Post-translational regulation of TFEB/3 activity

Supervised by

Professor Colin Goding

This thesis has been submitted to the Nuffield Department of Medicine, University of Oxford in partial fulfilment of the requirements for the degree of Doctor of Philosophy in Clinical Medicine.

Sarah Andrews

St Edmund Hall, University of Oxford

2025

Disclaimer

I declare that the work presented in this thesis is my own, unless otherwise stated. To the best of my knowledge, it does not contain material written by another person nor has it been previously submitted as an academic piece of work to this university or to another. Any work presented that is not my own is declared in the relevant figure legend and here: **Table 8** (Linxin Li, Ludwig, Oxford), **Figure 15** (Georgina Berridge, TDI, Oxford), **Figure 16** (Val Millar, TDI, Oxford and Linxin Li, Ludwig, Oxford), **Figure 19** (Val Millar, TDI, Oxford), **Figure 20 (**Val Millar, TDI, Oxford and Linxin Li, Ludwig, Oxford), **Figure 28** (Linxin Li, Ludwig, Oxford and myself), **Figure 30** (Hiroko Isoda, University of Tsubaka). The first drug screen was performed by Linxin Li but all subsequent follow-up experiments were designed and performed by myself unless otherwise stated. **Supplemental Figure 10** was generated by Pakavarin Louphrasitthiphol. **Supplemental Figure 12** and **Supplemental Figure 13** are produced by myself and are published.

Acknowledgments

Firstly, I would like to thank my supervisor, Professor Colin Goding for all of his support and guidance over the years. Despite my battle with ongoing health issues, he has never once doubted my capabilities and commitment to completing my DPhil. In fact, he is probably the main reason I did not give up. It may not be the PhD that I had hoped for but no one, including myself, could have anticipated the events that unfolded. I never got that first author paper that I had dreamt of but I am forever grateful that his belief in my ability as a scientist never faded.

I am grateful to my ex-lab partners Linxin Li and Hans Friedrichsen who I worked closely with at the beginning of my DPhil and who started the project that I continued working on. I also would like to thank my brilliant colleagues Sizhu Lu, Alice Bellini, Erica Oliveira, Yurena Vivas Garcia and Romuald Binet for being such a pleasure to work alongside. To Pakavarin, I will be forever thankful for all of your help and support throughout my time as a DPhil student and pushing me to finally submit. Without your kind words of encouragement, I would have either quit or never submitted and ended up as the eternal PhD student!

To other people who have made my time at the Ludwig so special, Michael McClellan, Claudia Zagami, Antonella D'Amore and George Maier thank you for all giving me words of encouragement and help when things have gone wrong. To Claudia in particular, thank you for always being straight to the point with me. Your honesty is what I admire about you the most.

A big shoutout to Robert Crickley who helped me immensely with optimising the macro in order to quantify all of the immunofluorescence images in my follow-up experiments. Val Millar, you really are a superstar! Your attention to detail is astounding. The TDI are very lucky to have you! You always helped me to remain calm during our time working together at the TDI. I really did enjoy working on the drug screen together, especially learning how all of the equipment worked. I am so happy we have remained in touch after all of these years.

To my parents who have supported my academic endeavours (despite not ever really knowing what I actually do!) and have helped me immensely throughout my battle with ME/CFS and more recently, uterine fibroids. Without you guys telling me to keep going, I may have quit when things got tough. To my boyfriend Jan Traulsen, thank you for always believing in me and telling me that I am good enough to do a DPhil. Thank you for helping me at my lowest points when I couldn't get out of bed. You never gave up on me and I will always be forever grateful for that. Here is to the next chapter of our lives. To our dogs, Heston and Poppy, I love you both dearly. Although Poppy sadly passed away recently, thank you for giving me unconditional love! Poppy, you will be forever in my heart.

Lastly, I would like to acknowledge myself for not giving up despite everything that has happened over these years. You did it!

List of Abbreviations

Aβ	β-amyloid
AD	Alzheimer’s disease
AMP	adenosine monophosphate
AMPK	adenosine monophosphate-activated protein kinase
AKT	RAC-alpha serine/threonine-protein kinase/protein kinase B/AKT
ATG	autophagy related gene
ATF4	activating transcription factor 4
ATP	adenosine triphosphate
bHLH-LZ	basic-helix-loop-helix leucin-zipper
BafA	bafilomycin A
BSA	bovine serum albumin
C-terminal	carboxyl-terminal
CAD	carbamoyl-phosphate synthetase
CDKN1A	cyclin-dependent kinase inhibitor 1A
ChIP-seq	chromatin immunoprecipitation followed by sequencing
CLEAR	coordinated lysosomal expression and regulation
CREB	cAMP response element binding protein
CRM1	chromosomal region maintenance 1
CsA	cyclosporine
DAPI	4′, 6-diamidino-2-phenylindole
DMEM	Dulbecco’s modified eagle medium
DMSO	dimethyl sulfoxide
DNA	deoxyribonucleic acid
EGFP	enhanced green fluorescent protein

EGFR	epidermal growth factor receptor
ER	endoplasmic reticulum
ERK2	mitogen-activated protein kinase 1
FDA	food and drug administration
FKBP12	FK506 binding protein 12
FLCN	folliculin
GAP	guanosine triphosphate hydrolase activating protein
GDP	guanosine diphosphate
GEF	guanine-nucleotide exchange factor
GFAT1	glutamine: fructose-6-phosphate amidotransferase 1
GFP	green fluorescent protein
GLUT1	glucose transporter 1
GSK3β	glycogen synthase kinase 3 β
GST	glutathione S-transferase
GTP	guanosine triphosphate
GTPase	guanosine triphosphate hydrolase
HA	human influenza hemagglutinin
HBSS	Hank’s balanced salt solution
HD	Huntington’s disease
HER2	human epidermal growth factor receptor 2
HK1	hexokinase 1
HIF1α	hypoxia-induced factor 1 subunit α
IF	immunofluorescence
IGF-1	insulin/insulin-like growth factor-1
IPO	nuclear importin
IRS1	insulin receptor substrate 1

kDa	kilodalton
KO	Knockout
LAMP2	lysosomal associated membrane protein 2
LC3B	microtubule associated protein 1 light chain 3 B
LDL	low-density lipoprotein
LKB1	serine/threonine kinase 11/liver kinase B1
LPS	liposaccharide
LSD	lysosomal storage disorder
MAPK	mitogen-activated protein kinase
MAP4K3	mitogen-activated protein kinase kinase kinase kinase 3
MCOLN1	mucolipin 1
MEK	mitogen-activated protein kinase kinase 1
MHC	major histocompatibility complex
MITF	microphthalmia associated transcription factor
mLST8	mammalian lethal with Sec13 protein 8
mRNA	messenger ribonucleic acid
mTOR	mechanistic target of rapamycin
mTORC1	mechanistic target of rapamycin complex 1
mTORC2	mechanistic target of rapamycin complex 2
N-terminal	amine-terminal
NES	nuclear export signal
NLS	nuclear localisation signal
TBST	tris-buffered saline with Tween
TCA	tricarboxylic acid
TCGA	The Cancer Genome Atlas
TFEB	transcription factor EB

TFE3	transcription factor E3
TSC	tuberous sclerosis complex
TYR	tyrosinase
PBS (T)	phosphate-buffered saline (with Tween)
PCR	polymerase chain reaction
PD	Parkinson’s disease
PDAC	pancreatic ductal adenocarcinoma
PDK1	phosphoinositide-dependent kinase 1
PERK	PRKR-Like Endoplasmic Reticulum Kinase
PFK	phosphofructokinase
PGC1-α	peroxisome proliferator-activated receptor γ coactivator 1 α
PI3K	phosphoinositide 3-kinase
PKB	protein kinase B/AKT
PKC	protein kinase C
PP2A	protein phosphatase 2A
PRAS40	proline-rich AKT substrate of 40 kDa
PTEN	phosphatase and tensin homolog
qRT-PCR	quantitative real-time PCR
RRAGD	Ras-related GTP-binding protein D
RANKL	Receptor activator of nuclear factor kappa-B ligand
RAPTOR	regulatory protein associated with TOR
RCC	renal cell carcinoma
Rheb	Ras homologue enriched in brain
RNA	ribonucleic acid
RNAi	RNA interference
RICTOR	rapamycin insensitive companion of mTOR

Rb	retinoblastoma
S6	ribosomal protein S6
S6K	ribosomal protein S6 kinase/p70 S6 kinase
SBMA	spinal and bulbar muscular atrophy
SD	standard deviation
SGK1	glucocorticoid-induced protein kinase 1
shRNA	small hairpin RNA
siRNA	small interfering RNA
SREBP	sterol responsive element binding protein
SSMD	strictly standardised mean difference
ULK1	Unc-51 like autophagy activating kinase 1
UPR	unfolded protein response
v-ATPase	vacuolar-type H+- adenosine triphosphate hydrolase
WT	wild-type
XPO1	nuclear exportin 1

Table of contents

List of Figures

List of Supplementary Figures

List of Tables

Abstract

Post-translational regulation of TFEB/3 activity

Sarah Andrews, St Edmund Hall, University of Oxford, 2025

The ability of cells to sense and adapt to changes in their environment is critical for their survival. Cancer cells acquire the ability to promote cell growth and proliferation independently of growth factors, whilst retaining the ability to sense and adapt to changes in nutrient availability. During tumorigenesis, poor vascularisation results in the promotion of catabolic processes, such as autophagy. Transcription factor EB (TFEB), a member of the microphthalmia/transcription factor E (MiT/TFE) family has been coined as the master regulator of autophagy and lysosomal biogenesis. In response to nutrient deprivation, TFEB is dephosphorylated and rapidly accumulates in the nucleus to promote expression of the CLEAR network. In tumours that exhibit high levels of TFEB/3-dependent autophagy, TFEB is constitutively nuclear and hyperactivated, contributing to cancer pathogenesis. Conversely, in neurodegenerative diseases, such as Alzheimer's disease, lysosomal function and autophagy are often impaired. Over-expression or activation of TFEB can ameliorate disease pathogenesis through promoting intracellular clearance.

In this study, we show that TFEB accumulates in the nucleus in response to both amino acid and glucose depletion which is readily reversed upon nutrient replenishment. Furthermore, glucose deprivation does not inhibit mTORC1 but instead, activates the mTORC2-AKT signalling pathway. We demonstrated that GSK3β can phosphorylate TFEB/MITF on Ser138/Ser69 but only when Ser142/Ser73 is first phosphorylated by ERK2 or mTORC1, highlighting that this dual phosphorylation event is required for nuclear export of TFEB.

Additionally, we performed two reciprocal, high-throughput image-based screens to explore the regulatory mechanisms which govern TFEB subcellular localisation. The first screen allowed us to identify 50 FDA-approved drugs that could promote nuclear accumulation of TFEB as well as increase lysosomal staining. We identified pimozide as a potential candidate for drug re-purposing for neurodegenerative diseases as it displayed neuroprotection in cell-based models of neurodegenerative disease. The second screen identified 10 kinase inhibitors from the PKISI/II library (GSK) that may have cancer therapeutic potential, being able to attenuate nuclear accumulation of TFEB in response to glucose and/or amino acid deprivation. GW869516X was able to partially rescue mTORC1 activity whilst inhibiting mTORC2 signalling in response to amino acid and glucose starvation respectively. Additionally, GW869516X inhibited AMPK signalling and can directly bind to AMPK. Overall, this work contributes to our understanding of how TFEB activity is regulated through dynamic phosphorylation events. The results obtained from our screens provide a reservoir of drugs that can modulate TFEB subcellular localisation, warranting further investigation.

Chapter 1: Introduction

1.1 Glucose and amino acid metabolism in cancer

Cancer is a broad term used to describe a multitude of diseases involving the dysregulation of proliferation by transformed cells which have the ability to adapt and evolve to changes in their environment whilst having the potential to migrate to distant sites (Brown et al. 2023). In 2022, the risk of a person receiving a cancer diagnosis before the age of 75 was around 21.8% for males and 18.5% for females, highlighting cancer as a major global health issue (WHO).

In 2006, Pavlova and Thompson organised cancer-associated metabolic phenotypes into six 'hallmarks' of cancer metabolism: (1) Dysregulated uptake of glucose and amino acids; (2) use of opportunistic modes of nutrient acquisition; (3) use of glycolysis/TCA cycle intermediates for biosynthesis and NADPH production; (4) increased demand for nitrogen; (5) alterations in metabolite-driven gene regulation; and (6) metabolic interactions with the microenvironment (Pavlova and Thompson 2016). In this chapter, we will discuss these metabolic hallmarks of cancer.

- *Cancer cells rewire their metabolism to promote tumorigenesis*

The complexity of tumour composition, in addition to environmental stimuli such as nutrient limitation, oxygen deprivation as well as the cooperation of immune cells, all contribute to how cells rewire their metabolism in order to survive (Hanahan and Weinberg 2000). Nearly 100 years ago, the German physiologist Otto Warburg observed aberrant metabolism in cancer, demonstrating that tumours use significantly more glucose than normal cells (Otto Warburg, Wind, and Negelein 1927). Furthermore, he noted that cancer cells preferentially rely upon glycolysis instead of mitochondrial oxidative phosphorylation, even in the presence of oxygen (Warburg 1956).

It remained unclear as to why cancer cells would opt to use a less efficient way of generating ATP even in the presence of oxygen (Kang et al. 2023). Warburg and others first speculated that this metabolic rewiring could be the consequence of mitochondrial dysfunction, thus impairing the ability of cancer cells to utilise oxidative phosphorylation to generate ATP (Warburg 1956). Although mitochondrial dysfunction can contribute to the rewiring of metabolism (Tan et al. 2015), there are other factors that drive changes in cancer cell metabolism.

At first glance, the primary advantage would be to enable cancer cells to proliferate under low oxygen conditions, often observed during tumour development due to poor vascularisation.

However, glycolysis serves two purposes in cellular metabolism: firstly, to generate ATP and secondly, to produce intermediates for biosynthetic pathways (Fadaka et al. 2017). Thus, a clear survival advantage of upregulating glycolysis would be to upregulate biosynthesis of nucleotides, membrane lipids, and proteins required for cell growth and proliferation (Hsu and Sabatini 2008). In addition, glycolysis allows cells to increase glucose uptake and glucose utilisation through increasing expression of glucose transporters and glycolytic genes (Fadaka et al. 2017).

Whether or not the Warburg effect is simply an adaptation to reduced nutrient and oxygen supply to promote tumorigenesis or a consequence of cancer-initiating genetic alterations was disputed for quite some time. For instance, one study demonstrated that introducing cancer-promoting oncogenes in a step-wise manner transformed primary fibroblasts and at the same time, promoted glycolysis (Ramanathan, Wang, and Schreiber 2005). Another study introduced similar factors into human mesenchymal stem cells and demonstrated transformation is associated with increased dependence on glycolysis and upregulation of glycolytic genes which could be reversed upon oxygen restoration (Funes et al. 2007). Taken together, the evidence suggests both genetic alterations and nutrient availability in the tumour microenvironment mediate these metabolic adaptations.

- *Cancer cells uptake more glucose and amino acids than normal cells in a growth factor and ECM-independent manner*

To sustain cell proliferation, cancer cells require higher levels of glucose and amino acids than normal, differentiated cells (Pavlova and Thompson 2016). In order to balance their ‘supply’ with their ‘demand’, cancer cells must increase their ability to uptake glucose and amino acids from their external environment. The two main nutrients required for proliferation are glucose and glutamine. The catabolism of these two nutrients provide cells with a large, diverse pool of carbon intermediates which are the essential ‘building blocks’ of cells. Furthermore, oxidation of glucose and glutamine allows cells to capture their reducing power as Nicotinamide adenine dinucleotide with hydrogen (NADH) or Flavin adenine dinucleotide with hydrogen (FADH2), enabling the transfer of electrons to the electron transport chain to fuel ATP production. In addition, the related cofactor NADPH provides reducing power for a wide variety of biosynthetic reactions, as well maintaining cellular redox capacity (Pavlova and Thompson 2016).

As previously mentioned, cancer cells exhibit increased glucose uptake (Otto Warburg, Wind, and Negelein 1927) which has been confirmed by others in a variety of tumours contexts

(Fukuda et al. 1982). These observations are now exploited by clinicians through the use of position emission tomography (PET)-based imaging whereby cancer cells demonstrate increased uptake of a fluorinated glucose analogue (18F-fluorodeoxyglucose (18F-FDG) compared to normal cells, enabling medical specialists to diagnose and monitor tumour progression (Almuhaideb, Papathanasiou, and Bomanji 2011).

Although the observation that cancer cells uptake more glucose than normal cells was made in 1927 (Otto Warburg, Wind, and Negelein 1927), higher levels of glutamine uptake was not observed until 1957, by the American physiologist, Harry Eagle (Eagle 1955). Eagle demonstrated that HeLa cells required a 10-100-fold molar excess of glutamine compared to other amino acids. In addition, others demonstrated glutamine was the most rapidly consumed amino acid by cancer cells (Brand 1985) and often, tumours deplete glutamine from their environments (Pallett et al. 2021). The observation that tumour cells uptake more glutamine than non-cancer cells has led to the development of fluorinated glutamine analogues which have shown promise in preclinical and early clinical studies (Lieberman et al. 2011) and are particularly useful for imaging tumours that are in regions of the body that exhibit high levels of glucose utilisation, such as the brain, making the use of glucose analogues not feasible.

Glutamine catabolism not only provides cells with a source of carbon, but also nitrogen. Nitrogen is required for the biosynthesis of purine and pyrimidine nucleotides, glucosamine-6-phosphate, as well as non-essential amino acids (Pavlova and Thompson 2016). In addition to the catabolism of glutamine promoting cell survival, glutamine itself also plays a role in the uptake of essential amino acids that cannot be synthesised by cells themselves. For instance, the import of leucine through L-type amino acid transporter 1 (LAT1) on the plasma membrane is coupled to the efflux of glutamine (Nicklin et al. 2009). Furthermore, others have demonstrated that efflux of intracellular glutamine is also coupled to the import of other essential amino acids through LAT1, including isoleucine, valine, methionine, tyrosine, tryptophan and phenylalanine, essential for protein translation and mammalian target of rapamycin complex 1 (mTORC1) activity (Yanagida et al. 2001).

In normal, differentiated cells, glucose and glutamine uptake is dependent upon growth factor signalling and the extracellular matrix (Thompson 2011). For instance, studies have demonstrated that when lymphocytes are deprived of growth factors, they fail to consume glucose in quantities sufficient to maintain cellular bioenergetics, resulting in a reduction in cell size and higher rates of apoptosis despite glucose remaining abundant (Rathmell et al. 2000). However, survival of growth-factor deprived cells could be rescued by over-expressing the plasma membrane glucose transporter 1 (GLUT1) and the first enzyme of the glycolytic pathway hexokinase (HK) (Rathmell et al. 2003). In addition, culturing mammary epithelial

cells in suspension, whereby they are detached from the extracellular matrix, compromises glucose uptake and impairs mitochondrial function. However, this effect could be reversed by over-expression of Erb-b2 receptor tyrosine kinase 2 (ErbB2) which restored glucose uptake, through stabilisation of epidermal growth factor receptor (EGFR) and activation of phosphoinositide 3-kinase (PI3K) (Schafer et al. 2009).

- *Cancer cells accumulate genetic mutations to promote proliferation independently of environmental cues*

Cancer cells accumulate mutations in genes to promote cell survival independently of environmental cues. In particular, genetic alterations that target phosphoinositide 3-kinase (PI3K) and its negative regulators, phosphatase and tensin homolog (PTEN) and inositol polyphosphate 4 (INPP4B), as well as mutations and gene amplifications in upstream receptor tyrosine kinases (RTKs) result in constitutive uptake of glucose and amino acids to fuel cancer cell metabolism (Vogelstein and Kinzler 2004).

Many signaling pathways downstream of RTKs converge on PI3K/AKT (alpha serine/threonine-protein kinase) signalling, which is the main pathway regulating glucose uptake (Hoxhaj and Manning 2020). PI3K/AKT signalling promotes the expression of the plasma membrane glucose transporter GLUT1 and its translocation to the cell surface (Barthel et al. 1999). Additionally, AKT phosphorylates hexokinase II, promoting its ability to phosphorylate glucose molecules to prevent their efflux (David J. Roberts et al. 2013). In addition, AKT also phosphorylates and stabilises phosphofructokinase (PFK) which catalyses a key irreversible step in glycolysis (Lee et al. 2017). Collectively, PI3K/AKT signalling is a critical bottleneck for cancer cell survival through its control of glycolysis and glucose uptake and as a consequence, is often mutated in cancers. Other oncogenic pathways, such as Ras signalling have been found to upregulate GLUT1 expression to increase glucose uptake (Murakami, et al. 1992). For instance, cancers harbouring gain-of-function mutations in KRAS or BRAF exhibit higher levels of GLUT1 leading to increased glucose uptake and glycolysis (Yun et al. 2009).

Another gene that is often mutated in cancer is that encoding the transcription factor, cellular myelocytomatosis oncogene (c-Myc). In many cancers, c-Myc is overexpressed and/or constitutively active (Miller et al. 2012) and is a major driver of proliferation through promoting glutamine uptake and utilisation (Wise et al. 2008). For instance, transcriptional targets of c-Myc include the glutamine transporters: alanine serine cysteine transporter 2 (ASCT2) and sodium-coupled neutral amino acid transporter 2 (SN2) as well as enzymes required for

glutamine utilisation such as glutaminase 1 (GLS1), phosphoribosyl pyrophosphate synthetase 2 (PRPS2) and carbamoyl-phosphate synthetase 2 (CAD), which support transporter-facilitated glutamine uptake by converting glutamine to glutamate (Gao et al. 2009a) (Eberhardy and Farnham 2001). Furthermore, the resulting glutamate cannot exit the cell and accumulates, promoting the replenishment of TCA intermediates (anaplerosis), stimulating cysteine uptake by acting as an exchange substrate for the cysteine antiporter xCT (Conrad and Sato 2012).

In addition to gain-of-function mutations or amplifications leading to increased c-Myc activity, loss-of-function mutations in the retinoblastoma (Rb) gene also contribute to upregulation and utilisation of glutamine via increased activity of the Early region 2 binding factor (E2F) that can promote expression ASCT2 and GLS1 (W. Du et al. 2009). Furthermore, E2F activity also promotes nucleotide synthesis required for DNA synthesis (Ishida et al. 2001).

- *Cancer cells adapt their behaviour to balance their nutrient supply with their demand*

One of the biggest challenges in the development of anti-cancer therapies is tumour heterogeneity. Within one tumour, different subpopulations exist that harbour distinct genetic or epigenetic alterations and as a consequence, exhibit different phenotypes (Meacham and Morrison 2013). The ability of cancer cells to reversibly adapt to changes in their environment and alter their behaviour is referred to as ‘phenotypic-switching’, a phenomenon well studied in melanoma (Hoek and Goding 2010).

Melanoma has the highest mortality rate of all skin cancers and arises due to oncogenic transformation of cells of the melanocytic lineage (Shain and Bastian 2016). Furthermore, melanoma is a good model for demonstrating phenotypic heterogeneity and exploring the mechanisms underpinning phenotypic-switching; a process required for metastasis, as there are well-defined markers that highlight specific phenotypic subpopulations (Falletta, Goding, and Vivas-García 2022). For instance, levels of the microphthalmia-associated transcription factor (MITF) that controls many aspects of melanoma biology (Goding and Arnheiter 2019) are associated with different phenotypes: low levels of MITF are associated with invasion, senescence and therapy resistance, whereas higher levels of MITF are associated with proliferation and sensitivity to anti-cancer drugs, or differentiation. In addition, cells that exhibit stem cell-like properties have the ability to self-renew, seed and maintain tumours, providing a reservoir of cells that are resistant to therapy and maintain tumorigenesis (Hoek and Goding 2010).

The plasticity of cancer cell metabolism facilitates phenotypic-switching. For instance, one study demonstrated that three different melanoma cell lines, each representing different phenotypic states, displayed vast differences in their gene-expression and metabolomic profiles in response to oxygen deprivation (Louphrasitthiphol et al. 2019). Another demonstrated that low glutamine levels drive translational reprogramming in melanoma, promoting phenotype-switching from a proliferative to invasive phenotype through changes in MITF levels mediated by loss of MITF translation and by activating transcription factor 4 (ATF4)-mediated transcriptional silencing of the MITF gene (Falletta et al. 2017).

Taken together, cancer cells acquire mutations in genes that control cell proliferation as well as rewiring their metabolism by acquiring mutations in genes involved in the uptake and utilisation of glucose and amino acids. Furthermore, changes in the tumour microenvironment can reversibly alter cancer cell behaviour through driving transcriptional, translational and metabolic changes ensuring survival, maintenance of tumorigenesis and even drive metastasis.

1.2 Introducing the mTORC1 and mTORC2 complexes

In the 1960s, a naturally occurring compound was isolated from soil samples collected on Easter Island (Rapa Nui) and was found to exhibit anti-fungal properties (Sehgal, Baker, and Vézina 1975). Later it was shown that Rapamycin also exhibited immunosuppressive (Dumont and Su 1995) and anti-tumour properties (Eng, Sehgalt, and Vezina 1984), although its mode of action remained elusive for quite some time. In the 1990s, genetic studies identified the target of rapamycin 1 and 2 (TOR1 and TOR2) genes as mediating the toxic effects induced by rapamycin in yeast (Cafferkey et al. 1993) and biochemical studies revealed rapamycin forms a complex with FKBP12 to inhibit cell proliferation in mammalian cells (Chung et al. 1992) via inhibition of a protein kinase that was homologous to that in yeast, which was named the mechanistic/mammalian target of rapamycin (mTOR) (Sabatini et al. 1994).

As mTOR is a key regulator of maintaining nutrient homeostasis, allowing cells to maintain survival and proliferation in response to environmental changes, it has been widely studied and has been implicated in numerous diseases(Laplante and Sabatini 2012). The mTOR protein kinase forms two structurally and biologically distinct protein kinase complexes with regulatory subunits, which are called mTOR Complex 1 and 2 (mTORC1/2).

mTORC1 consists of the regulatory protein associated with TOR (RAPTOR) (Hara et al. 2002), the mammalian lethal with Sec13 protein 8 (mLST8) (Kim et al. 2003) and two negative regulatory subunits called the proline-rich AKT substrate of 40 kDa (PRAS40) (Sancak et al. 2007), and the DEP domain-containing mTOR-interacting protein DEPTOR (Peterson et al.

2009). In comparison, mTORC2 which shares the same core protein kinase, mTOR, has different regulatory subunits and is insensitive to the rapamycin-FKBP12 complex. Instead, mTORC2 is comprised of rapamycin insensitive companion of mTOR (RICTOR), (Sarbassov et al. 2004), mammalian stress-activated protein kinase interacting protein 1 (mSIN1) (Frias et al. 2006), protein observed with Rictor-1/2 (Protor1/2) (Pearce et al. 2007). The compositions of mTORC1 and mTORC2 are demonstrated below in **Figure 1**:

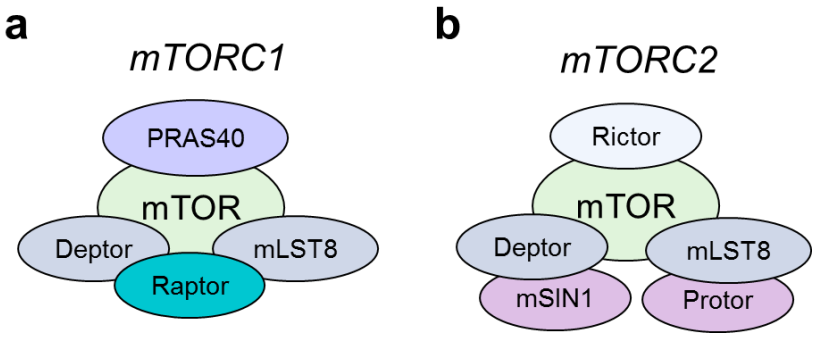

Figure 1 Composition of the mTOR complexes. (a) mTORC1 contains: the catalytic subunit mTOR, the positive regulatory subunits mLST8 and RAPTOR, and the negative regulatory subunits DEPTOR, PRAS40 and is sensitive to the FKBP12-rapamycin complex. (b) mTORC2 contains: the core mTOR kinase, the positive regulatory subunits mLST8, RICTOR and mSIN1, and the negative regulatory subunits DEPTOR and Protor1/2. mTORC2 is insensitive to the FKBP12-rapamycin complex.

1.2.1 Regulation of mTORC1

- *Growth factors and cytokines*

Numerous growth factors converge on mTORC1 signaling through inhibition of the Tuberous Sclerosis Complex (TSC), a negative regulator of mTORC1. The TSC consists of three proteins: TSC1, TSC2 and TBC1D7 (Dibble et al. 2012) and acts as a GTPase activating protein (GAP) for the small GTPase Rheb (Inoki et al. 2003). The TSC GAP activity towards Rheb leads to the conversion of GTP-bound to GDP-bound Rheb, rendering it inactive. Only when Rheb is GTP-bound can it directly bind to and activate mTORC1 (Long et al. 2005). In response to insulin or insulin-like growth factor-1 (IGF-1), phosphoinositide 3-kinase (PI3K) is activated and in turn, phosphorylates and activates alpha serine/threonine-protein kinase (AKT) on Thr308. Activated AKT phosphorylates TSC2, promoting its dissociation from the lysosomal membrane, preventing its GAP function towards Rheb and thereby enabling mTORC1 activity (Inoki et al. 2002b). Simultaneously, AKT can directly phosphorylate and inhibit PRAS40, a negative regulatory subunit of the mTORC1 complex, further promoting

mTORC1 activity (Sancak et al. 2007). In parallel, insulin/insulin growth factor receptor 1 (IGFR-1) also activates the mitogen-activated protein kinase (MAPK) pathway, leading to phosphorylation and inhibition of TSC2 (W. Zhang, Liu, and Tu 2002) and phosphorylation and activation of Raptor (Carrière et al. 2008).

Other growth factors and cytokines can activate mTORC1 (**Figure 2**)**Figure 2 Regulation of mTORC1 and mTORC2.**. For instance, activation of Wingless-related integration site (Wnt) signalling leads to phosphorylation and inhibition of TSC2 by glycogen synthase kinase 3 β (GSK3β) (Inoki et al. 2006). Additionally, activation of Tumour Necrosis Factor Alpha (TNFα) signalling leads to activation of the Inhibitor of Kappa b kinase β (IKKβ), which can phosphorylate TSC1 (D. F. Lee et al. 2007).

- *Amino acids*

Amino acids regulate mTORC1 activity through two main mechanisms (**Figure 2**). Firstly, the recruitment of mTORC1 to the lysosomal surface is dependent on amino acids and involves the heterodimeric Rag GTPases: Rag A/B and Rag C/D (Sancak et al. 2008) which are tethered to the lysosomal surface through binding with the Ragulator complex (Sancak et al. 2010). When amino acids are present, the active forms of Rag GTPases (RagA/B-GTP-RagC/D-GDP) bind to RAPTOR, recruiting mTORC1 to the lysosomal surface, and allowing Rheb to activate mTORC1 (Parmar and Tamanoi 2010). The second mechanism involves the sensing of amino acids in the cytosol and within the lysosome. For instance, when arginine is present inside the lysosome, the lysosomal amino acid transporter, human member 9 of the solute carrier family 38 (SLC38A9) is activated (Rebsamen et al. 2015). Activation of SLC38A9 is mediated by the lysosomal v-ATPase which promotes the guanine exchange factor (GEF) function of the Ragulator complex towards RagA/B (Bar-Peled et al. 2012). At the same time, cytosolic arginine and leucine activate mTORC1 through inhibition of the GAP Activity Towards Rags complex 1 (GATOR1). GATOR2 is upstream of GATOR1 and inhibits the GAP activity of GATOR1 in response to amino acids (Sahu and Ben-Sahra 2023). This occurs through the binding of arginine and leucine to Cytosolic Arginine Sensor for mTORC1 Subunit 1 (CASTOR1) (Xia et al. 2016) and Sestrin1/2 (Wolfson et al. 2016), respectively. Binding of leucine to Sestrin1/2 leads to inhibition of GAP function of GATOR1 towards RagA/B (Chantranupong et al. 2014). Whereas binding of arginine to CASTOR1, prevents CASTOR1-CASTOR2 dimerization, a complex that activates GAP function of GATOR1 towards RagA/B (Chantranupong et al. 2016).

Whilst RagA/B are regulated by the GATOR1/2 complex, RagC/D are regulated by the tumour suppressor Folliculin (FLCN) and the Folliculin-interacting protein 1/2 (FNIP1/2) complex. When amino acids are present, the FLCN-FNIP2 complex functions as a GAP for RagC/D which also activates mTORC1 (Tsun et al. 2013).

In comparison, glutamine and asparagine activate mTORC1 independently of Rag GTPases but instead, require the ADP-ribosylation factor-1 (Arf1) (Meng et al. 2020). In the absence of glutamine and asparagine, Arf1 GTPase-activating protein 1 (ArfGAP1) interacts with mTORC1, preventing its recruitment to the lysosome (Jewell et al. 2015). Low glutamine levels also inhibit mTORC1 activity through another amino acid sensor; general control nonderepressible 2 (GCN2). In response to glutamine withdrawal, activation of GCN2 activates ATF4, leading to increased expression of Sestrin 2 which is required to sustain repression of mTORC1 by preventing its lysosomal localisation (Ye et al. 2015). Overall, mTORC1 activity is maintained by amino acids through multiple mechanisms (**Figure 2**).

- *Lipids and glucose*

mTORC1 also senses the levels of lipids and glucose. For instance, cholesterol is a lipid that is a precursor of steroid hormones, bile acids and vitamin D, as well as being an important component of the cell membrane. Cholesterol is transported throughout the body in low-density lipoproteins (LDL) and then taken up by cells by endocytosis. When degraded by the lysosomes, cholesterol is exported out of the lysosomal lumen by the Niemann-Pick-C1 (NPC1) protein and interacts with the amino acid transporter SLC38A9, resulting in mTORC1 activation (Castellano et al. 2017).

In comparison, glucose is sensed by mTORC1 indirectly, through activation of AMP-activated protein kinase (AMPK). Low glucose levels lead to changes in the abundance of glycolytic intermediates, such as fructose-1-6-bisphosphate (FBP) levels. An enzyme called Aldolase binds to FBP and when levels of FBP are low, Aldolase instead promotes the formation of a lysosomal complex containing the lysosomal v-ATPase, Ragulator, Axin, Liver kinase B1 (LKB1) and AMPK (Zhang et al. 2017). The interaction of LKB1 with AMPK is required for AMPK activation via phosphorylation of its catalytic domain on Thr172 (Shackelford and Shaw 2009). In addition, low glucose levels are sensed by an increase in the AMP/ATP and/or ADP/ATP ratios. Binding of AMP and/or ADP leads to allosteric changes in AMPK which promote binding to upstream kinases such as LKB1 required for its activity (Ke et al. 2018). Once AMPK is activated, it inhibits mTORC1 signaling by phosphorylation and inhibition of the positive regulatory subunit of mTORC1, RAPTOR (Gwinn et al. 2008a) and phosphorylation

and activation of the negative regulator of mTORC1, TSC2 (Inoki, Zhu, and Guan 2003a). In addition, low glucose levels also inhibit mTORC1 signaling through inhibition of the Rag GTPases independently of AMPK through recruitment of AXIN to the lysosomal membrane (Li et al. 2023).

1.2.2 Regulation of mTORC2

- *Growth factors and cytokines*

Although mTORC1 and mTORC2 share the same catalytic subunit (mTOR), they are composed of different regulatory subunits which alter their regulation and function. mTORC2 primarily functions as a downstream effector of insulin/IGF-1 signalling. mTORC2 contains a negative regulatory subunit called mammalian stress-activated protein kinase-interacting protein 1 (mSIN1) which contains a pleckstrin homology (PH) domain; a 100-120 amino acid module that binds to phosphoinositides present in cell membranes (Frias et al. 2006b). In response to insulin/IGF-1 signalling, PI3K becomes activated and phosphorylates Phosphatidylinositol 4,5-bisphosphate ($PI(4,5)P_2$) to generate Phosphatidylinositol-3,4,5-triphosphate ($PI(3,4,5)P_3$) at the surface of the plasma membrane (**Figure 2**). This reaction is opposed by the phosphatase and tension homolog (PTEN). When $PI(3,4,5)P_3$ is abundant, AKT and its activating kinase, PDK1 are recruited to the plasma membrane via interactions with their PH domains. This recruitment allows PDK1 phosphorylation of AKT at Thr308, promoting its activation. Additionally, when PI(3,4,5)P3 levels are high, it binds to the PH domain of mSIN1, preventing it from inhibiting mTOR kinase activity (Gan et al. 2011) but also allowing recruitment of mTORC2 to the plasma membrane (Liu et al. 2015). At the same time, activated AKT phosphorylates mTORC2 on Thr86 of the mSIN1 domain, further promoting mTORC2 activation (Sun et al. 2023). Activation of mTORC2, through inhibition of mSIN1, then leads to phosphorylation of Ser473, further promoting AKT activation (Baffi et al. 2021a), resulting in a positive feedback loop that maintains mTORC2-AKT signalling (G. Yang et al. 2015).

- *Glutamine and glucose*

mTORC2 is also responsive to intracellular nutrients and metabolites. Unlike mTORC1, mTORC2 activity is enhanced by withdrawal of glutamine and glucose (Moloughney et al. 2016). During glucose deprivation, AMPK directly phosphorylates mTOR on S1261 and RICTOR in the presence of minimal PI3K activity, promoting mTORC2 activation (Kazyken et

al. 2019). Although glutamine levels influence mTORC2, the mechanism through which this occurs remains unclear. However, Sestrin 1/2 is suspected to play a role in this process. For instance, Sestrin 2 is upregulated in lung cancer cells during glutamine deprivation and associates with mTORC2 to promote activation of AMPK and at the same time, suppressing mTORC1 (Byun et al. 2017). Conversely, high glutamine levels have been shown to cause hyperactivation of mTORC1, leading to repression of mTORC2 (Gayatri et al. 2022). Therefore, the evidence suggests that glutamine withdrawal promotes activation of mTORC2 indirectly through inhibition of mTORC1, but also through up-regulation of Sestrin-2. Sestrin-2 activates mTORC2 through activation of AKT and by directly to mTORC2, promoting Sestrin-2 stability and thus creating a positive feedback loop.

- *Lysosomal positioning and ribosomal binding*

Due to PI3K-dependent generation of $PI(3,4,5)P_3$ occurring at the plasma membrane, mTORC2 regulation is thought to occur primarily there. Although mTORC2 and AKT are known to be widely distributed within the cell, AKT, mTORC2 and PI3K all harbour PH domains, essential for membrane recruitment. However, others have demonstrated that pools of active mTORC2 are physically associated with ribosomal membranes, and PI3K activation promotes mTORC2-ribosome binding, suggesting that ribosomes activate mTORC2 directly (Zinzalla et al. 2011). Another study showed perinuclear clustering of lysosomes delayed reactivation of not only mTORC1 but also mTORC2 and AKT upon serum replenishment. This finding demonstrates the existence of pools of mTORC2 and AKT that are sensitive to lysosomal positioning (Jia and Bonifacino 2019), suggesting that compartmental localisation of mTORC2 is also important for its activity in response to growth factor signalling.

Additionally, mTORC2-ribosomal binding promotes constitutive, co-translational phosphorylation and stability of AKT on the turn motif (Thr450), preventing co-translational ubiquitination and subsequent proteasomal degradation of AKT. Unlike PI3K-induced, mTORC2-dependent phosphorylation of AKT on Ser473, this function is independent of growth factors and happens constitutively due to the turn motif of AKT being accessible, whereas the hydrophobic motif (Ser473) is not accessible in the ribosomal tunnel (Oh et al. 2010). This latter function demonstrates that mTORC2 activity is not only transiently induced by growth factors but is mediated by other nutrients or conditions that promote translation.

- *Mechanical stress*

In yeast, TORC2 has been shown to respond to mechanical stress via redistribution of its partner, Slm which harbours a PH domain (Berchtold et al. 2012). In mammals, inhibition of mTORC2-AKT signaling in bone marrow-derived mesenchymal cells prevents cytoskeletal reorganisation in response to mechanical strain and prevents osteoclasts from differentiating and instead, promoted adipogenesis (Sen et al. 2014), thus demonstrating that mTORC2 is not only activated by depletion of glucose, glutamine or energetic stress, but also by mechanical strain/osmotic pressure.

- *mTORC1 inhibits mTORC2 activity*

The ability of mTORC1 to inhibit mTORC2 is mediated through a negative feedback loop whereby mTORC1 inhibition of insulin receptor substrate 1 (IRS1)-PI3K signalling and growth factor receptor-bound protein 10 (GRB10) dampens mTORC2/AKT signalling. For instance, S6K1 has been shown to phosphorylate IRS1 at multiple sites to promote its proteasomal degradation, preventing prolonged mTORC2 activation in response to IGF signalling (Yoneyama et al. 2018). However, others have demonstrated that mTORC1 can also inhibit mTORC2 via IRS1-independent mechanisms. For instance, one study demonstrated that mTORC1 activation inhibited mTORC2 signalling by promoting phosphorylation of mSIN1 (an essential component of mTORC2) either by S6K or AKT (cell line dependent) at Thr86 and Thr398, promoting dissociation from RICTOR and mTOR and suppression of mTORC2-induced AKT activation (Liu et al. 2013).

Overall, although mTORC2 regulation is less well understood, coordination of both the mTORC1 and mTORC2 signalling networks are essential for enabling cells to respond to changes in their environment. The integration of signalling pathways upstream of mTORC1 and mTORC2 are shown below in **Figure 2**:

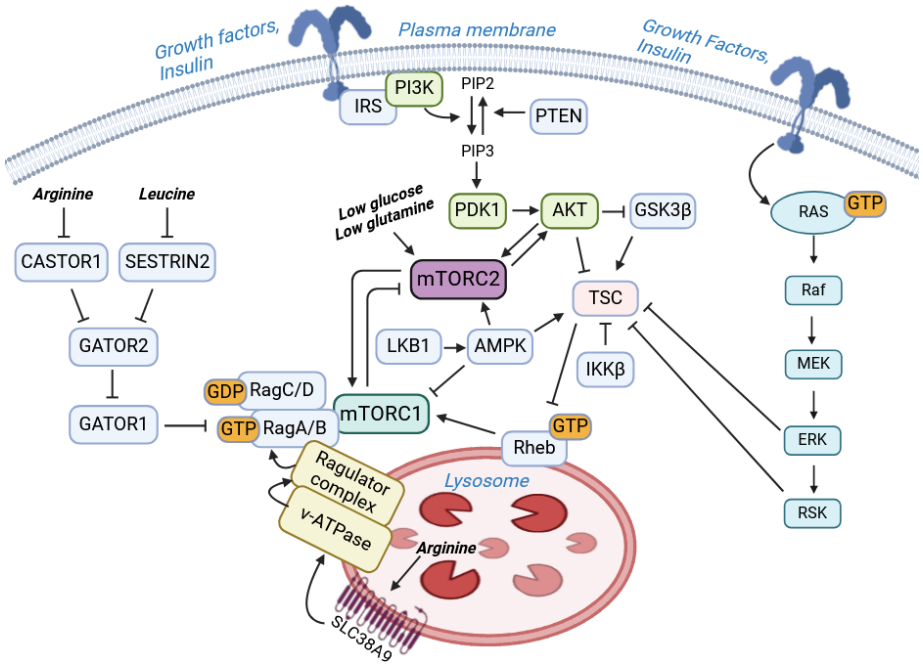

Figure 2 Regulation of mTORC1 and mTORC2.
A simplified schematic demonstrating the integration of numerous signalling pathways upstream of mTORC1 and mTORC2. mTORC1 and mTORC2 activity is regulated by the availability of growth factors, amino acids and glucose. mTORC1 is recruited to the surface of the lysosome via recruitment with Rag GTPases (RagA/B-GTP-RagC/D-GDP) where it can interact and phosphorylate its substrates.
Figure made by the candidate using BioRender.

1.2.3 mTORC1 and mTORC2 have distinct, yet connected biological functions

- *mTORC1 promotes anabolism and inhibits catabolism to maintain cell growth and proliferation*

mTORC1 and mTORC2 have different, yet connected functions enabling cells to adapt to changes in their environment. mTORC1 plays a key role in maintaining protein translation and achieves this through activation of downstream targets such as p70 S6 Kinases 1 and 2 (S6K1/2) and the eukaryotic initiation factor (eIF4E) which are involved in mRNA translation (Burnett et al. 1998; Von Manteuffel et al. 1997). Studies have shown mTORC1 and S6K1 control protein translation through associating and disassociating with the eukaryotic initiation factor 3 (eIF3) translation initiation complex. When mTORC1 is inactive (for instance due to low amino acids), S6K1 associates with the eIF3 complex whilst the mTORC1 complex does not. Activation of mTORC1 by amino acids/growth factors leads to its recruitment to the eIF3 complex and phosphorylation of S6K1. This promotes disassociation of S6K1 from the complex enabling it to phosphorylate the eukaryotic initiation factor 4B (eIF4B) and the 40S ribosomal protein S6, enabling their recruitment to the translation initiation complex at the 5' cap (Hay and Sonenberg 2004). At the same time, mTORC1 promotes translation by

phosphorylating and inhibiting the eIF4E-binding proteins (4E-BPs), which are inhibitors of the translation initiation factor eIF4E to promote 5'cap-dependent translation.

In addition to protein translation, mTORC1 is also involved in the synthesis of lipids; an essential component of cell membranes and organelles. Lipid biosynthesis is regulated by the sterol responsive element binding proteins (SREBPs), a transcription factor family that promotes the expression of genes involved in synthesising fatty acids and cholesterol (Horton, Goldstein, and Brown 2002). mTORC1-dependent activation of AKT leads to nuclear translocation of SREBP and transcription of SREBP target genes in order to maintain cell growth and proliferation (Porstmann et al. 2008). At the same time, mTORC1 can regulate SREBP transcriptional activity by inhibiting nuclear entry of lipin 1, a phosphatidic acid phosphatase that promotes nuclear remodelling to dampen SREBP promoter activity (Peterson et al. 2011)

Furthermore, mTORC1 is able to regulate biosynthesis of nucleotides. One way is via S6K-dependent phosphorylation and activation of carbamoyl-phosphate synthetase 2, aspartate transcarbamoylase, dihydroorotase (CAD), an enzyme that catalyses the first three steps of de novo pyrimidine synthesis (Ben-Sahra et al. 2013). Additionally, mTORC1 phosphorylates activation transcription factor 4 (ATF4), promoting transcription of its target genes including methylenetetrahydrofolate dehydrogenase 2 (MTHFD2), thereby enabling production of purine via enhancing the mitochondrial tetrahydrofolate (mTHF) cycle (Ben-Sahra et al. 2016).

mTORC1 also plays an important role in glucose metabolism. For instance, hyperactivation of mTORC1 activity leads to increased levels of hypoxia-induced factor 1 subunit α (HIF1α), a transcription factor that drives the expression of several glycolytic enzymes, promoting a shift from oxidative phosphorylation towards aerobic glycolysis referred to as the Warburg effect, allowing cells to generate biosynthetic intermediates (Otto Warburg, Wind, and Negelein 1927). This occurs via both mTORC1-dependent activation of STAT3-mediated HIF1α transcription, as well as promotion of translation of HIF1α mRNA through 4E-BP1/eIF4E, S6K1 as mentioned previously (Dodd et al. 2015).

In addition to promoting anabolism (the production of biosynthetic intermediates required for cellular proliferation and growth), mTORC1 inhibits catabolism; namely by inhibiting autophagy and lysosomal biogenesis. There are three main types of autophagy: macro-autophagy, micro-autophagy, and chaperone-mediated autophagy, all of which promote proteolytic degradation of cytosolic components through lysosomes (Glick, Barth, and Macleod 2010). This process of 'self-catabolism' allows cells to adapt to survive stress, such as nutrient deprivation as well as promoting clearance of misfolded proteins or damaged organelles. Through this process, cells are able to recycle cellular components (Klionsky and

Emr 2000). One of the ways mTORC1 inhibits autophagy is through inhibition of Unc-51-like kinase 1 (ULK1), a serine/threonine kinase homologous to ATG13 in yeast, required for the formation of autophagosomes (Turco, Fracchiolla, and Martens 2020). Under nutrient-rich conditions, mTORC1 is active and phosphorylates ULK1 on Ser757, preventing it from interacting with AMPK. However, in response to amino acid starvation, mTORC1 is inactive, allowing AMPK to interact with and phosphorylate ULK1, promoting its activity and inducing autophagosome production (Zhao and Klionsky 2011). Additionally, mTORC1 inhibits the activity of the microphthalmia/transcription factor E (MiT/TFE) family of transcription factors. This family comprises four proteins: MITF, TFEB, TFE3, and TFEC that can form homo and heterodimers with one another (Hemesath et al. 1994). TFEB is a master regulator of lysosomal biogenesis, promoting the expression of many lysosomal genes, including hydrolases, lysosomal membrane permeases, and lysosome-associated proteins required for lysosomal function (Sardiello et al. 2009). When mTORC1 is active, it phosphorylates TFEB on numerous sites resulting in its cytoplasmic retention, preventing its transcriptional activity (Martina et al. 2012). In addition to inhibiting autophagy, mTORC1 also inhibits proteasome assembly through inhibition of Mpk1/ERK5 (Rousseau and Bertolotti 2016).

- *mTORC2 promotes cell survival, glycolysis, glucose uptake and changes in cytoskeletal dynamics*

mTORC2 promotes cell proliferation and survival in response to environmental stresses. One of the main effectors implicated in mTORC2 signalling is AKT. As mentioned previously, in response to mTORC2 activation AKT is fully phosphorylated by mTORC2 at Ser473, after it is phosphorylated by PI3K-activated PDK1 on Thr308 (Sarbassov DD et al. 2005). AKT has numerous substrates involved in glycolysis. For instance, AKT phosphorylates hexokinase (HK) leading to increased mitochondrial binding and mitochondrial protection which also contributes to inhibition of mTORC1 (Roberts and Miyamoto 2015). Furthermore, AKT phosphorylates and stabilises phosphofructokinase (PFK) through preventing binding of TRIM21 E3 ligase and subsequent proteasomal degradation (Lee et al. 2017b). Stabilisation of both HK and PFK promote aerobic glycolysis, enabling cells to survive glucose deprivation.

Another substrate of mTORC2-activated AKT is glycogen synthase kinase (GSK3β), a kinase which phosphorylates and inhibits the rate-limiting enzyme of glycogen synthesis (Ali, Hoeflich, and Woodgett 2001) but also can regulate several components of the mTORC1/mTORC2 signalling network, including TSC2, RICTOR, PTEN and AKT as part of a feedback loop. AKT phosphorylates Ser9 of GSK3β, inhibiting its activity to promote glycolysis (Cross et al. 1995). Furthermore, phosphorylation of TSC2 by AKT leads to activation of

mTORC1 to promote cell survival (Inoki et al. 2002a). Additionally, AKT inhibits a sub-family of the forkhead box family (FOXO) to promote cell survival and autophagy (Zhang et al. 2011)., mTORC2 also phosphorylates and activates the serum and glucocorticoid-induced protein kinase 1 (SGK1) to regulate ion transport, hormone release, inflammation, cell proliferation and apoptosis (Lang et al. 2010).

mTORC2 plays a role in lipid biogenesis through modulation of SREBP1 via GSK3β. When mTORC2 is inactive, GSK3β phosphorylates SREBP1 targeting it for proteasomal degradation by the E3 ubiquitin ligase, FBXW7 (Koo et al. 2015). Upon glucose deprivation for instance, mTORC2 becomes activated and inhibits GSK3β, and thus stabilises SREBP1, promoting fatty acid synthesis and cholesterol production (Horton, Goldstein, and Brown 2002).

Upon glutamine depletion, mTORC2 is activated and promotes expression and nuclear accumulation of the glutamine:fructose-6-phosphate amidotransferase 1 (GFAT1) to promote biosynthesis of hexosamine (Moloughney et al. 2016). Although mTORC1 can sense changes in glutamine levels, mTORC2 responds to declining levels of glutamine catabolites to restore metabolic homeostasis.

mTORC2 activity has also been implicated in controlling cytoskeleton dynamics (Sarbassov et al. 2004). For example, when mTORC2 signalling is depleted, bone marrow-derived mesenchymal cells are unable to undergo cytoskeletal re-organisation and lineage selection demonstrating the importance of mTORC2 in mediating cytoskeletal dynamics (Sen et al. 2014). Moreover, mTORC2 can directly phosphorylate several members of the protein kinase C (PKC) family (Baffi et al. 2021). The PKC proteins regulate cytoskeleton arrangement, cell shape and migration (Larsson 2006).

Overall, although mTORC1 and mTORC2 have distinct cellular functions, both are important in responding to changes in the external environment and ultimately enable cell survival. Regulation of mTORC1 and mTORC2, along with their downstream targets are shown below in:

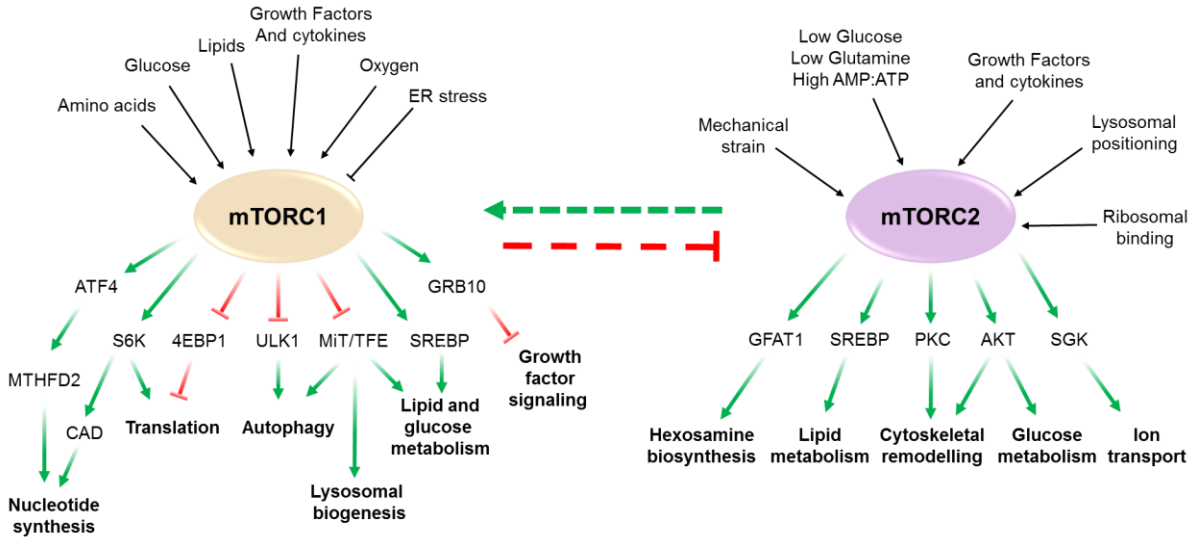

Figure 3 Summary of how mTORC1 and mTORC2 are regulated and their biological functions. mTORC1 and mTORC1 have distinct yet connected biological functions to enable cell survival and proliferation. They are regulated by different physiological stimuli, such as growth factors, cytokines and nutrients. The green arrows indicate positive regulation, whereas the red arrows with blunt ends indicate inhibitory regulation. *Figure made by the candidate using PowerPoint.*

1.3 mTOR activity is hijacked in cancer

Given the importance of mTORC1 and mTORC2 in not only promoting cell growth and proliferation, but allowing cells to adapt to changes in their environment, it is unsurprising that mTOR activity is dysregulated in many diseases. The pathological relevance of promoting mTOR activity is particularly clear in cancer, with over 70% of cancers exhibiting hyperactivation of mTOR activity (Forbes et al. 2011).

There are three main ways through which cancers can hijack mTOR activity to promote cell survival and tumorigenesis. The most obvious is through acquiring mutations in mTOR itself or mutating the regulatory subunits of the mTORC1 and mTORC2 complexes. mTOR itself is mutated in around 11% of all cancers, several mutations lead to constitutive activation of mTORC1 to promote proliferation (Grabiner et al. 2014). For instance, several point mutations in mTOR and Rheb have been identified in patients with clear cell renal cell carcinoma. These included hyperactivating mutations in the FAT (FRAP-ATM-TRAP) domain of mTOR, leading to increased mTORC1 and mTORC2 activity, alongside mutations that reduced the binding of the negative regulator of mTOR, PRAS40. Furthermore, the recurrent Rheb mutation found in patients with renal cell carcinoma is resistant to the GAP activity of TSC2 (Ghosh et al. 2015)

Importantly, cancer cells often acquire mutations in upstream genes that mediate mTORC1 and mTORC2 activity, either by acquiring loss-of-function mutations in repressors or by acquiring gain-of-function mutations in activators. For example, mutations leading to hyperactivation of the PI3K pathway which is upstream of both mTORC1 and mTORC2 are

observed. For instance, gain-of-function mutations in the PIK3CA gene encoding the p110α catalytic subunit (Samuels et al. 2004) enhance PI3K signalling and are found in 15% of metastatic colorectal cancer patients (Zhang, Roberts, and Shivdasani 2011). Whereas loss-of-function mutations in PTEN, a negative regulator of PI3K signalling are found in 20-40% of colorectal cancer patients (Roock et al. 2011). Loss of PTEN function is also observed in myeloma (Hyun et al. 2000), breast cancer (deGraffenried et al. 2004), endometrial cancer (Milam et al. 2007), and prostate cancer (Jamaspishvili et al. 2018), making these cancers particularly sensitive to PI3K inhibition.

Furthermore, loss-of-function mutations in TSC1 and TSC2 which form the TSC complex and negatively regulate mTORC1 activity are found in around 15% of urothelial cancers, as well as exhibiting gain-of-functions mutations in the PIK3CA and PI3KR1 gene (Sjödahl et al. 2011). Additionally, loss-of-function mutations in TS1 and TSC2 lead to the development of tuberous sclerosis (Rosset, Netto, and Ashton-Prolla 2017), an autosomal dominant neurocutaneous and progressive disorder, characterised by the occurrence of numerous tumours in different organs (Northrup, Koenig, and Pearson 1999). Alongside gain-of-function mutations, cancers often exhibit copy number amplifications in tumour promoters such as the PI3KCA gene. For example, small cell lung carcinomas exhibit mutations in the PI3KCA as well as copy number amplifications (Yamamoto et al. 2008).

Alongside the PI3K pathway, the RAS/RAF/MAPK signalling pathway acts upstream of mTOR and is also often mutated in cancers (Santarpia, Lippman, and El-Naggar 2012). Gain-of-function mutations in members of the RAS family (HRAS, KRAS, and NRAS) comprise up to 30% of all human cancers (Shields et al. 2000). Furthermore, mutations in BRAF such as the V600E mutation have been identified in melanoma, colorectal cancer, multiple myeloma, and other types of cancers (Śmiech et al. 2020). Notably, 50% of melanomas harbour activating BRAF mutations, of which 90% are the V600E mutation (Ascierto et al. 2012). The BRAF V600E mutation results in constitutive activation of ERK, leading to uncoupling of LKB1 to AMPK, a negative regulator of mTORC1 (Esteve-Puig et al. 2009). Additionally, LKB1 is mutated in Peutz-Jeghers Syndrome and prevents AMPK-mediated inhibition of mTORC1 in response to energetic stress (Karuman et al. 2001).

Furthermore, components of the GATOR1 complex which acts as a GAP for the Rag GTPases are frequently mutated in glioblastoma and ovarian cancer (Bar-Peled et al. 2013) and results in highly active mTORC1, even in the absence of amino acids (Muller et al. 2024). Additionally, gain-of-function mutations in mTORC1 activators such as RagC are enriched in patients with follicular lymphoma (17%), an incurable B-cell lymphoma. Furthermore, more than half of the mutations co-occurred with mutations in ATP6V1B2 and ATP6AP1, components of the

lysosomal v-ATPase involved in mTORC1 sensing amino acids (Okosun et al. 2016). These mutations co-occurring not only increases recruitment of mTORC1 to the lysosomal surface, but also renders mTORC1 signaling resistant to amino acid deprivation.

Due to the role of mTOR in cancer, mTOR is an attractive therapeutic target for anti-cancer treatments. The first generation of rapamycin and its analogs (rapalogs) only inhibited mTORC1 and not mTORC2 which is likely why they have had little clinical success. This is because mTORC2 is also important in cancer cell survival, especially in the context of cancers that are dependent on PI3K/AKT hyperactivation. For instance, RICTOR levels and mTORC2 activity are upregulated in gliomas which leads to hyperactivation of AKT to promote cell growth and motility (Masri et al. 2007). Furthermore, knockdown of the mTORC2 component RICTOR reduces proliferation and induces apoptosis in colorectal cancer cell lines (Gulhati et al. 2009). mTORC2 also promotes cancer cell migration, including downstream from human epidermal growth factor 2 (HER2) in breast cancer cells (Collins et al. 2023) and inhibition of mTORC2 can prevent migration and induce apoptosis in breast cancer (Li et al. 2012).

In addition to the important roles mTORC2 plays in cancer, inhibition of mTORC1 leads to inhibition of mTOR-dependent phosphorylation of the insulin receptor substrate-1(IRS-1) which promotes it for proteasomal degradation (Haruta et al. 2000). This triggers activation of insulin-like growth factor-I (IGF-I) signaling and downstream phosphatidylinositol3-kinase (PI3K)/AKT (O'reilly et al. 2006), which is referred to as the IRS1 feedback loop (Shi et al. 2005). The IRS1 feedback loop is one of the ways in which cells become resistant to mTORC1 inhibition.

Inhibition of mTORC1 may not always be beneficial for treating cancer due mTORC1 inhibiting autophagy. The role of autophagy in cancer is complex and context-dependent. Studies have shown that although autophagy suppresses cancer initiation, it can promote tumorigenesis, allowing cancer cells to survive despite poor vascularisation. For instance, in pancreatic adenocarcinoma (PDAC), high levels of MiT/TFE-mediated autophagy are required for pathogenesis (Perera et al. 2015). Therefore, inhibition of mTORC1 in PDAC would not be beneficial. Furthermore, mTORC1 inhibition has been shown to facilitate micropinocytosis (a process where cells engulf extracellular nutrients), enabling tumours with poor vascularisation to grow (Palm et al. 2015).

In summary, although the mTORC1 and mTORC2 complexes are important mediators of tumorigenesis, targeting them as a therapeutic strategy has been more challenging than anticipated. Currently, the idea of a combinatorial approach whereby not only mTORC1 but also mTORC2 and PI3K/AKT activity is inhibited may circumvent the issues associated with inhibited mTORC1 alone. However, another idea would be to target the key downstream

effectors of mTORC1 and mTORC2 that mediate cancer cell initiation and tumorigeneses. For example, the MiT/TFE family of transcription factors: MITF, TFEB and TFE3 have been implicated in numerous diseases, including several cancers. Therefore, there is a clinical need to identify modulators of the MiT/TFE family in the context of cancer but also in other diseases.

1.4 Introducing the MiT/TFE family of transcription factors

MITF is a well-defined lineage specific transcription factor crucial for melanocyte differentiation and development. In 1942, Hertwig observed that the offspring of X-ray irradiated mice had abnormally small eyes and were not pigmented (Hertwig 1942) and named the mutant gene locus *m*, later expanded to *mi* and eventually to *Mitf.* Furthermore, various *Mitf* mutant mice exhibited hearing loss, due to a lack of developed melanocytes in the inner ear as well as defective osteoclasts and mast cells. In the 1990s, Hodgkinson et al. used transgenic insertional mutagenesis and identified *Mitf* as the gene responsible for the phenotypes observed (Hodgkinson et al. 1993). Mutations in the human homologue, MITF have been linked to Waardenburg Syndrome type IIA; an autosomal dominant syndrome resulting in hearing loss and pigmentary disturbances (Hughes et al. 1994; Tassabehjil, Newton, and Read 1994). Later, molecular studies revealed that MITF functions as a transcription factor and is able to directly bind to and regulate the expression of pigmentation genes (Hoek et al. 2008). MITF promotes melanocyte differentiation through regulation of Tyrosinase (TYR) and Dopachrome Tautomerase (DCT), genes involved in melanin synthesis or melanogenesis (Yasumoto,' Kouji Yokoyama,' et al. 1994), as well as genes involved in melanosome biogenesis, such as Premelanosome Protein (PMEL) and Melan-A (MLANA) (Du et al. 2003).

The MITF gene has a split promoter design, resulting in several isoforms of MITF with distinct promoters and 5' exons (Hershey and Fisher 2005). The expression patterns of these isoforms range from widely expressed to tissue-specific. For instance, the m-MITF isoform is almost exclusively expressed in melanocytes and melanoma (Maruotti et al. 2012). Furthermore, loss-of-function mutations in the bHLH domain not only affect melanocyte development, but also osteoclasts, mast cells and retinal epithelial cells (Steingrimsson et al. 1994). More recently, MITF has been implicated in cardiomyocytes; mediating cardiac growth and hypertrophy (Tshori et al. 2006) as well as regulation of pancreatic β cell function (Mazur et al. 2013). Taken together, MITF has a diverse array of cell-type specific functions.

MITF also plays a key role in determining phenotypic identity of melanoma cells. For instance, cells expressing low levels of MITF exhibit an invasive and stem-like phenotype, cells with intermediate levels of MITF are proliferative and thus sensitive to anti-cancer drugs, whereas melanoma cells expressing high levels of MITF are more differentiated and G1 arrested (Hoek

and Goding 2010b). This exemplifies that not only the presence, but levels of MITF are important for determining cell behaviour in melanoma.

Unlike MITF, TFEB and TFE3 are more widely expressed. TFEB was discovered in the 1990s by screening a bacteriophage expression library with a probe containing the binding site for adenovirus major late promoter transcription factor (Carr and Sharp 1990). TFE3 was first isolated from cDNA in the 1990s and identified as activating transcription through the immunoglobulin enhancer μE3 motif (Beckmann, Su, and Kadesch 1990).

In 2009, a new role for the MiT/TFE family emerged, as TFEB and TFE3 were shown to be able to bind to CLEAR motifs (Coordinated Lysosomal Expression and Regulation), a 10 base pair sequence (GTCACGTGAC) found in the promoter region of lysosomal genes suggesting their involvement in promoting lysosomal biogenesis (Sardiello et al. 2009). These genes include hydrolases, lysosomal membrane permeases, and lysosome-associated proteins (Palmieri et al. 2011).

The microphthalmia family (MITF, TFEB, TFE3 and TFEC) of transcription factors are emerging to be global regulators of cell survival. They all share structural domains such as a basic helix-loop-helix (bHLH) leucine zipper (LZ) motif and an identical basic region required for DNA binding (Beckmann, Su, and Kadesch 1990; Sato et al. 1997). Due to the MiT/TFE family all sharing a basic-helix-loop-helix-leucine zipper (bHLH-LZ) domain, they can form homodimers and heterodimers with one another. In addition, TFEB, TFE3 and MITF also contain a conserved transactivation domain (TAD), essential for their transcriptional activation. In comparison, TFEC, the most divergent family member, lacks this domain and has been shown to form heterodimers with TFE3 to inhibit, rather than activate transcription (Zhao et al. 1993).

MITF, TFEB and TFE3 share significant similarity in their N-terminal and C-terminal regions, which are involved in regulation of protein localisation and stability. Additionally, they are subject to a variety of post-translational modifications such as phosphorylation, acetylation, SUMOylation, oxidation and ubiquitination that are also conserved between family members (Puertollano et al. 2018; Goding and Arnheiter 2019). Notably, some key residues involved in their regulation are conserved across species, suggesting that their regulation is evolutionarily conserved (Settembre et al. 2011;Martina et al. 2012).

Like other transcription factors with a bHLH domain, they are able to bind to CANNTG E-boxes in the promoters and enhancers of their transcriptional targets. For MITF, an additional T residue at the 5' end of a CATGTG or CACGTG E-box is required for high-affinity DNA binding (Aksan and Goding 1998). Furthermore, the TCATGTG motif is highly conserved in the promoters of melanocytic-specific genes, and is referred to as an M-box (Aksan and Goding

1998). A schematic demonstrating the structural similarities and differences in the MiT/TFE family of transcription factors are highlighted in **Figure 4.**

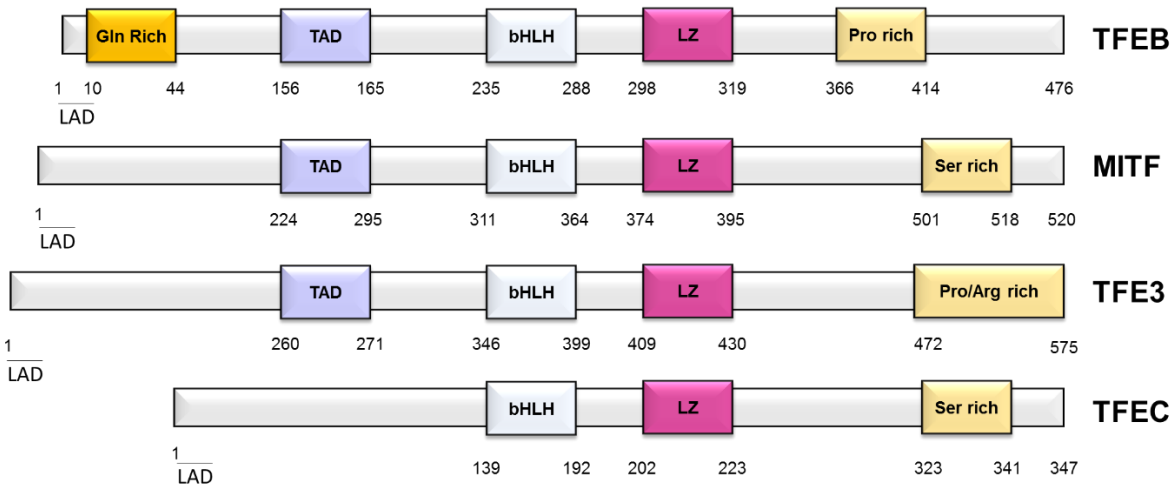

Figure 4 The protein structure of the MiT/TFE family of transcription factors
Schematic representation of TFEB, MITF, TFE3 and TFEC proteins, highlighting similarities and differences in their structures. TFEB, MITF, TFE3 and TFEC all share a Lysosomal attachment domain (LAD) at their C-termini, allowing for lysosomal recruitment. TFEB, MITF and TFE3, unlike TFEC, all share transactivation domain (TAD); required for their transcriptional activity, a basic helix-loop-helix domain (bHLH); allowing homo- and heterodimerisation and a Leucine Zipper domain (LZ); required for DNA binding. TFEC, the most divergent member of the family lacks a TAD and is thought to inhibit rather than promote transcription of its targets. TFEB, MITF and TFE3 all share conserved C- and N-terminal sequences, important in their regulation and stability. Notably, MITF has a split promoter design, allowing the generation of multiple, biologically distinct proteins, all with differing C-termini. The melanocytic specific m-MITF lacks the lysosomal attachment domain (LAD), also referred to as the Rag binding domain, allowing binding of MITF to the lysosome. The numbers correspond to the amino acid position of each protein above. *Figure made by the candidate using PowerPoint.*

1.5 Regulation of TFEB

TFEB is primarily regulated via post-translational modifications that alter their subcellular localisation. In order to be transcriptionally active, they have to be imported into the nucleus. To ensure cell survival in response to nutrient deprivation, cells have to first sense nutrient availability. As previously described, mTORC1 is the main sensor of amino acids, and when amino acids are abundant, it is localised to the surface of the lysosome. This localisation is important for maintaining mTORC1 activity, allowing cells to promote anabolic processes required for cell proliferation and growth, such as protein translation and lipid synthesis. At the same time, mTORC1 prevents catabolic processes such as lysosomal biogenesis and autophagy. One of the main ways by which mTORC1 prevents catabolism is through inhibition of TFEB and TFE3. When amino acids are abundant, mTORC1 is active and prevents nuclear entry of TFEB and TFE3. In fully-fed cells, mTORC1 and TFEB/3 are recruited to the lysosomal surface by the Rag GTPases (Sancak et al. 2008; Martina and Puertollano 2013). Importantly,

the mitogen-activated protein kinase kinase kinase kinase 3 (MAP4K3) phosphorylates TFEB on Ser3, a phosphorylation required for its interaction with the Rags (Hsu et al. 2018). Inhibition of MAP4K3 prevents recruitment of the TFEB to the lysosomal surface, allowing nuclear entry despite mTORC1 activity (Hsu et al. 2018).

After recruitment of mTORC1 and TFEB to the surface of the lysosome, mTORC1 directly phosphorylates multiple sites. For instance, phosphorylation of Ser211 on TFEB enables binding of the cytoplasmic chaperone 14-3-3, sequestering TFEB in the cytoplasm (Martina et al. 2012). Later it was found mTORC1-dependent phosphorylation of TFEB on Ser122 is also required for cytoplasmic retention. Using site-directed mutagenesis, whereby the residue was mutated from a serine to an aspartic acid, (S122D), nuclear entry of TFEB was blocked, despite mTORC1 inhibition. However, mutating the serine to an alanine (S122A) could not induce nuclear translocation of TFEB, indicating that nuclear entry of TFEB is regulated by multiple phosphorylation events (Vega-Rubin-de-Celis et al. 2017).

Conversely, when cells are starved of amino acids, inactivation of MAP4K3 prevents recruitment of TFEB to the lysosomal surface through prevention of de novo phosphorylation of Ser3. Inactivation of mTORC1 prevents de novo phosphorylation of TFEB at the surface of the lysosome on Ser211. At the same time, amino acid deprivation leads to Ca^{2+} release from lysosomes and activation of calcineurin which promotes active dephosphorylation of TFEB (Medina et al. 2015). Others have demonstrated that Protein Phosphatase 2A, activated by oxidative stress can actively dephosphorylate TFEB on specific residues Ser109, Ser114, Ser122 and Ser211, but not on Ser142 or Ser138. Altogether, these events lead to the nuclear entry of TFEB (Martina and Puertollano 2018).

mTORC1 is not the only kinase that regulates the subcellular localisation of the TFEB. For instance, AKT has been shown to phosphorylate TFEB on Ser467, preventing nuclear entry and inhibition of AKT using the pharmacological inhibitor Trehalose, induces nuclear accumulation of TFEB (Palmieri et al. 2017). Furthermore, mTORC1 and ERK2 can phosphorylate TFEB on Ser142. Site-directed mutagenesis revealed mutating Ser142 to an alanine (Ser142A) prevented cytoplasmic retention (Settembre et al. 2011). In addition, PKC activation was reported to lead to inhibition of GSK3β which can phosphorylate TFEB on Ser134 and Ser138 leading to nuclear localisation (Li et al. 2016).

Phosphorylation events can also promote TFEB activity. For example, in osteoclasts when PKCβ is activated in response to cytokine treatment (RANKL) it can phosphorylate Ser461, Ser466 and Ser468 in the c-terminus of TFEB, stabilising TFEB and promoting transcriptional activity (Ferron et al. 2013). Furthermore, AMPK-dependent phosphorylation of TFEB on Ser466, Ser467 and Ser469 is required for transcriptional activity (Paquette et al. 2021).

Due to the structural similarities of the MiT/TFE family of transcription factors, MITF and TFE3 activity is controlled in a similar fashion. However, due to the structure of the MITF gene, featuring numerous alternative promoters in exon 1, there are several isoforms of MITF that generate structurally and biologically distinct proteins (Hershey and Fisher 2005). All MITF isoforms, except for the m-MITF isoform contain the domain encoded by exon 1B1b which is required for lysosomal recruitment (Lu et al. 2010). Therefore, the m-MITF isoform generally exhibits nuclear localisation due to lacking the n-terminal Rag binding domain (Takebayashi et al. 1996) and its subcellular localisation is regulated mainly through its nuclear localisation signal and nuclear transport machinery. The regulation of TFEB subcellular localisation is demonstrated in **Figure 5**.

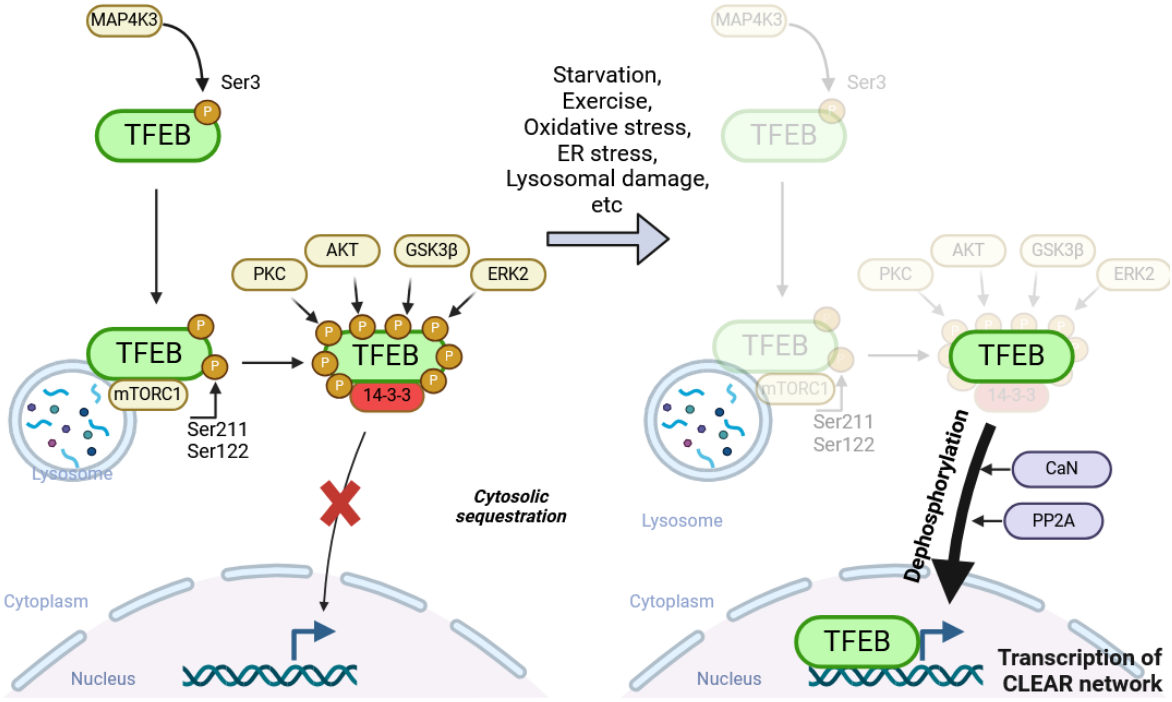

Figure 5 Current model demonstrating regulation of TFEB subcellular localisation. Under nutrient rich conditions, TFEB is firstly phosphorylated by MAP4K3 on Serine 3, promoting its lysosomal recruitment. At the surface of the lysosome, TFEB is phosphorylated by mTORC1 on Serine 122 and Serine 211. Phosphorylation on Serine 211 is required for cytoplasmic sequestration by the cytoplasmic chaperone protein 14-3-3. In addition, numerous kinases have also been demonstrated to play a role in regulating TFEB activity, such as AKT, PKC, GSK3β and ERK2, although these phosphorylation marks are less well characterised. Conversely, under starvation/stress conditions, MAP4K3 and/or mTORC1 are inactivated, preventing de novo phosphorylation of TFEB. At the same time, TFEB is actively dephosphorylated by calcineurin (CaN) and/or protein phosphatase 2A (PP2A) allowing rapid re-localisation of TFEB to the nucleus to promote TFEB-dependent gene transcription. Orange circles with letter 'p' represent phosphorylation marks. *Figure made by the candidate using BioRender.*

1.6 Physiological functions of TFEB

- *Lysosomal biogenesis and autophagy*

In 2009, TFEB and TFE3 were shown to bind to CLEAR motifs (Coordinated Lysosomal Expression and Regulation), a 10 base pair sequence (GTCACGTGAC) found in the promoter region of lysosomal genes suggesting their involvement in promoting lysosomal biogenesis (Sardiello et al. 2009). This finding was further corroborated by genome-wide chromatin immunoprecipitation followed by sequencing (ChIP-seq), demonstrating the ability of TFEB to directly bind to CLEAR elements (Palmieri et al. 2011b). As previously mentioned, under nutrient-rich conditions, TFEB co-localises with mTORC1 on the lysosomal membrane, allowing mTORC1 to phosphorylate and inhibit the nuclear translocation of TFEB. Conversely, pharmacological inhibition of mTORC1 as well as starvation and lysosomal disruption lead to nuclear translocation of TFEB and transcription of lysosomal and autophagic genes (Settembre et al. 2012).

Overexpression of TFEB induces transcriptional activation of genes involved in lysosomal biogenesis and function, including several subunits of the v-ATPase, lysosomal membrane proteins, lysosomal hydrolases and increased the number of lysosomes (Sardiello et al. 2009). Additionally, Martina et al. identified transcription factor E3 (TFE3) as another regulator of lysosomal homeostasis. In response to amino acid deprivation, TFE3 also translocates to the nucleus and induces expression of genes involved in autophagy and lysosomal biogenesis (Martina et al. 2014).

Not only can TFEB increase the number of lysosomes, but it can change their distribution. For instance, overexpression of TFEB leads to redistribution of the lysosomes to the surface of the plasma membrane and promotes fusion. TFEB and TFE3 mediate exocytosis by raising intracellular Ca^{2+} levels through increasing the expression of the lysosomal calcium channel Mucolipin (MCOLN1) (Medina et al. 2011). In osteoclasts, stimulation with RANKL activates PKCβ which in turn, stabilises TFEB through phosphorylation events as previously mentioned. This is important in osteoclasts as they require high levels of lysosomal exocytosis in order to release proteases required for bone resorption (Ferron et al. 2013).

MITF regulates the biogenesis of melanosomes, a melanocyte-specific lysosome-related organelle (Lowings, Yavuzer, and Goding 1992). Additionally, MITF expression strongly correlates with a subset of lysosomal genes containing CLEAR elements in their promoters as well as an increase in vesicular structures, and increased expression of late endosomal proteins, such as Rab7, LAMP1, and CD63 (Ploper et al. 2015). Further corroborating these findings, MITF has been shown to transcriptionally regulate the lysosomal v-ATPase in drosophila (Bouché et al. 2016) and human melanocytes (Zhang et al. 2015). Therefore, the

MITF/TFE family are considered to be the master regulators of lysosomal biogenesis and autophagy.

- *Lipid metabolism*

TFEB not only regulates autophagy and lysosomal biogenesis in response to amino acid deprivation but also is involved in the catabolism of lipids. One study using mice, demonstrated that overexpression of TFEB induces the expression of many genes required for lipid uptake, mitochondria oxidative metabolism and peroxisomes, and is associated with downregulation of genes involved in lipid biosynthesis (Settembre et al. 2013). For example, TFEB overexpression increased transcription of the peroxisome proliferator-activated receptor γ coactivator 1 α (PGC1α), a key mediator of liver lipid metabolism (Puigserver and Spiegelman 2003). They also demonstrated that TFEB could directly bind to two CLEAR box motifs in the promoter of PGC1α, in a starvation-dependent manner, demonstrating PGC1α was a direct transcriptional target of TFEB. In the absence of PGC1α, TFEB-mediated transcription of genes involved in lipid catabolism was impaired, demonstrating that PGC1α is not only a transcriptional target of TFEB but also mediates TFEB transcriptional activity in the liver as part of a positive feedback loop (Settembre et al. 2013). In addition, during starvation PGC1α regulates lipid metabolism in the liver via the downstream nuclear receptor peroxisome proliferator activated receptor α (PPARα) suggesting that PGC1α may mediate TFEB function by controlling the activity of PPARα. In wildtype mice, starvation caused induction of the PPARα target genes but could not in TFEB knockout mice, suggesting TFEB is essential for PPARα activation by starvation. Additionally, in the absence of PPARα, starvation could not induce the majority (74%) of genes that could be induced by TFEB overexpression. Overall, this study highlighted the role of TFEB in mediating lipid catabolism in response to nutrient starvation (Settembre et al. 2013).

Notably, mTORC1 can also sense lipid levels. The lysosome is important for acquiring and catabolising dietary cholesterol. Receptor-mediated endocytosis allows cells to uptake cholesterol and fatty acids which are then broken down in the lysosomal lumen (Goldstein and Brown 2015). The sterol transport system composed of the Niemann-Pick C1 (NPC1) and NPC2 proteins localises specifically at the late endosome or lysosome where it can bind cholesterol and mediate its export (Kwon et al. 2009). When cholesterol is abundant within the lysosomal lumen, SLC38A9 activates mTORC1 independently of arginine (Castellano et al. 2017). The NPC1 protein, which regulates cholesterol export from the lysosome, forms a complex with the transmembrane lysosomal protein SLC38A9 to inhibit mTORC1 function

(Castellano et al. 2017). Inhibition of mTORC1 leads to prevention of de novo phosphorylation of TFEB, allowing its nuclear entry and activity.

- *Glucose metabolism and mitochondrial biogenesis*

In muscle cells, TFEB is involved in controlling metabolic flexibility during exercise, independently of its effects on PGC1α. In response to physical activity, TFEB translocates to the myonuclei (nuclei found in skeletal muscle cells which are multinucleated) and upregulates genes involved in promoting glucose uptake, such as glucose transporters and glycolytic enzymes as well as genes involved in mitochondrial biogenesis, fatty acid oxidation and oxidative phosphorylation (Mansueto et al. 2017). Nuclear translocation of TFEB in response to exercise is thought to be in part due to calcium influx activating the protein phosphatase calcineurin which as previously mentioned, actively dephosphorylates TFEB (Medina et al. 2015; Gehlert, Bloch, and Suhr 2015). Through the generation of mice overexpressing *Tcfeb*, (the mouse homologue of human TFEB), or genetic ablation of *Tcfeb,* Mansueto et al. identified several gene categories that were regulated by TFEB in skeletal muscle. They demonstrated that genes related to cellular metabolism including lipid and glucose homeostasis, were upregulated in mice overexpressing TFEB and downregulated in TFEB knockout mice (Mansueto et al. 2017).

Furthermore, they found TFEB directly promoted the expression of nuclear respiratory factors 2 (NRF2) as well as its downstream genes including the mitochondrial transcription factor A (TFAM). In addition, TFEB overexpression increased mitochondrial number and size, whilst TFEB depletion led to dysfunctional mitochondria. As the tricarboxylic acid cycle (TCA) and β-oxidation of lipids take place at mitochondria (Y. Wang et al. 2019), TFEB therefore mediates energy metabolism. Overall, they demonstrated that TFEB regulates mitochondrial biogenesis and function as well as glucose homeostasis in skeletal muscle. This response ultimately allows muscle cells to optimise the usage of mitochondrial substrates and enhance ATP production and thus energy capacity (Mansueto et al. 2017)

- *Endoplasmic reticulum (ER) stress*

Endoplasmic reticulum (ER) stress is caused by the accumulation of misfolded proteins in the ER. Cells sense the accumulation of misfolded proteins and in doing so, activate the unfolded protein response (UPR) (Harding et al. 2003). It has been previously demonstrated that upon ER stress, TFEB and TFE3 translocate to the nucleus and activate not only genes involved in promoting autophagy and lysosomal biogenesis, but also genes involved in mediating the

stress response and apoptosis (Martina et al. 2016). Martina et al. demonstrated that TFEB and TFE3 translocate to the nucleus upon treatment with ER stressors independently of mTORC1 but instead, dependent on protein kinase R (PKR)-like endoplasmic reticulum kinase (PERK) and calcineurin (José A Martina et al. 2016). They found upon induction of ER stress, TFEB and TFE3 induced expression of activating transcription factor 4 (ATF4); a master regulator of the integrated stress response (Di Wu and Liang 2024). ATF4 promotes cell survival by upregulating genes required for autophagy, redox homeostasis and amino acid import and synthesis (Harding et al. 2003). Furthermore, under prolonged ER stress, TFEB and TFE3 contributed to cell death (José A Martina et al. 2016). Overall, this work demonstrated that TFEB and TFE3 not only respond to nutrient deprivation but also allows cells to sense and respond to different types of environmental stresses.

- *Innate and adaptive immune responses*

TFEB also plays a role in mediating immune responses in macrophages and other cells of the innate immune system in response to exposure to pathogens (Pastore et al. 2016). Pastore et al demonstrated that upon treatment with lipopolysaccharides (LPS) TFEB and TFE3 translocate to the nucleus independently of mTORC1 activity. Through the use of ChIP-Seq, followed by ChIP-PCR, they identified direct targets of TFE3 including lysosomal and proinflammatory genes with CLEAR motifs in their promoters. They also demonstrated that upon treatment with LPS, TFEB and TFE3 double knockout macrophages had impaired cytokine induction compared to wildtype macrophages. Some of the cytokines that were significantly reduced included key mediators of the inflammatory response, such as colony-stimulating factor 2 (CSF2), interleukin 1β (IL1 β), IL2 and IL27, and genes involved in macrophage differentiation including colony-stimulating factor 1 (CSF1). In addition, genes involved in macrophage infiltration and migration to sites of inflammation, such as chemokine (C-C motif) ligand 2 (CCL2) which was reduced by 90% compared to wildtype, demonstrating TFEB and TFE3 are also important in the functioning of macrophages (Pastore et al. 2016).

In another study investigating phagocytosis in macrophages, they found upon treatment with aggregated IgG (AIgG) immune complexes, Fcγ receptor activation caused nuclear translocation of TFEB (Gray et al. 2016). Furthermore, silencing TFEB expression repressed Fcγ receptor-induced degradation and bacterial killing. Silencing of MCOLN1, a lysosomal Ca^{2+} channel, prevented phagosome completion and is required for TFEB nuclear translocation upon treatment with AIgG. (Gray et al. 2016).

TFEB is implicated in innate immunity in *Caenorhabditis elegans (C. elegans)* (Visvikis et al. 2014). Visvikis et al. demonstrated that after exposure to *Staphylococcus aureus*, HLH-30 (homologous to human TFEB) was activated and induced upregulation of close to 80% of

genes involved in host responses, including antimicrobial and autophagy genes that are essential for allowing host survival. Additionally, they showed that this response was conserved in murine macrophages where TFEB was activated upon *S. aureus* infection, and induced the expression of several proinflammatory cytokines and chemokines (Visvikis et al. 2014). More recently, studies have implicated AMP-activated protein kinase (AMPK) and its negative regulator Folliculin (FLCN) in acting upstream of TFEB and TFE3 in the innate immune response (El-Houjeiri et al. 2019a). In nematodes, they demonstrated that loss of FLCN or overexpression of AMPK confers pathogen resistance via activation of TFEB/3-dependent transcription of antimicrobial genes. Similarly, in mammalian cells, they observed loss of FLCN or pharmacological activation of AMPK induces TFEB/TFE3-dependent pro-inflammatory cytokine expression (El-Houjeiri et al. 2019). In murine macrophages, treatment with LPS reduced intracellular ATP levels, resulting in activation of AMPK and subsequent TFEB nuclear localisation. Overall, the fact that TFEB and TFE3 regulate innate immunity in nematodes as well as mammalian cells demonstrate these functions are evolutionarily conserved.

TFEB and TFE3 also mediate adaptive immunity. As previously mentioned, TFE3 was originally discovered in the 1990s and was identified as activating transcription through binding the immunoglobulin enhancer μE3 motif (Holger Beckmann, Su, and Kadesch 1990). Since then, TFEB and TFE3 have been shown to be essential for mediating thymus-dependent humoral immunity via $CD4^+$ T cell activation. Inactivation of both TFEB and TFE3 resulted in hyper-immunoglobulin M syndrome, caused by impaired expression of the CD40 ligand in $CD4^+$ T cells. Furthermore, TFEB and TFE3 could directly bind to the promoter of the CD40 ligand induce its expression (Huan et al. 2006).

In order for T cells to function, antigen presenting cells, such as dendritic cells, macrophages and B cells have to present antigens for recognition. Cytosolic antigens are digested by the proteasome and presented through the major histocompatibility complex (MHC) class I to $CD8^+$ T cells (Burgdorf and Kurts 2008). In comparison, exogenous antigens are engulfed through endocytosis and are broken down into peptides by lysosomal proteases in endolyososomes and presented to CD4+ T cells through MHC class II molecules (Burgdorf and Kurts 2008). It was originally believed that only cytosolic peptides derived by proteins synthesised by the cell itself could be presented on MHC class I to $CD8^+$ T cells. However, in some cases, exogenous antigens can be presented through MHC class I to $CD8^+$ T cells via a process called cross-presentation, a phenomenon originally thought to occur in transplant patients (Rock and Shen 2005). However, cross-presentation is the only way the immune system can detect and respond to viral infections or mutations that exclusively occur in

parenchymal cells rather than in bone marrow-derived antigen-presenting cells (Rock and Shen 2005).

Dendritic cells are the principal cells with the capacity to cross-present antigens (Gutiérrez-Martínez et al. 2015). The switch of antigen presentation from MHC class I to MHC class II has been found to be regulated by TFEB (Samie and Cresswell 2015), and TFEB expression was inhibited by the presentation of exogenous antigens by MHC class I whilst enhancing presentation by MHC II. In addition, TFEB activation was regulated during dendritic cell maturation and phagosomal acidification was impaired when TFEB expression was silenced. Overall, their data demonstrated TFEB acts as a molecular switch allowing dendritic cells to switch between presenting on MHC I or MHC II.

Taken together, TFEB and TFE3 mediate both innate and adaptive immunity, not only through their ability to induce autophagy, lysosomal biogenesis and the expression of cytokines but also through modulating antigen presentation switching in dendritic cells.

- *Cell fate and differentiation*

TFEB has also been implicated in osteoblast differentiation (Yoneshima et al. 2016). Osteoblasts are bone forming cells that produce large amounts of collagen type I and various bone matrix proteins. During osteoblast development, TFEB expression was upregulated, as well as genes involved in lysosomal biogenesis. TFEB silencing resulted in a marked reduction in osteoblast differentiation compared with control cells whilst TFEB overexpression enhanced osteoblastogenesis (Yoneshima et al. 2016). Knockdown of TFEB resulted in increased expression of activating transcription factor 4 (ATF4) and CCAAT/enhancer-binding protein homologous protein (CHOP), proteins already known to be essential for osteoblast differentiation (Yoneshima et al. 2016).

Furthermore, TFEB mediates myeloid cell differentiation (Yun et al. 2021). Yun et al. demonstrated that acute myeloid leukaemia (AML) and myeloid progenitor cell growth are dependent upon MYC-mediated inhibition of TFEB expression and function. Notably, TFEB functions as a tumour-suppressor in AML, whereby it promotes AML cell differentiation and death through inducing the expression of isocitrate dehydrogenase-1 (IDH1) and IDH2, resulting in global hydroxylation of 5-methycytosine. Overall, they concluded that epigenetic control by MYC-TFEB dictated myeloid cell fate and high levels of MYC were required to suppress TFEB-dependent epigenetic changes to maintain AML (S. Yun et al. 2021).

TFEB also plays an important role in lineage commitment in the liver (Pastore et al. 2020). During development and upon regeneration in response to injury, TFEB drives the

differentiation of murine liver progenitor cells (LPCs) into the progenitor/cholangiocyte lineage whilst inhibiting hepatocyte differentiation. Pastore et al demonstrated that Sox9, a marker of precursor and billary cells was a direct transcriptional target of TFEB and the primary mediator of its effects on liver cell fate (Pastore et al. 2020).

1.7 TFEB in cancer

- *Renal cell carcinoma*

Renal cell carcinoma (RCC) is considered the most well-known example of how TFEB and TFE3 are implicated in cancer. Translocation RCCs (tRCCs) are categorised by their chromosomal breakpoint, as well as the genes that are fused to TFEB and TFE3 (Kauffman et al. 2014). The first documented case of a chromosomal rearrangement in RCC was the Xp11.2 translocation, t(X;1)(p11.2;q21.2) which was first described in a 2-year-old child with RCC in 1986 (de Jong et al. 1986). It was not until 1995, that it was shown to cause the fusion of the TFE3 gene on Xp11.2 to the Proline Rich Mitotic Checkpoint Control Factor (PRCC) gene at 1q21.2, producing the PRCC-TFE3 fusion gene (Shipley et al. 1995). More recently, others have demonstrated that the nuclear-aggregated PRCC-TFE3 fusions constitutively activate expression of the target gene E3 ubiquitin ligase PRKN, leading to rapid PINK1-PRKN-dependent mitophagy and promoted cell survival (Wang et al. 2021). In addition, PRCC-TFE3 fusion proteins accelerated mitochondrial turnover by activating the PPARGC1A/PGC1α-NRF1 pathway. They concluded that PRCC-TFE3 fusion proteins promote mitophagy, mitochondrial biogenesis and proliferation of PRCC-TFE3 tRCCs (Wang et al. 2021).

Since then, other TFE3 fusions in tRCC have been uncovered, such as SFPQ-TFE3, NONO-TFE3, ASPSCR1-TFE3 and CLTC-TFE3 suggesting that TFE3, rather than the fusion partners, is the critical factor for the development of tRCC. Notably, only three of these five TFE3 gene fusions (PRCC-TFE3, ASPL-TFE3, and PSF-TFE3) are confirmed as being ‘recurrent’ by being detected in multiple RCC patients with differing gene fusion boundaries. Whilst NONO-TFE3 and CLTC-TFE3 have so far only been observed in one patient (Kauffman et al. 2014).

Although translocations involving TFEB are not as common as for TFE3, they are still implicated in tRCC. One example is the translocation t(6;11)(p21;q12), resulting in the fusion of the MALAT1 gene to TFEB. MALAT1 is an intron-less gene and the fusion involves rearrangement with the first intron of TFEB, upstream of the initiation ATG, thus preserving the entire TFEB coding sequence (Davis et al. 2003). As a result, TFEB expression is driven by

the promoter of the Alpha gene, resulting in over-expression. Furthermore, the MALAT1-TFEB fusion protein results in constitutively nuclear expression patterns. In fact, the nuclear localisation of TFEB protein is a highly sensitive and specific diagnostic marker for these tRCCs (Argani et al. 2005). Recently, other genes have been identified as fusion partners in TFEB rearranged renal cell carcinomas such as, ASPSCR1-TFEB, ACTB-TFEB and NEAT1-TFEB. An interesting observation was that many of these TFEB fusion proteins results in constitutive expression of Programmed Cell Death Ligand 1 (PDL1) (Caliò et al. 2021).

Common to all TFE3 and TFEB fusion proteins is the retention of the wild-type protein C-terminus, including the bHLH domain (dimerisation), the leucine zipper (DNA-binding), and nuclear localisation signal (Kauffman et al. 2014). Interestingly, the transactivation domain is not always retained. Despite this, the most widely accepted model explaining how TFE-fusion proteins lead to the development of RCC remains to be the introduction of a constitutively active promoter leading to dysregulated TFE transcriptional activity (Kauffman et al. 2014). Nonetheless, numerous pathways that are well-implicated in cancer are regulated by TFEB and/or TFE3. These include the activation of TGFβ and ETS transcription factors, E-cadherin expression, CD40L-dependent lymphocyte activation, mTORC1 signaling, insulin-dependent metabolism regulation, folliculin signaling, and Rb-dependent cell cycle arrest (Kauffman et al. 2014). However, it is still unclear as to which of these pathways is involved in mediating carcinogenesis observed in TFEB/3 tRCCs.

- *Pancreatic ductal adenocarcinoma*

Pancreatic ductal adenocarcinoma (PDAC) is a subtype of pancreatic cancer and is one of the most lethal diseases with an average 5-year survival rate of 10% (Sarantis et al. 2020). PDAC is characterised by its poor vascularisation and high levels of autophagy, which is thought to be a therapeutic sensitivity (Piffoux, Eriau, and Cassier 2021; Yang et al. 2011). Furthermore, a study investigating the role of autophagy in PDAC demonstrated that regardless of nutrient status and mTORC1 activity, PDAC cell lines exhibited higher levels of TFEB and TFE3 than non-PDAC cell lines and were constitutively nuclear (Perera et al. 2015). They also demonstrated that the high levels of autophagy observed in PDAC cell lines were the result of TFEB/3-dependent transcription (Perera et al. 2015). Using proteomic approaches, they revealed importin 8 (IPO8), a member of the Importin-β family of nucleocytoplasmic transporters (Raices and D'Angelo 2012) was significantly higher in TFE3 immunoprecipitates obtained from PDAC cell lines than non-PDAC cell lines. Furthermore, knockdown of IPO8 in PDAC cell lines reduced the nuclear proportion of TFE3 as well as reducing overall levels but not in non-PDAC cell lines. Combined knockdown of IPO8 and its

most closely related homolog, IPO7 (Yao et al. 2008) produced similar effects for MITF and TFEB, suggesting that IPO7 and IPO8 not only import the MiT/TFE family members into the nucleus, but also regulate their stability (Perera et al. 2015). They concluded that the high levels and nuclear localisation of the MiT/TFE family members in PDAC is IPO8-dependent and led to constitutive activation of lysosomal and autophagic genes as well as increased macropinocytosis, thus promoting cell proliferation and survival (Perera et al., 2015).

Since then, other groups have investigated the role of the MiT/TFE family in PDAC and have identified non-autophagic roles of TFEB that also contribute to PDAC pathogenesis (Kim et al. 2021). For instance, Kim et al. demonstrated PDAC exhibited significantly higher TFEB expression compared with non-PDAC tissue samples and knockdown of TFEB using shRNA inhibited glutamine and mitochondrial metabolism. Although knockdown inhibited PDAC growth both in vitro and in vivo, they observed no significant effect on autophagic flux under nutrient-rich conditions. Instead, they observed reduced transcription of glutaminase; an enzyme involved in glutamine metabolism. They later showed glutaminase was a direct transcriptional target of TFEB, thus highlighting non-autophagic roles of TFEB in PDAC (et al. 2021).

- *Colorectal cancer*

Although TFEB is expressed at a lower level in colorectal cancer (CRC) than in normal tissue, one study demonstrated that there was a significant positive correlation between TFEB expression in CRC cancer tissues and malignant progression (Liang et al. 2018). Furthermore, they observed patients with CRCs that expressed higher levels of TFEB expression exhibited deeper infiltration and higher rates of metastasis to lymph nodes (Liang et al. 2018). Liang et al. found CRC patients with high TFEB levels always had poor survival and, using a multivariate analysis demonstrated that high TFEB levels in CRC patients could be used as a predictor of survival. Knockdown and/or knockout of TFEB in CRC cell lines significantly reduced cell proliferation and migration under amino acid starvation. Additionally, they showed TFEB knockdown inhibited Beclin1 expression in CRC. Beclin1 is a mammalian ortholog of the yeast autophagy-related gene 6 (ATG6/VPS30) and is required for the formation of biogenesis of autophagosomes (Tran, Fairlie, and Lee 2021).

(iii) Lung cancer

One study using 98 non-small cell lung cell cancers (NSCLCs), revealed by immunohistochemistry that overexpression of TFEB, LAMP2a and Cathepsin D was exhibited

in 47.9%, 43.9% and 39.8% of cases respectively (Giatromanolaki et al. 2015). Furthermore, they demonstrated that expression of TFEB, LAMP2a and Cathepsin D were positively correlated each other and with adenocarcinomas, resulting in a poorer prognosis (Giatromanolaki et al. 2015). In addition, they showed silencing TFEB in lung cancer cell lines reduced cell migration (Giatromanolaki et al. 2015)

Another study demonstrated that the tumour suppressor p53 can also regulate nuclear translocation and activity of TFEB in lung cancer cell lines (Zhang et al. 2017). For instance, deletion or pharmacological inhibition of p53 with pifithrin-α promoted nuclear translocation of TFEB and increased lysosomal and autophagosomal biogenesis. which could be reversed upon re-introduction of p53. In addition, they demonstrated the effect of p53 expression on lysosomal and autophagosomal biogenesis was TFEB-dependent as knockdown of TFEB abolished these effects. Although the authors speculate the role of p53 in regulating TFEB subcellular localisation is indirect and is likely mediated by mTORC1 activity, this study revealed a novel role of p53 in mediating TFEB activity in lung cancer (Zhang et al. 2017).

- *Melanoma*

In 2002, it was revealed that cutaneous melanoma is a molecularly heterogenous disease with approximately 40-60% of melanomas harbouring an activating mutation in the serine/threonine kinase protein kinase B-raf (BRAF) gene with 90% of these mutations being a one base pair substitution, resulting in a valine to glutamate amino acid substitution at position 600 (V600E) (Davies et al. 2002). In cells harbouring the $BRAF^{V600E}$ mutation, BRAF is constitutively active and leads to constant activation of the MAPK pathway and is thought to drive cancer cell survival independently of growth factors (Tian and Guo 2020). Interestingly, ERK is part of the MAPK pathway and can directly phosphorylate TFEB on Ser142 and prevents nuclear accumulation of TFEB (Settembre et al. 2011).

One study demonstrated that in $BRAF^{V600E}$ melanoma, TFEB mediates therapy resistance to BRAF inhibition (Li et al. 2019). They showed inhibition of BRAF prevented de novo phosphorylation of TFEB on Ser142 by ERK which caused nuclear translocation, independently of mTORC1 activity. Preventing BRAFi-induced transcriptional activation of autophagy and lysosomal biogenesis enhanced tumour progression, EMT, transdifferentiation, and metastatic dissemination in mouse melanoma xenografts. Moreover, chemoresistance was associated with a TFEB-dependent increase in TGFβ levels and signalling whilst inhibition of TGFβ restored tumour differentiation and responsiveness to BRAF inhibitors (Li et al. 2019).

Overall, this study highlighted pharmacological inhibition of BRAF results in nuclear translocation and activation of TFEB and is thought to contribute to chemoresistance.

1.8 TFEB in neurodegenerative diseases

- *Alzheimer's disease*

Alzheimer's disease (AD) is a genetic and sporadic neurodegenerative disease characterised by the presence of extracellular β-amyloid (Aβ)-containing plaques and intracellular tau-containing neurofibrillary tangles (Knopman et al. 2021) consisting of hyper-phosphorylated Tau proteins (Ricciarelli and Fedele 2017) and causes cognitive impairments such as memory loss and confusion, significantly impairing quality of life. Certain mutations have been identified as risk factors for AD, including amyloid beta precursor protein (APP), Presenilin-1 (PSEN1), PSEN2, and Apolipoprotein E (APOE). Mutations in the APP gene lead to increased expression of longer Aβ peptides, especially those ending at residue 42 (Aβ42) which are prone to rapid aggregation (Tcw and Goate 2017).

In Alzheimer's disease (AD), abnormal sphingolipid metabolism has been reported (Haughey et al. 2010). Sphingolipids constitute a family of lipids, including sphingosine, ceramide, sphingosine-1-phosphate (S1P) and ceramide-1-phosphate (Hannun and Obeid 2018). Interestingly, acid sphingomyelinase (ASM); an enzyme responsible for catalysing the breakdown of sphingomyelin to ceramide and phosphorylcholine (Schuchman 2010), is higher in fibroblasts, brain and/or plasma from AD patients or AD mice. This increase in ASM is associated with defective autophagic degradation of Aβ and Tau plaques due to lysosomal dysfunction (Lee et al. 2014). Genetic ablation of ASM in AD mice ameliorated the autophagic defect by restoring lysosomal biogenesis and reducing Aβ deposition (Lee et al. 2014). Interestingly, they also demonstrated that treating cells with ASM, decreased TFEB expression as well as reducing its nuclear localisation. Furthermore, inhibition of ASM by genetic disruption or treatment with amitriptyline, restored TFEB-dependent lysosomal activity and autophagy (Lee et al. 2014). This study provided evidence that defective autophagy caused by increased levels of ASM in AD is due to impaired TFEB-dependent lysosomal biogenesis.

Other studies have also implicated TFEB as a potential therapeutic target in AD. For instance, one study demonstrated in astrocytes that overexpression of TFEB promoted Aβ clearance (Xiao et al. 2014). Another study demonstrated in mice TFEB expression promotes the degradation of p-Tau and Neurofibrillary tangles and ameliorates disease pathogenesis (Polito et al. 2014). Together, these studies provide evidence that targeting TFEB activity may be an effective therapeutic strategy for the treatment of AD patients.

- *Parkinson's disease*

Parkinson's disease is the next most common neurodegenerative disease and is characterised by the accumulation of Lewy bodies and degeneration of dopaminergic substantia nigra neurons (Grimes and Bulman 2002). Lewy bodies are formed by the accumulation of abnormal protein aggregates, including α-synuclein and cause neuronal dysfunction and is thought to be the result of impaired lysosomal function (Dehay et al. 2013). Mutations have now been identified in inherited forms of Parkinson's disease such as α-synuclein (4q21.3-23), parkin (6q25.2-27), and ubiquitin carboxy terminal hydrolase-L1 (4p16.3) (Grimes and Bulman 2002). Symptoms of Parkinson's disease include involuntary movements, rigidity, difficulty with motor coordination and later dementia.

One study demonstrated the importance of TFEB in Parkinson's disease by using an *in vivo* model of α-synuclein toxicity. They demonstrated that excess cellular levels of α-synuclein in nigral dopamine neurons resulted in a reduction in lysosomal markers and cytoplasmic retention of TFEB (Decressac et al. 2013). Interestingly, α-synuclein exhibits structural and functional homology to the cytoplasmic chaperone 14-3-3 (Ostrerova et al. 1999) which can sequester TFEB in the cytoplasm (Napolitano and Ballabio 2016). Furthermore, they demonstrated that over-expression of TFEB or, pharmacological inhibition of mTORC1, led to nuclear translocation of TFEB, activation of autophagy and clearance of α-synuclein aggregates (Decressac et al. 2013).

Furthermore, another study showed protein levels of NLRP3, ASC and caspase-1 are increased in the α-synuclein mutation (A53T) Parkinson's disease mouse model (Chen et al. 2021). Moreover, p38 is activated by overexpression of the α-synuclein A53T mutant and inhibits TFEB activity. In addition, they demonstrated NLPR3 is degraded by chaperone-mediated autophagy in microglial cells which is inhibited by overexpression of the α-synuclein A53T mutant through p38-dependent inhibition of TFEB. Overall, they showed inhibition of p38 exhibits a neuroprotective effect in the Parkinson's disease mouse model through preventing inhibition of TFEB and promoting TFEB-dependent chaperone-mediated degradation of NLPR3 (Chen et al. 2021).

However, others have demonstrated that impaired macroautophagy (a process of breaking down intracellular cargo for energy) in dopaminergic neurons can have opposing effects. For instance, overexpression of α-synuclein with impaired macroautophagy in dopaminergic neurons caused typical Parkinson's neuropathology but paradoxically improved Parkinsonian behaviour in mouse models (Hunn et al. 2019). Taken together, although many studies have demonstrated that impaired autophagy contributes to the neuropathogenesis observed in Parkinson's disease. The observation that inducing autophagy may worsen motor

performance is a consideration that should not be overlooked, especially in clinical trials of new Parkinson's drugs.

- *Huntington's disease*

Huntington's disease is a rare, incurable, autosomal dominant, genetically inherited neurodegenerative disease (Ojalvo-Pacheco et al. 2024), with an average age onset of 40 years (Ross and Tabrizi 2011). Pathologically, Huntington's disease is characterised by a chronic and progressive accumulation of misfolded protein aggregates in the cytoplasm and nucleus of specific neurons in the brain (particularly in the striatum and cortex), leading to their dysfunction and death (Ojalvo-Pacheco et al. 2024). Clinical manifestations of Huntington's disease include involuntary movements, cognitive decline and psychiatric issues (Ross and Tabrizi 2011).

Huntington's disease is caused by an abnormal expansion of a CAG repeat in the huntingtin (HTT) gene, encoding a large protein of 3,144 amino acids. The CAG repeat in HTT codes for a polymorphic polyglutamine (polyQ) stretch. In people without Huntington's disease, the CAG sequence is repeated 9 to 35 times, with an average median of between 17 and 20 repeats (Kremer et al. 1994). However, in patients with Huntington's disease, the CAG expansion exceeds 35 repeats. Interestingly, the age of onset of the disease is proportional to the length of the CAG expansion, with juvenile onset being associated with CAG expansions of 75 or more repeats. Therefore, the length of the CAG expansion in the HTT gene can be used to predict the age of onset in patients (Lee et al. 2012). Ultimately, CAG expansion in the HTT gene ultimately leads to its misfolding and pathogenesis (MacDonald et al. 1993).

Studies have observed that in Huntington's disease models, including neuronal cells and mice, TFEB and PGC1α expression is significantly reduced. For instance, one study demonstrated that mutant huntingtin (HTT) results in impaired mitochondrial function by directly binding to the PGC1α promoter and preventing CREB/TAF4-dependent transcription (Cui et al. 2006). Furthermore, another study demonstrated that induction of PGC1α virtually eliminated HTT protein aggregation and ameliorated neurodegeneration through activation of TFEB. Overexpression of TFEB alone was capable of reducing HTT aggregation, demonstrating PGC1α acts upstream of TFEB (Tsunemi et al. 2012).

- *Spinal and bulbar muscular atrophy*

Similarly, to Huntington's disease, spinal and bulbar muscular atrophy (SBMA), also referred to as Kennedy's disease, is caused by CAG expansion in a polyglutamine (polyQ) stretch but in a different gene, encoding the androgen receptor (AR), resulting in a mutant AR protein, referred to as polyQ-AR (Spada et al. 1991). Wildtype AR interacts with TFEB and acts as a coactivator of TFEB-dependent transcription. Despite the pathogenic polyQ-AR protein retaining its ability to bind to TFEB, it interferes with its activity, causing defects in autophagic flux and lysosomal biogenesis (Cortes et al. 2014). Furthermore, TFEB over-expression has been shown to rescue autophagic defects in a SBMA stem cell model (Cortes et al. 2014).

1.8 Summary and aims

The ability of cells to respond to their environment is fundamental for survival. Cells must sense changes in the availability of resources, such as amino acids, glucose, growth factors and cytokines. Integral to cellular homeostasis is the ability of mTORC1 and mTORC2 to integrate environment cues. Importantly, mTORC1 coordinates cellular metabolism; when nutrients are abundant mTORC1 is active and promotes anabolic processes such as protein translation, lipid biosynthesis and nucleotide synthesis, whilst inhibiting catabolic processes such as autophagy through the inhibition of the MiT/TFE family of transcription factors through cytoplasmic sequestration. Conversely, in response to nutrient deprivation, namely amino acid withdrawal, mTORC1 is inactivated and as a result, anabolic processes such as protein translation and biosynthesis of lipids and nucleotides are inhibited. At the same time, phosphatases such as calcineurin are activated and mTORC1 de novo phosphorylation of the MiT/TFE family of transcription factors is inhibited, allowing their nuclear entry to promote autophagy and lysosomal biogenesis through binding to the CLEAR network. The MiT/TFE family promote catabolism through inducing transcription of genes involved in lysosomal biogenesis, autophagy, lipid catabolism, glucose uptake and mitochondrial biogenesis. This response to nutrient withdrawal enables cells to adapt and attempt to rebalance their nutrient supply with their demand.

mTORC2 also plays a key role in maintaining cellular homeostasis, although its regulation is less well understood than that of mTORC1. In response to glutamine withdrawal and glucose limitation mTORC2 is activated and is known to mediate cell mobility and migration through mediating cytoskeletal remodelling, promote hexosamine biosynthesis (the addition of an amine group to a hexose sugar) as well as promoting catabolic processes such as lipid metabolism and glucose metabolism.

Overall, the regulation of MiT/TFE family members, particularly TFEB, in response to amino acid levels is fairly well understood. Currently, we know that when amino acids are present, MAP4K3 phosphorylates TFEB on Ser3, which is crucial for its recruitment to the lysosomal surface through binding to Rag GTPases. At the same time, mTORC1 is recruited to the surface of the lysosome by Rag GTPases. Once both TFEB and mTORC1 have been recruited to the lysosomal membrane, mTORC1 phosphorylates TFEB on numerous residues such as Ser122, Ser142 and Ser211. Phosphorylation of Ser211 is particularly important for retaining TFEB in the cytoplasm as it is required for binding to the cytoplasmic chaperone protein, 14-3-3. This cytoplasmic sequestration is essential for keeping TFEB out of the nucleus and keeping it transcriptionally inactive. Conversely, in response to amino acid withdrawal, mTORC1 is inactivated and de novo phosphorylation of TFEB is inhibited. Simultaneously, activation of phosphatases, such as calcineurin, actively dephosphorylate TFEB. Both of these events result in nuclear translocation of TFEB and promote its transcriptional activity of the CLEAR network.

In addition to mTORC1, other kinases have been shown to phosphorylate and regulate TFEB activity. For instance, AKT phosphorylates TFEB at Ser467, GSK3β at Ser138, PKCβ at Ser461, Ser466 and Ser468 as well as AMPK at Ser466, Ser467 and Ser469. However, the importance of these phosphorylation marks is less clear than that described by mTORC1, and the way cells integrate these signals to finely tune subcellular localisation is not well understood as often they are studied in isolation. Given that TFEB not only activates genes involved in amino acid metabolism, but also glucose and lipid metabolism, it is unsurprising that TFEB can be phosphorylated by numerous kinases that are key effectors in metabolism. However, the ability of TFEB to respond to changes in glucose levels for instance, has not yet been explored.

Furthermore, mTORC1 and mTORC2 activity is often highjacked in cancers to promote growth and proliferation. Cancer cells do this through the acquisition of mutations either in mTOR itself or in the genes that act upstream in order to rewire their metabolism. In addition, TFEB has been implicated in cancers such as melanoma, lung cancer, renal cell carcinoma and pancreatic ductal adenocarcinoma whereby TFEB is over-expressed and/or constitutively nuclear, promoting autophagy, lysosomal biogenesis as well as non-autophagic functions such as, genes involved in metabolism as well as promoting cell migration.

Although TFEB activity is important in cancer pathogenesis, TFEB has been identified as a potential therapeutic target in the context of neurodegenerative diseases. Numerous studies have demonstrated that over-expression or activation of TFEB can provide neuroprotection in Alzheimer’s, Parkinson’s, Huntington’s as well as Spinal and bulbar muscular atrophy.

We hypothesise that understanding how we can attenuate or promote nuclear accumulation of TFEB to inhibit or promote its activity in cancers and neurodegenerative diseases respectively would therefore be therapeutically beneficial.

The first chapter of this thesis will explore the signalling pathways that control TFEB nuclear-cytoplasmic shuttling in response to amino acid and glucose withdrawal, aiming to expand our knowledge of how TFEB is regulated by nutrients other than amino acids. In addition, upon re-establishment of nutrients, how TFEB exits the nucleus to be retained in the cytoplasm is unclear.

The second part of this thesis will explore the feasibility of promoting nuclear accumulation and activity of TFEB using a library of FDA-approved drugs. To do this, we performed a high throughput image-based screen and after, performed functional validation experiments to visualise TFEB-dependent effects on lysosomal biogenesis and autophagy. The results from this screen may provide novel insights into how drugs that are already clinical-approved have the potential to be re-purposed for treatment of neurodegenerative diseases or lysosomal storage disorders.

The third and final chapter of this thesis will explore the feasibility of preventing nuclear accumulation of TFEB either by preventing nuclear import or promoting nuclear export in response to amino acid and glucose deprivation respectively. To do this, we performed a high-throughput image-based screen using the PKISI/II libraries from GSK to assess which compounds could attenuate nuclear accumulation of TFEB. After, we performed follow-up experiments to determine drug mode of action. The results of this screen may provide novel insights into how we can therapeutically prevent TFEB activity in cancers that rely upon high levels of autophagy.

Chapter 2: Materials and methods

2.1 Bacterial methods

2.1.1 Bacterial strains

(i) For general cloning purposes, the *E.* coli sub-cloning efficiency DH5α competent cells (ThermoFisher Scientific, Cat No. 18265017), were used. The genotype of the DH5α *E. coli* strain is F^- Φ80lacZΔM15 Δ(lacZYA-argF) U169 recA1 endA1 hsdR17(r_k^-, m_k^+) phoA supE44 thi-1 gyrA96 relA1 λ^-.

(ii) For site-directed mutagenesis, the *E.* coli XL10-Gold ultracompetent cells (Agilent, Cat No. 200315), were used. The genotype of the XL10-Gold strain of *E. coli* is Tetr Δ(mcrA)183 Δ(mcrCB-hsdSMR-mrr)173 endA1 supE44 thi-1 recA1 gyrA96 relA1 lac Hte [F' proAB lacIqZ ΔM15 Tn10 (Tetr) Amy Camr].

(iii) For recombinant expression of eukaryotic proteins, the *E.* coli Rosetta BL21(DE3)-R3-pRARE2 cells, phage-resistant derivative of BL21(DE3) strain, with a pRARE plasmid encoding codon tRNAs rarely used in *E.* coli *(Sigma Aldrich, Cat No. 70954)* were used.

2.1.2 Growth conditions

E. coli was cultured in autoclaved Bacterial Luria-Bertani (LB) media (10 g/L Tryptone, 5 g/L Yeast Extract, and 5 g/L NaCl). LB agar plates were prepared using agar powder (10 g/L Peptone 140, g/L Yeast Extract, and 5 g/L NaCl, 12 g agar, ThermoFisher Scientific) diluted in ddH_20, autoclaved and then poured onto 10 cm petri dishes (Sterilin, Newport, UK). LB Agar plates were supplemented with the corresponding antibiotics required for selection: 100 µg/mL Ampicillin, 34 µg/mL Chloramphenicol (Sigma Aldrich, Cat No. C0378) and 50 µg/mL kanamycin (ThermoFisher Scientific).

When using *E. coli* strains for plasmid propagation and cloning (DH5α and XL10-Gold), liquid cultures were incubated at 37 °C overnight, shaking at 225 rpm, whilst solid cultures were grown in a humidified incubator at 37 °C overnight to allow for colony formation. For information regarding growth conditions for *E. coli* strains for recombinant protein expression (Rosetta), refer to section **2.1.4 Recombinant protein expression and purification**.

2.1.3 Transformation by heat shock

- *E. coli strains DH5α and Rosetta*

Briefly, cells were thawed on ice before adding 10-50 ng DNA and incubating on ice for 20 min. Cells were then heat shocked at by incubating at 42 °C for 30 s then on ice for 2 min. After, 150 µL of Super Optimal broth with Catabolite repression (SOC) medium was added before incubating at 37 °C, shaking at 225 rpm for 30 min before spreading onto LB agar plates.

- *E. coli strain XL10-GOLD*

Prior to transformations, 14 mL BD Falcon polypropylene round-bottom tubes were pre-chilled on ice, SOC media was pre-heated at 42 °C and cells were thawed on ice. Once thawed, 100 µL of cells were transferred into each pre-chilled tube. 4 µL of β- mercaptoethanol was added to each tube and swirled gently. Cells were incubated on ice for 10 min, swirling gently every 2 min. After, 0.1-50 ng of DNA (or 2 µl of a ligation mix) was added to each tube and swirled gently and incubated on ice for 30 min. Cells were heat-shocked by incubating at 42 °C for 30 sec then on ice for 2 min. After, 0.9 mL of preheated SOC was added before incubating at 37 °C for 1 hr, shaking at 225-250 rpm. The transformation mixture (200 µl) was spread onto LB agar plates containing the appropriate antibiotic. Plates were incubated OVERNIGHT at 37 °C.

2.1.4 Recombinant protein expression and purification

E. coli Rosetta BL21(DE3)-R3-pRARE2 cells were transformed with either the pNIC 6xHis TFEB 1-200 or pNIC 6xHis MITF 1-105 vectors, selected using 50 µg/mL Kanamycin (Sigma Aldrich, Cat No. BIK0126) and amplified at 37 °C in LB medium with 50 µg/mL Kanamycin and 34 µg/mL Chloramphenicol (Sigma Aldrich, Cat No. C0378) (Sigma Aldrich, Cat No. C0378). Once an OD_{600} of 0.6 was reached, the culture was cooled to 18 °C and recombinant protein expression induced by adding 0.1 mM IPTG (Sigma Aldrich, Cat No. 16758) and incubating overnight at 18˚C. Cells were harvested by centrifugation at 6,000 g for 15 min before lysing under denaturing conditions (6 M urea, 25 mM HEPEs pH 7.5, 0.5 M NaCl, 5% Glycerol, 20 mM Imidazole, buffer pH 7.5) using a French Press homogeniser. The lysate was then cleared by centrifugation at 25,000 g for 15 min.

10 mL Ni-NTA agarose (QIAGEN, Cat No. 30210) was washed twice using 10 mL Lysis Buffer before cleared lysate was added to the resin and incubated at 4 ˚C, rotating for 1 hr. The lysate-resin mixture was applied to a gravity-flow column before washing twice with 10 mL wash buffer (6 M urea, 25 mM HEPES pH 7.5, 0.5 M NaCl, 5% Glycerol, Buffer pH 7.5) and once with Lysis Buffer. Protein was eluted using increasing concentrations of Imidazole (50-

250 mM). Eluted fractions were pooled and dialysed using 3-5 kDa DiaEasy Dialyzer tubes (Biovision, Cat No. K1012) and buffers prepared with decreasing concentrations of urea (25 mM HEPES pH 7.5, 0.5 M NaCl, 5% Glycerol, 4.0-0.0 M urea). Protein fractions were dialysed for 1.5 hr at each urea step at 4˚C on a magnetic stirrer starting with 1 L of 4 M urea (two times), then 2 M urea, and then 1 M urea before transferring to 0.5 M urea at 4˚C on a magnetic stirrer overnight. The next morning, samples were dialysed against 1 L of urea-free buffer for 3.0 hr at 4˚C on a magnetic stirrer. Once dialysis was complete, samples were aliquoted, flash frozen in liquid nitrogen before transferring to –80 ˚C for long-term storage.

2.2 Mammalian methods

2.2.1 Cell culture conditions

HT29 and HeLa cells were cultured in Dulbecco's Modified Eagle Medium DMEM, high glucose, GlutaMAX™ Supplement, HEPES media (DMEM, ThermoFisher Scientific, Cat No. 10564011) supplemented with 10% Foetal Bovine Serum (FBS, Sigma-Aldrich, Cat No. F7524) and 1% Penicillin-Streptomycin (ThermoFisher Scientific, Cat No. 15140122). All cell lines were grown in a humidified incubator, with 5% CO_2 at 37 °C.

All cell lines were passaged by removing the media, washing with sterile 1X PBS, adding Trypsin to cover the plate/dish and incubating at 37 °C for 3-5 min to allow for detachment. After, Trypsin was neutralised with an equal volume of media containing FBS. To store, cells were frozen in in FBS containing 10% DMSO and stored at -80 °C and then moved into a liquid nitrogen tank to ensure long-term preservation.

2.2.2 Transient transfection of plasmid DNA

Cells were plated at a density of $3x10^5$ cells/well on 6-well plates the day prior to transfection to ensure approximately 30-50% confluency. The FuGENE 6 (Promega, Cat No. E2692) was used according to the manufacturer's guidelines. Per transfection, 7 µL FuGENE 6 reagent was added to 100 µL RT Opti-MEM (ThermoFisher, Cat No. 31985062) and incubated for 5 min at RT before adding 0.5–2 µg DNA and incubating for a further 15 min at RT. The transfection mixture was then added drop-wise to each well and mixed gently to ensure even coverage. Cells were incubated for 24-72 hr before experiments were performed.

2.2.3 Transient gene knock-down using siRNA

Cells were plated onto 6-well plates in antibiotic-free media. The next day, or when cells had reached 50-60% confluency, cells were subject to transfection using the RNAiMAX protocol. Firstly, two mixes were prepared; Mix A (150 µL of OptiMEM and 9 µL of Lipofectamine RNAiMAX) and Mix B (150 µL of OptiMEM and 3 µL siRNA (10 µM). Mixtures were inverted to ensure they were homogenous and then incubated at RT for 5 min. After, Mix A and Mix B were combined and inverted gently a couple of times before incubating for 20 min at RT. After, 250 µL (per well) of the transfection mixture was added to cells drop-wise. Cells were incubated at 37 ºC, 5% CO_2 for 1-3 days post-transfection to ensure sufficient knock-down of the target gene(s).

2.2.4 Generating stable over-expression cell lines by transfection

To generate stably expressing (Piggybac) cell lines by transfection, three plasmids were co-transfected: a PiggyBac vector containing the gene to be ectopically expressed (downstream of a tetracycline-responsive promoter), a vector expressing the PiggyBac transposase enzyme and a vector containing the trans-activator required for transposase activity. These three plasmids were transfected at a ratio of 10:1:1 respectively using the FuGENE 6 reagent as outlined previously (Section 2.2.2). For a 6 well plate, 2 µg of the PiggyBac Vector was used along with 200 ng of both the transposase and transactivator plasmids. After transfection (48 hr), the appropriate antibiotic selection was added to cells to enrich for transfected cells with PiggyBac integration(s) for approximately 1-2 weeks (or until the non-transfected control cells had died).

2.2.5 Generating stable over-expression cell lines by transduction

To generate stably expressing cell lines (shRNA knock-down or over-expression using PiggyBac), cells were plated the day prior to transduction. The appropriate amount of lentivirus or retrovirus was added dropwise to each well (6-well plate). After 24 hr, the supernatant was removed and replaced with media containing the appropriate antibiotics to select for transduced cells. Cells were kept under selection for 1-2 weeks (or until the un-transduced control cells died) before performing experiments.

2.3 Nucleic acid methods

2.3.1 Plasmid purification

For plasmid purification, a colony resulting from a transformation would be picked into 10-100 mL of LB media (depending on how much plasmid was needed) containing the appropriate antibiotics for selection. Cultures were grown at 37 °C, shaking at 225 rpm overnight. The next morning, cells were pelleted by centrifugation at 4,600 g and plasmids purified using either the QIAprep Spin Miniprep Kit (QIAGEN) for small scale (10 mL) plasmid production or the Plasmid Midiprep Kit (QIAGEN) for medium scale (100 mL) plasmid production. Plasmid DNA was eluted in an appropriate volume of ddH_20 (10-100 µL) and after, concentration was measured using the NanoDrop 2000 spectrophotometer (ThermoFisher Scientific). Plasmids generated from cloning were sequenced using Sanger Sequencing (Eurofins).

2.3.2 Gel electrophoresis

To separate DNA fragments by molecular weight 1% agarose gels were prepared by dissolving Agarose (Web Scientific) in an appropriate volume of 1x Tris/Borate/EDTA (TBE) buffer (100 mM Tris, 90 mM boric acid, 1 mM EDTA) by heating gently in the microwave. Once cooled to below 60 °C, peqGREEN (PEGLAB) was added to the gel (1:10,000) before pouring the gel into the cassette. Samples were prepared by adding 1 volume of 6X orange gel loading dye (New England Biolabs) to 5 volumes of sample. To measure DNA fragment size(s), 5 µl of either the HyperLadder 50 bp or HyperLadder 1 kb (Bioline) were used. Samples were separated at 150 V for 20-30 min in 1x TBE buffer.

2.3.3 Polymerase Chain Reaction (PCR)

- *PCR for cloning*

When using PCR for cloning purposes, the high fidelity Accuprime Taq polymerase (ThermoFisher Scientific) was used to amplify DNA regions as per the manufacturer's guidelines. Once the PCR mixtures were prepared, heat-cooling cycles were performed using a Veriti Thermal Cycler (Applied Biosystems, ThermoFisher). Heat-cooling cycles were performed in the Veritis Thermal Cycler using the programme shown in **Table 1**.

Table 1. PCR programme for cloning

Step	Temperature	Time	Cycles
Initial denaturation	95 °C	2 min	1X
Denaturation	95 °C	30 sec	
Annealing	55-65 °C	30 sec	30X
Extension	68 °C	1 min/kb	
Final Extension	68 °C	5 min	1X

After PCR reactions were complete, samples were either checked by agarose gel electrophoresis and/or purified.

- *Colony PCR*

For colony PCR, a DNA mixture was prepared by picking bacterial colonies from LB agar plates into 10 µL of ddH_20. PCR reactions were prepared using the MyTaq Red mix (Bioline) using the manufacturers guidelines (1 µL of the DNA mixture was used per PCR). Heat-cooling cycles were performed in the Veritis Thermal Cycler using the programme shown in **Table 2**.

Table 2. PCR programme for Colony PCR

Step	Temperature	Time	Cycles
Initial denaturation	95 °C	2 min	1X
Denaturation	95 °C	15 sec	
Annealing	60 °C	15 sec	30X
Extension	72 °C	30 sec	
Final Extension	72 °C	5 min	1X

After PCR reactions were complete, samples checked by agarose gel electrophoresis.

- *Site-directed mutagenesis by PCR*

Site-directed mutagenesis by PCR was performed using the Quikchange Lightning kit (Agilent) to introduce insertions, deletions or point mutations into a gene of interest. Primers were designed using the online tool: https://www.genomics.agilent.com/primerDesignProgram.jsp. Reactions were prepared in a total volume of 50 µL. Heat-cooling cycles were performed in the Veritis Thermal Cycler using the programme shown in **Table 3**.

Table 3. PCR programme for site-directed mutagenesis

Step	Temperature	Time	Cycles
Initial denaturation	95 °C	2 min	1X
Denaturation	95 °C	30 sec	
Annealing	60 °C	10 sec	25X
Extension	68 °C	30 sec/kb	
Final Extension	68 °C	5 min	1X

Template DNA was selectively degraded by adding 1 µL of the methylation-specific restriction enzyme, Dpn1 (New England Biolabs) and incubating at 37 °C for 10 min. After digestion, 2 µL of the PCR product was used to transform 30 µL of XL10-Gold ultracompetent cells and colonies were screened for mutations by Sanger Sequencing (Eurofins).

2.3.4 Digesting DNA

Enzymatic digestion using restriction enzymes (New England Biolabs) were performed using the manufacturer's guidelines. Per 20 µL reaction, 2 µg DNA was used. To prevent re-ligation of digested fragments, DNA was dephosphorylated by adding 2 µL of Shrimp Alkaline Phosphatase (rSAP) to each reaction and incubating at 37 °C for 30 min. Digestion products were then analysed by gel electrophoresis and/or purified.

2.3.5 DNA fragment clean-up for cloning

DNA fragments generated from cloning steps (PCR and digestion) were purified using the QIA quick PCR Purification Kit (QIAGEN) following the manufacturer's protocol.

2.3.6 Ligating DNA

Purified DNA fragments were ligated together using the T4 DNA ligase kit (New England Biolabs) per manufacturer's guidelines (molar ratio of insert DNA to vector DNA of 10:1). Reactions were incubated at room temperature for 1 h. After, 2 µL of the ligation products were used to transfect 30 µL of DH5α cells.

2.4 Protein methods

2.4.1 Whole cell lysate preparation

Cells were grown to approximately 70-80% confluency. Cells were harvested and denatured by directly applying an appropriate volume of 1X Laemmli buffer (0.0625 M Tris base, 2% SDS, 10% glycerol, 5% β-mercaptoethanol with a dash of Bromphenol blue). Cells were scraped into the 1X Laemmli buffer using a P1000 Gibson pipette and lysates were transferred into 1.5 mL Eppendorf tubes before boiling at 95°C for 5 min.

2.4.2 Subcellular fractionation

Cells were grown to approximately 70-80% confluency. Subcellular fractionation was performed using the Rapid, Efficient And Practical (REAP) method. Briefly, cells were washed in ice-cold 1X PBS before being scraped into 200 µL of ice-cold 1X PBS with 0.1% NP-40 (containing 1 tablet of the cOmplete Protease Inhibitor Cocktail (Roche, Cat No. 11697498001) and 1 tablet of the PhosSTOP Phosphatase Inhibitor Cocktail (Roche, Cat No. 4906837001)), triturated 5 times using a Gibson P200 pipette and transferred into 1.5 mL Eppendorf tubes. After, 60 µL was removed and transferred to a 1.5 mL Eppendorf tube labelled 'whole cell fraction'. The remaining 140 µL was centrifuged using a table-top centrifuge (10 sec, 5000 g, 4 ºC). After, 60 µL of the supernatant was removed and transferred to a 1.5 mL Eppendorf tube labelled 'cytoplasmic fraction'. The remaining supernatant was removed, leaving only the insoluble pellet. The pellet was washed by resuspending in 200 µL of ice-cold 1X PBS containing 0.1% NP-40 before centrifuging using a table-top centrifuge (10 sec, 5000 g, 4 ºC). The supernatant was removed and discarded before resuspending the pellet in 60 µL ice-cold 1X PBS containing 0.1% NP-40 and labelled 'nuclear' fraction. The 'whole cell' and 'nuclear' fractions were sonicated for 30 sec at 4 ºC. After, 20 µL of 4X Laemmli buffer was added to all samples before boiling at 95 ºC for 5 min. Samples were stored at -20 °C.

2.4.3 Immunoprecipitation

Cells were grown on 60 cm plates until 70-80% confluent. Cells were washed in 1 mL of ice-cold 1XPBS before scraping into 1 mL of ice-cold immunoprecipitation (IP) buffer (50 mM Tris-HCL pH 7.5, 150 mM NaCl, 1 mM EDTA, 1% Triton X-100) containing 1 tablet of the cOmplete Protease Inhibitor Cocktail (Roche, Cat No. 11697498001) and 1 tablet of the PhosSTOP Phosphatase Inhibitor Cocktail (Roche, Cat No. 4906837001) and incubated on ice for 20 min. Lysates were sonicated to shear genomic DNA for 3 min at 4°C. After, lysates were centrifuged at 16,000 g for 15 min at 4°C before removing 50 µL of supernatant and transferring to a fresh Eppendorf tube labelled as 'input'. The rest of the supernatant was transferred to a fresh Eppendorf tube and labelled as 'pull-down' and the pellets containing genomic DNA were discarded. To the samples labelled 'pull-down', 0.4 µg of primary antibody was added and incubated overnight at 4°C, rotating. The next day, 8 µL of Protein A (anti-rabbit IgG) or Protein G (anti-mouse IgG) dynabeads were added and incubated for 2 hr at 4°C. Using a magnetic separator stand, the supernatant was removed from the dynabeads. The beads were washed three times with 400 µL of ice-cold IP lysis buffer, incubating at 4°C for 10 min, rotating each time. The supernatant was then removed and the beads were resuspended and boiled in 40 µL of 1X Laemmli buffer for 5 min at 95 °C. Equal volumes of 'input' and 'pull-down' samples were loaded to assess the efficiency of the IP. Samples were stored at -20 °C.

2.4.4 Sodium dodecyl-sulfate polyacrylamide gel electrophoresis (SDS-PAGE)

Protein samples were separated by sodium dodecyl sulphate polyacrylamide gel electrophoresis (SDS-PAGE). The resolving gel that separates proteins by molecular weight, consisted of 10-15% acrylamide (made from 30% Acrylamide solution, (Severn Biotech, Cat. No. 20-9001-10), 375 mM Tris, 0.1% SDS, pH 8.8. Ammonium persulphate (APS) and tetramethylethylenediamine (TEMED) were added to a final concentration of 0.1 % to allow polymerisation. After pouring the resolving gel to approximately 70% of the total volume of the gel cassette, a layer of 100% Isopropanol was added to create a smooth edge to layer the stacking gel on top of. After the resolving gel had set, the isopropanol was removed and the stacking gel (comprised of 3.75% acrylamide, 125 mM Tris, 0.1% SDS, pH 6.8, 0.17 % APS and 0.083% TEMED) was added to the gel cassette. Immediately, either a 1.0 mm or 1.5 mm comb (with 10 or 15 lanes) was added to allow lane formation. Proteins were separated by electrophoresis for around 20 min at 100V before increasing the voltage up to 150V for a further 40-60 min in 1X Running Buffer (25 mM Tris, 192 mM glycine, 0.1 % SDS) using the Mini-PROTEAN Tetra Cell (Bio-Rad, Cat No. 1658001). Molecular weight of proteins was estimated by using Precision Plus Dual Colour Protein Standards (Bio-Rad, Cat No. 1610374).

2.4.5 Immunoblotting

After protein separation by SDS-PAGE, proteins were transferred onto a methanol-activated Polyvinylidene difluoride (PVDF) membrane in 1X Transfer Buffer (25 mM Tris, 192 mM glycine, 20 % isopropanol) at 100 V for 60-80 min using the Mini Trans-Blot Module (Bio-Rad, Cat No. 1703935). After, non-specific antibody binding was blocked by incubating the membranes with 5% milk in 1X PBS containing 1% Tween-20 (v/v) for 1 hr before membranes were incubated with primary antibodies at 4°C overnight. The next morning, membranes were washed repeatedly in 1X PBS-T before incubating with the secondary antibodies for 1 hr at RT. Proteins were visualised using the ECL Prime Western Blotting Detection Reagent (GE Healthcare Amersham, Cat No. 12316992) using X-ray films (Fujifilm). For phospho-antibodies, blocking was performed in 5% Milk in 1X TBS-T, washes with 1X TBS-T and antibody dilution in 5% BSA in TBS-T. Primary antibodies used frequently were diluted in 5% BSA in TBS-T containing sodium azide (0.02%) to prevent bacterial growth and stored at 4°C to be used repeatedly.

2.4.6 *In vitro* kinase assay

For in vitro kinase assays (22 µl total volume), reaction mixes were prepared using 2 µg of recombinant TFEB (1-200 6X nHis), 0.3 mM cold ATP (Invitrogen, Cat No. 55082) and 100 ng of ERK2 (Sigma Aldrich, Cat No. E1283-10UG) and/or 100 ng of GSK3β (Abcam, Cat No. ab60863). All reactions were made up to 22 µl with Kinase Dilution Buffer (KDB). KDB was prepared by diluting Kinase Assay Buffer (25 mM MOPS pH 7.2, 12.5 mM glycerol 2-phosphate, 25 mM $MgCl_2$, 5 mM EGTA, and 2 mM EDTA) 1:5 in ddH20 before adding DTT (0.25 mM). Reactions were incubated for a total of 1 hr at 37˚C. ERK2 was added at the beginning of the experiment, whereas GSK3β was added after 30 min (kept consistent among all samples). Afterwards, 10 mM EDTA was added to chelate Mg_2+ ions in order to prevent further kinase activity. After performing the in vitro kinase assay, 1X volume of 2X SDS buffer was added to samples before boiling at 95°C for 5 min. After, samples were analysed by SDS polyacrylamide gel electrophoresis (SDS-PAGE) by loading ¼ of each reaction mix. Samples were onto a 12% acrylamide gel (37.5:1 acrylamide:bis-acrylamide; Severn Biotech, Kidderminster, UK). Gels were run at 170 V for 1 hr. As an indicator of molecular weight, 1 µl of the Precision Plus Protein All Blue Protein Standard (Bio-Rad) was used. For coomassie staining, gels were incubated with the Instant blue Coomassie staining reagent (Expedeon, Cat No. ISB1L) for 1 hr and de-stained using water before imaging. For western blotting, proteins were transferred onto methanol-activated (30 sec, room temperature (RT)) polyvinylidene difluoride (PVDF) membranes (Whatman, Kent, UK) by electroblotting at 100V for 70 min on ice in transfer buffer (25 mM Tris, 192 mM glycine and 20% methanol).

Membranes were blocked in 5% milk in TBS-T for 1 hr at RT, shaking before incubating with the primary antibodies at 4°C overnight. The next morning, membranes were washed three times for 10 min in TBS-T and then incubated with the secondary antibodies at RT, shaking for 1 h. The membranes were then washed three times for 10 min in 1XTBS-T before incubating with the enhanced chemiluminescence (ECL) reagent (Amersham, Uppsala, Sweden). Excess ECL was removed before exposing the membranes to X-ray films (Fujifilm).

2.4.7 Validating custom-made phospho-antibodies by peptide array

Membranes were re-hydrated by rinsing three times with 100% ethanol and then equilibrated by washing in 1X PBS-T. After, membranes were blocked in 5% BSA in 1X PBS-T for 8 hr at RT. Membranes were washed with 1X PBS-T before incubating with custom-made phospho-specific antibodies from Rabbit serum (Generon) diluted in 5% BSA PBS-T or the anti-p-S138 rabbit antibody (Andrea Ballabio Lab) diluted 1:1000-1:10,000 in 5% BSA PBS-T overnight at 4˚C, shaking. After, membranes were washed in 1X PBS-T before re-blocking in 5% BSA 1X PBS-T at RT for 1 h, shaking. Membranes were washed in 1X PBS-T before incubating with the horseradish peroxidase (HRP)-conjugated secondary antibody (Bio-Rad) in 5% BSA 1X PBS-T for 1 h, at RT, shaking. Membranes were washed with 1X PBS-T at RT, shaking, before incubating with enhanced chemiluminescence (ECL) reagent (Amersham, Uppsala, Sweden). Excess ECL was removed before imaging with the ImageQuant Las-4000 Camera.

2.5 Cell Biology methods

2.5.1 Flow cytometry

Cells were seeded onto 12-well plates at $1x10^5$ cells/well and incubated overnight. LysoTracker Deep Red 647 (ThermoFisher Scientific) was added to a working concentration of 50 nM, 30 min before the end of each experiment. Cells were de-attached from plates by washing with PBS before adding 500 µL 0.05% Trypsin-EDTA and incubating at 37°C for 5 min. Trypsin was neutralised using 500 µL of DMEM with 10% FBS. Cells were pelleted by centrifugation at 600 xg for 4 min and after, re-suspended in 400 µL PBS and transferred to 15 mL flow cytometry tubes (BD Biosciences) for FACs. Data was acquired using the FACS Canto flow cytometer (BD Biosciences) with BD FACSDiva software. Live cells were gated using Forward Scatter (FSC) and Side Scatter (SSC). Depending on the purpose of the experiment the appropriate channel was used. For example, to measure lysosomal number using LysoTracker deep red 647 dye (ThermoFisher), the APC channel was used. For detecting eGFP or mCherry the FITC and PE channels were used.

2.5.2 Fluorescent-assisted cell sorting

For generating CRISPR/Cas9 TFEB and TFE3 knock-out cell lines, cells were sorted for the top 10% of GFP expression (capped at 10,000 cells) and collected in 15 mL Falcon tubes by Andrew Worth.

2.5.3 Immunofluorescence microscopy

Cells were seeded onto 8-well coverglass chambered slides (VWR International Ltd, Cat No. 155411) and incubated overnight. The next day, cells were treated with a variety of conditions. After, cells were washed with 1X PBS, fixed before fixing and permeabilising using the BD Cytofix/Cytoperm™ Fixation/Permeabilization Kit as per the manufacturer's guidelines. Primary antibodies were diluted 1:200 in 1X Perm/Wash buffer before incubating overnight at 4°C. The next day, cells were washed 3X in 1X Perm/Wash buffer before incubating with the secondary antibody diluted 1:1000 in 1X Perm/Wash buffer in the dark at RT for 1 hr. After, DAPI was diluted in 1:5000 in 1X Perm/Wash buffer before adding to samples and incubating in the dark at RT for 15 min. Afterwards, cells were washed three times in 1X Perm/Wash buffer, and a further three times in 1X PBS. Images were acquired using Zeiss LSM710 confocal microscope and analysed using ZEN 2012 and ImageJ software.

2.5.4 Image-based high-throughput screen procedure

The screen was performed using the PKISI/II libraries provided by the TDI. Information in regards to PKSI can be found: https://pubmed.ncbi.nlm.nih.gov/26501955/, and information in regards to PKSII can be found: https://www.ncbi.nlm.nih.gov/pubmed/28767711

- *Day one: cell plating*

Using the Flex drop dispenser HT29 (3,500 cells/well) were plated into 384 well Cell Carrier Imaging Plates. Cells were incubated overnight at 37°C and 5% CO_2.

- *Day two: compound dilution, cell treatment, fixation and primary antibody staining*

The next day, using the ECHO 550, 758 compounds (PKSI/II library) and controls (Torin and DMSO) were dispensed into 384 well CoStar 3656 round bottom plates for a final concentration of 10 mM. Using the Janus MDT cells media (DMEM, DMEM with no glucose or HBSS) was added to the compound plates to dilute the compounds to a final concentration of 10 µM. After, cells were washed twice with PBS before adding the test compounds (diluted in corresponding media) to the cells and incubated at 37°C at 5% CO_2 for 2 hrs. After

treatment, cells were fixed and permeabilised for 10 mins at RT using PERM/FIX solution (BD Cytofix/Cytoperm Fixation/Permeabilization Kit) and then washed three times with the 1X PERM/WASH solution (diluted in ddH_20). Using the Janus MDT, the TFEB primary antibody (Cell Signaling, Cat No.4240) was diluted (1:200) in PERM/WASH buffer and added to cell plates. Cell plates were spun down at 500 xg for 2 mins and incubated o/n at 4^oC on an orbital shaker.

- *Day three: addition of secondary antibody and DAPI staining*

Using the Janus MDT, all plates were washed three times with 1X PERM/WASH buffer (diluted in ddH_20) before the addition of the secondary donkey anti-Rabbit IgG (H+L) Highly Cross-Adsorbed Secondary Antibody, Alexa Fluor 488 (Thermo Fisher, Cat No. A-21206) diluted in 1X PERM/WASH buffer (1/1000). Plates were spun down 1000RPM for 2 mins before incubation on an orbital shaker at RT, in the dark for 2 hrs. Using the Janus MDT, plates were washed with three times with 1X PERM/WASH buffer and then twice with 1XdPBS.

Examples of plate layouts are demonstrated in **Supplemental Figure 9. Example of plate layouts used for high-throughput image-based screen.**

2.5.5 Macro for measuring nuclear vs cytoplasmic ratios

Using a nuclear marker in channel 2 this macro creates a set of nuclear regions of interests (ROIs) using STARDIST. It then constricts these ROIs by a defined number of pixels to eliminate cytoplasmic contamination of the analysed area. It measures area, perimeter, and grey value on a per nucleus basis and outputs a .csv results table for each image. Additionally, this macro has been expanded to create a ringed ROI to encompass the cytoplasmic region surrounding the nucleus and measure it to allow for ratiometric analysis of levels of fluorescence between cytoplasm and nucleus. It also has an inbuilt quality control mechanism; by superimposing the ROIs generated over the original image the macro saves an image of the ROI overlaid on the original nuclei to allow the user to check the fidelity of their segmentation. The outputs of this macro should be 2 .csv files which contain an equal number of labelled ROIs as well as two images of the nuclear ROI and the Ringed cytoplasmic ROI overlaid on an image. Robert Crickley wrote the macro to measure TFEB nuclear/cytoplasmic ratios (see pages 206-208, supplementary materials) and examples of ROI generation is shown in **Supplemental Figure 8**.

2.5.6 Intracellular Kinase Assay

To perform the Intracellular Kinase Assay for AMPK, the NanoBRET TE (Promega, K-10) kit was used. The protocol was as follows:

- *Day one: Transfection and Cell Seeding*

HT29 cells were diluted to $2x10^5$ cells/mL in OptiMEM (no phenol red) containing 1% FBS. Transfections were performed firstly by diluting the NanoLuc PRKAA1 plasmid (1 µg/mL) and transfection carrier DNA (9 µg/mL) in 1 mL OptiMEM (no phenol red) before the addition of 30 µL of FuGENE HD. The transfection mix was inverted gently 5-10 times before incubating at RT for 20 min. In a 50 mL falcon tube, the 1 mL of transfection mix was added to 20 mL of cell suspension and gently inverted 5-10 times. The cell suspension (100 µL/well). was poured into a sterile reagent trough and transferred to a White, TC-treated 96-well plate using a multi-channel pipette. Cells were incubated incubating at 37 °C, 5% CO2, overnight.

- *Day two: Drug treatment and BRET measurement*

A 1:2 serial dilution of the test compound was performed by dilution in DMSO for a total of 11 steps. The highest concentration used was the stock concentration, 10 mM (1000X final concentration). After, all of the serially-diluted concentrations of the test compound were diluted 1:100 in OptiMEM containing no phenol red to achieve a 10X final concentration. From this plate, 10 µL/well of the serially diluted (10X) test compound was added to the experimental plate containing the cells. After, the NanoBRET Tracer reagent was diluted to 2.6 µM (20X final concentration) in Tracer Dilution Buffer before adding 5 µL/well to the experimental plate containing the cells. To the 'no tracer' control wells, 5 µL Tracer Dilution Buffer was added.

The experimental plate was then placed on an orbital shaker for 15 sec at 900 rpm before incubating at 37 °C, 5% CO2 for 2 hr. The experimental plate was removed from the incubator and allowed to cool at RT for 15 min. Whilst cooling, the 3X Complete Substrate plus Inhibitor Solution (CSI) was prepared in a 15 mL falcon tube. Per 5 mL of OptiMEM (no phenol red), 30 µL Nano-Glo Substrate and 10 µL NanoLuc Inhibitor was used. The 3X CSI solution was mixed by inverting 5-10 times before adding 50 µL to each well. The experimental plate was incubated for 2-3 min before using the CLARIOstar plate reader to take readings at ~450 nm and ~610 nm. BRET ratios were generated by dividing the acceptor emission value (610 nm) by the donor emission value (450 nm) for each sample. The BRET ratios were corrected by subtracting the BRET ratio in the absence of the tracer (average of the no-tracer control samples) from all samples. The raw BRET units were then converted to milliBRETs units (mBU) by multiplying each raw BRET value by 1000. The calculation is shown below:

BRET Ratio (mBU)=

$$[(Acceptor_{sample}/Donor_{sample}) - (Acceptor_{no\text{-}tracer\ control}/Donor_{no\text{-}tracer\ control})] \times 1000$$

2.6 Chemicals and reagents

2.6.1 Chemicals

Torin 1 was purchased from Tocris (Bristol, UK). Bafilomycin A was purchased from Cell Signalling Technology (Danvers, USA). EGFR inhibitor (CAS 879127-07-8), an ALK5 inhibitor (CAS 446859-33-2) and a PI3K inhibitor (TGX-221) were purchased from Sigma Aldrich. The Pharmakon 1,600 small compound library and PKS I/II libraries were provided by Dr. Daniel Ebner's laboratory. Hits from drug screen 1 using the Pharmakon library were ordered from vendors and are shown below in **Table 4**. Hits from the PKS I/II libraries could not be re-ordered as they are not commercially available. However, GW869516X was custom made Wuxi AppTech.

Table 4. Drug screen 1 'hits' using the Pharmakon 1,600 library of FDA-approved small compounds

Compound Name	Vendor	Catalogue No.
Escitalopram Oxalate	Sigma-Aldrich Co Ltd	E4786
Benazepril Hydrochloride	Abcam	Ab141166-50mg
Naftopidil	Abcam	Ab120756-10mg
Doxepin Hydrochloride	Insight Biotechnology Ltd	Sc-203930
Eticlopride Hydrochloride	Abcam	Ab120602-10mg
Famotidine	Abcam	Ab120760-500mg
Amlodipine Besylate	Abcam	Ab141777-10mg
Fluphenazine Hydrochloride	Cambridge Bioscience Ltd	F4584-1 G
Abamectin	Cambridge Bioscience Ltd	19201-100 Mg-Cay
Pizotyline Malate	Cambridge Bioscience Ltd	P3597-1 G
Digoxin	Bio-Techne (R&D Systems	4583/50
Carvedilol Phosphate	Cambridge Bioscience Ltd	C0366-1 G
Nortriptyline Hydrochloride	Cambridge Bioscience Ltd	15904-10 Mg-Cay
Pimozide	Cambridge Bioscience Ltd	16222-50 Mg-Cay
Prazosin Hydrochloride	Cambridge Bioscience Ltd	15023-50 Mg-Cay
Trifluoperazine Hydrochloride	Cambridge Bioscience Ltd	15068-1 G-Cay
Perhexiline Maleate	Cambridge Bioscience Ltd	16982-5 Mg-Cay

Quinacrine Hydrochloride	Cambridge Bioscience Ltd	15041-100 Mg-Cay
Paroxetine Hydrochloride	Cambridge Bioscience Ltd	14998-10 Mg-Cay
Thioridazine Hydrochloride	Cambridge Bioscience Ltd	14400-1 G-Cay
Desloratidine	Cambridge Bioscience Ltd	21847-1 Mg-Cay
Alexidine Hydrochloride	Cambridge Bioscience Ltd	13876-10 Mg-Cay
Cepharanthine	Cambridge Bioscience Ltd	19648-50 Mg-Cay
Toremiphene Citrate	Cambridge Bioscience Ltd	20854-50 Mg-Cay
Maprotiline Hydrochloride	Cambridge Bioscience Ltd	15892-50 Mg-Cay
Metergoline	Cambridge Bioscience Ltd	21336-10 Mg-Cay
Doxorubicin	Cambridge Bioscience Ltd	15007-5 Mg-Cay
Loperamide Hydrochloride	Cambridge Bioscience Ltd	L5660-5 G
Sertraline Hydrochloride	Cambridge Bioscience Ltd	14839-5 Mg-Cay
Raloxifene Hydrochloride	Cambridge Bioscience Ltd	10011620-50 Mg-Cay
Amoxapine	Cambridge Bioscience Ltd	17347-100 Mg-Cay
Doxazosin Mesylate	Cambridge Bioscience Ltd	18633-100 Mg-Cay
Carvedilol	Cambridge Bioscience Ltd	15418-50 Mg-Cay
Florfenicol	Cambridge Bioscience Ltd	19458-500 Mg-Cay
Azelastine Hydrochloride	Cambridge Bioscience Ltd	Cay20873-10 Mg
Trimipramine Maleate	Cambridge Bioscience Ltd	15921-1g-Cay
Tilorone Hydrochloride	Cambridge Bioscience Ltd	17868-50 Mg-Cay
Aripiprazole	Cambridge Bioscience Ltd	19989-5 Mg-Cay
Terfenadine	Cambridge Bioscience Ltd	20305-500 Mg-Cay
Primaquine Phosphate	Cambridge Bioscience Ltd	18223-1 G-Cay
Daunorubicin	Cambridge Bioscience Ltd	14159-5 Mg-Cay
Mitoxantrone Hydrochloride	Cambridge Bioscience Ltd	14842-10 Mg-Cay
Etodolac	Cambridge Bioscience Ltd	20833-1 G-Cay
Tolazoline Hydrochloride	Cambridge Bioscience Ltd	18865-5 G-Cay
Astemizole	Cambridge Bioscience Ltd	16967-25 Mg-Cay
Mitomycin	Cambridge Bioscience Ltd	11435-1 Mg-Cay

Nisoldipine	Cambridge Bioscience Ltd	20998-100 Mg-Cay
Perhenazine	Cambridge Bioscience Ltd	20735-1 G-Cay
Chloramphenicol Sodium Succinate	Fisher Scientific Uk Ltd	15529483
Amitriptyline Hydrochloride	Fluorochem Ltd	463103-5g
Acriflavinium Hydrochloride	Insight Biotechnology Ltd	Sc-214490
Suloctidil	Insight Biotechnology Ltd	Sc-236957
Benzethonium Chloride	Insight Biotechnology Ltd	Sc-239299
Hexetidine	Insight Biotechnology Ltd	Sc-228301
Pyronaridine Tetraphosphate	Insight Biotechnology Ltd	Sc-205828
Mebhydrolin Naphthalenesulfonate	Insight Biotechnology Ltd	Sc-263459
Prochlorperazine Edisylate	Insight Biotechnology Ltd	Sc-296136b
Chloropyramine Hydrochloride	Insight Biotechnology Ltd	Sc-234345
Oxyclozanide	Insight Biotechnology Ltd	Sc-236264
Triflupromazine Hydrochloride	Insight Biotechnology Ltd	Sc-251335
Lobeline Hydrochloride	Insight Biotechnology Ltd	Sc-203114a
Thonzonium Bromide	Insight Biotechnology Ltd	Sc-396750
Cloperastine Hydrochloride	Insight Biotechnology Ltd	Sc-234405
Chlorhexidine Dihydrochloride	Insight Biotechnology Ltd	Sc-203886
Sodium Phenylbutyrate	Insight Biotechnology Ltd	Sc-200652
Reserpine	Cambridge Bioscience Ltd	16474-1 G-Cay
Methylene Blue	Scientific Laboratory Supplies Limited	Che2584
Ivermectin	Sigma-Aldrich Co Ltd	I8898-250mg
Thiothixene	Sigma-Aldrich Co Ltd	1665003-250mg
Trimeprazine Tartrate	Sigma-Aldrich Co Ltd	1689001-200mg
Citalopram Hydrobromide	Sigma-Aldrich Co Ltd	Phr1640-1g
Penbutolol Sulfate	Sigma-Aldrich Co Ltd	P0307000
Fluoxetine	Sigma-Aldrich Co Ltd	F-918-1ml
Benzyl Isothiocyanate	Sigma-Aldrich Co Ltd	252492-5g
Proflavine Hemisulfate	Sigma-Aldrich Co Ltd	P2508-10g
Thiram	Sigma-Aldrich Co Ltd	T24201-5g
Amsacrine	Sigma-Aldrich Co Ltd	A9809-10mg

Perphenazine	Sigma-Aldrich Co Ltd	P6402-1g
Gentian Violet	Sigma-Aldrich Co Ltd	48770-25g
Emetine Dihydrochloride	Sigma-Aldrich Co Ltd	E2375-500mg
Thimerosal	Sigma-Aldrich Co Ltd	30376-100mg
Merbromin (Mercury) Dibromofluorescin Disodium)	Sigma-Aldrich Co Ltd	M7011-10g
Methylbenzethonium Chloride	Sigma-Aldrich Co Ltd	M7379-10g
Ouabain	Sigma-Aldrich Co Ltd	O3125-250mg
Hexachlorophene	Sigma-Aldrich Co Ltd	40323
Progesterone	Sigma-Aldrich Co Ltd	P8783-1g
Arsenic Trioxide	Sigma-Aldrich Co Ltd	202673-5g
Desipramine Hydrochloride	Sigma-Aldrich Co Ltd	D3900-1g
Dichlorophen	Sigma-Aldrich Co Ltd	133221-50g
Menadione	Sigma-Aldrich Co Ltd	M5750-25g
Dibucaine Hydrochloride	Sigma-Aldrich Co Ltd	D0638-1g
Pridinol Methanesulfonate	Sigma-Aldrich Co Ltd	P4419-5g
Benzalkonium Chloride	Sigma-Aldrich Co Ltd	12060-5g
Crotamiton	Sigma-Aldrich Co Ltd	128201-5g
Pyridostigmine Bromide	Sigma-Aldrich Co Ltd	P9797-1g
Penfluridol	Stratech Scientific Ltd	S4151-Sel-50mg
Sirolimus	Stratech Scientific Ltd	S1039-Sel-5mg
Chloroxylenol	Stratech Scientific Ltd	S4518-Sel-100mg

2.6.2 Antibodies

The antibodies used in this study are listed below in

Table 5. List of Antibodies

Antibody	Vendor	Cat No.	Dilution (Application)
TFEB rabbit polyclonal	Cell Signaling	4240	1:1000 (WB), 1:250 (IF)
TFE3 rabbit polyclonal	Sigma-Aldrich	HPA023881	1:5000 (WB)
MITF			1:1000 (WB)
Actin (AC-40) mouse monoclonal	Sigma-Aldrich	A4700	1:1000 (WB)
HA (HA-7) mouse monoclonal	Sigma-Aldrich	H3663	1:500 (IF)
ERK (C-14) rabbit polyclonal	Santa Cruz	sc-154	1:10000 (WB)
GAPDH rabbit polyclonal	Sigma-Aldrich	G9545	1:20000 (WB)
Histone H3 rabbit polyclonal	Abcam	ab1791	1:5,000 (WB)
p70 S6 Kinase (C-18) rabbit polyclonal	Santa Cruz	sc-230	1:1000 (WB)
S6 Ribosomal Protein (5G10) rabbit monoclonal	Cell Signaling	2217	1:1000 (WB)
Phospho ERK1/2 (T202/Y204) rabbit polyclonal	Cell Signaling	4377	1:1000 (WB)
Phospho p70 S6 Kinase (T389) rabbit polyclonal	Cell Signaling	9205	1:1000 (WB)
Phospho-S6 Ribosomal Protein (Ser235/236) rabbit polyclonal	Cell Signaling	2211	1:1000 (WB)
Phospho-AKT (Ser473) rabbit polyclonal	Cell Signaling	9271	1:2000 (WB)
AKT rabbit polyclonal	Cell Signaling	9272	1:2000 (WB)
Phospho-GSK3β (S9) rabbit polyclonal	Cell Signaling	9336	1:2000 (WB)

GSK3α/β (21A) mouse monoclonal	Life Technologies	44-610	1:2000 (WB)
Phospho-ULK1 (S757) rabbit polyclonal	Cell Signaling	6888	1:1000 (WB)
ULK1 (D8H5) rabbit monoclonal	Cell Signaling	8054	1:1000 (WB)
SGK1 rabbit polyclonal	Cell Signaling	12103	1:1000 (WB)
LC3B rabbit polyclonal	Cell Signaling	2775	1:1000 (WB)
Phospho-TFEB (Ser142) Rabbit polyclonal	Generon,	Custom-made	1:1000 (WB)
Phospho-TFEB (Ser138) Rabbit polyclonal	Generon,	Custom-made	1:1000 (WB)
Phospho-TFEB (Ser122) Rabbit polyclonal	Generon,	Custom-made	1:1000 (WB)
Phospho-TFEB (Ser211) Rabbit polyclonal	Generon,	Custom-made	1:1000 (WB)
Donkey anti-Rabbit IgG (H+L) Highly Cross-Adsorbed Secondary Antibody, Alexa Fluor 488	Thermo Fisher Scientific	A-21206	1:5000 (IF)
Donkey anti-Mouse IgG (H+L) Highly Cross-Adsorbed Secondary Antibody, Alexa Fluor 546	Thermo Fisher Scientific	A10036	1:5000 (IF)

2.6.3 Plasmids

The plasmids used in this study are listed below in **Table 6**.

Table 6. List of Plasmids

Number	Name	Description	Source
1	pPB-iCMV-TFEB-GFP	Full-length human TFEB tagged N-terminally with GFP in a Tet-on piggybac vector containing transposon elements	Available in the laboratory
2	pPB-iCMV-TFEB (S138A)-GFP	Same as #1 but Serine 138 mutated to an Alanine by SDM	Available in the laboratory
3	pPB-iCMV-TFEB(S142A)-GFP	Same as #1 but Serine 142 mutated to an Alanine by SDM	Available in the laboratory
4	pPB-iCMV-TFEB(S211A)-GFP	Same as #1 but Serine 211 mutated to an Alanine by SDM	Available in the laboratory
5	pPB-iCMV-TFEB(S122A)-GFP	Same as #1 but Serine 211 mutated to an Alanine by SDM	Prepared by the candidate
6	pPB-iCMV-TFEB-3XHA	Full-length human TFEB tagged N-terminally with 3XHA in a Tet-on piggybac vector containing transposon elements	Available in the laboratory
7	NanoLuc®-PRKAA1 Fusion Vector	Transfection-ready DNA to express full-length PRKAA1 kinase fused to NanoLuc® Luciferase. Measures kinase target engagement in live cells. Used with the NanoBRET® TE Intracellular Kinase Assay.	Promega

2.6.4 Primers and Oligos

The primers and oligos used in this study are listed below in **Table 7**.

Table 7. List of primers/oligos

Name	Description	Sequence (5'→3')
siRNA control	Control siRNA	Scrambled
Human TFEB siRNA	Knockdown	GGUUCAACAUCAAUGACCGTT
Human TFE3 siRNA	Knockdown	TCGCAGGCGATTCAACATTAA
Human MITF siRNA	Knockdown	AGCAGUACCUUUCUACCACTT
TFEB gRNA Ex.3.3 TS	CRISPR/CAS9 KO	CACGTGGACGGGGGTATTGATGGCA
TFEB gRNA Ex.3.3 BS	CRISPR/CAS9 KO	AAACGCCATCAATACCCCCGTCCAC
TFEB gRNA Ex.5.3 TS	CRISPR/CAS9 KO	CACGTTTCAGGATTGATGTAGCCAA
TFEB gRNA Ex.5.3 BS	CRISPR/CAS9 KO	AAACTGGCTACATCAATCCTGAAAC
TFE3 gRNA Ex1.3 TS	CRISPR/CAS9 KO	CACGTCGAGCCGTGTTCGTGCTGTA
TFE3 gRNA Ex1.3 BS	CRISPR/CAS9 KO	AAACACAGCACGAACACGGCTCGAC
TFE3 gRNA Ex2.3 TS	CRISPR/CAS9 KO	CACGACTCTTTGCTTCCGGAATCCA
TFE3 gRNA Ex2.3 BS	CRISPR/CAS9 KO	AAACGGATTCCGGAAGCAAAGAGTC

Chapter 3: Nutrient availability influences nuclear import and nuclear export of TFEB via changes in phosphorylation status

3.1 Introduction

The ability of cells to respond to environmental changes is critical for their survival and homeostasis. In response to nutrient deprivation, the MiT/TFE family members of transcription factors undergo a plethora of rapid post-translational modifications in order to facilitate nuclear translocation. Two of the family members, Transcription Factor EB (TFEB) and Transcription Factor binding to the IGHM Enhancer 3 (TFE3) are primarily regulated through tight control of their subcellular localisation. Under nutrient-rich conditions, TFEB/3 interact with Rag proteins at the surface of the lysosome via their N-terminal lysosomal attachment domain (LAD) and are phosphorylated by mTORC1 on serine 211 and serine 321, respectively. This phosphorylation event leads to their cytoplasmic retention, enabling the binding of the 14-3-3 chaperone protein. Additionally, mTORC2 can indirectly regulate TFEB and TFE3 subcellular localisation via post-translational modifications made by downstream kinases such as Protein Kinase B (PKB/AKT) and Glycogen Synthase Kinase 3 (GSK3β).

Conversely, when cells are deprived of amino acids, mTORC1 becomes inactivated and can no longer phosphorylate TFEB/3 on their respective phosphorylation sites. Simultaneously, phosphatases such as the calcium activated Calcineurin, and Protein Phosphatase 2A (PP2A) can actively dephosphorylate TFEB/3 in response to nutrient-limitation, lysosomal dysfunction and oxidative stress which also enhance nuclear translocation. Once in the nucleus, TFEB/3 promote the expression of genes to restore the balance between nutrient supply and demand, as well as promoting cell survival under prolonged stress.

Although nuclear import of the MiT/TFE family in response to amino acid deprivation has been well studied, the following questions remained:

1. How do cells respond to different types of nutrient stress, such as glucose deprivation?
2. How do the transcription factors TFEB/3 get exported back into the cytoplasm when the balance between nutrient supply and demand is restored?

This chapter aims to address these questions and focuses on how cells integrate different types of nutritional stress and how both nuclear import and export are tightly regulated through dynamic, reversible phosphorylation events.

3.2 Results

3.2.1 TFEB exhibits dynamic and reversible cytoplasmic-nuclear shuttling in response to changing amino acid and glucose levels

With a focus on TFEB and TFE3 post-translational regulation, we first selected the cancer cell lines HeLa and HT29 that express both TFEB and TFE3 but not MITF, allowing us to study them in isolation. To explore the dynamics of TFEB subcellular localisation in response to nutrient-limitation, we firstly starved cells of amino acids for up to 6 hr. After, we performed immunofluorescence to visualise changes in subcellular localisation of TFEB and western blot analysis to examine the signaling pathways implicated.

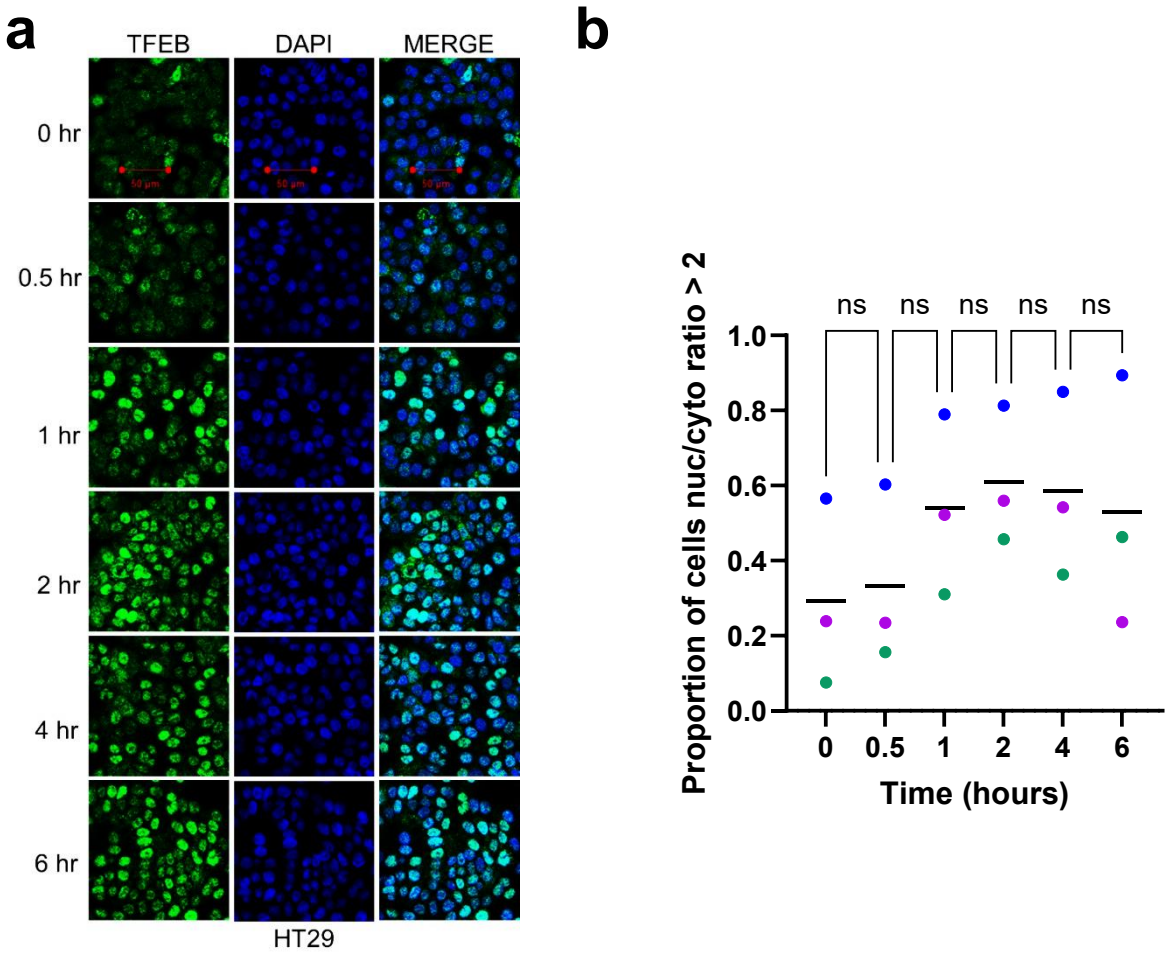

Figure 6. TFEB translocates to the nucleus upon amino acid deprivation
(a) Representative immunofluorescence images taken of HT29 starved of Amino Acids for 0-6 hrs using an antibody against endogenous TFEB (green) and DAPI as a nuclear dye (blue) along with merged image of both TFEB and DAPI to show co-localisation. Scale bars are shown in red (50 μM). (b) Scatter plot showing proportion of cells exhibiting nuclear TFEB staining (defined as having a TFEB nuc/cyto ratio of 2 or greater) from the immunofluorescence images (black bars = mean). Biological replicates are colour coded. TFEB accumulates in the nucleus over time in response to amino acid deprivation. One-Way Anova was performed on three biological replicates (n>1000 cells per condition, N=3). ns = not significant, *= p value < ****P < 0.0001, *** P < 0.001, ** P < 0.01, * P < 0.05.

Despite the immunofluorescence images demonstrating amino acid starvation induced rapid changes in TFEB subcellular localisation, there was no significant change in the proportion of cell exhibiting nuclear TFEB staining (**Figure 6**). However, this is likely due to biological variation exhibited by the replicates (colour coded). Despite this, the proportion of cells exhibiting nuclear staining does increase visually. The effect of amino acid starvation upon nuclear translocation of TFEB appears to be time-dependent with the proportion of cells exhibiting nuclear TFEB staining increasing over time and plateauing from 2 hr onwards.

Most studies have focussed on amino acid limitation as regulating TFEB/3 subcellular localisation, largely neglecting the effects of other carbon sources. Therefore, we investigated how glucose limitation regulates TFEB subcellular localisation by performing a time-course experiment (0-6 hr) followed by immunofluorescence **(Figure 7).** We chose to only starve cells for up to 6 hr to observe early changes in the adaptive response to starvation.

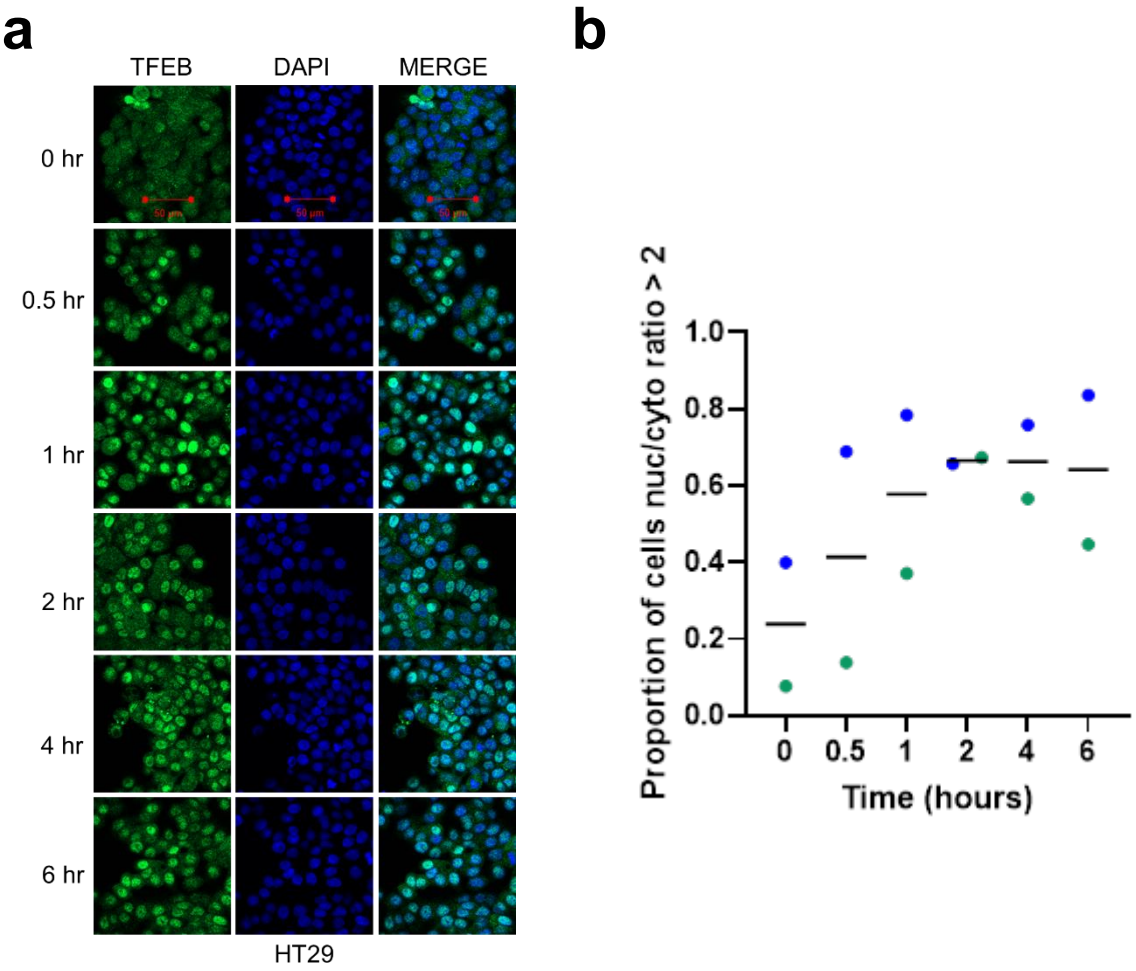

Figure 7. TFEB translocates to the nucleus upon glucose deprivation
(a) Representative immunofluorescence images from two independent experiments demonstrating in HT29, TFEB translocates to the nucleus upon glucose deprivation in a time-dependent manner. Scale bars are shown in red (50 μM). (b) Scatter plot showing proportion of cells with a nuc/cyto ratio of 2 or greater from the immunofluorescence images (black bars = mean). Biological replicates are colour coded. TFEB accumulates in the nucleus over time in response to glucose deprivation.

Similarly, glucose starvation promoted a time-dependent increase in the proportion of cells exhibiting nuclear TFEB staining, increasing over time and plateauing from 2 hr onwards. **(Figure 7).**

To illustrate the dynamics of TFEB subcellular localisation, cells were starved of amino acids, glucose or treated with Torin 1 (an mTORC1/2 inhibitor) for 2 hr. After, samples were subjected to subcellular fraction (**Figure 8**).

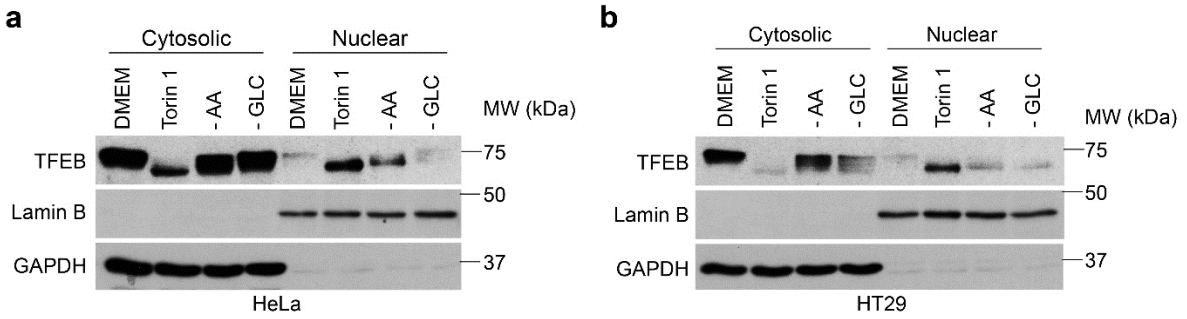

Figure 8. Demonstrating TFEB translocation dynamics in response to glucose starvation, amino acid starvation or pharmacological inhibition of mTORC1/2 with Torin. (a-b) Western blot analysis of cytoplasmic and nuclear fractions, illustrating TFEB cytoplasmic-nuclear shuttling in response to glucose starvation (2 hr), amino acid starvation (2 hr) and pharmacological inhibition of mTORC1 and mTORC2 with Torin (10 μM, 2 hr) in HeLa and Ht29 cell lines respectively.

As expected, in response to mTORC1/2 inhibition by Torin treatment, both HeLa and Ht29 exhibited higher levels of TFEB in their nuclear fraction vs their cytosolic fraction using Lamin B and GAPDH as markers of the fractionated extracts (Fig 3 a, b). In response to amino acid deprivation, both cell lines exhibited higher levels of TFEB in their nuclear vs cytosolic fractions than when compared to the unstarved (DMEM) control. However, in response to glucose deprivation, only a slight increase in the nuclear vs cytoplasmic ratio of TFEB was observed. Notably, pharmacological inhibition of mTORC1/2 by Torin promotes nuclear translocation more robustly than physiological starvation. However, there is an observable shift in the ratio of nuclear vs cytoplasmic retention of TFEB dependent on nutrient availability. Interestingly, HeLa appear to be less responsive to glucose starvation than HT29, as evidenced by TFEB still remaining largely cytoplasmic. In addition, we observed a decrease in the total levels of TFEB in response to glucose deprivation, a phenomenon we also observe in later chapters**.**

To visualise the reversibility of TFEB subcellular localisation upon nutrient refeeding, cells were starved for 2 hr or starved for 1.5 hr before ‘refeeding’ and immunofluorescence was

performed **(Figure 9)**. Torin 1 and DMSO (0.1%) were used as a positive and negative control respectively.

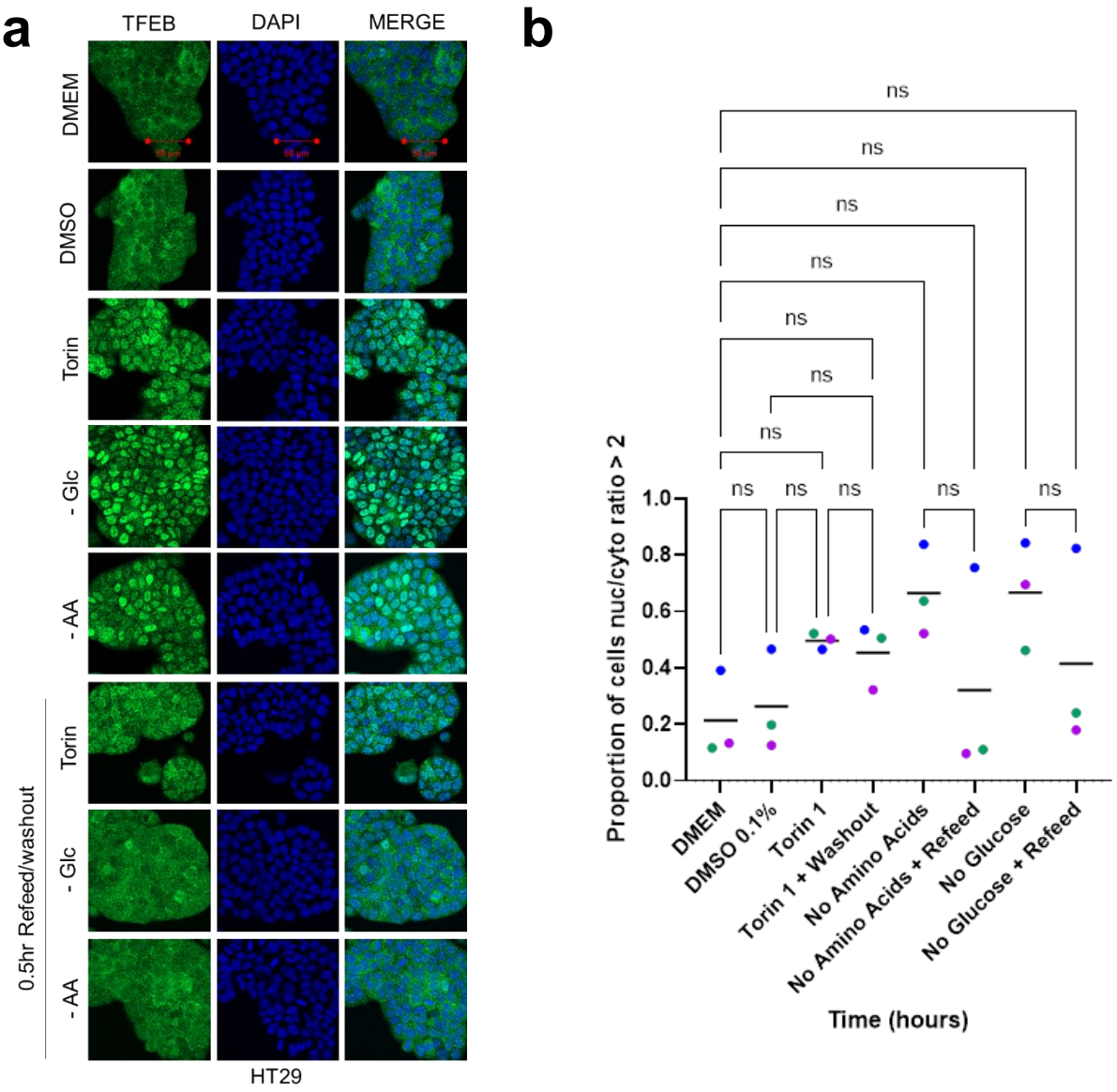

Figure 9. Nuclear translocation of TFEB is reversible
(a) Representative immunofluorescence images demonstrating in HT29, TFEB translocates to the nucleus upon starvation of either amino acids and glucose deprivation or treatment with Torin (10 μM) for 2 hr. However, upon re-addition of nutrients or drug washout (30 min), whereby the media is replaced with DMEM, TFEB translocates out of the nucleus. Scale bars are shown in red (50 μm). (b) Scatter plot showing proportion of cells with a TFEB nuc/cyto ratio of 2 or greater from the immunofluorescence images (black bars = mean). Biological replicates are colour coded. One-Way Anova was performed on two biological replicates (n>1000 cells per condition, N=2). ns = not significant, *= p value < ****P < 0.0001, *** P < 0.001, ** P < 0.01, * P < 0.05.

Despite TFEB translocation appearing to be readily reversible within 30 mins of re-feeding starved cells with glucose/amino acids from the immunofluorescence images **(Figure 9a),** changes in the proportion of cells exhibiting nuclear TFEB staining were not statistically

significant **(Figure 9b)**. As previously mentioned, this is likely due to large biological variation exhibited by the replicates. Notably, removal of Torin 1 was less efficient at reversing translocation of TFEB visually when compared to the reversal observed when starved cells were re-fed **(Figure 9a and b)**. This is likely due to Torin 1 still being present intracellularly, despite replacement of media. Additionally, the TFEB nuclear/cytoplasmic ratio did not return to that of unstarved/untreated cells. However, if given longer to recover after the media was replenished, we would expect it would do so.

Overall, these results demonstrate that although translocation of TFEB appears to be reversible visually, our quantification method did not detect any significant changes, most likely due to large biological variation exhibited by the replicates.

3.2.2 Amino acid deprivation inhibits mTORC1 whereas glucose deprivation activates mTORC2

We next performed a starvation time-course in HeLa **(Figure 10)** and HT29 **(Figure 11)** to demonstrate the different signalling pathways that are affected by amino acid or glucose deprivation. After being starved, whole cell protein lysates were collected and the mTORC1 and mTORC2 pathways interrogated by western blot analysis.

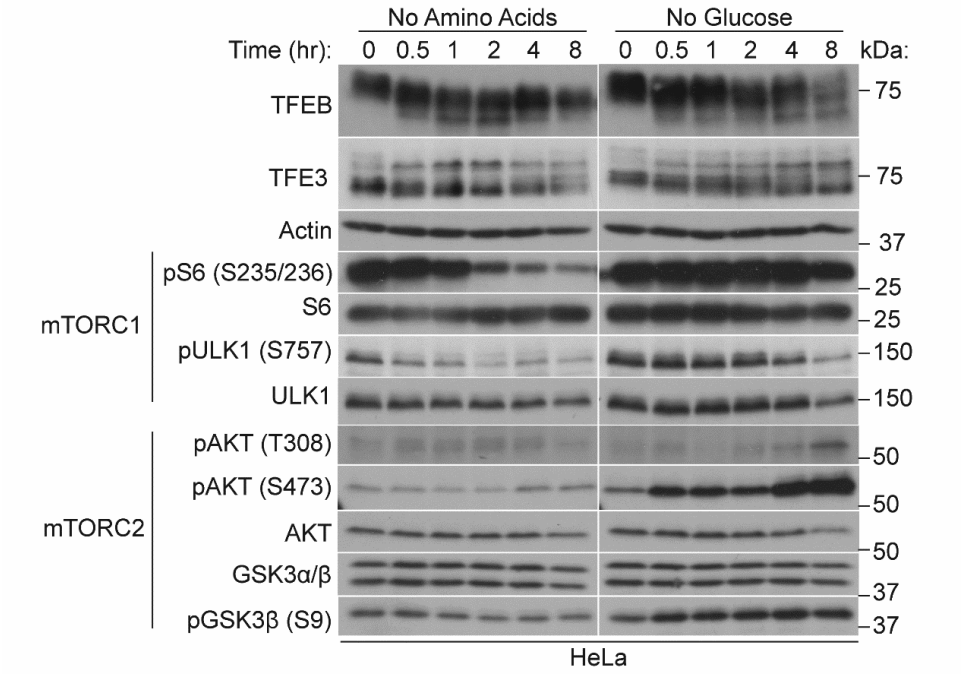

Figure 10. Amino acid deprivation inhibits mTORC1, whereas glucose deprivation activates mTORC2
Western blot analysis of HeLa starved of either amino acids or glucose (0-8 hr). The activity of the mTORC1/2 complexes were assessed by visualising the phosphorylation of downstream targets. Additional loading controls used are shown in Supplemental Figure 1.

As expected, in response to amino acid deprivation, there is a notable mobility shift observed for both TFEB and TFE3 in HeLa **(Figure 10, left panel)**, presumably due to loss of numerous phosphorylation marks enabling their nuclear entry. By 2 hr, there is a notable decrease in mTORC1 activity; indicated by an observable decrease in phosphorylation of downstream targets S6 and ULK1 **(Figure 10, left panel).** In comparison, mTORC2 activity is largely unaffected and appears to remain inactive with no observable changes to phosphorylation of its downstream target S473 AKT, or the AKT target S9 GSK3β **(Figure 10, left panel)**.

Similarly, in response to glucose deprivation, there is a notable mobility shift observed for both TFEB and TFE3 **(Figure 10, right panel).** However, mTORC1 remains active; indicated by no observable changes in pS6 or pULK1 levels up to 4 hr after glucose deprivation **(Figure 10, right panel).** However, by 2 hr, mTORC2 becomes active and by 4 hr, even more so, as visualised by incremental increases in pSer473 AKT levels **(Figure 10, right panel).** Additionally, by 8 hr we observed a small increase PI3K activity, as observed by an increase in pThr308 AKT levels **(Figure 10, right panel).**

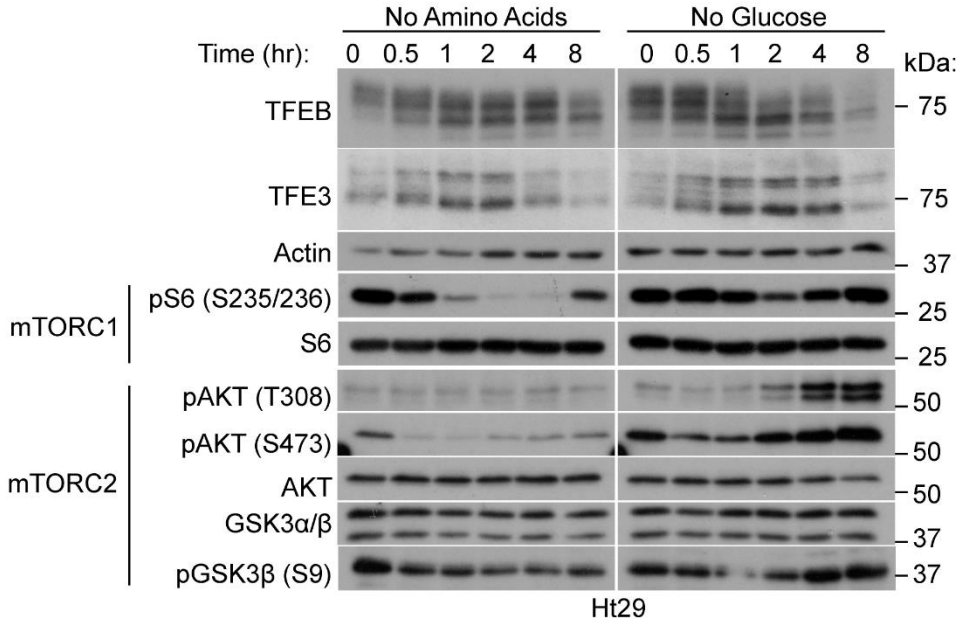

Figure 11. Amino acid deprivation inhibits mTORC1, whereas glucose deprivation activates mTORC2
Western blot analysis of HT29 starved of either amino acids or glucose (0-8 hr). The activity of the mTORC1/2 complexes were assessed by visualising the phosphorylation of downstream targets. Additional loading controls used are shown in Supplemental Figure 2.

Similarly, to the results observed in HeLa **(Figure 10)**, in response to amino acid deprivation in HT29 cells, we observed a mobility shift for both TFEB and TFE3 **(Figure 11, left panel),** most likely due to loss of numerous phosphorylation marks enabling their nuclear entry. By 1 hr, there is a notable decrease in mTORC1 activity; indicated by an observable decrease in pS6 levels **(Figure 11, left panel)**. In comparison, mTORC2 activity remains largely unaffected with minimal changes in the phosphorylation status of pS9 GSK3β. Notably, there was a slight increase in the phosphorylation status of pS473 AKT after the initial loss observed by 0.5 hr **(Figure 11, left panel).**

Similarly, in response to glucose deprivation, there is a notable mobility shift observed for both TFEB and TFE3 **(Figure 11, right panel)**. Unlike amino acid deprivation, mTORC1 activity remains largely unaffected, although a small decrease in pS6 levels was observed at 2 hr, but increases again by 4 hr. **(Figure 11, right panel)**. Conversely, by 2 hr, mTORC2 becomes active and by 4 hr, even more so, as indicated by increases in pSer473 AKT levels **(Figure 11, right panel)**. Additionally, by 2 hr we observed a small increase in PI3K activity as observed by an increase in pThr308 AKT which further increases by 8 hr **(Figure 11. right panel)**.

Although there are minor differences between the perceived speed at which, HeLa and HT29 respond to amino acid and glucose deprivation, both cell lines respond in similar fashion in a time-dependent manner.

3.2.3 TFEB and MITF have a conserved nuclear export signal that requires hierarchal phosphorylation events

Whilst exploring how the MiT/TFE family members are re-exported out upon re-feeding, our lab identified a conserved nuclear export signal in TFEB and MITF and their importance in cytoplasmic-nuclear shuttling in response to nutrient availability. After, they demonstrated that nuclear export could be blocked by mutating phospho-sites (serine to alanine) on sites serine 138 and 142 in TFEB and serine 69 and 73 in MITF.

Interestingly, it has already been demonstrated that GSK3β can phosphorylate TFEB *in vitro* on serine 134 and 138 (Li et al. 2016). However, this group failed to recognise that GSK3β favours a consensus sequence of S/T-XX-X-pS/pT (S: serine, T: threonine, pS: phospho-serine, pT: phospho-threonine, X: any amino acid) (Dianqing Wu and Pan 2010) and thus requires a priming phosphorylation event to bind.

Our group previously demonstrated that mutation of phosphorylation sites S142 or S138 in TFEB; adjacent to an evolutionarily conserved nuclear export signal blocked nuclear export

upon nutrient refeeding (Li et al., 2018). Furthermore, inhibition of GSK3β using a pharmacological inhibitor; BIO, also prevented nuclear export of TFEB.

Taken together, this data suggested that GSK3β promotes TFEB nuclear export via phosphorylation of S138. Using a peptide array, we demonstrated that GSK3β could indeed phosphorylate S138/S69 on TFEB/MITF, but only when S142/S73 was phosphorylated. However, peptide arrays may yield false positive results due to the short length of the peptides. To circumvent this, we performed an *in vitro* kinase assay using much longer protein fragments.

Firstly, we expressed and purified N-terminally histidine-tagged TFEB/MITF fragments using gravity-flow columns with an Ni-NTA resin. Molecular weights were confirmed by SDS-PAGE followed by Coomassie-staining. Due to the insoluble nature of these transcription factors, we only expressed the N-terminal half of both TFEB and MITF (excluding their DNA-binding domains) and protein fractions were purified under denaturing conditions. After, eluted fractions were pooled and dialysed for 48 hr to remove urea and imidazole **(Figure 12a, b)**. The precise molecular weights of 6xHis-TFEB (1-200) and 6xHis-MITF (1-105) were confirmed by Time-of-Flight Mass Spectrometry **(Figure 12c, d)**.

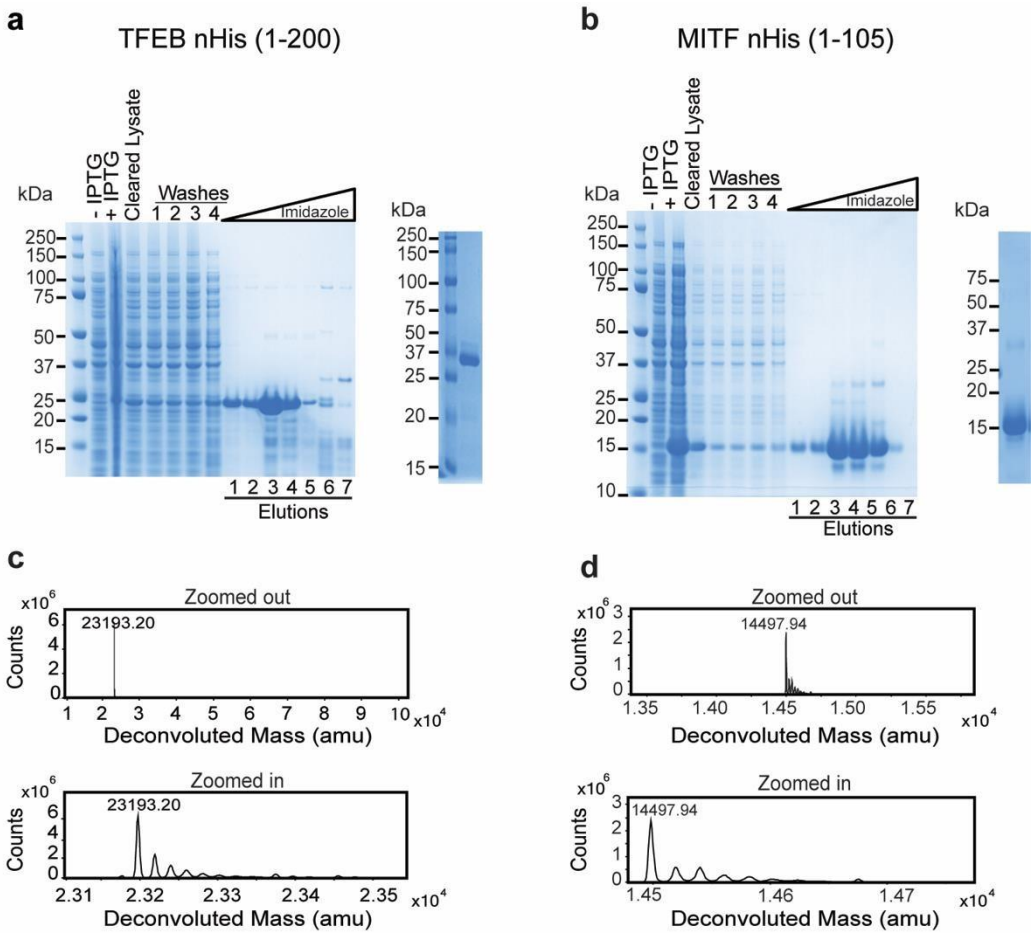

Figure 12. Purification of bacterially-expressed N-terminally histidine-tagged TFEB (1-200 aa) and MITF (1-105) (a-b) Left, Coomassie-stained gels of bacterially expressed and purified 6xHis-tagged TFEB (1-200 aa.) ladder with molecular weights shown (kDa), before induction with IPTG, after induction with IPTG (0.1 mM), and MITF (1-105 aa) respectively under denaturing conditions (6 M urea). From left to right: protein cleared lysate, 4 washes with lysis buffer, 7 elution steps with increasing imidazole concentrations (50-250 mM). Right, Coomassie-stained gels of dialysed 6XHis-TFEB (1-200 aa) and 6XHis-MITF (1-105) after purification. (c-d) Deconvoluted spectra (top: zoomed out and bottom: zoomed in) from ToF MS of 6XHis TFEB (1-200 aa) and 6XHis-MITF (1-105 aa) showing correct molecular weights of 23.193 kDa and 14.498 kDa. *Data shown was generated by the candidate and is published in Li et al., 2018 and Ngeow et al., 2018 respectively.*

After successfully purifying 6xHis-TFEB (1-200) and 6xHis-MITF (1-105) from bacteria, we set out to demonstrate the hierarchal phosphorylation events that occur. We ordered custom-made antibodies to recognise the specific phosphorylation events involved in TFEB nuclear import/export; pS138, pS142, pS122 and pS211. In order to validate antibody specificity, we performed western blot analysis in HT29 over-expressing either wild-type TFEB or phospho-mutant forms whereby the respective phosphorylation site was mutated from a serine to an alanine; S122A, S138A, S142A and S211A **(Figure 13)**.

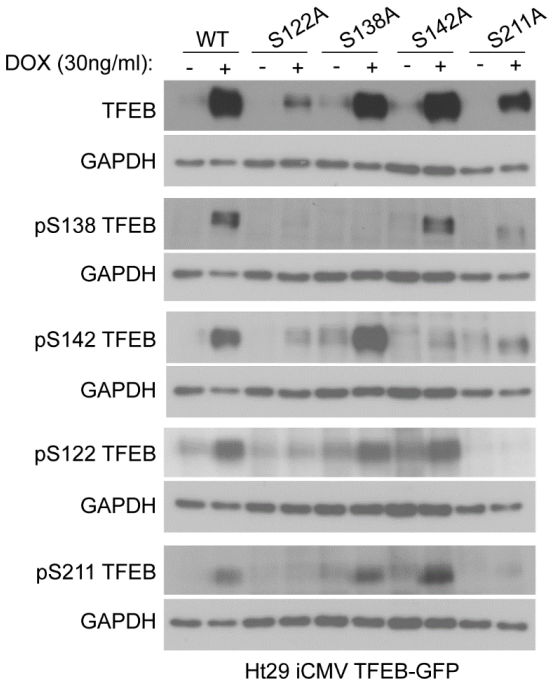

Figure 13. Validation of custom-made antibodies using TFEB phospho-mutants
Western blot analysis of HT29 over-expressing Wild-Type TFEB, or phospho-mutants S122A, S138A, S142A or S122A all tagged with a c-terminal GFP tag. Expression of TFEB-GFP was induced with 30 ng/mL doxycycline overnight before whole cell lysates were collected. Immunoblotting was performed using an antibody that can recognise total levels of TFEB and custom-made antibodies.

As expected, when over-expressing WT TFEB-GFP, there was a signal obtained using all five antibodies **(Figure 13, Lanes 1, 2)**. When over-expressing S122A TFEB-GFP and using the custom-made TFEB pS122 antibody, we saw a reduction in signal compared to the WT TFEB-GFP cell line **(Figure 13, Lanes 3, 4)**. However, we observed a reduction in signal when using all antibodies, including the antibody recognising total TFEB levels, demonstrating that the total expression level of TFEB-GFP was lower in this cell line. Therefore, we could not conclude that the pS122 antibody was specific or if the decrease in signal intensity was simply due to there being less TFEB-GFP expressed in this cell line. When over-expressing S138A TFEB-GFP and using the TFEB pS138 antibody, we observed complete ablation of the signal **(Figure 13, Lanes 5, 6)**. However, when using the other antibodies, recognising pS122, pS142 and pS211, the intensity of the signal remained unchanged, demonstrating the specificity of the pS138 antibody. Similarly, when we over-expressed pS142 TFEB-GFP, and used the pS142 TFEB antibody we saw a reduction in the signal compared to the WT TFEB-GFP expressing cell line **(Figure 13, lanes 7, 8)**. However, when using the other antibodies, recognising pS122, pS142 and pS211, the intensity of the signal remained unchanged, demonstrating the specificity of the pS142 TFEB antibody. Furthermore, while the pS211 antibody recognised the WT TFEB-GFP protein, the signal was ablated when the S211A

mutant was expressed, demonstrating antibody specificity. However, we also observed that mutating S211 (S211A) reduced the ability of all the phospho-antibodies to recognise TFEB. This could be because the mutation of S211 prevented phosphorylation of TFEB on other sites, for example by increasing the proportion of nuclear TFEB which would not be accessible to cytoplasmic kinases. An unexpected finding was that despite our previous work demonstrating that GSK3 can only phosphorylate S138 when S142 is first phosphorylated (L. Li et al. 2018), the pS138 antibody could still recognise S142A TFEB-GFP **(Figure 13, lane 8, row 3)**. This raised questions as to the specificity of the pS138 antibody.

To further validate the pS138 and pS142 specific antibodies, we performed a peptide array whereby short peptides including these residues were printed onto a membrane and then immunoblotted against (**Figure 14a, b**). The results from the peptide array **(Figure 14a, b)** confirmed that the custom-made antibodies designed to recognise pS138 and pS142 are specific as they were only able to recognise the peptides when phosphorylated at S138 and S142 respectively and not when unphosphorylated or converted to alanine.

To determine if phosphorylation of S138/69 is dependent upon phosphorylation of S142/73 in TFEB and MITF respectively, we performed an *in vitro kinase assay* using the recombinant 6xHis-TFEB (1-200) and 6xHis-MITF (1-105). To do this we used four different conditions: No kinase control, ERK only, GSK3β only or ERK and GSK3β. After the kinase assay, SDS-PAGE was performed followed by Coomassie-staining to demonstrate equal protein loading. After, western blot analysis was performed using the phospho-specific antibodies **(Figure 14c, d)**. The *in vitro* kinase assay revealed that GSK3β was only able to phosphorylate TFEB or MITF on S138/69, when also phosphorylated by ERK on S142/73 respectively.

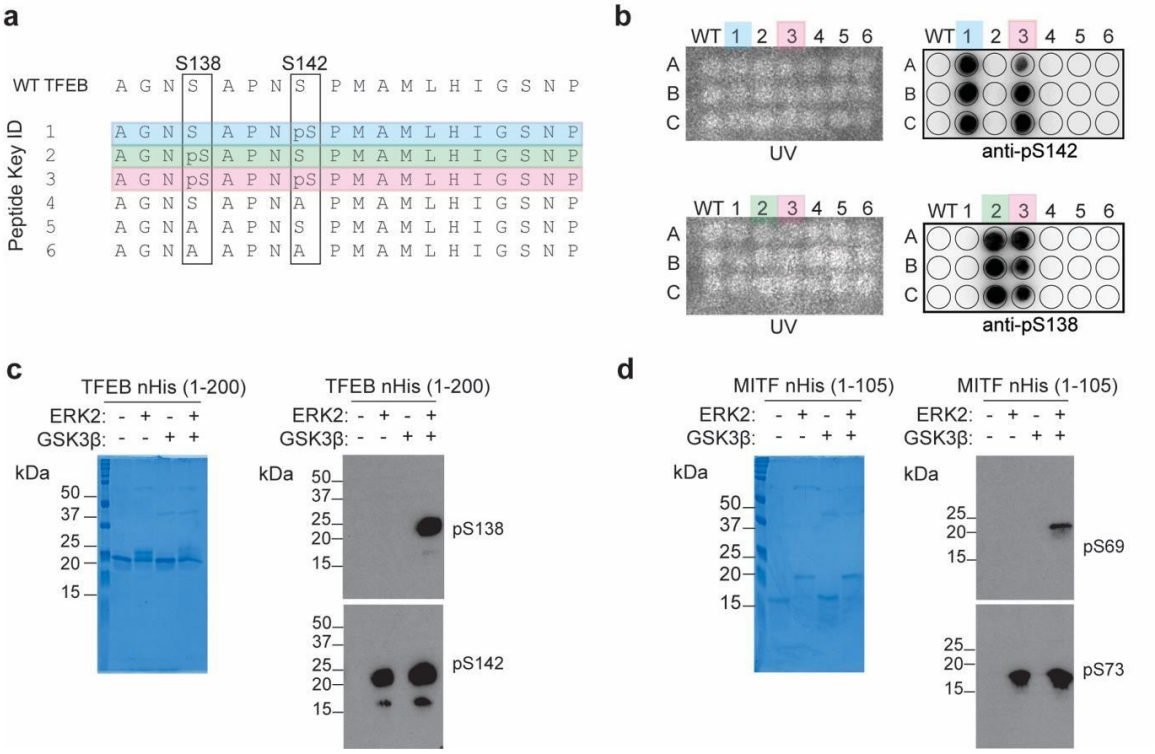

Figure 14. Phosphorylation of S142 and S73 primes for phosphorylation of S138 and S69 by GSK3β in TFEB and MITF respectively. (**a)** Peptide array aa. sequences with the identifying ID numbers labelled 1-6. **(b)** Peptide array probed with either the α-pS142 or the α-pS138 antibody. Left panels show UV traces to illustrate equal peptide printing on dot blot. Right panel shows signal (chemiluminescence) observed when peptide arrays are incubated with α-pS142 and α-pS138 antibodies diluted 1:10,000 in 5% BSA in PBS-T. **(c-d)** *In vitro* kinase assay performed on bacterially-expressed TFEB (1-200) and MITF (1-105) with ERK2 and GSK3β followed by Coomassie stain and western blot analysis with custom-made pS142 and pS138 antibodies. *Data shown was generated by the candidate and is published in Li et al., 2018 and Ngeow et al., 2018 respectively.*

After confirming the *in vitro* kinase assay worked, samples were sent to the Target Discovery Institute (TDI) for phospho-proteomic analysis (George Berridge and Roman Fischer). Peptides with and without phosphorylation on S73/S142 and S69/S138 were detected and spectral counts were calculated **(Figure 15 a, b)**.

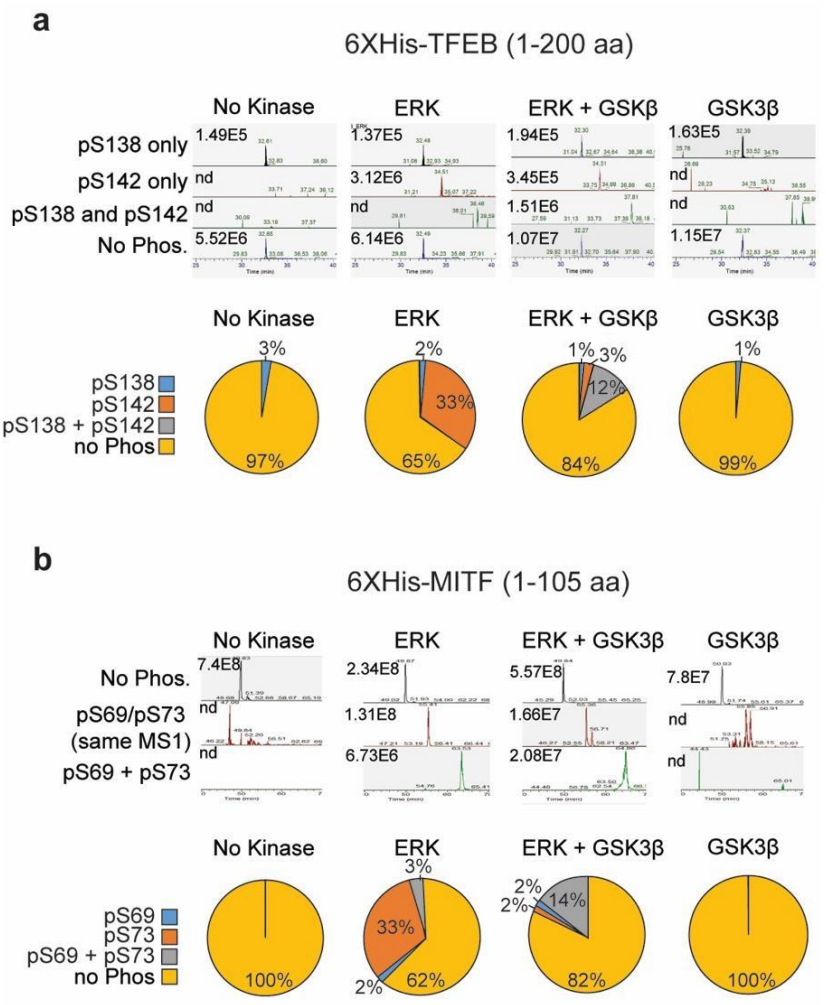

Figure 15. Hierarchal phosphorylation of TFEB and MITF by ERK and GSK3β
(a) Top panel: EICs of tryptic peptides covering S138 and S142 of 6XHis-TFEB (1-200 aa) in their differential phosphorylation states after kinase treatments. Peptides with a single phosphorylation on S138 were detected at low intensity in all samples, including those not treated with GSK3β (background level), while peptides with a phosphorylation event on S142 were only detected in the ERK and GSKβ+ERK treated samples. Peptides dually phosphorylated on both S138 and S142 were detected only after GSKβ+ERK treatment. Numbers represent maximum ion count for each peptide/phospho -peptide. Bottom Panel: Quantification of TFEB in vitro kinase/Mass Spec data. Pie charts show the signal contribution of each (phospho-) peptide variant to total signal intensity covering the analysed phosphorylation locus after different kinase treatments. Assuming that each peptide variant has identical ionization characteristics, the charts reflect the stoichiometry of the different phospho-proteoforms of TFEB (1 -200) after kinase treatment. Data analysis performed by Georgina Berridge (TDI, Oxford) adapted from Li *et al.*, 2018. (b) Top panel: EICs of tryptic peptides covering S73 and S69 of 6XHis MITF (1-105) in their differential phosphorylation states after indicated kinase treatment. A peptide with a single phosphorylation on S69 was detected at low levels only in ERK -treated and ERK+GSK3β samples but not in the no kinase control or in GSK3β-treated samples. A peptide with a single phosphorylation event on S73 was detected at high levels (33%) in the ERK -treated sample and at low levels in the GSKβ+ERK treated samples but not in the no kinase control or in GSK3β -treated samples. Peptides dually phosphorylated on both S73 and S69 were detected only after GSKβ+ERK treatment. Numbers represent maximum ion count for each pep tide/phospho-peptide. Bottom panel: Quantification of MITF in vitro kinase/Mass Spec data. Pie charts show the signal contribution of each phospho-peptide variant to total signal intensity covering the analysed phosphorylation locus after different kinase treatments. Assuming that each peptide variant has identical ionization characteristics, the charts reflect the stoichiometry of the different phospho proteoforms of TFEB after kinase treatment. *Samples produced by the candidate, data analysis performed by Georgina Berridge (TDI, Oxford) adapted from Ngeow et al., 2018*

The majority of the recombinant 6XHis-TFEB (1-200) and 6XHis MITF (1-105) peptides detected were unphosphorylated, indicating that the *in vitro* kinase wasn't 100% efficient **(Figure 15 a, b, first pie chart)**. However, 33% of peptides detected from the ERK only samples for both TFEB and MITF were phosphorylated on S142 and S73 respectively **(Figure 15 a, b, second pie chart)**. Furthermore, we observed peptides detected from the GSK3β only samples for both TFEB and MITF were not phosphorylated on S138/S69 **(Figure 15 a, b, third pie chart)**. Dually phosphorylated peptides for both TFEB and MITF were only detected from samples treated with both ERK and GSK3β S142/73 and S138/69 respectively **(Figure 15 a, b, fourth pie chart)**. These results supported previous work from our lab demonstrating that phosphorylation of TFEB/MITF at S142/73 is a pre-requisite for phosphorylation by GSK3β of S138/69 respectively (Li et al. 2018, Ngeow et al. 2018) A schematic showing our current understanding of how TFEB is modulated through various phosphorylation events is shown below in **Figure 16**.

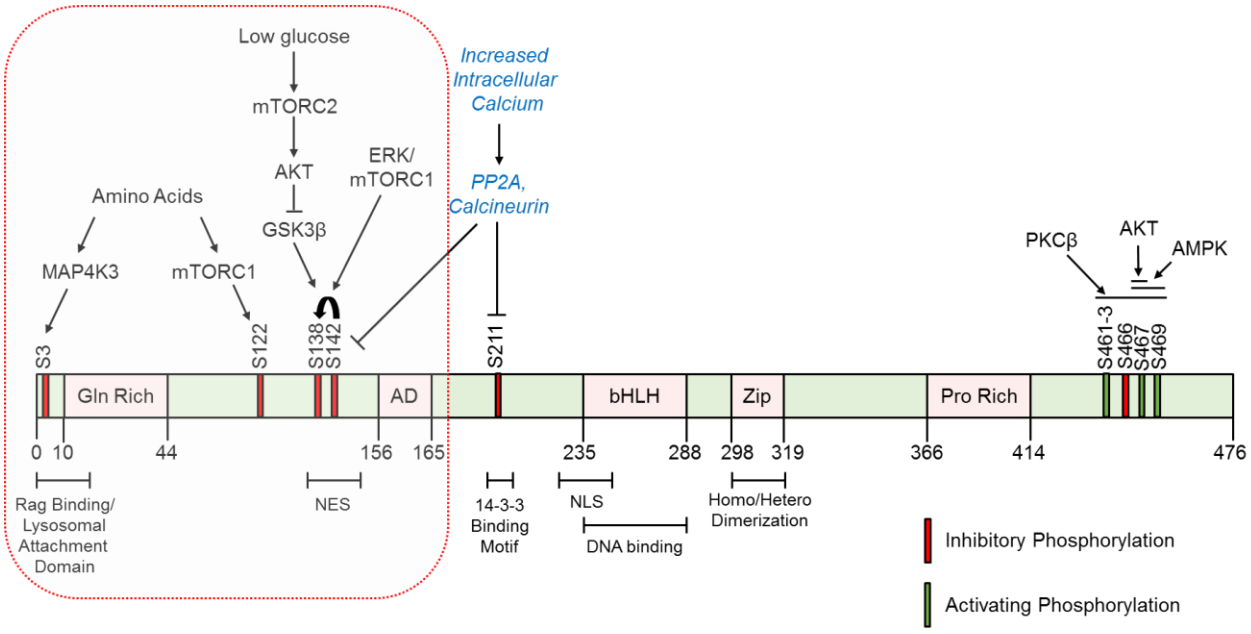

Figure 16. Current understanding of how cells integrate glucose and amino acid availability to elicit changes in TFEB subcellular localisation via phosphorylation events
Diagram demonstrating the complex signaling pathways that are able to control TFEB subcellular localisation in response to changes in amino acid or glucose availability. The work shown in this chapter provided evidence supporting the hypothesis that TFEB nuclear export is regulated by two phosphorylation events. TFEB has to first be phosphorylated on S142 by ERK/mTORC1 before GSK3β can phosphorylate S138; a phosphorylation site our lab had previously shown is required for nuclear export.

3.3 Discussion and future perspectives

Over the last decade, TFEB has emerged to be a key transcription factor in mediating the effects of amino acid limitation. Under nutrient-rich conditions, TFEB is phosphorylated by mTORC1 on S211, a phosphorylation site required for its cytoplasmic retention by the chaperone protein 14-3-3. In response to amino acid deprivation, mTORC1 becomes inactivated, preventing the de novo phosphorylation of TFEB. Synergistically, the activation of phosphatases such as Calcineurin (Medina et al. 2015) and Protein Phosphatase 2A (Martina and Puertollano 2018), lead to active de-phosphorylation of TFEB, further promoting nuclear entry. Upon nuclear entry, TFEB promotes the transcription of genes involved in lysosomal biogenesis, lipid catabolism and autophagy as well as glucose uptake and utilisation. Activation of TFEB in response to amino acid limitation allows cells to adapt in an attempt to re-establish their nutrient supply. Without a nuclear export signal, TFEB would remain nuclear and therefore active, even after nutrient replenishment. Eventually this would be catastrophic to a cell and lead to autophagy-induced apoptosis.

Furthermore, most studies investigating subcellular regulation of TFEB have focused on the effects of amino acid limitation, neglecting other nutrients such as glucose. We demonstrated that glucose deprivation also promotes rapid nuclear accumulation of TFEB. This is unsurprising when considering TFEB targets include genes involved in glucose uptake and utilisation (Mansueto et al. 2017). Additionally, although nuclear import of TFEB and TFE3 have been thoroughly investigated, understanding how cells re-establish cytoplasmic retention of TFEB and TFE3 upon nutrient-replenishment had not been explored.

By immunofluorescence and western blot analysis, we demonstrated that although glucose and amino acid deprivation both provoked nuclear accumulation of TFEB which could be later reversed upon nutrient replenishment, these effects were driven by two distinct mechanisms. We found amino acid deprivation led to inactivation of mTORC1 and subsequent loss of TFEB cytoplasmic retention through loss of phosphorylation marks, namely S211 required for binding to the cytoplasmic anchoring by 14-3-3 (Settembre et al. 2011). Although previous studies have demonstrated that glucose deprivation can lead to inhibition of mTORC1 via activation of AMPK, either directly via inhibition of the mTORC1 component regulatory-associated protein of mTOR (Raptor) (Gwinn et al. 2008), or indirectly through activation of the mTOR negative regulator tuberous sclerosis complex 2 (TSC2) (Inoki, Zhu, and Guan 2003). We found glucose starvation does not impair mTORC1 signaling but instead, activates mTORC2, leading to inhibition of GSK3β activity and prevention of nuclear export (Li et al. 2018), an observation now corroborated by others (Moloughney et al. 2016).

Furthermore, our lab identified a novel nuclear export signal conserved in TFEB, TFE3 and MITF. Mutation of this export signal and adjacent serines resulted in increased nuclear accumulation of TFEB and MITF and an inability to restore cytoplasmic retention of TFEB upon nutrient replenishment. Although a previous study demonstrated the ability of GSK3β to phosphorylate TFEB on S134 and S138 (Li et al. 2016), they did not consider GSK3β requires a priming phosphorylation to bind (Dianqing Wu and Pan 2010). Our results highlight that phosphorylation of S138 by GSK3β can only occur when TFEB is phosphorylated on S142 by ERK/mTORC1 (Li et al., 2018). This hierarchal phosphorylation event required for nuclear export of TFEB, not only allows the rapid reversal of TFEB localisation upon nutrient replenishment, but integration of nitrogen and carbon sources to finely tune TFEB activity. Other groups have since also corroborated our findings by investigating the importance of this nuclear export signal in TFEB (Napolitano et al. 2018).

The identification of the same, conserved nuclear export signal in the melanocyte-specific MITF isoform (MITF-M) is intriguing (Ngeow et al. 2018), owing to the fact it is largely nuclear even under nutrient-rich conditions. However, the MITF gene has a split promoter design (Hershey and Fisher 2005), allowing production of different structurally and biologically distinct proteins; MITF-A, MITF-B, MITF-C, MITF-H, and MITF-M (Hershey and Fisher 2005). The expression of these isoforms ranges from ubiquitous to cell-type specific. For instance, MITF-M is expressed exclusively in melanocytes and melanoma cells, whereas MITF-A and MITF-H are expressed in multiple tissue types, including retinal pigment epithelium, cervical cancer, osteoclasts, and mast cells (Yasumoto et al. 1998). Intriguingly, all of these isoforms, apart from MITF-M, share an n-terminal region (Shibahara et al. 2001) which is remarkably similar to TFEB and TFE3 (Yasumoto et al. 1998) allowing for recruitment to lysosomes required for regulation by mTORC1 and subsequent cytoplasmic retention (Jose A. Martina and Puertollano 2013). Therefore, it appears having a nuclear export signal is perhaps more functionally important in allowing mTORC1-dependent regulation of the other MITF isoforms, enabling their cytoplasmic retention when nutrients are plentiful.

Another notable point is many studies that have used immunofluorescence to measure TFEB subcellular localisation do so by categorising cells as having either nuclear or cytoplasmic TFEB. Not only is this highly subjective, our work demonstrates TFEB subcellular localisation is dynamic, whereby a balance between both nuclear import and export is tightly modulated by nutrient availability. As a consequence, cells do not exhibit exclusively nuclear or cytoplasmic TFEB staining, rather changes in the ratio of nuclear vs cytoplasmic TFEB. To corroborate this, we have recently demonstrated that even under nutrient-rich conditions, when mTORC1 is active, there is still a proportion of TFEB in the nucleus as observed using

ChIP-seq (Dias et al. 2024). In this chapter, we used a reproducible, high-throughput method to quantify changes in subcellular localisation of TFEB in populations of cells, in response to a given treatment removing this subjectivity.

To summarise, these results provide novel insights into the ability of cells to sense and integrate the availability of nitrogen and carbon sources to elicit changes in TFEB and MITF subcellular localisation; through regulating nuclear import and export. Understanding how nuclear export is controlled provides us with more information as to how TFEB activity can be fine-tuned and even targeted therapeutically.

Chapter 4: Re-purposing FDA-approved drugs to promote TFEB nuclear translocation

4.1 Introduction

The MIT/TFE family of transcription factors have been coined 'the master regulators of autophagy and lysosomal biogenesis' (Settembre et al. 2011). Promoter analysis of lysosomal genes demonstrated that they share a common 10-base E-box-like palindromic sequence (GTCACGTGAC), in most cases, within 200 bp pairs of the transcription initiation site. This sequence is often referred to as a 'Coordinated Lysosomal Expression and Regulation' (CLEAR) element. TFEB and TFE3 bind directly to these CLEAR elements to promote autophagy and lysosomal biogenesis (Peskin et al. 2009). These processes are often impaired in a range of neurodegenerative diseases such as Alzheimer's (Sooyeon, Yutaka, and Nixon 2011) and Parkinson's disease (Tanji et al. 2011). It is thought insufficient levels of autophagy and lysosomal biogenesis, leads to the accumulation of misfolded proteins, and the formation of plaques, impairing neuronal cell function.

Many studies have discovered the potential therapeutic benefits of increasing TFEB levels or activities in ameliorating in neurodegenerative disease models. For instance, Gypenoside XVII, a naturally occurring compound found in ginseng, was shown to enhance lysosomal biogenesis and autophagy flux through activation of TFEB in PC12 cells expressing the Swedish mutant of APP695 (APP695swe) and APP/PS1 mice (Meng et al., 2016). Another study demonstrated that activation of TFEB promoted clearance of amyloid-β(1-42) (Aβ(1-42)) in a cell based model of Alzheimer's disease (Xiao et al., 2014). Additionally, TFEB overexpression was shown to ameliorate Aβ(1-42) plaque-induced pathogenesis in an Alzheimer's mouse model (Zhang & Zhao, 2015).

Notably, over-expressing TFEB in humans using viruses is not necessarily a practical therapeutic strategy. Instead, TFEB activity can be increased by promoting nuclear translocation or blocking nuclear export rather than increasing overall protein levels. Thus, exploring how we can fine-tune TFEB subcellular localisation in order to promote lysosomal biogenesis is potentially a promising therapeutic approach.

Re-purposing clinically-approved drugs is a potential way of circumventing challenges associated with drug development, such as the time and expense (GNS et al. 2019). There have been numerous success stories of drugs being successfully re-purposed. One of the most successful examples of drug re-purposing is Sildenafil, a drug originally developed as an anti-hypertensive drug which was later re-marketed by Pfizer as 'Viagra' to treat erectile dysfunction. In 2012, Viagra held a market-leading 47% share of the erectile dysfunction drug

market, with worldwide sales of $2.05 billion (Juárez-López and Schcolnik-Cabrera 2021). Another example is thalidomide originally developed for morning sickness in 1957. Although it became apparent in the 1960s that thalidomide treatment during pregnancy resulted in severe birth defects (Kim & Scialli, 2011), it was later re-purposed to treat multiple myeloma (Eema et al. 1927).

To explore the feasibility of targeting TFEB/3 activity therapeutically via promotion of nuclear translocation, we performed an image-based high-throughput screen using the Pharmakon library of 1600 FDA-approved drugs. Our aims were to investigate the feasibility of drug re-purposing to promote TFEB and/or TFE3 activity through targeting their subcellular localisation. Additionally, we aimed to uncover novel regulatory pathways that are involved in modulating TFEB/3 subcellular localisation.

4.2 Results

4.2.1 Performing a high-throughput, image-based screen

Due to the TFE3 antibodies available at the time not being adequate for immunofluorescence (IF), we exploited the Tet-ON system to ectopically express a c-terminally HA tagged TFE3 in HT29 cells (i-CMV-TFE3-HA HT29). Due to the nature of drug-entry and kinetics, two time points of 2 and 12 hr were used. Because the library is so large, and to avoid missing potential hits, a single concentration of 10 μM was used. After drug treatment, immunofluorescence was performed using an anti-TFEB and anti-HA antibody. Nuclear translocation of TFEB/3 was determined by calculating the ratio of nuclear to cytoplasmic (Nuc/Cyto) TFEB/3 using the FITC channel and DsRed channel respectively. In addition, DAPI staining was used to identify the nuclear area. Assay robustness was determined by calculating the Z-factor (a statistical measure used to assess the quality of assays) for each plate. All liquid handling including cell seeding, addition of compounds and the immunofluorescence procedure was performed using the robotic BioStar liquid handling system. High-content image analysis was performed using the INCELL analyser 6000 (GE healthcare) and image-processing was performed using a customised protocol developed by Val Millar in GE Developer Toolbox software. Hits that were identified from the screen (Z-score of 2 or greater), were further investigated to elucidate their mode of action and their TFEB/3-dependent effects upon autophagy and lysosomal biogenesis. The drug screen was performed by Linxin Li and further experiments were performed by the candidate. A schematic of the work flow is demonstrated in **Figure 17**.

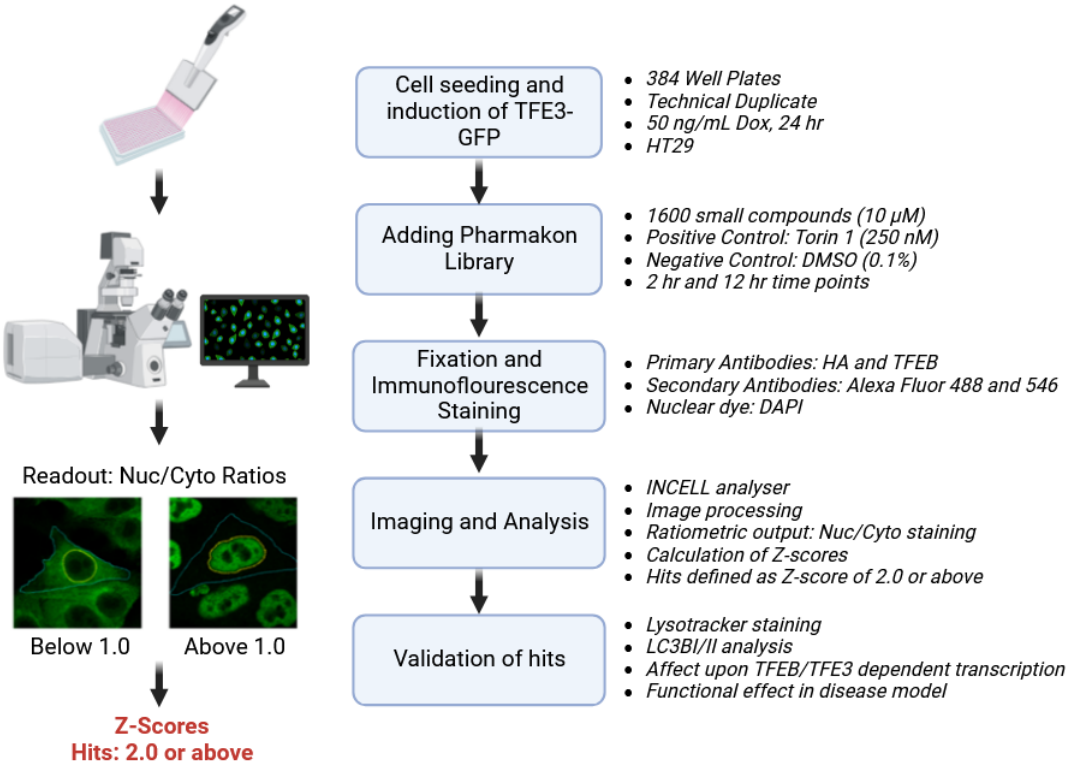

Figure 17. Flow-chart outlining the screening procedure to identify potential TFEB and/or TFE3 agonists.
The ratiometric output of nuclear to cytoplasmic TFEB/3 was determined. The Z factor and SSMD were used as quality control metrics for each plate. A good assay has a Z' >0.5 and SSMD >5. Replicate plates were compared using Pearson Correlation and RSQ. Duplicate plates were then averaged before calculating Z-scores. Using Z-scoring, we identified hits as having a Z-score of 2 or greater (2 standard deviations away from the mean). Z-scores were calculated as follows: *the raw nuc/cyto value minus the mean nuc/cyto value for the library divided by the standard deviation of the library.* The channel used to calculate nuc/cyto ratios of TFEB and TFE3-HA were the 488 and 546 channels respectively. DAPI staining was used to as a nuclear marker to create a distinct nuclear collar.

Two masking methods were used to measure TFEB Nuc/Cyto ratios and derive Z-scores for the drug screen. The first method utilised DAPI staining as a marker of nuclear area and TFEB/TFE3-HA as a cytoplasmic marker. The second method utilised, referred to as an 'eroded nucleus', involved creating an inner collar around the exterior of the nucleus. The cytoplasmic area was determined by creating a second outside collar around the exterior of the nucleus. Due to the un-even distribution of TFEB staining throughout the cytoplasm; the intensity of TFEB being greatest closer to the nucleus and fainter around the edges of the cell, the second method improved the signal-to-noise ratio and thus was used for the screen. The two masking methods described are shown in **Figure 18**.

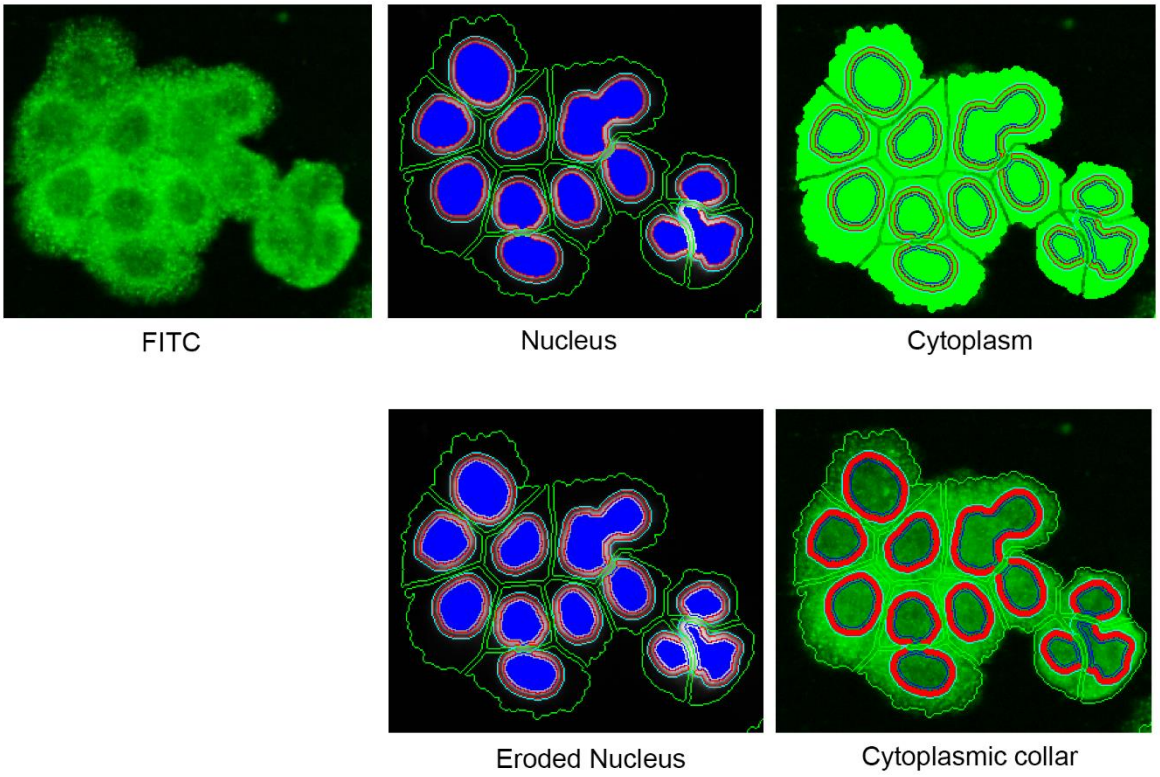

Figure 18. Two masking methods to isolate cytoplasmic and nuclear areas.
The first method (top row): nuclear area was determined by utilising DAPI which stains nuclear DNA. The cytoplasmic area was determined TFEB staining using the FITC channel (top). Alternatively, the second method (second row): the eroded nucleus was created to represent nuclear area and a cytoplasmic collar around the nucleus was selected to represent the cytoplasmic area (bottom). (Image processing protocol is developed by Val Millar). The second protocol was implemented due to varying levels of TFEB staining intensity throughout the cytoplasm and reduced variability.
Figure produced by Val Millar

4.2.2 Image-based screen results

High-throughput image-analysis was automated using a customised protocol developed by Val Millar (TDI). Z-factor and the Strictly Standardised Mean Difference (SSMD) were measured from all plates (each plate was in duplicate) to assess the robustness of the screen and acted as a quality control measure for the positive and negative controls. The Z-factor was calculated by the following calculation:

$$\mathrm{Z-factor} = 1 - (3(\sigma P + \sigma N))/(\mu P - \mu N)$$

Where σP and σN are the standard deviation of the positive (P) and negative (N) controls, μP and μN are the means of the positive (P) and negative (N) controls. A robust assay is expected to have a Z-factor between 0.5-1.0. The Z-factors obtained for each duplicate plate were calculated (**Table 8**). Z-factors calculated using the FITC channel (TFEB) from plates treated with compounds for 2 hr were robust with Z-factors ranging from 0.43-0.72. However, Z-factors

calculated using the FITC channel (TFEB) from plates treated with Torin as a positive control for 12 hr were less robust with Z-factors greater or lower than the indicated range required to pass the quality control measure (**Table 9**). In comparison, when using the DsRed channel (TFE3), Torin was a robust positive control at both the 2 hr and 12 hr time-points.

A possible explanation for this is the positive control used being Torin 1, which strongly induces TFEB nuclear translocation as soon as 30 min after treatment. Torin 1 is most potent at 1 hr but its effects start to reduce after around 3 hr, consistent with previous work (Zapata et al., 2016). However, Torin 1 as a positive control for TFE3-3xHA nuclear translocation gave robust results at both time points. These observations may suggest that TFEB and TFE3 are regulated slightly differently, or it may be an artefact of ectopically expressing TFE3-3xHA.

A second quality control test was performed by calculating the SSMD as follows:

$$\mathrm{SSMD} = (\mu\mathrm{P} - \mu\mathrm{N})/\sqrt{({\sigma_\mathrm{P}}^2 + {\sigma_\mathrm{N}}^2)}$$

Where $\mu\mathrm{P}$ and $\mu\mathrm{N}$ is the means of the positive (P) and negative (N) controls and σP and σN are the standard deviation of the positive (P) and negative (N) controls. This measure of robustness also takes into account the effect of the positive and negative controls. Controls with an SSMD larger than 5 are considered robust. Similarly, to the Z-factor, the SSMD derived from the DsRed Channel (TFE3) Nuc/Cyto ratios were robust at both 2 hr and 12 hr. However, the SSMD calculated from the FITC channel (TFEB) Nuc/Cyto ratios were only robust at 2 hr (**Table 9**). Calculating the Nuc/Cyto ratios using either masking method made no difference to the robustness of the assay.

Table 9. Z-factor and SSMD were used as a quality control measure for high-throughput image analysis. Values highlighted in red did not pass the quality control tests (Z-factors and SSMD).

Plate_Time	QC criteria	Ratio Nuc/Cyto FITC (Cytoplasm)	Ratio Nuc/Cyto FITC (Cytoplasmic Collar)	Ratio Nuc/Cyto DsRed (Cytoplasm)	Ratio Nuc/Cyto DsRed (Cytoplasmic Collar)
P1_2h	Z-factor	0.67	0.72	0.73	0.84
P1_12h	Z-factor	0.19	0.24	0.79	0.88
P2_2h	Z-factor	0.65	0.64	0.82	0.87
P2_12h	Z-factor	-1.48	-1.36	0.83	0.87
P3_2h	Z-factor	0.62	0.63	0.61	0.72
P3_12h	Z-factor	-1.29	-2.00	0.78	0.83
P4_2h	Z-factor	0.43	0.46	0.71	0.76
P4_12h	Z-factor	10.08	4.98	0.79	0.84
P5_2h	Z-factor	0.62	0.57	0.64	0.76
P5_12h	Z-factor	2.19	2.28	0.81	0.86
P1_2h	SSMD	12.75	14.99	14.27	23.10
P1_12h	SSMD	5.18	5.58	18.08	31.90
P2_2h	SSMD	12.00	11.75	21.30	30.62
P2_12h	SSMD	1.70	1.79	20.73	28.76
P3_2h	SSMD	10.98	11.36	10.84	14.74
P3_12h	SSMD	1.82	1.38	18.06	23.53
P4_2h	SSMD	6.62	7.20	14.80	17.56
P4_12h	SSMD	-0.47	-1.06	20.04	27.07
P5_2h	SSMD	9.60	9.62	11.71	17.81
P5_12h	SSMD	-3.45	-3.30	22.26	30.55

To assess if the calculation of Z-scores would be affected by the masking method, the two masking methods and the Z-scores they produced were compared using the Pearson product-movement correlation coefficient; a statistical measurement of the correlation between two data sets. This was calculated as follows:

$$r = \sum(x - xm)(y - ym)/(\sqrt{\sum(x - xm)^2 \sum(y - ym)^2})$$

If the value is close to +1, this indicates a strong positive correlation and if r is close to -1, this indicates a strong negative correlation.

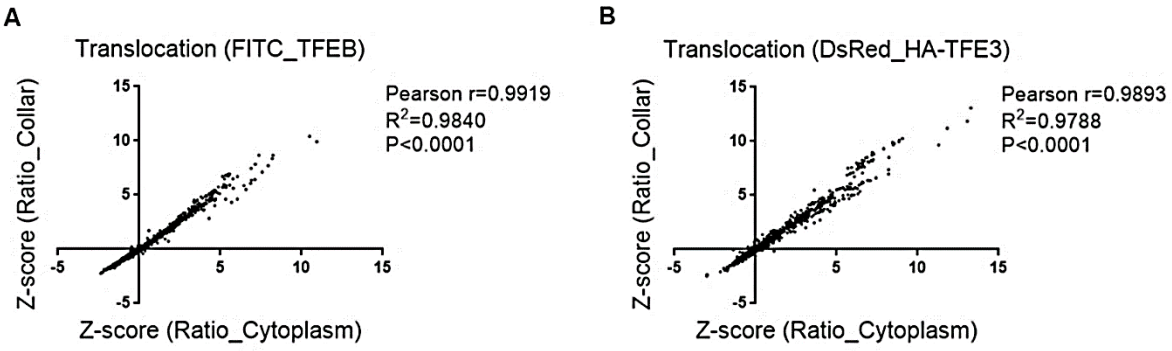

Figure 19. The two masking methods displayed no significant difference in generating Z-scores of compounds. (a) Linear correlation between Z-scores derived from the Nuc/Cyto ratios using the whole cytoplasm masking method (Ratio_Cytoplasm) and the cytoplasmic collar masking method (Ratio_Collar) for TFEB in the FITC channel. (b) Linear correlation between Z-scores derived from the Nuc/Cyto ratios using the whole cytoplasm method (Ratio_Cytoplasm) and the cytoplasmic collar masking method (Ratio_Collar) for HA-TFE3 in the DsRed channel. *Disclaimer: data generated by Linxin Li and Val Millar.*

We demonstrated that the choice of masking method used did not have a significant effect upon the calculation of Z-scores with both the FITC channel (TFEB) and the DsRed channel (TFE3), having r values of 0.9919 and 0.9893 respectively **(Figure 19)**.

Of the 1,600 compounds, 94 promoted TFEB/3 nuclear translocation of which 86 caused TFEB/3 translocation at 2 hr, whereas only 56 drugs did so at 12 hr, having a Z-score of 2.0 or greater **(Figure 20a, b)**. We also examined the fluorescence intensity of the FITC channel to check for drugs that increased TFEB protein levels **(Figure 20c)**, however owing to the nuclear translocation of TFEB causing an increase in perceived fluorescence intensity, we could not reliably screen for drugs that could increase TFEB levels. 24 drugs significantly decreased TFEB levels after 12 hr, having a Z-score of -2.0 or below **(Figure 20c)**. Although most drugs that increased nuclear translocation of TFEB also caused translocation of TFE3-HA, a small proportion had a greater effect upon nuclear translocation of TFE3-HA than TFEB at 2 hr **(Figure 20d)**. At 12 hr, there was greater variability exhibited with some drugs affecting TFEB nuclear translocation more than TFE3-HA and vice versa **(Figure 20e)**. This could be due to differential regulation of TFEB and TFE3, or an artefact of ectopically expressing TFE3-HA. Because of this, we chose to focus on TFEB translocation and function.

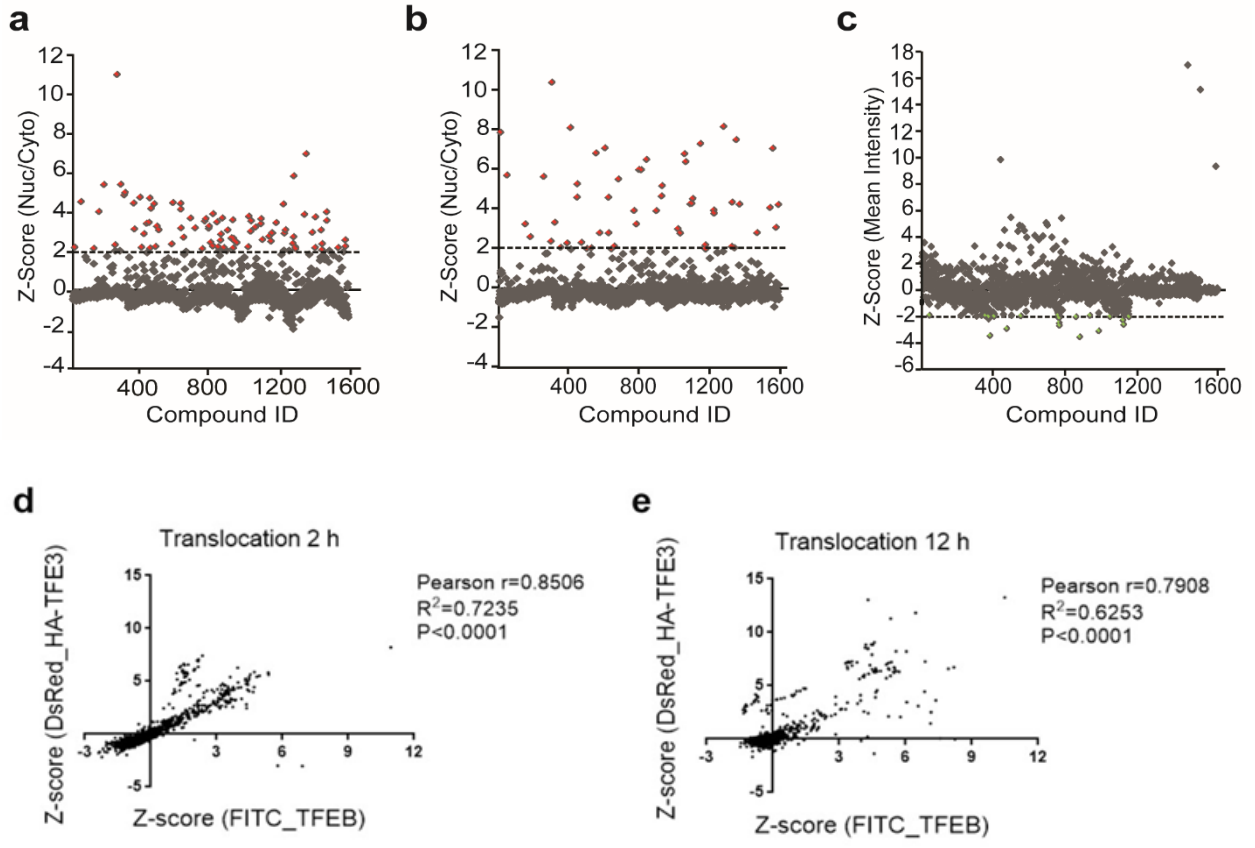

Figure 20. Image-based TFEB/3 translocation screen. (a-b) Scatter dot plot showing the effect of the small compounds (Z-scores) upon TFEB nuclear translocation at 2 hr and 12 hr respectively. Red indicates a Z-score of 2 or above. **(c)** Scatter dot plot showing the effect of the small compounds (Z-scores) upon TFEB fluorescence intensity at 12 hr. Green indicates a Z-score of -2 or below. (d-e) Linear correlation of Z-scores of all compounds for nuclear translocation between TFEB and HA-TFE3 at 2 hr and 12 hr respectively. *Data produced by Linxin Li, quantification performed by Val Millar, graphs adapted by the candidate.*

4.2.3 Validating hits and their mode of action

The 94 drugs that were able to promote TFEB/TFE3 translocation fell into four main groups: neurotransmitter-related, cardiac glycosides, histamine-related and anti-malarials. As an initial trial, we tested several compounds from each group to determine if we could reproduce the results from the screen. To do this, we treated HT29 for 2 hr with each compound at 10 μM and performed immunoflourescene using an antibody against endogenous TFEB. After, we quantified TFEB nuclear vs cytoplasmic (nuc/cyto) ratios **(Figure 21)**.

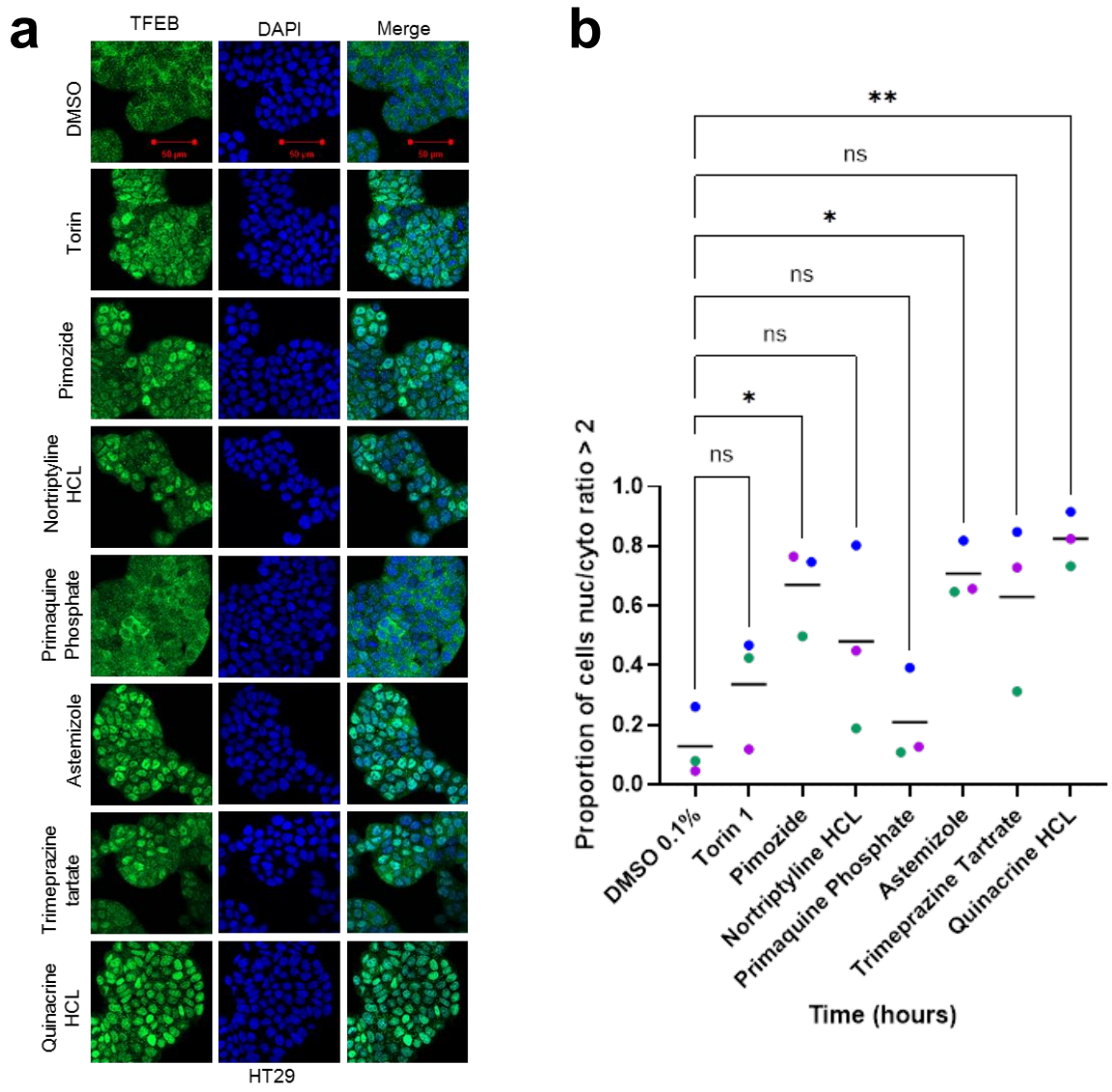

Figure 21. Validation of 'hits' from drug screen 1 that promoted nuclear translocation
(a) Representative immunofluorescence images of three independent experiments demonstrating in HT29, TFEB translocates to the nucleus upon treatment of Torin 1 (250 nM), Pimozide, Nortriptyline HCL, Astemizole, Trimeprazine tartrate and Quinacrine HCL (all 10 μM) but not when treated with Primaquine Phosphate. Scale bars are shown in red (50 μm). (b) Scatter plot showing proportion of cells with a TFEB nuc/cyto ratio of 2 or greater from the immunofluorescence images (black bars = mean). Biological replicates are colour coded. One-Way Anova was performed on three biological replicates (n>1000 cells per condition, N=3). ns = not significant, *= p value < ****P < 0.0001, *** P < 0.001, ** P < 0.01, * P < 0.05.

Immunoflourescence analysis revealed 5 out of the 6 drugs tested visually increased the proprtion of cells displaying nuclear TFEB staining, including the positive control, Torin 1 **(Figure 21a).** However, not all 6 drugs signifcantly increased the proportion of cells exhibiting nuclear TFEB staining **(Figure 21b)**. Of the six drugs tested, only pimozide, astemizole and quinacrine hydrochloride were able to signifcantly increase the proportion of cells with nuclear

TFEB staining. Once again, we hypohtesise that the lack of statistical signifcance observed when treating cells with Torin 1, along with other 'hits' tested is likely due to the large variation exhibited by the biological replicates.

To investigate the mode of action of these compounds, we first explored the possibility that these drugs may affect mTORC1 and/or mTORC2 signalling. To do this, we treated cells with each compound (10 μM, 2 hr). After, whole cell lysates were collected and used for western blot analysis (**Figure 22**).

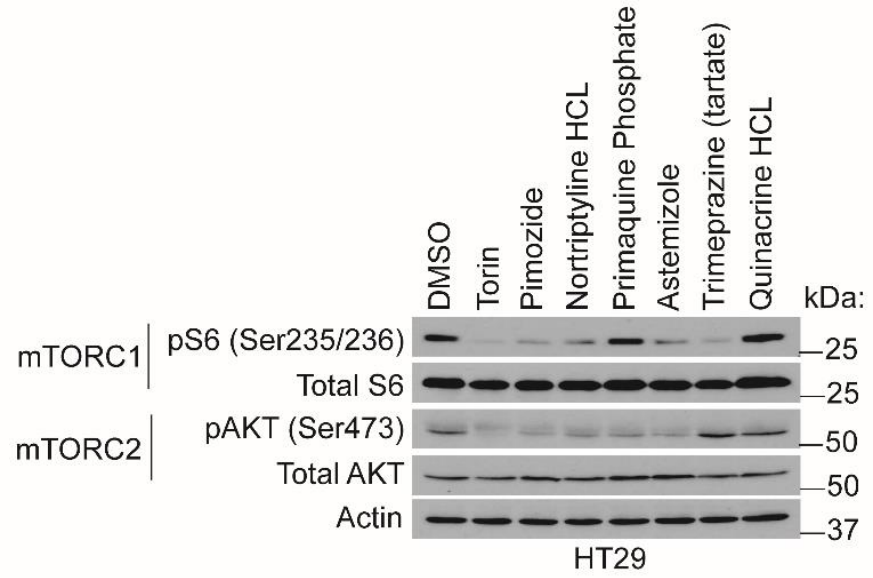

Figure 22. Example of 'hits' and their effect on mTORC1 and mTORC1 signalling
Western blot analysis of HT29 treated with DMSO as a negative control (0.1%), Torin 1 as a positive control known to inhibit mTORC1 and mTORC1 (250 nM), Pimozide, Nortriptyline HCL, Primaquine HCL, Astemizole, Trimeprazine tartrate, Quinacrine HCL (all 10 μM, 2 hr).

As expected, Torin 1 inhibited both mTORC1 and mTORC2, as observed by decreases in the phosphorylation of downstream targets S6 and AKT respectively **(Figure 22, column 2).** Treatment with pimozide, nortriptyline hydrochloride, astemizole and trimeprazine tartate all led to reduced mTORC1 signaling, viualised by a decrease in phosphorylation of S6 **(Figure 22, columns 3,4,6 and 7).** Pimozide, nortriptyline hydrochloride and astemizole also reduced mTORC2 signaling as seen by a decrease in phosphorylation of AKT **(Figure 22, columns 3,4 and 6)**. Trimeprazine tartate only reduced mTORC1 signaling whereas quinacrine hydrochloride did not alter mTORC1 or mTORC2 signaling. Interestingly, although primaquine phosphate did not alter TFEB subcellular localisation visually in our follow-up immunoflourescence experiment **(Figure 21)** it inhibited mTORC2 signaling. This is interesting considering we have previously demonstrated that activation, not inhibition, of mTORC2 promotes nuclear translocation of TFEB (Li et al. 2018).

To functionally validate the 94 compounds that induced TFEB nuclear translocation, and narrow down our 'hit list' in an unbiased manner, we used LysoTracker (deep red) dye which selective stains for lysosomes, allowing us to visualise drug-induced changes in lysosomal number, a process mediated by TFEB/3. To optimise the conditions for this functional screen, we tested the ability of a known inhibitor, (Bafilomycin A (BafA)) and inducers of autophagy (Rapamycin (Rapa) and Torin 1) to induce detectable changes in LysoTracker staining in HeLa and Ht29 cells **(Figure 23)**. Single cells were gated using side scatter and forward scatter **(Figure 23a)**. Fold changes in LysoTracker staining was measured **(Figure 23b, c)** and quantified **(Figure 23d, e)**.

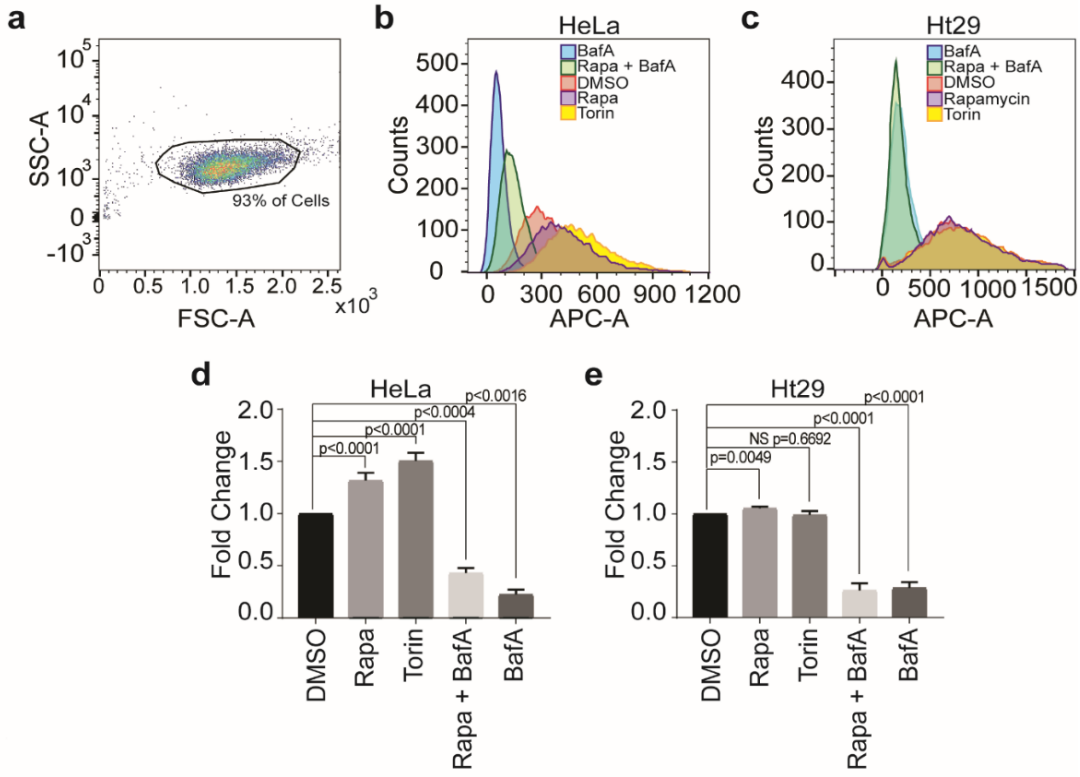

Figure 23. Optimising control conditions for functional validation experiments using Lysotracker Deep Red Dye. Fluorescence-Assisted Cell sorting (FACs) of HeLa and Ht29 cells with the APC-A channel after treatment with DMSO (0.1%, 3 hr) Torin (1 μM, 3 hr), Rapamycin (Rapa, 250 nM, 3 hr), Rapa and Bafilomycin A (BafA) (250 nM, 3 hr and 10 nM respectively, 1 hr) or BafA only (10 nM, 1 hr) followed by 30 min incubation with LysoTracker Deep Red Dye. (a) Illustrates typical gating of cells. (b-c) Histograms profiles of singlets after treatments showing mean Fluorescence intensity measured with the APC -A channel against counts (number of cells). (d-e) Quantification of LysoTracker deep red staining calculated as fold change in mean intensity of staining normalised to DMSO. Student's *t*-test: ****$P < 0.0001$, ***$P < 0.001$. Error bars = SD. N>8,000 cells, n=3.

As expected, we found that Bafilomycin A; a drug that inhibits autophagosome-lysosome fusion (Mauvezin and Neufeld, 2015), significantly decreased staining in both HeLa and Ht29

(Figure 23d, e). Furthermore, Torin (mTORC1 and mTORC2 inhibitor) and Rapamycin (mTORC1 inhibitor), caused the opposite effect and increased LysoTracker staining. Rapamycin induced a significant increase in lysotracker staining in both cell lines, whereas Torin only induced a significant increase in HeLa. Furthermore, the decreased LysoTracker staining intensity caused by BafA treatment could be partially rescued by Rapamycin in HeLa but not in HT29 **(Figure 23d, e)**. The variability in drug sensitivity of the two cell lines is likely due to different basal levels of autophagic flux or lysosomal-number. Based on this, we chose to use HeLa for future experiments. We performed a secondary 'functional validation' screen using LysoTracker staining to test all 94 drugs (10 μM, 4 hr) in HeLa. Based on our previous translocation screen, where we see translocation as soon as, 2 hr, we used a slightly longer time point of 4 hr with the aim of visualising increased TFEB/3 activity through LysoTracker staining. Fold changes in lysotracker staining were calculated (relative to DMSO) and plotted against $-\log_{10}$(P-Value) **(Figure 24)**.

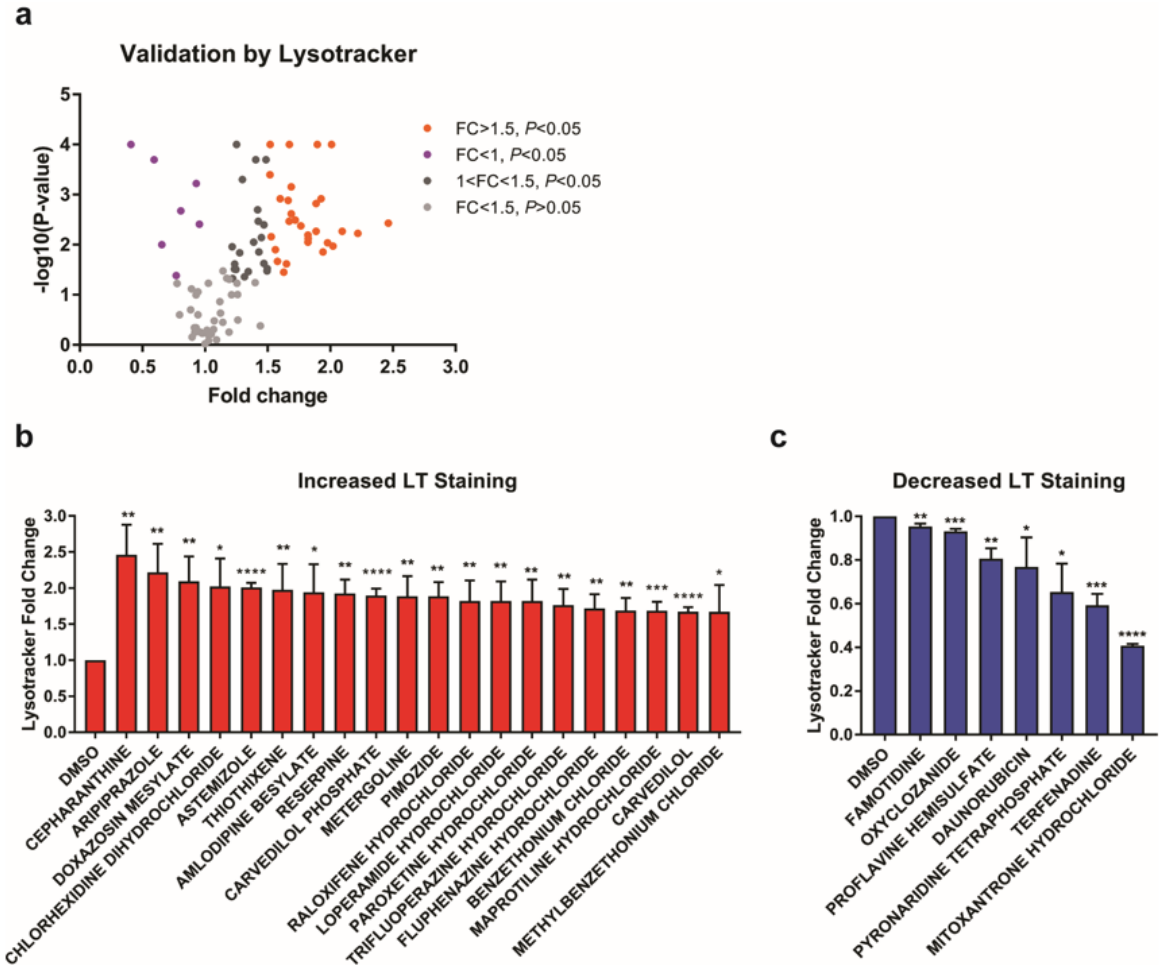

Figure 24. Functional validation of translocation hits using LysoTracker staining. (a) Volcano plot of the translocation hits screened using LysoTracker staining. The -log10 (P-value) of each hit was plotted against its fold change in LysoTracker staining (relative to DMSO control). (b) Bar graph showing the fold change in LysoTracker staining of the top 20 hits. (c) Bar graph showing fold change in LysoTracker staining of hits that caused decrease in LysoTracker staining. N>8,000 cells per condition. All experiments were performed using HeLa (n=3). Student's t-test ****P < 0.0001, ***P < 0.001, **P < 0.01, *P < 0.05. Error bars = SD.

We observed 50 drugs significantly increased LysoTracker staining, whilst 7 significantly decreased LysoTracker Staining (P <0.05) **(Figure 24a)**. Of the drugs that increased LysoTracker staining, Cepharanthine had the greatest effect **(Figure 24b)**. Cepharanthine is a biscoclaurine alkaloid extracted from *Stephania cepharantha* and is known to inhibit the activity of the efflux transporter ABCC10 (Multidrug resistance-associated protein 7) (Zhou et al. 2009)and Hsp90 (Heat Shock Protein 90) with a binding Kd of 15 nM (Haginaka et al. 2015). Hsp90 plays an important role in autophagy through mTOR signalling (X. Xiao et al. 2018) and studies have demonstrated that Cepharanthine can induce apoptosis, G0/G1 cell cycle arrest and autophagy through inhibition of the Akt/mTOR pathway (S. Gao et al. 2017) (Gao et al., 2017). However, the involvement of TFEB/3 in orchestrating these downstream

responses has not yet been discussed. Of the drugs that decreased LysoTracker staining, Mitoxantrone hydrochloride had the greatest effect **(Figure 24c)**. Mitoxantrone hydrochloride is a type of chematherapeutic agent called an anthracycline which inhibits topoisomerase; an enzyme required for DNA repair (Wu et al., 2013). Additionally, Daunorubicin, another topoisomerase inhibitor (Aubel-Sadron and Londos-Gagliardi 1984) also decreased lysotracker staining.

We then focused on two of the drugs that were able to increase TFEB nuclear accumulation and also increase lysotracker staining; Nortriptyline Hydrochloride and Pimozide. One of the reasons for selecting these drugs is that they are both neurotransmitter-related and can cross the blood-brain barrier. Nortriptyline hydrochloride is a tricyclic antidepressant used to treat major depression and is also used off-label for chronic pain and other conditions. It acts by inhibiting the reuptake of serotonin and norepinephrine by the presynaptic neuronal membrane, thereby increasing the concentration of these neurotransmitters in the synapse. Additionally, nortriptyline has been shown to inhibit the activity of histamine, 5-hydroxytryptamine, and acetylcholine. Interestingly, Nortriptyline has already been shown to inhibit growth cancer cells through induction of oxidative stress by triggering the Keap1-Nrf2 pathway (Zhu et al. 2024) and inhibition of fatty acid uptake (Chu et al. 2023). In contrast, nortriptyline exhibits a neuroprotective effect in cases of cerebral ischemia (W. H. Zhang et al. 2008) but the potential involvement of TFEB has not yet been explored.

Pimozide is neuroleptic drug of the diphenylbutylpiperidine class and is currently used for Tourette's syndrome (Pringsheim and Marras 2009) and delusional disorders such as Schizophrenia (Mothi and Sampson 2013). It's mode of action in cases of Tourette's syndrome is thought to be via inhibition of the dopamine recptor D2 (DRD2) and thus decreases dopamine activity. However, in cases such as neuropathic pain, it has been shown to inhibit T-type Ca2+ channels (Kasanami et al. 2022). Pimozide has also been shown to have anti-cancer properties. For example, one study demonstrated Pimozide could inhibit the PI3K/AKT/MDM2 signaling pathway to inhibit breast cancer growth (Li et al., 2022). Interestingly, pimozide has also been shown to inhibit the growth of brain cancer cell lines by promoting STAT3-mediated autophagy, inducing apoptosis (Ranjan, Kaushik, and Srivastava 2020). Furthermore, pimozide has already been identified as an activator of autophagy in an independent high-throughput screen (Zhang et al., 2007) although the role TFEB/3 may play in mediating autophagy has not yet been explored.

4.2.4 Pimozide and Nortriptyline Hydrochloride induce an increase autophagosome number in a partially TFEB-dependent manner

We then investigated whether Nortriptyline Hydrochloride or Pimozide could induce changes in autophagic flux through observing changes in the conversion of the microtubule-associated protein light chain 3 (LC3) from LC3BI to LC3BII. LC3B is firstly synthesised as cytosolic precursor referred to as Pro-LC3B. When autophagy is induced, ATG4 cleaves Pro-LC3B near its c-terminus to generate LC3BI. LC3BI is then conjugated to phosphatidyl ethanolamine, generating membrane-bound LC3BII on the surface of the autophagosome. LC3BII is then recycled by ATG4 by a process called delipidation (removal of phosphatidyl ethanolamine) to further promote autophagosome production. Therefore, LC3BII levels correlate to the number of autophagosomes. The standard procedure of measuring autophagic flux is to compare the conversion of LC3BI and LC3BII induced by a particular treatment when in the absence or presence of an autophagy inhibitor, such as Bafilomycin A (BafA) which inhibits the acidification of lysosomes as well as inhibiting the fusion of autophagosomes and lysosomes (Mauvezin and Neufeld, 2015).

To do this, cells were treated with Torin 1, Pimozide or Nortriptyline for 0-8 hr with and without BafA. Samples were collected for western blot analysis and endogenous levels of LC3B I and II were visualised **(Figure 25)**.

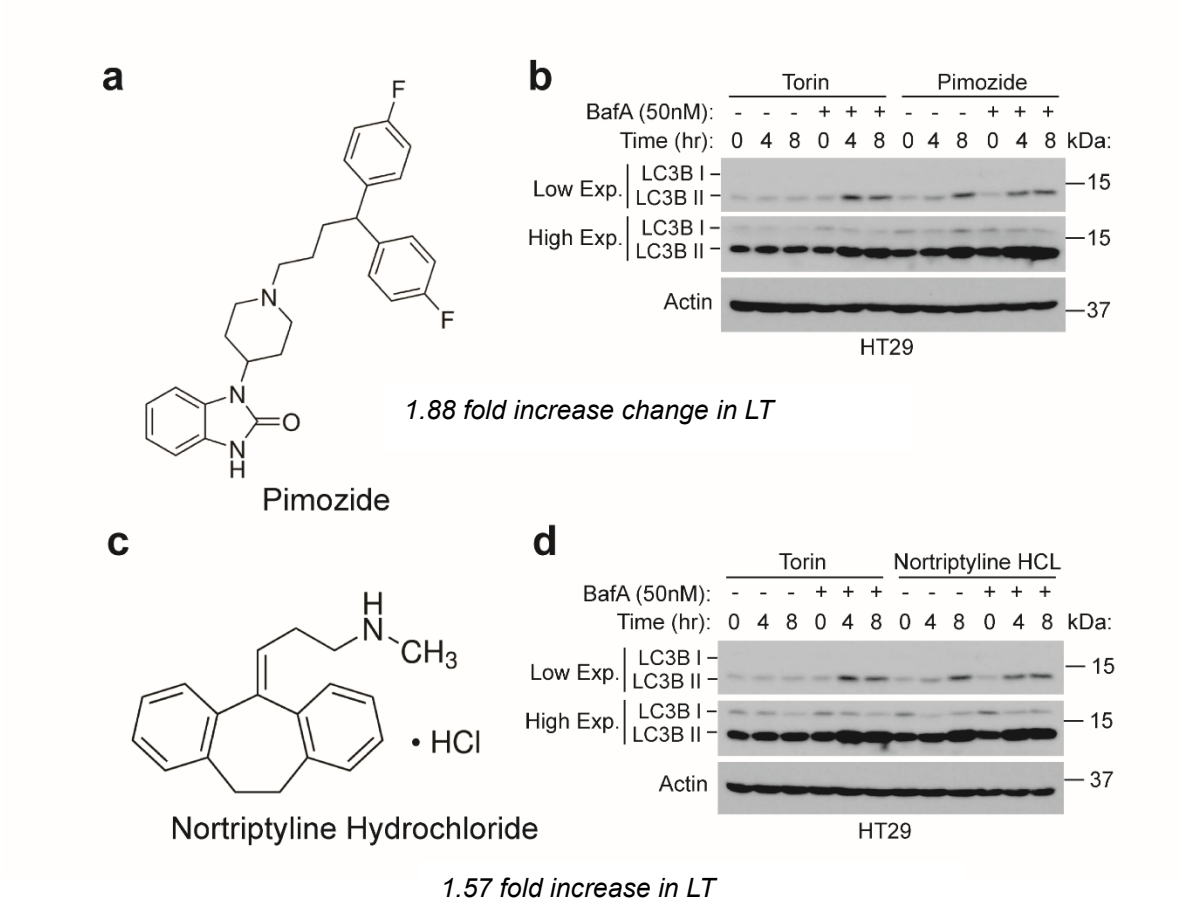

Figure 25. Pimozide and Nortriptyline increase levels of LC3BII
(a) Chemical structure of Pimozide with the fold change in Lysotracker (LT) Staining. (b) western blot analysis of HT29 treated with Torin 1 (250 nM) or Pimozide (10 μM) with and without Bafilomycin A (50 nM) for 0, 4 or 8 hours (hr). (c) Chemical structure of Nortriptyline Hydrochloride (HCL) with the fold change in LT staining. (d) Western blot analysis of HT29 treated with Torin 1 (250 nM) or Pimozide (10 μM) with and without BafA (50 nM) for 0, 4 or 8 hours.

As expected, Torin 1 induces autophagy by 4 hr, as observed by an increase in the ratio of LC3BII/I when co-treated with BafA which blocks autophagosome-lysosome fusion. Similarly, both Pimozide and Nortriptyline hydrochloride increased the ratio of LC3BII/LC3BI in the presence of BafA by 4 hr. However, unlike treatment with Torin 1, Pimozide and Nortriptyline Hyrochloride increased the ratio of LC3BII/I even in the absence of BafA by 8 hr, indicating an increase in the number of autophagasomes.

After, we investigated if these changes in autophagic flux were TFEB-dependent. To do this, we transiently knocked down TFEB expression using siRNA and measured the ratio of LC3BI/II induced by Pimozide and Nortriptyline Hydrochloride with and without BafA compared this to cells transfected with non-targeting siRNA as a control (siCON). To check that the

knockdown of TFEB was efficient, we also immunblotted against endogenous TFEB **(Figure 26)**.

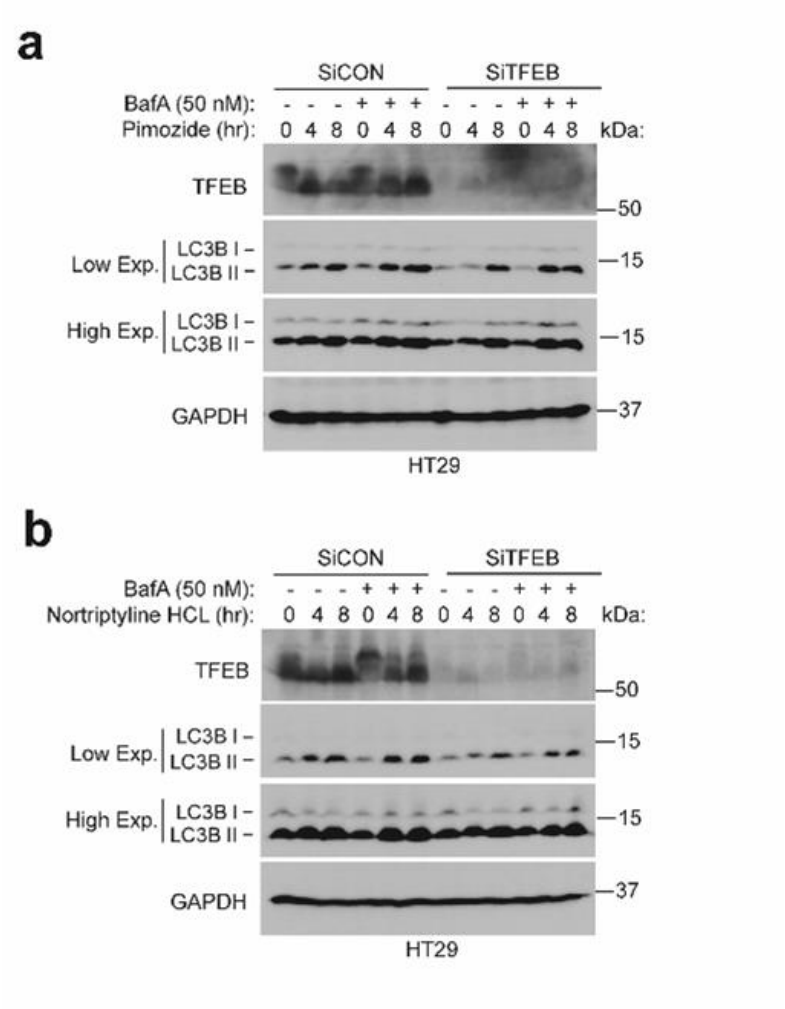

Figure 26. Pimozide and Nortriptyline increase levels of LC3BII in a partially TFEB-dependent manner. Western blot analysis of HT29 transfected with either siCON or siTFEB to reduce TFEB expression and subsequently treated with either (a) Pimozide or (b) Nortriptyline HCL for 0-8 hr with or without BafA (50 nM).

We observed that Pimozide and Nortriptyline Hydrochloride caused an increase in the LC3BII/I ratio in a time-dependent manner which was increased in the presence of BafA **(Figure 26a, b respectively).** The samples tranfected with siRNA targeting TFEB had markedbly lower TFEB protein levels, indicating the knockdown was efficient. We observed that both Pimozide and Nortriptyline Hydrochloride were still able to induce an increase in the LC3BII/I ratio when TFEB expresion was reduced by siRNA, although to a lesser degree. This indicates that the induction of autopahagosome number induced by Pimozide and Nortriptyline Hydrochloride may be at least partly mediated by TFEB.

As we previously demonstrated that HeLa are more responsive to inducers of autophagy than HT29 **(Figure 23)**, we generated TFEB and TFE3 knockout cell lines in HeLa using CRISPR/Cas9 **(Figure 27a)**. As part of the validation process, we examined if the induction of autophagy was impaired in TFEB and TFE3 knockout cell lines (TFEB KO and TFE3 KO respectively) compared to Wild-type (WT) **(Figure 27b, c)** To do this, cell lines were treated with Torin 1 and the ratio of LC3BI/II was measured by western blot analysis **(Figure 27c)** and quantified by densitometry **(Figure 27d)**.

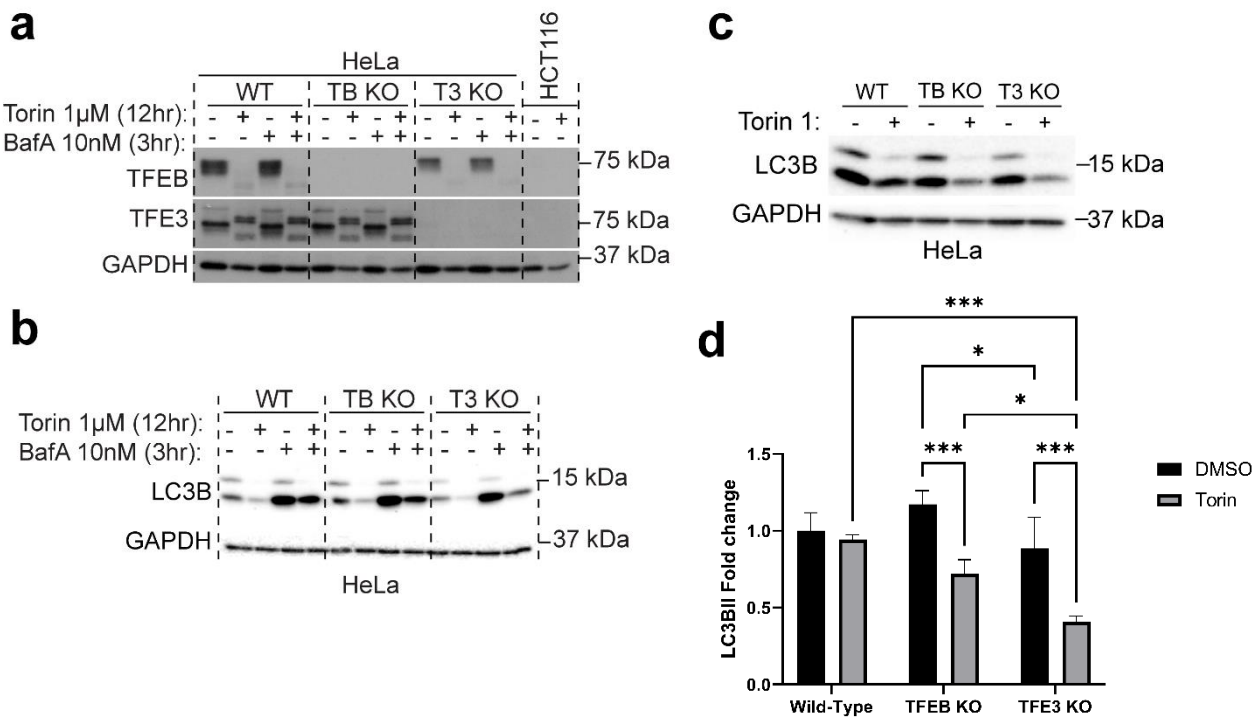

Figure 27. Knocking out TFEB or TFE3 reduces LC3BII levels when cells are treated with Torin (a) Western blot analysis of Wildtype (WT), TFEB knock-out (TB KO) and TFE3 knock-out (T3 KO) generated in HeLa compared to HCT116 (negative control); a cell line that does not express TFEB or TFE3. Cell lines were treated with 1μM of Torin 1 for 12 hr in the presence or absence of 10 nM of Bafilomycin A (BafA) for 3 hr. (b) Western blot analysis using the same samples as shown in (a) immunoblotting against LC3B. (c) Representative western blot analysis (n=3) of WT, TB KO and T3 KO cell lines treated with Torin 1 immunoblotted against LC3B. (d) Fold changes in LC3BII levels induced by Torin 1 treatment demonstrated TB KO and T3 KO cell lines had a greater reduction in LC3BII than WT when treated with Torin 1 (n=3), One-Way Anova was performed on three biological replicates (n=3), *= p value < ****P < 0.0001, *** P < 0.001, ** P < 0.01, * P < 0.05. All three replicates are shown in *Supplemental Figure 3*.

Western blot analysis revealed that knocking out TFEB and TFE3 expression in HeLa (TB KO and T3 KO) was succesful as demonstrated by complete ablation of expression when compared to wildtype HeLa **(Figure 27a)**. The HCT116 cell line was used as a control as it does not express either TFEB or TFE3. As expected, treatment with Torin 1 induced a mobility

shift in both TFEB and TFE3. However, Torin 1 also induced a decrease in the total levels of TFEB; a phenomenon that has previously been observed (Wang et al. 2022).

We then examined the effect of knocking out TFEB or TFE3 on the induction of autophagy resulting from Torin 1 treatment in the presence and absence of BafA **(Figure 27b and c)**. Although we observed Torin 1 treatment decreased LC3BII levels in all three cell lines, the wild-type cell line did not display a statistically signicant reduction in LC3BII levels when treated with Torin 1 **(Figure 27d)**. In comparison, the TFEB and TFE3 knockout cell lines displayed a signifcant reduction in LC3BII levels when treated with Torin 1 **(Figure 27d)**, indicating autophagosome production is impaired when TFEB and/or TFE3 is knocked out. Treatment with Torin 1 and BafA (**Figure 27c)**, induced slightly higher LC3BII levels in wildtype than in TFEB and TFE3 knockout cell lines, with the TFE3 knockout cell line having the lowest levels visually, although this was not quantified.

Once we confirmed knocking out TFEB and TFE3 was successful, we focussed primarily on Pimozide for further functional assays due to its ability to increase autophagosome number more effectively than Nortriptyline hydrochloride. To do this, we treated wildtype, TFEB knockout and TFE3 knockout cell lines with Torin 1 and Pimozide for 4 hr as this was a timepoint that worked well previously **(Figure 23)**. During the last 30 min of treatment, we added Lysotracker Dye to selectively stain for lysosomes before performing FACs analysis. We quantified the change in lysotracker staining induced by either Torin 1 or Pimozide treatment and then normalised to the wildtype cell line **(Figure 28)**.

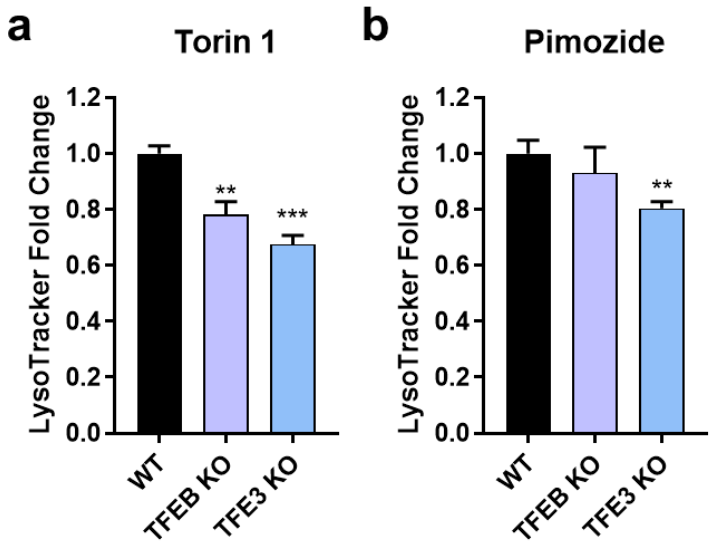

Figure 28. Torin 1 and Pimozide increase lysosomal staining in a partially TFEB/3-dependent manner. Quantification of FACs analysis of Lysotracker staining induced by either Torin 1 or Pimozide treatment in wildtype, TFEB knockout and TFE3 knockout cell lines. (a) Wildtype, TFEB knockout (sgTFEB #3-1-3) and TFE3 knockout (sgTFE3 #1-2-4) cell lines generated in HeLa were treated with Torin 1 (250 nM, 4hr). 30 min before the end of treatment, Lysotracker (deep red) dye was added to cells. Fold changes in Lysotracker staining were normalised to wildtype cells. (b) Wildtype, TFEB knockout (sgTFEB #3-1-3) and TFE3 knockout (sgTFE3 #1-2-4) cell lines generated in HeLa were treated with Pimozide (10 μM, 4 hr). 30 min before the end of treatment, Lysotracker (deep red) dye was added to cells. Fold changes in Lysotracker staining were normalised to wildtype cells. N>8,000 cells per condition. All experiments were performed using HeLa (n=3). Student's t-test ****P < 0.0001, ***P < 0.001, **P < 0.01, *P < 0.05. Error bars = SD. *Data produced by Linxin Li and the candidate.*

We observed TFEB knockout and TFE3 knockout cell lines had significantly reduced lysotracker staining induced by Torin 1 **(Figure 28a)** ; indicative of reduced lysosomal biogenesis**.** These results corroborate other studies that have demonstrated the importance of TFEB and TFE3 in the regulation of lysosomal biogenesis and autophagy. However, only the TFE3 knockout cell line exhibited a reduction in lysotracker staining when treated with Pimozide **(Figure 28b),** demonstrating that pimozide promotes an increase in lysosomal staining in a partially TFE3-dependent manner. Perhaps if cells were treated for longer, the effect sizes observed would be further increased.

To assess the potential neuroprotective potential of Pimozide, we pre-treated SH-SY5Y; a human neurotypic cell line dervied from human neuroblastoma with Pimozide for 1 hr before adding Amyloid-β (1-42) or Lipolysaccharides for 24 hr. A schematic demonstrating how this experiment is performed is shown in **(Figure 29)**. Afterwards, cell viability was measured using an MTT assay **(Figure 30)**.

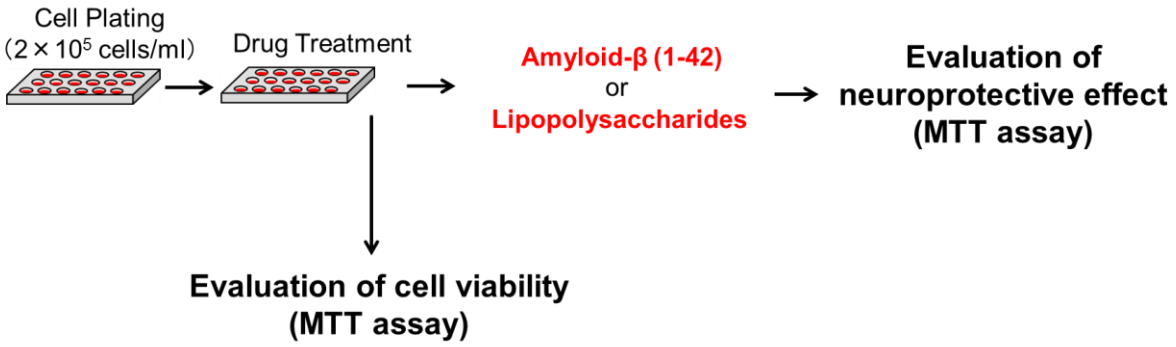

Figure 29. Schematic demonstrating experimental design
The neuroprotective effect of Pimozide against Amyloid-β (1-42) or Lipopolysaccharides was assessed using SH-SY5Y; a human neurotypic cell line derived from human neuroblastoma. SH-SY5Y are widely used as a cell-based model for evaluating neuronal function. Firstly, cells are plated, then treated with Pimozide for 1hr before incubating with Amyloid-β (1-42) or lipopolysaccharides for 24 hr, 10 μM. Cytotoxity was then assessed using the MTT (3-[4,5-dimethylthiazol-2-yl]-2,5 diphenyl tetrazolium bromide) assay.

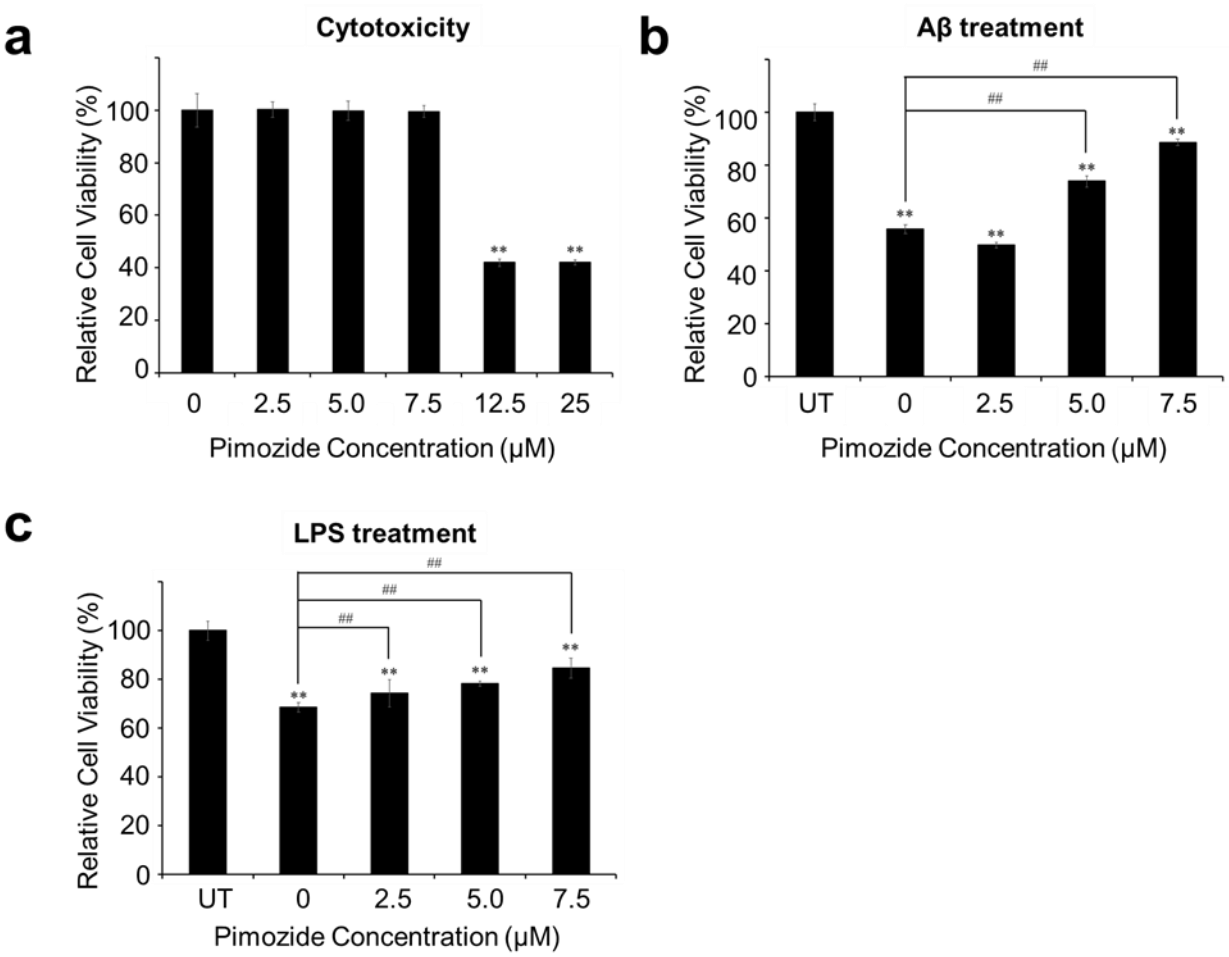

Figure 30. Pimozide has a neuroprotective effect in SH-SY5Y, rescuing cell viability in response to Aβ and LPS treatment. (a) Cytotoxicity of pimozide was determined using a range of concentrations (0-25 μM) using an MTT assay. Concentrations of 12.5 μM and above reduced cell viability. (b) Pimozide exhibited neuroprotection against treatment with synthetic Amyloid β (1-42) oligomers (Aβ) when using concentrations of 5-7.5 μM. (c) Pimozide exhibited neuroprotection against treatment with Lipopolysaccharides (LPS) when using concentrations of 2.5-7.5 μM. (n=3). *Disclaimer: experiment and data produced were anlaysed by Hiroko Isoda, Univ. Tsukuba and figure adapted by the candidate.*

We observed Pimozide exhibited cytotoxicty when using concentrations of 12.5-25 μM; visualised by a significant reducion in cell viability **(Figure 30a)**. Therefore in the neuroprotection assays, Pimozide was only used in concentrations up to 7.5 μM.

As expected, Aβ (1-42) treatment, signifcantly reduced cell viability **(Figure 30b)**. However, treating cells with 5-7.5 μM of Pimozide signifcantly increased cell viability in response to Amyloid β (1-42) treatment. Interestingly, pimozide further reduced cell viability when using concentrations of 5-7.5 μM. Furthermore, treatment with Lipopolysaccharides decreased cell viability which could be significantly rescued by pimozide using concentrations as low as 2.5 μM and improved with increasing concentrations **(Figure 30c)**.

Taken together, we observed pimozide exhibited neuroprotection in SH-SY5Y against Amyloid β (1-42), Dexamethasone and Lipoplysaccharide treatment. Increasing concentrations of pimozide further protected cells against each treatment, with the exception of dexamethasone treatment whereby pimozide only exhibited neuroprotection when using the lowest concentration of 2.5 μM.

4.3 Discussion and future perspectives

The MIT/TFE family of transcription factors have been coined 'the master regulators of autophagy and lysosomal biogenesis' (Settembre et al. 2011). These processes are often impaired in a range of neurodegenerative diseases such as Alzheimer's (Sooyeon, Yutaka, and Nixon 2011) and Parkinson's disease (Tanji et al. 2011). It is thought insufficient levels of autophagy and lysosomal biogenesis, leads to the accumulation of misfolded proteins, and the formation of plaques, impairing neuronal cell function. Many studies have discovered the potential therapeutic benefits of increasing TFEB levels or activities in ameliorating disease pathogenesis in neurodegenerative disease models. For instance, one study demonstrated that activation of TFEB promoted clearance of amyloid-β(1-42) (Aβ(1-42)) in a cell based model of Alzheimer's disease (Xiao et al. 2014). Another, showed TFEB overexpression ameliorated Aβ(1-42) plaque-induced pathogenesis in an Alzheimer's mouse model (Zhang and Zhao 2015).

Thus, there is a clinical need to find TFEB/TFE3 agonists to drive autophagy and lysosomal biogenesis for the treatment of neurodegenerative diseases. To explore the feasibility of targeting TFEB/3 activity therapeutically via promotion of nuclear translocation, we performed an image-based, high-throughput screen using the Pharmakon library of 1600 FDA-approved drugs. Our aims were to investigate the feasibility of drug re-purposing to promote TFEB and/or TFE3 activity through targeting their subcellular localisation. In addition, we aimed to discover novel regulatory mechanisms that govern TFEB/3 subcellular localisation to expand our knowledge.

We found of the 1,600 drugs tested, 94 drugs could promote nuclear accumulation of TFEB and/or TFE3. We found these 94 drugs could be categorised into four main groups: neurotransmitter-related, cardiac glycosides, histamine-related or anti-malarial. We selected 6 drugs representing each of these groups (aside from cardiac glycosides): pimozide, nortriptyline hydrochloride, astemizole and trimeprazine tartate, primaquine phosphate and quinacrine for some follow-up experiments. We found pimozide, astemizole, trimeprazine tartrate and quinacrine hydrochloride could visually promote nuclear accumulation of TFEB despite only astemizole, trimeprazine tartrate and quinacrine hydrochloirde signifcantly

increasing the proportion of cells displaying nuclear TFEB staining. However, considering our positive control, Torin 1 also failed to yield signifcant a increase in cells with nuclear staining, it is likely a reflection of the large amount of biological variation observed between the replicates. Future studies should look to repeat these experiments in a bid to reduce variation between experimental replicates.

Furthermore, we found pimozide, nortriptyline hydrochloride and astemizole inhibited both mTORC1 and mTORC2, trimeprazine tartrate inhibited mTORC1, and quinacrine hydrochloride did impair mTORC1 or mTORC2 activity. Interestingly, quinacrine hydrochloride is an anti-malarial compound which has shown to be an inhibitor of autophagy (Goodall et al. 2014), despite its ability to promote nuclear accumulation of TFEB/3. However, previous studies have shown quinacrine hydrochloride induces lysosomal membrane permeabilisation (Bredahl Hansen et al. 2021). Based on our currently knowledge of how TFEB subcellular localisation is regulated, permeabilisation of the lysosomal membrane could promote nuclear accumulation of TFEB through prevention of mTORC1-mediated phosphorylation on S211, required for its cytoplasmic retention (Vega-Rubin-de-Celis et al. 2017). Although interesting mechanistically, if quinacrine hydrochloride impairs lysosomal function despite promoting nuclear accumulation of TFEB, it would not be a good candidate to re-purpose for the treatment of neurodegenerative diseases.

Due to this finding highlighting that some of these drugs may be promoting nuclear accumulation of TFEB despite being inhibitors of autophagy, we next validated hits by measuring drug-induced changes in lysosomal staining rather than qRT-PCR. We found of the 94 drugs that could promote nuclear accumulation of TFEB, 50 were able to significantly increase lysosomal staining, indicative of an increase in lysosomal number. Conversely, we found 7 drugs significantly reduced lysosomal staining, indicating a decrease in lysosomal number. The fact not all of the hits that promoted nuclear accumulation of TFEB led to functional changes in lysosomal number demonstrates the need to consider the chemical properties of the drugs we are investigating. For instance, two of the compounds that decreased lysosomal staining were daunorubicin and terfenadine; lipophilic weak basic therapeutic agents that are lysosomotropic due to their ability to penetrate the lysosomal membrane and prevent lysosomal acidification (Stark et al. 2020). By using this secondary screen to check for lysosomal staining, it enabled us to exclude lysosomotropic agents from our hit list.

Notably, others have also performed similar image-based screens to identify TFEB/3 agonists. For instance, one study used a novel multi-parameter screen involving measuring TFEB/3 subcellular localisation, as well as using DQ-BSA to assess lysosomal function. By using this

methodology, they identified a set of quinazoline-derivative compounds that induced TFEB and TFE3 translocation whilst retaining lysosomal function (Carling et al. 2023).

Critically, by implementing this two-step screening method, we excluded drugs that could promote lysosomal biogenesis in a TFEB/3-independent manner. Additionally, an increase in lysosomal staining, indicating an increase in lysosomal number is not always due to an increase in lysosomal biogenesis, but could be the result of impaired lysosomal degradation (Han et al. 2022). Therefore, when interpreting these results, we must appreciate that autophagic flux is a dynamic process involving biogenesis, fusion and degradation of intracellular vesicles.

An alternative strategy to assess drug-induced changes on autophagic flux would be to use the dual fluorescent mCherry-EGFP-LC3B tandem vector (Kimura, Noda, and Yoshimori 2007). Under nutrient-rich conditions, mCherry-EGFP-LC3B staining appears diffusely localised throughout the cell (red and green) and upon induction of autophagy, there is recruitment of mCherry-EGFP-LC3B to the autophagosomes and puncta can be visualised (red and green). However, upon fusion of autophagosomes to lysosomes, EGFP becomes quenched by the low pH, whereas mCherry does not, resulting in a decrease in green fluorescence but no change in red fluorescence (Kimura, Noda, and Yoshimori 2007). Therefore, using this tandem vector would provide us more information in regards to changes in autophagic flux through visualising changes in the ratio of green vs red fluorescence. Although we did generate a stable cell line expressing mCherry-EGFP-LC3B in HT29, we were unable to optimise the control conditions due to lack of time **(Supplemental Figure 4).**

Future experiments could therefore utilise the cell line expressing the mCherry-EGFP-LC3B tandem vector to visualise drug-induced changes in autophagic flux over time. Moreover, performing dose and time-course experiments would allow us to assess the pharmokinetics of the drugs, such as IC50 or the optimal time-points to use to observe changes in autophagic flux.

Nonetheless, we further validated two neuro-transmitter related drugs; pimozide and nortriptyline hydrochloride. We selected these two drugs as potential candidates for drug re-purposing as they promoted nuclear transloation of TFEB, increased lysosomal staining and have the ability to cross the blood-brain barrier which is a useful consideration when re-purposing drugs for neurodegenerative diseases. Interestingly, an independent screen identified pimozide, loperamide and trifluoperazine as inducers of autophagy (L. Zhang et al. 2007) but did not explore the involvement of TFEB/3 in mediating these effects.

Pimozide is currently used to treat schizophrenia (Mothi and Sampson 2013), Tourette's syndrome (Pringsheim and Marras 2009), and somatic pain (Kasanami et al. 2022) but also

exhibits anti-cancer activity in brain tumours (Ranjan, Kaushik, and Srivastava 2020) and breast cancer (J. Li et al. 2022). It is thought to treat schizophrenia through its inhibition of the dopamine D2 receptor (Wisner and Schaefer 2015), whereas in Tourette's syndrome, its mode of action is via inhibition of T-type calcium channels (Pringsheim and Marras 2009). Interestingly, calcium signalling has already been implicated in the regulation of TFEB. However, previous studies have demonstrated that an increase in intracellular Ca^{2+} leads to activation of Calcineurin-dependent de-phosphorylation of TFEB (Medina et al. 2015), making it appear unlikely that inhibition of Ca^{2+} channels would lead to activation of Calcineurin. Others have demonstrated that a decrease in intracellular cytosolic Ca^{2+} can promote Ca^{2+} release from intracellular stores (Park et al. 2020). We hypothesise that this sudden change in calcium release may trigger activation of Calcineurin which in turn, leads to de-phosphorylation of TFEB. Future studies should measure changes in intracellular Ca^{2+} using calcium dyes such as Fura-2 AM (Barreto-Chang and Dolmetsch 2009) to confirm this.

Nortriptyline hydrochloride is a tricyclic antidepressant used to treat major depression (Nierenberg et al. 2003) and is also used off-label for neuropathic pain (Derry et al. 2015). It acts by inhibiting the reuptake of serotonin and norepinephrine by the presynaptic neuronal membrane, resulting in increased concentrations of these neurotransmitters in the synapse. Interestingly, nortriptyline has already been shown to exhibit anti-cancer properties by triggering the Keap1-Nrf2 pathway, leading to induction of oxidative stress (Zhu et al. 2024) and inhibition of fatty acid uptake (Chu et al. 2023). Additionally, nortriptyline has been shown to exhibit a neuroprotective effect in cases of cerebral ischemia (Zhang et al. 2008). However, the potential involvement of TFEB has not yet been explored.

By western blot analysis we demonstrated that both pimozide and nortriptyline hydrochloride promoted an increase in the ratio of LC3BII vs LC3BI indicating an increase in autophagic flux (Mizushima and Yoshimori 2007) and that this response was dampened when expression of TFEB/3 were reduced by siRNA. Although this provided evidence that TFEB and TFE3 are partly mediating this effect, the dampening effect was minimal, indicating TFEB or TFE3 are not solely responsible for mediating this effect. However, due to the functional redundancy of TFEB and TFE3 (Huan et al. 2005), it is plausible that a greater effect may be observed when expression of both TFEB and TFE3 are reduced. Although, this may be dependent on the cell line used as we have recently shown in melanoma cell lines, the MiT/TFE family members have functionally distinct functions (Dias et al. 2024). Future studies would benefit from repeating these experiments by either knocking down/out expression of both factors simultaneously.

Through the use of neuroprotection assays, using cell-based models of neurodegenerative diseases, we demonstrated pimozide exhibited neuroprotection against Aβ (1-42) and lipopolysaccharides, providing further evidence that pimozide may be a good candidate to further validate for its potential to be re-purposed for neurodegenerative diseases. Previous studies have demonstrated that overexpression or activation of TFEB can promote intracellular clearance of Aβ (X. Meng et al. 2016), we have not demonstrated the neuroprotective effects exhibited by pimozide are TFEB and/or TFE3 dependent. Future studies should employ the use of a double knockout cell line to repeat these experiments to assess the importance of TFEB and/or TFE3 in mediating these effects. In addition, performing genetic rescue experiments by overexpressing either wildtype TFEB/3 or the △Basic mutant that cannot enter the nucleus, will help elucidate if this neuroprotective effect is mediated by TFEB/3-dependent transcription **(Supplemental Figure 5)**. Although we generated stable cell lines expressing wildtype TFEB-GFP and the △ Basic TFEB-GFP mutant, unexpectedly, wildtype TFEB-GFP could not translocate to the nucleus upon glucose or amino acid deprivation **(Supplemental Figure 6)**. Given that wildtype TFEB-GFP could translocate to the nucleus upon treatment with Torin **(Supplemental Figure 5)**, it suggests that the presence of the c-terminal GFP tag interferes with the post-translation regulation of TFEB in response to physiological starvation. We have since generated alternative cell lines whereby replacing the tag with a much smaller 3xHA tag which can translocate to the nucleus upon starvation. Due to lack of time, we could not use them in this study.

In summary, we performed an image-based, high-throughput screen using 1,600 FDA-approved small compounds. We identified 94 drugs that could promote nuclear accumulation of TFEB, of which 50 induced increases in lysosomal staining. Nortriptyline hydrochloride and pimozide are neuro-transmitter related drugs that inhibited mTORC1 and mTORC2 signaling. Although the exact mode of action is unclear, pimozide is known to inhibit T-type calcium channels. Based on our current knowledge of regulation of TFEB and TFE3, changes in intracellular calcium could play a part in mediating these changes in TFEB subcellular localisation. Furthermore, inhibition of mTORC1 is required for promoting nuclear entry of TFEB and TFE3 through loss of cytoplasmic tethering (Jose A. Martina et al. 2012). Further analysis demonstrated pimozide and nortriptyline hydrochloride induced changes in autophagic flux, which were partly dependent upon TFEB/3 expression. Furthermore, pimozide exhibited a neuroprotective effect in a cell-based model of neurodegenerative disease. Ultimately, our screen highlights drug repurposing as a valuable resource in finding novel ways of targeting TFEB and TFE3 activity therapeutically. Furthermore, our results could provide insight into the novel regulatory mechanisms that control subcellular localisation of TFEB and TFE3.

Chapter 5 - Preventing the adaptive response to starvation by preventing TFEB translocation

5.1 Introduction

The MIT/TFE family of transcription factors have been implicated in a plethora of disease contexts. The importance of TFEB/3 in regulating lysosomal biogenesis and autophagy has been demonstrated by numerous studies and as such, they are often referred to as the 'master regulators of autophagy and lysosomal biogenesis'. Both autophagy and lysosomal biogenesis are important in the maintenance of nutrient homeostasis; allowing cells to sense and adapt to their ever-changing nutrient supply.

During cancer development, cellular metabolism is rewired. Normal, healthy differentiated cells primarily rely upon mitochondrial oxidative phosphorylation to generate the energy needed for cellular processes. However, cancer cells instead rely upon aerobic glycolysis, and is referred to as the 'Warburg effect' (Kang et al. 2023).

Autophagy is a highly regulated catabolic process used by cells to degrade cellular structures such as organelles and macromolecules, thereby allowing the recycling of bioenergetic components to promote cell survival. The role of autophagy in mediating cancer cell adaptation during tumorigenesis is complex. Studies have demonstrated that autophagy both inhibits cancer onset but can promote advanced tumour growth (Amaravadi, Kimmelman, and White 2016). For instance, the pathogenesis of pancreatic ductal adenocarcinoma (PDAC) requires high levels of autophagy and is thought to contribute to therapy-resistance (Yang et al., 2011). Furthermore, a study investigating the role of autophagy in PDAC demonstrated that regardless of nutrient status and mTORC1 remaining active, PDAC cell lines exhibited constitutively nuclear MiT/TFE caused by dysregulated nuclear import. They also demonstrated that the high levels of autophagy observed in PDAC cell lines were the result of MiT/TFE-dependent transcription (Perera et al. 2015).

Most studies investigating the role of MiT/TFE in mediating autophagy in the context of cancer have focused on altering TFEB/3 expression levels. However, practically it would be challenging to use such approaches in the clinic. Finding novel ways of preventing nuclear translocation of TFEB/3 to prevent their activity and thus, autophagy is therefore an appealing therapeutic strategy.

This chapter aims to explore the feasibility of inhibiting TFEB/3 activity through regulation of their subcellular localisation. To do this, we performed a reciprocal drug screen to that outlined in Chapter 2. Using the PKIS1/2 libraries of 758 compounds (GSK), provided by the Target

Discovery Institute, University of Oxford (TDI), we aimed to identify kinase inhibitors that could prevent nuclear translocation of TFEB in response to either amino acid and/or glucose deprivation.

5.2 Results

5.2.1 Performing a high-throughput image-based analysis screen to identify kinase inhibitors that can attenuate TFEB nuclear localisation in response to nutritional deprivation

A 2-hr time-point for starvation was selected for the drug screen due to it being a relatively short time but yet still effectively resulting in translocation of TFEB (**Figure 6** and **Figure 7**) Given that we do not know the pharmokinetics of the compounds in the PKIS I and II library, we chose to use one concentration of 10 μM in the hope of capturing all potential hits that could effectively prevent TFEB translocation.

After drug treatment, (10 μM, 2 hr) immunofluorescence was performed using an anti-TFEB antibody to visualize endogenous TFEB translocation. Nuclear translocation of TFEB was determined by calculating the ratio of nuclear to cytoplasmic (Nuc/Cyto) TFEB using the FITC channel. Assay robustness was determined by calculating the Z-factor for each plate using the ratio of Nuc/Cyto fluorescence intensity. To do this, a masking method developed by Val Millar (TDI) was used. All liquid handling including cell seeding, addition of compounds and the immunofluorescence procedure was performed using the robotic BioStar liquid handling system. High-content image analysis was performed using the INCELL analyser 6000 (GE healthcare) and image-processing was performed using a customised protocol developed by Val Millar in GE Developer Toolbox software. Hits that were identified from the screen (Z-score of-2 or lower), were further investigated to elucidate their mode of action and their TFEB-dependent effects upon autophagy and lysosomal biogenesis. The protocol procedure is outlined below in **Figure 31**.

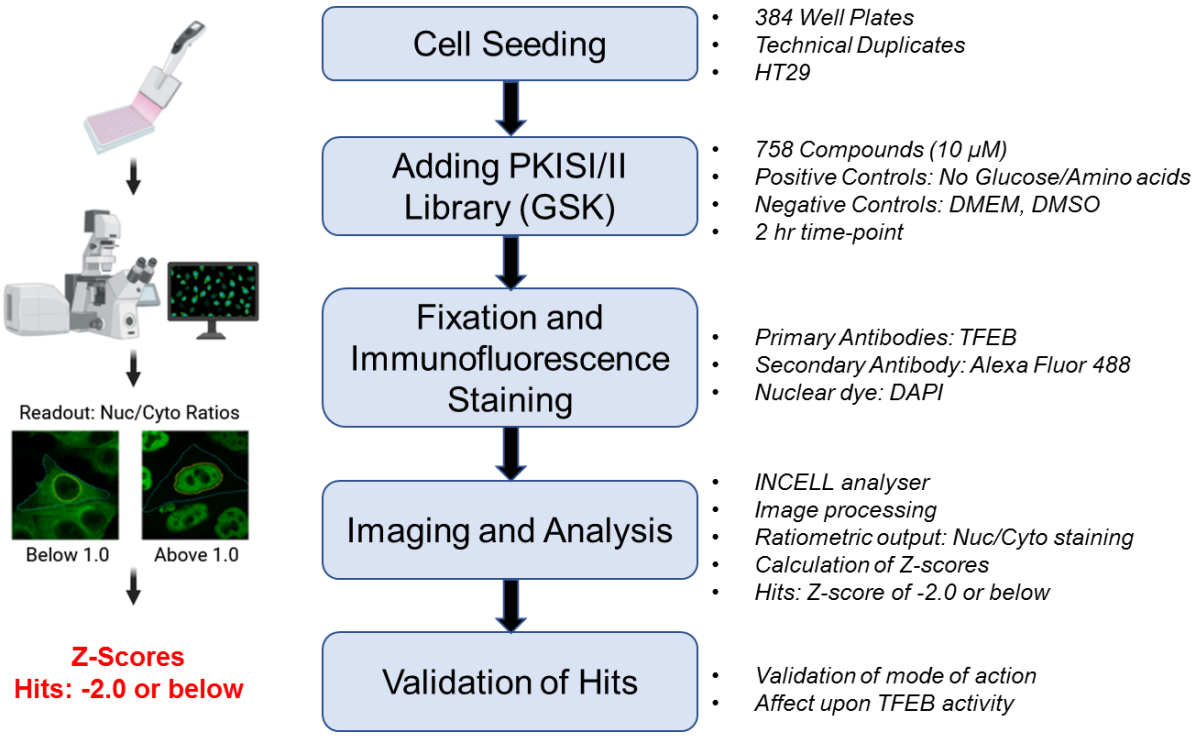

Figure 31 Flow-chart outlining the screening procedure to identify potential TFEB antagonists. The ratiometric output of nuclear to cytoplasmic TFEB was determined. The Z' prime and SSMD were used as quality control metrics for each plate. A good assay has a Z' >0.5 and SSMD >5. Replicate plates were compared using Pearson Correlation and RSQ. Duplicate plates were then averaged before calculating Z-scores. Using Z-scoring, we identified hits as having a Z-score of -2.0 or lower (2 STD away from the mean). Z-scores were calculated as follows: the raw nuc/cyto value minus the mean nuc/cyto value for the library divided by the SDV of the library. TFEB nuc/cyto ratios were calculated by measuring the intensity of staining (488 channel). DAPI staining was used to identify the nucleus and create a nuclear collar, a cytoplasmic collar was created around the nuclear collar, as previously described using the 'eroded nucleus' masking method (**Figure 18**).

High-throughput image-analysis was automated using a customised protocol developed by Val Millar (TDI). Z-factor and the Strictly Standardised Mean Difference (SSMD) were measured from all plates (each plate was in duplicate) to assess the robustness of the screen and acted as a quality control measure for the positive (starvation condition) and negative (Nutrient-rich DMEM with 0.1% DMSO) controls. The Z-factor and SSMD for each plate was calculated as previously outlined (Results Chapter 2). Controls were found to all have an SSMD larger than 5 and a Z-factor between 0.5-1.0 which are considered to be robust (**Table 10).**

Table 10. Z-factor and SSMD were used as a quality control measure for high-throughput image analysis. All values passed the quality control tests (Z-factors and SSMD).

Plate_Rep_condition	QC criteria	Ratio Nuc/Cyto FITC
P1_rep1 HBSS	Z-factor	0.87
P1_rep2 HBSS	Z-factor	0.78
P2_rep1 HBSS	Z-factor	0.70
P2_rep2 HBSS	Z-factor	0.81
P3_rep1 HBSS	Z-factor	0.80
P3_rep2 HBSS	Z-factor	0.51
P1_rep1 no glc	Z-factor	0.81
P1_rep2 no glc	Z-factor	0.83
P2_rep1 no glc	Z-factor	0.81
P2_rep2 no glc	Z-factor	0.79
P3_rep1 no glc	Z-factor	0.82
P3_rep2 no glc	Z-factor	0.76
P1_rep1 HBSS	SSMD	30.964
P1_rep2 HBSS	SSMD	16.540
P2_rep1 HBSS	SSMD	11.783
P2_rep2 HBSS	SSMD	21.859
P3_rep1 HBSS	SSMD	20.554
P3_rep2 HBSS	SSMD	6.806
P1_rep1 no glc	SSMD	20.266
P1_rep2 no glc	SSMD	25.317
P2_rep1 no glc	SSMD	22.780
P2_rep2 no glc	SSMD	19.928
P3_rep1 no glc	SSMD	23.561
P3_rep2 no glc	SSMD	15.492

Z-Scores obtained under glucose deprivation were plotted against compound ID numbers and representative images are shown in **Figure 32**.

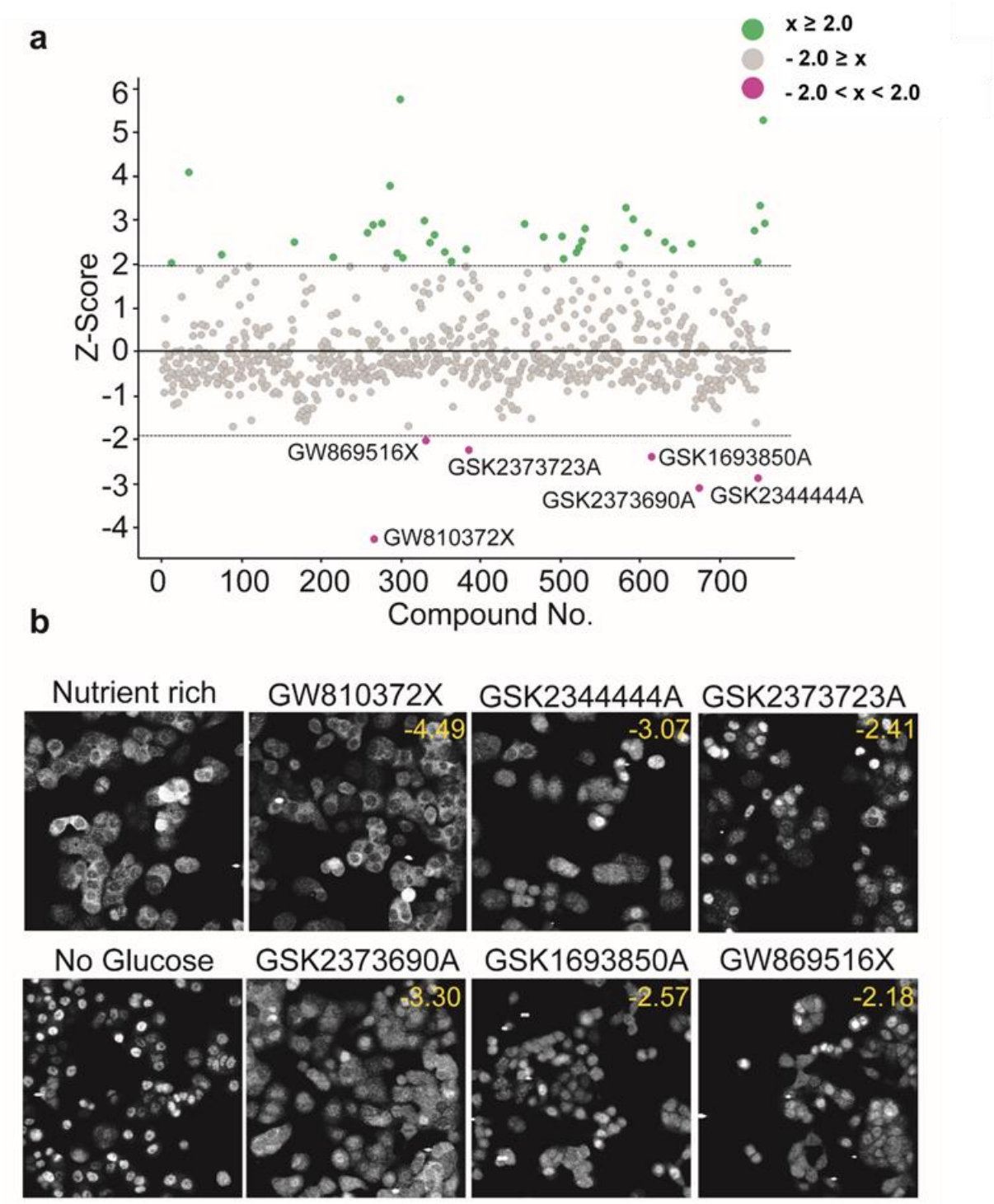

Figure 32 Image-based screen results for PKI libraries I and II under glucose deprivation in HT29 using a TFEB antibody. (a) Scatter dot plot showing the Z-scores of all compounds except columns 15 and 16 on each plate for TFEB translocation at 2 hr, 10 μM. Green indicates drugs with a Z-score of 2 or above (drugs that promote further nuclear translocation), Grey indicates drugs that did not promote nor prevent nuclear translocation in response to glucose deprivation. Magenta indicates drugs with a Z-score of -2 or below (drugs that prevent nuclear translocation), and thus were considered hits. (b) Representative images from the image-based screen showing TFEB localisation for each of the compounds.

Out of 758 drugs, 6 drugs prevented nuclear translocation in response to glucose deprivation **(Figure 32)**. Descriptions of 'hits' including full-names, known targets and Z-scores are shown in **Table 11**.

Table 11. Compounds that attenuated TFEB nuclear translocation in response to glucose deprivation ranked by Z-score.

Rank	Drug ID	Full name	Z-Score	Targets
1	GW810372X	Pyrazolo[1,5-b]pyridazine deriv. 43	-4.49	PKY2,AurC, DK2/CycE, CDK2/CYCA, GSK3A, GSK3B, CLK2, HIPK1, HIPK4,DYRK1B, DYRK1A
2	GSK2373690A	2-Methyl-5-[(2R)-2-methyl-4-morpholinyl]-3-[2-methyl-3-(trifluoromethyl)benzyl][1,2,4]triazolo[1,5-a]pyrimidin-7(3H)-one	-3.30	PI3K
3	GSK2344444A	2-Methyl-5-(2-methyl-4-morpholinyl)-3-[2-methyl-3-(trifluoromethyl)benzyl][1,2,4]triazolo[1,5-a]pyrimidin-7(3H)-one	-3.07	PI3K
4	GSK1693850A	3-Piperidin-1-ylsulfonyl-5-(4-pyridin-4-ylquinolin-6-yl)pyridin-2-amine	-2.57	PI3K
5	GSK2373723A	2-Methyl-5-[(2R)-2-methyl-4-morpholinyl]-3-[2-methyl-3-(trifluoromethyl)benzyl][1,2,4]triazolo[1,5-a]pyrimidin-7(3H)-one	-2.41	PI3K
6	GW869516X	7-(1H-Indol-2-yl)-5-methyl-N-(3,4,5-trimethoxyphenyl)imidazo[5,1-f][1,2,4]triazin-2-amine	-2.18	Numerous

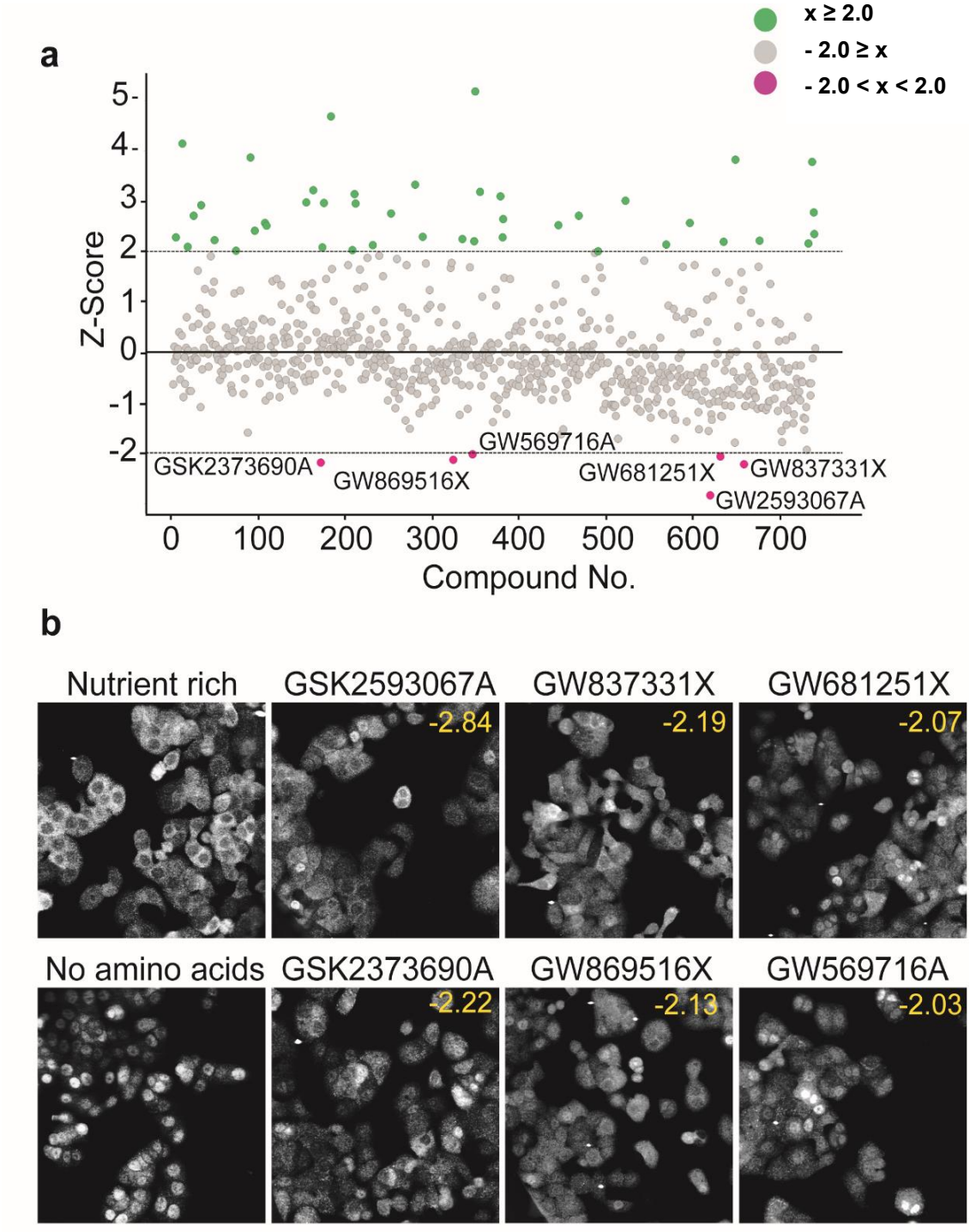

Figure 33. Image-based screen results for PKI libraries I and II under amino acid deprivation in HT29. (a) Scatter dot plot showing the Z-scores of all compounds for TFEB translocation at 2 hr, 10 μM. Green indicates drugs with a Z-score of 2 or above (drugs that promote further nuclear translocation), Grey indicates drugs that did not promote nor prevent nuclear translocation in response to glucose deprivation. Magenta indicates drugs with a Z-score of -2 or below (drugs that prevent nuclear translocation), and thus were considered hits. () Representative immunofluorescence images from the image-based screen showing TFEB localisation for each of the compounds.

Out of 758 drugs, 6 drugs prevented nuclear translocation in response to amino acid deprivation **(Figure 33)**. Descriptions of 'hits' including full-names, known targets and Z-scores are shown below in **Table 12**.

Table 12. Compounds that attenuated TFEB nuclear translocation in response to amino acid deprivation ranked by Z-score.

Rank	Drug ID	Full name	Z-Score	Targets
1	GSK2593067A	Could not be located in database	-2.84	PERK
2	GSK2373690A	2-Methyl-5-[(2R)-2-methyl-4-morpholinyl]-3-[2-methyl-3-(trifluoromethyl)benzyl][1,2,4]triazolo[1,5-a]pyrimidin-7(3H)-one	-2.22	PI3K
3	GW837331X	5-methyl-7-(3-(trifluoromethyl)phenyl)-N-(3,4,5-trimethoxyphenyl)imidazo[1,5-f][1,2,4]triazin-2-amine	-2.19	PLK1
4	GW89516X	7-(1H-Indol-2-yl)-5-methyl-N-(3,4,5-trimethoxyphenyl)imidazo[5,1-f][1,2,4]triazin-2-amine	-2.13	Numerous
5	GW681251X	2-(4-chlorophenyl)-4-(3-(pyridin-2-yl)-1H-pyrazol-4-yl)pyridine	-2.07	TGFBR1 (ALK5)
6	GW569716A	N-(1-Benzyl-1H-indazol-5-yl)-6-[2-({[2-(methylsulfonyl)ethyl]amino}methyl)-1,3-thiazol-4-yl]-4-quinazolinamine	-2.03	EGFR

Interestingly, both GW89516X and GSK2373690A were able to prevent nuclear accumulation in response to both amino acid and glucose deprivation whereas the other compounds were only able to block translocation in response to either amino acid or glucose deprivation. This suggests that GW89516X and GSK2373690A may act upstream of both mTORC1 and mTORC2 pathways.

Four out of six of the compounds that prevented TFEB translocation in response to glucose deprivation (GSK2373690A, GSK2344444A, GSK1693850A and GSK2373723A) are annotated to be PI3K inhibitors. This is unsurprising given that PI3K is upstream of the AKT – mTOR pathway and five PI3K inhibitors have already been approved by the FDA for the treatment of breast cancer with PIK3CA mutations and blood disorders (Hongyao Li et al. 2024).. However, while GSK2373690A is also annotated as a PI3K inhibitor in the PKIS library, it also prevents translocation in response to amino acid starvation. This suggests that the mechanism through which it prevents translocation of TFEB under amino acid deprivation is via an alternative mechanism. GW89516X is an interesting candidate to further validate as it has numerous potential targets including AMPK which has been shown to directly phosphorylate TFEB (Paquette et al. 2021). Other interesting candidates to further investigate are GSK2593067A (PERK inhibitor), GW569716A (EGFR inhibitor) and GW681251X (ALK5 inhibitor) due to their novelty as the kinases they inhibit have not yet been shown to affect TFEB translocation.

5.2.2 Validation of 'hits' that prevent TFEB nuclear translocation in response to amino acid or glucose deprivation

To check the reproducibility of the results from the drug screen, we obtained small aliquots of the hits from the screening facility (TDI) and performed dose responses of the compounds to see if the affect upon TFEB translocation is dose-dependent.

The first drug we tested, GSK2593067A is annotated to be a PERK inhibitor and is able to prevent translocation of TFEB in response to amino acid deprivation using a concentration as low as 1 μM **(Figure 34)**.

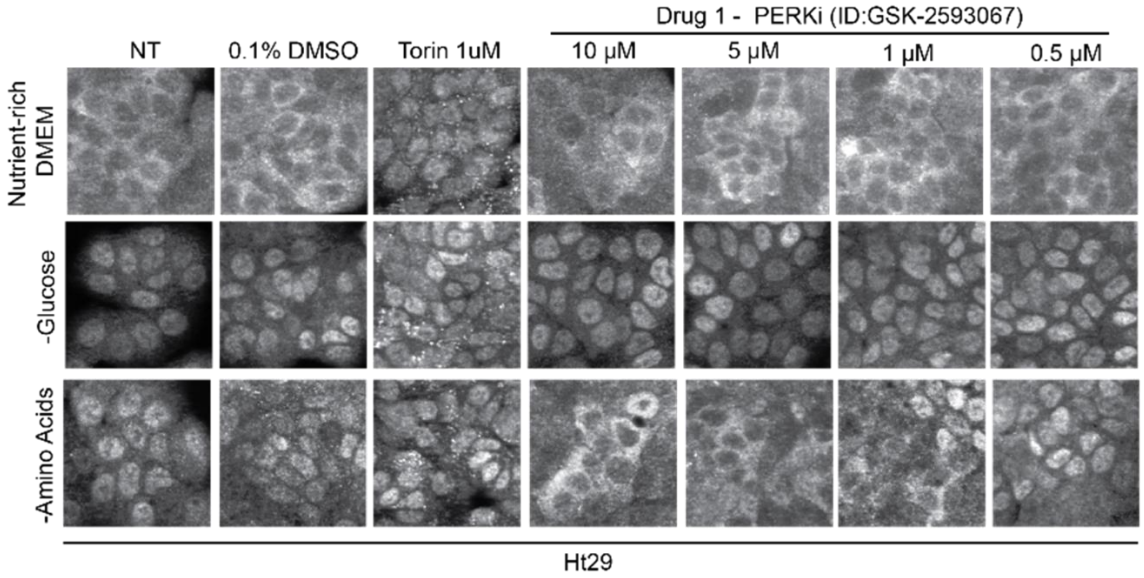

Figure 34 Drug 1, Regno ID: GSK2593067A a PERK inhibitor attenuates nuclear localisation of TFEB in response to amino acid deprivation.
Columns 1-3 are representative immunofluorescence images of endogenous TFEB subcellular localisation under the control conditions used for the screen (nutrient-rich DMEM, no glucose, no amino acids) with or without 0.1% DMSO or Torin (1 μM). These controls were used for figures 17-25 as these experiments were performed in parallel and thus share the same controls. Columns 4-8 show immunofluorescence images of endogenous TFEB subcellular localisation under the control conditions plus the addition of varying concentrations of drug GSK2593067A (10 μM, 5 μM, 1 μM, 0.5 μM) for 2 hours in HT29 (N=1).

The second drug we tested, GSK2373690A is annotated as a PI3Ki that blocks TFEB translocation in response to amino acid and glucose deprivation. The compound was able to sufficiently block translocation of TFEB in response to glucose deprivation and amino acid deprivation using a concentration as low as 1 μM and 0.5 μM respectively **(Figure 35)**.

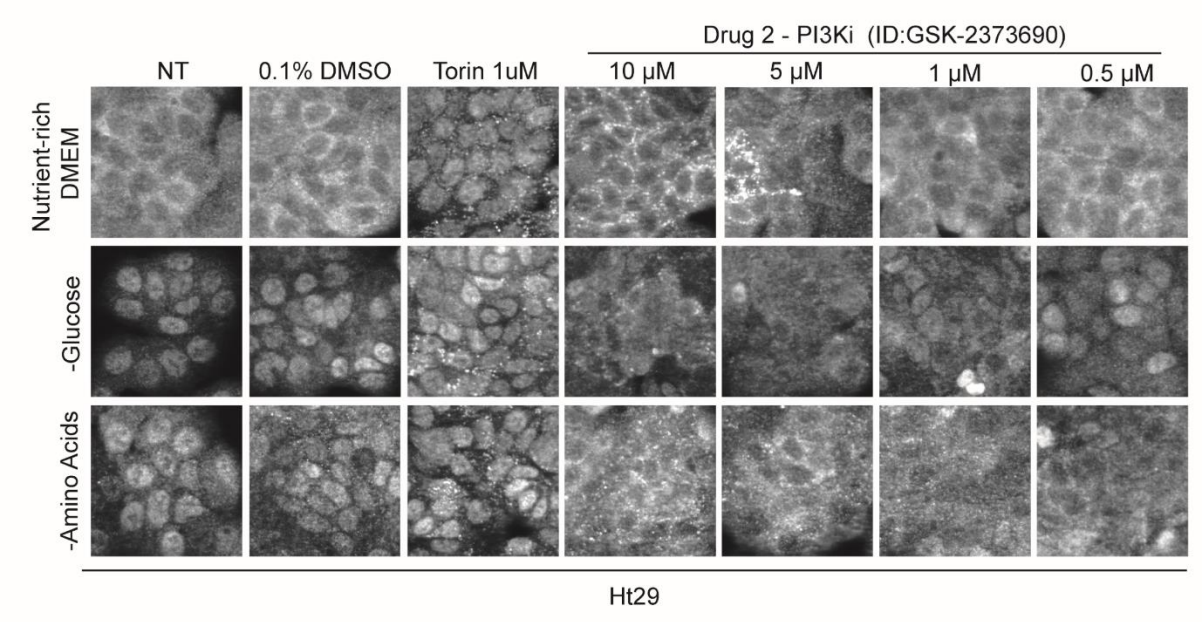

Figure 35. Drug 2, Regno ID: GSK2373690A a PI3K inhibitor attenuates nuclear localisation of TFEB in response to both glucose and amino acid deprivation.
Columns 1-3 are representative immunofluorescence images of endogenous TFEB subcellular localisation under the control conditions used for the screen (nutrient-rich DMEM, no glucose, no amino acids) with or without 0.1% DMSO or Torin (1 μM). These controls were used for figures 17-25 as these experiments were performed in parallel and thus share the same controls. Columns 4-8 show immunofluorescence images of endogenous TFEB subcellular localisation under the control conditions plus the addition of varying concentrations of drug GSK2373690A (10 μM, 5 μM, 1 μM, 0.5 μM) for 2 hours in HT29 (N=1).

Drug GW837331X was annotated as a PLK1 inhibitor and could not prevent translocation in response to glucose deprivation but could attenuate translocation in response to amino acid deprivation using concentrations as low as 1 μM **(Figure 36)**.

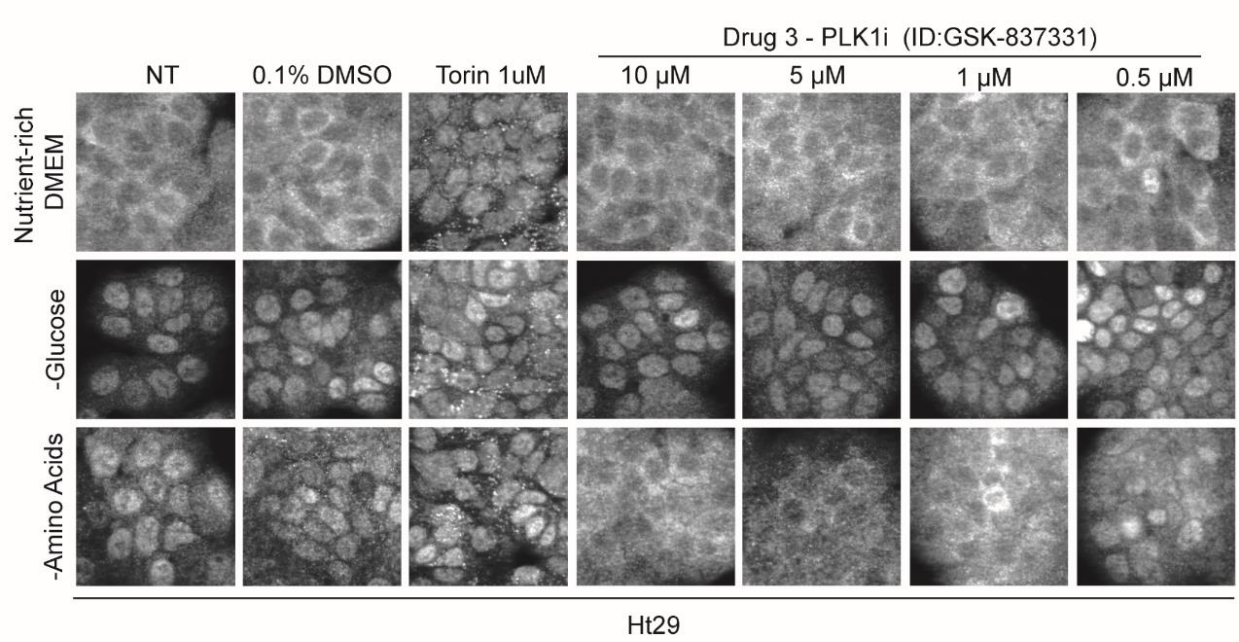

Figure 36. Drug 3, Regno: GSK837331X, a PLK1 inhibitor attenuates nuclear localisation of TFEB in response to amino acid deprivation.
Columns 1-3 are representative immunofluorescence images of endogenous TFEB subcellular localisation under the control conditions used for the screen (nutrient-rich DMEM, no glucose, no amino acids) with or without 0.1% DMSO or Torin (1 µM). These controls were used for figures 17-25 as these experiments were performed in parallel and thus share the same controls. Columns 4-8 show immunofluorescence images of endogenous TFEB subcellular localisation under the control conditions plus the addition of varying concentrations of drug GSK837331X (10 µM, 5 µM, 1 µM, 0.5 µM) for 2 hours in HT29 (N=1).

Drug GW681251X, annotated to be an ALK5 inhibitor, could not prevent translocation in response to glucose deprivation but could attenuate translocation in response to amino acid deprivation using concentrations as low as 0.5 µM **(Figure 37)**.

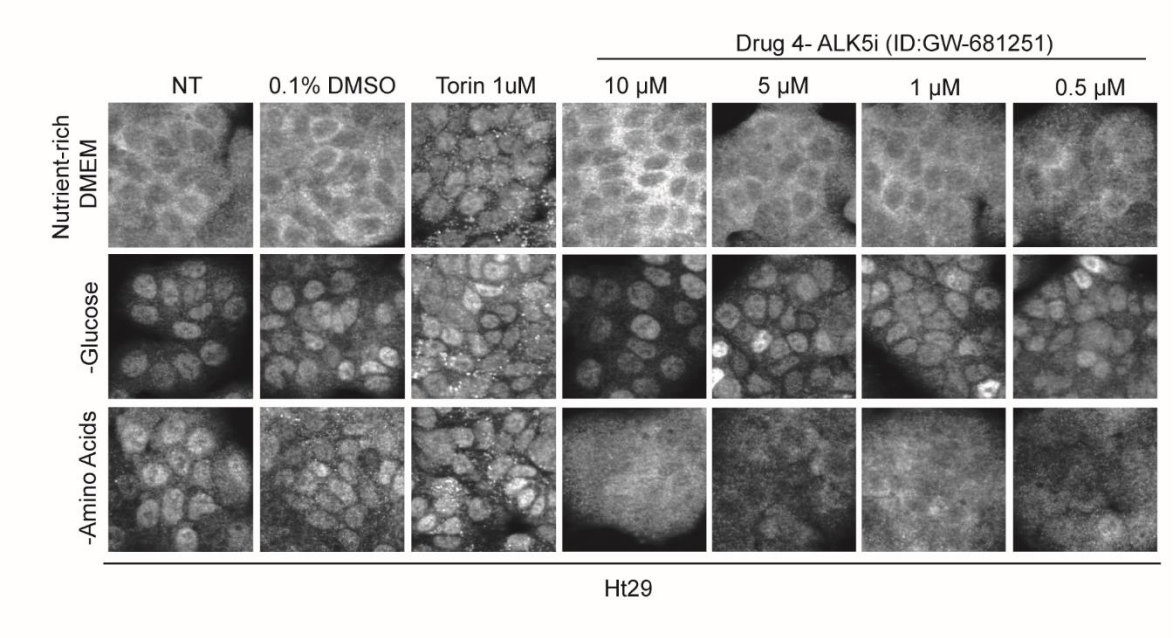

Figure 37. Drug 4, Regno GW681251X, an ALK5 inhibitor attenuates nuclear localisation of TFEB in response to amino acid deprivation.
Columns 1-3 are representative immunofluorescence images of endogenous TFEB subcellular localisation under the control conditions used for the screen (nutrient-rich DMEM, no glucose, no amino acids) with or without 0.1% DMSO or Torin (1 µM). These controls were used for figures 17-25 as these experiments were performed in parallel and thus share the same controls. Columns 4-8 show immunofluorescence images of endogenous TFEB subcellular localisation under the control conditions plus the addition of varying concentrations of drug GW681251X (10 µM, 5 µM, 1 µM, 0.5 µM) for 2 hours in HT29 (N=1).

Interestingly, when using drug GSK1693850A, annotated as a PI3K inhibitor, we could not reproduce the attenuation of translocation of TFEB in response to either glucose or amino acid deprivation at any concentration used (0.5-10 μM). Additionally, at 10 μM, it actually promoted TFEB translocation even under nutrient-rich conditions **(Figure 38)**. One potential explanation for this could be that at high concentrations, GSK1693850A could promote ER stress, promoting nuclear import of TFEB despite nutrients being plentiful.

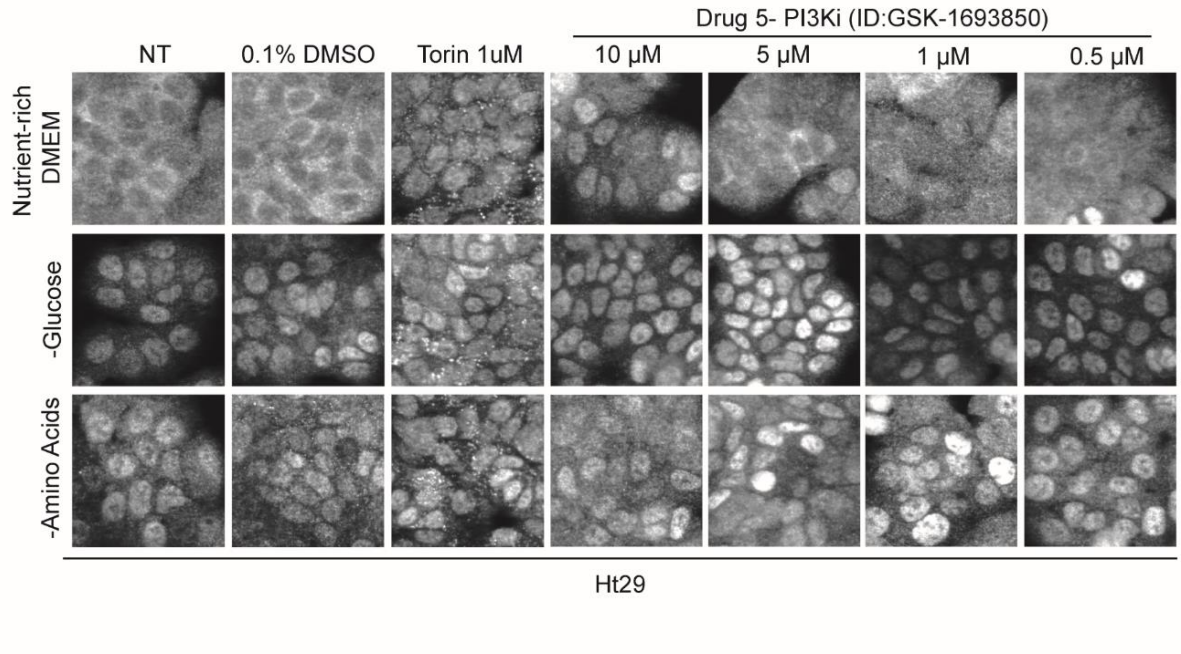

Figure 38. Drug 5, Regno GSK-1693850A, a PI3K inhibitor could not prevent TFEB nuclear translocation in response to either glucose or amino acid deprivation.
Columns 1-3 are representative immunofluorescence images of endogenous TFEB subcellular localisation under the control conditions used for the screen (nutrient-rich DMEM, no glucose, no amino acids) with or without 0.1% DMSO or Torin (1 μM). These controls were used for figures 17-25 as these experiments were performed in parallel and thus share the same controls. Columns 4-8 show immunofluorescence images of endogenous TFEB subcellular localisation under the control conditions plus the addition of varying concentrations of drug GSK-1693850A (10 μM, 5 μM, 1 μM, 0.5 μM) for 2 hours in HT29 (N=1).

GW89516X was able to attenuate translocation of TFEB in response to both glucose and amino acid deprivation using concentrations as low as 1 μM and 0.5 μM respectively **(Figure 39)**.

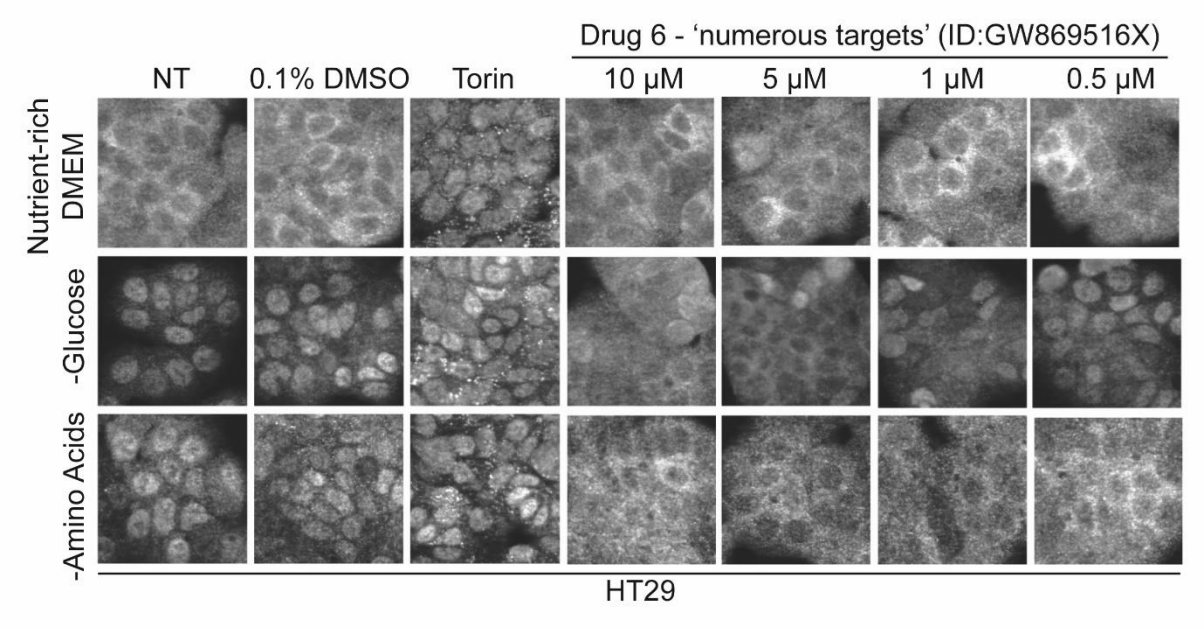

Figure 39. Drug 6, Regno GW869516X, a kinase inhibitor annotated to have numerous targets could prevent TFEB nuclear translocation in response to both glucose and amino acid deprivation.
Columns 1-3 are representative immunofluorescence images of endogenous TFEB subcellular localisation under the control conditions used for the screen (nutrient-rich DMEM, no glucose, no amino acids) with or without 0.1% DMSO or Torin (1 μM). These controls were used for figures 17-25 as these experiments were performed in parallel and thus share the same controls. Columns 4-8 show immunofluorescence images of endogenous TFEB subcellular localisation under the control conditions plus the addition of varying concentrations of drug GW869516X (10 μM, 5 μM, 1 μM, 0.5 μM) for 2 hours in HT29 (N=1).

GSK2344444A annotated as a PI3Ki was able to block nuclear translocation of TFEB in response to glucose and amino acid deprivation using concentrations as low as 5 μM and 0.5 μM respectively **(Figure 40)**.

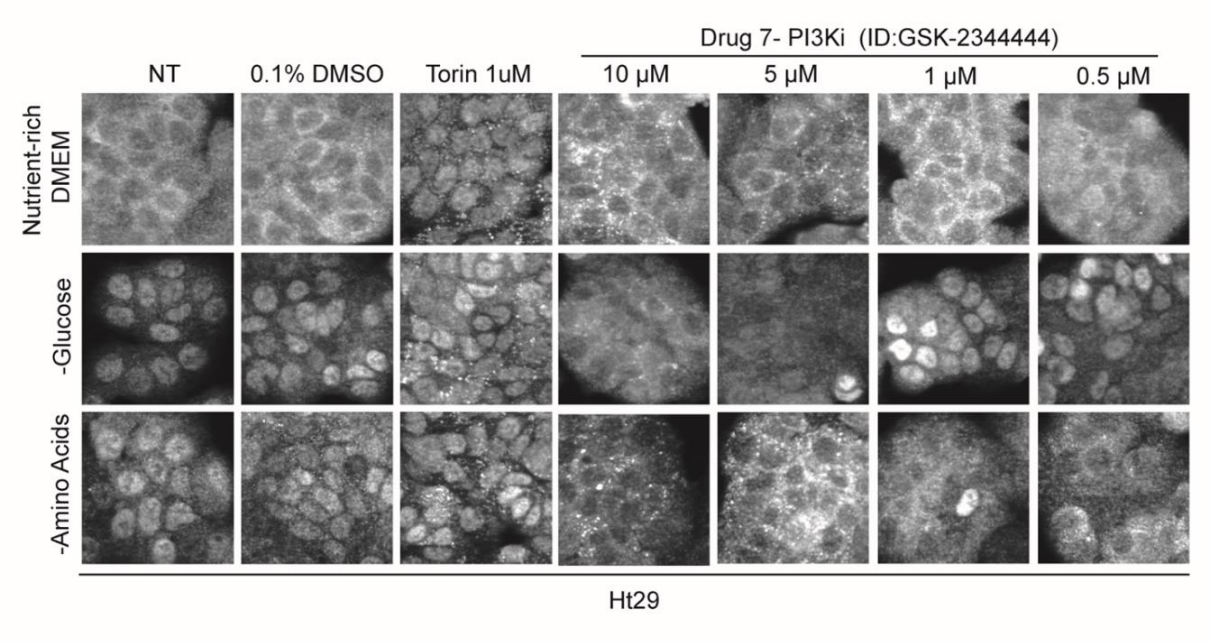

Figure 40. Drug 7, Regno GSK-2344444A, a PI3K kinase inhibitor could prevent TFEB nuclear translocation in response to both glucose and amino acid deprivation.
Columns 1-3 are representative immunofluorescence images of endogenous TFEB subcellular localisation under the control conditions used for the screen (nutrient-rich DMEM, no glucose, no amino acids) with or without 0.1% DMSO or Torin (1 μM). These controls were used for figures 17-25 as these experiments were performed in parallel and thus share the same controls. Columns 4-8 show immunofluorescence images of endogenous TFEB subcellular localisation under the control conditions plus the addition of varying concentrations of drug GSK-2344444A (10 μM, 5 μM, 1 μM, 0.5 μM) for 2 hours in HT29.

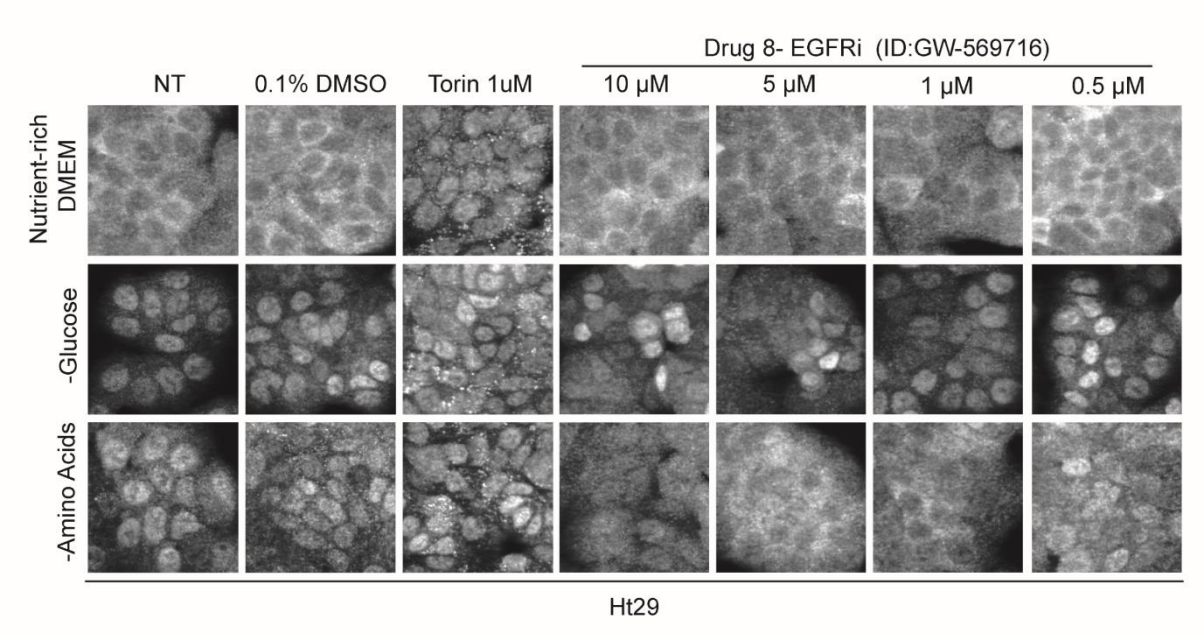

Figure 41. Drug 8, Regno: GW569716A, an EGFR inhibitor could attenuate TFEB nuclear translocation in response to amino acid deprivation.
Columns 1-3 are representative immunofluorescence images of endogenous TFEB subcellular localisation under the control conditions used for the screen (nutrient-rich DMEM, no glucose, no amino acids) with or without 0.1% DMSO or Torin (1 μM). These controls were used for figures 17-25 as these experiments were performed in parallel and thus share the same controls. Columns 4-8 show immunofluorescence images of endogenous TFEB subcellular localisation under the control conditions plus the addition of varying concentrations of drug GW569716A (10 μM, 5 μM, 1 μM, 0.5 μM) for 2 hours in HT29.

GW569716A annotated as an EGFR inhibitor, blocks TFEB translocation in response to deprivation of amino acids but not glucose using a concentration as low as 1 μM **(Figure 41)**. GW810372X, annotated to have numerous targets, seems to partially reduce TFEB nuclear translocation in response to amino acid deprivation but not glucose starvation only when using a concentration of 0.5 μM. However, an interesting observation is that when using higher concentrations, the compound does not prevent translocation **(Figure 42)**. This could be perhaps due to higher concentrations of the compound inducing ER stress and inducing nuclear translocation of TFEB.

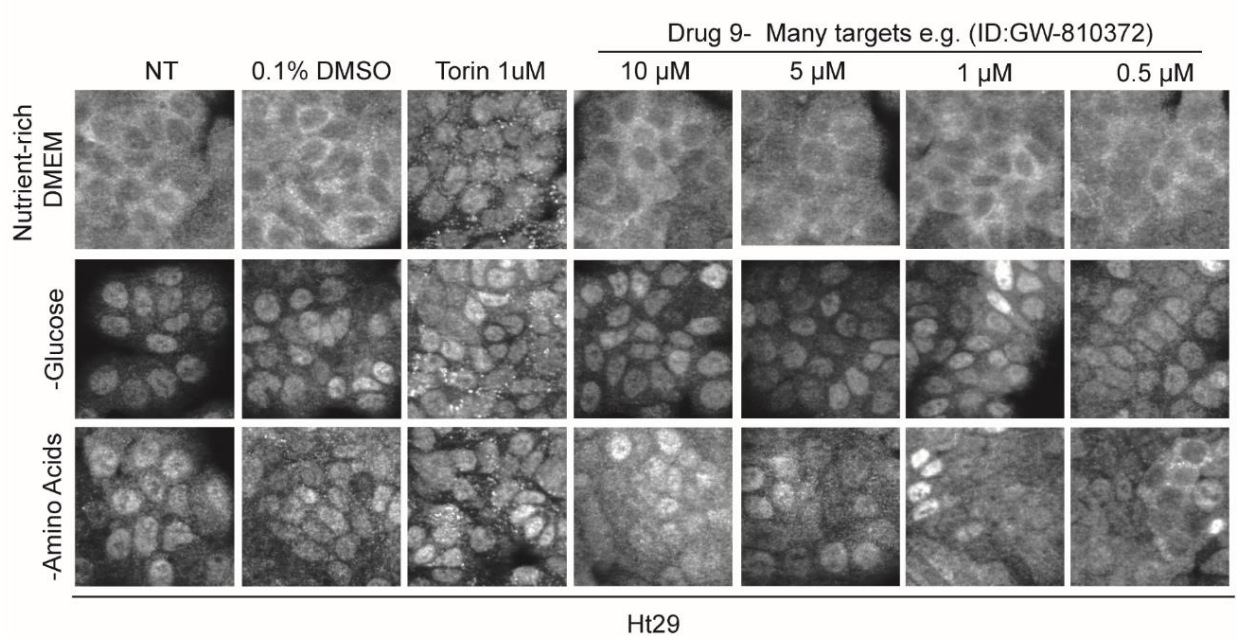

Figure 42. Drug 9, Regno: GW-810372X, annotated to have many targets could only attenuate nuclear translocation of TFEB in response to amino acid deprivation using a concentration of 0.5 μM.
Columns 1-3 are representative immunofluorescence images of endogenous TFEB subcellular localisation under the control conditions used for the screen (nutrient-rich DMEM, no glucose, no amino acids) with or without 0.1% DMSO or Torin (1 μM). These controls were used for figures 17-25 as these experiments were performed in parallel and thus share the same controls. Columns 4-8 show immunofluorescence images of endogenous TFEB subcellular localisation under the control conditions plus the addition of varying concentrations of drug GW-810372X (10 μM, 5 μM, 1 μM, 0.5 μM) for 2 hours in HT29.

In attempt to elucidate more information as to how these drugs prevent TFEB nuclear translocation, we examined the ability of the 'hits' to affect mTORC1 or mTORC2 signaling. To do this, HT29 cells were treated with each 'hit' in the context of nutrient-rich media (DMEM) or media lacking amino acids or glucose. We then examined the ability of each 'hit' to prevent changes in the apparent molecular weight of TFEB (indicative of phosphorylation status) and mTORC1 or mTORC2 signaling induced by amino acid or glucose starvation respectively **(Figure 43)**.

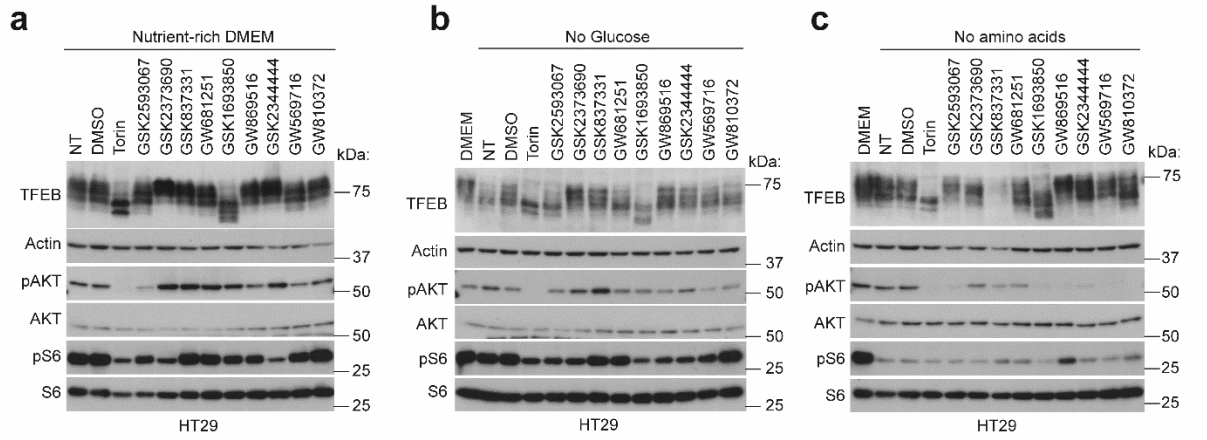

Figure 43. Deciphering mode of action of hits
Western blot analysis of HT29 unstarved (a), starved of amino acids (b) or starved of glucose (c) treated with DMSO (0.1%) as a negative control, Torin 1 (250 nM) as a positive control, and the PKIS hits (10 μM) for 2 hr. NT are non-treated samples where nothing additional was added. 'Normal media' refers to unstarved controls (DMEM). Changes in mTORC1 and mTORC2 signaling was observed by immunoblotting against downstream targets; AKT and S6 ribosomal protein respectively.

As expected, when using Torin 1 (positive control), we observed a reduction in the apparent molecular weight of TFEB (indicative of de-phosphorylation), a decrease in phosphorylation of the S6 ribosomal protein and a decrease in phosphorylation of AKT; downstream targets of mTORC1 and mTORC2 respectively **(Figure 43a)**. Additionally, DMSO (negative control), had no effect on these downstream targets.

Intriguingly, under nutrient rich conditions, two of the hits decreased mTORC1 signaling (GSK2373690 and GSK2344444) but also increase mTORC2 signaling as observed by a decrease in phosphorylation of Ser235/6 on S6 and an increase in phosphorylation of Ser473 on AKT respectively. Despite these changes normally being indicative of an increase in TFEB nuclear translocation, the western blot analysis showed no change in molecular weight of TFEB and our previous immunofluorescence experiment shows that TFEB remains cytoplasmic **(Figure 35 & Figure 40)**. Therefore, one can assume the ability of these drugs to prevent TFEB nuclear translocation in response to either glucose or amino acid starvation is most likely mTORC1/2 independent.

Another interesting observation is that GSK16983850, another kinase inhibitor annotated to target PI3K, induced a large mobility shift (similar to that observed with Torin treatment) in TFEB under nutrient-rich conditions but also under both glucose and amino acid deprivation, indicative of de-phosphorylation required for nuclear translocation of TFEB **(Figure 43a-c)**. These results also corroborate the immunofluorescence images taken demonstrating that at

10 μM, GSK16983850 promotes nuclear translocation of TFEB under nutrient-rich conditions **(Figure 38, lane 1)**. Ultimately, we were unable to re-produce the results from the drug screen as GSK16983850 was unable to prevent TFEB translocation in response to glucose or amino acid starvation **(Figure 38, lanes 2&3).**

Unfortunately, under amino acid or glucose starvation **(Figure 43b, c)**, a marked decrease in TFEB molecular weight was not observed and thus it is inconclusive as to whether the hits could prevent the TFEB mobility shift normally observed in response to starvation. Furthermore, glucose starvation only provoked a minimal increase in phosphorylation of AKT (Serine 473) indicative of increased mTORC2 activity. Because of this, we could not determine which of the hits impair mTORC2 signaling in response to glucose starvation.

However, amino acid starvation caused a large decrease in mTORC1 activity **(Figure 43c)** as observed by a decrease in phosphorylation of S6 (Serine 235/6). The only drug that was observed to partially rescue mTORC1 activity was GW869516X, as observed by an increase in phosphorylation of S6 **(Figure 43c)**. An interesting observation was that under amino acid deprivation, all of the hits were able to inhibit mTORC2 activity to varying degrees as observed by a decrease in phosphorylation of AKT (Serine 473).

Due to the inability to precure more of the compounds as they are not commercially available, we were unable to investigate all hits further. We instead purchased some commercially available inhibitors that targeted the same kinases implicated in the drug screen to see if we could recapitulate the results we observed. To do this, we purchased an EGFR inhibitor (CAS 879127-07-8), an ALK5 inhibitor (CAS 446859-33-2) and a PI3K inhibitor (TGX-221). Our first experiment was to investigate if the inhibitors could prevent the TFEB mobility shift caused by amino acid deprivation or glucose starvation **(Figure 44)**.

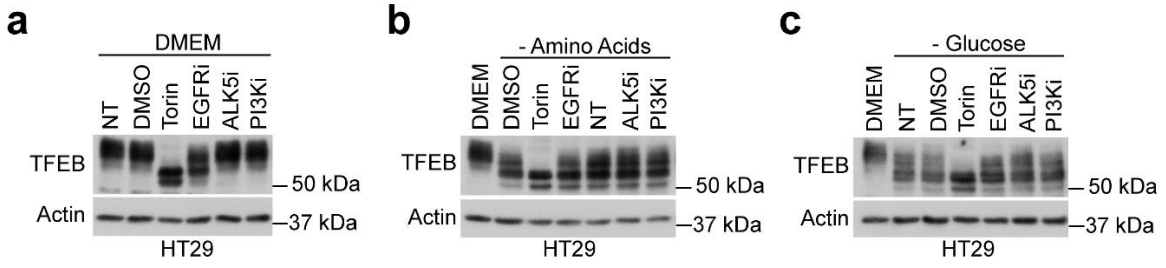

Figure 44. Commercially available kinase inhibitors of EGFR, ALK5 or PI3K are unable to prevent TFEB mobility shift
Western blot analysis of HT29 unstarved (a), starved of amino acids (b) or starved of glucose (c) treated with DMSO (0.1%), Torin 1 (250 nM), EGFR inhibitor (10 μM), ALK5 inhibitor (10 μM), or PI3K inhibitor (10 μM) for 2 hr. NT are non-treated samples where nothing additional was added.

As expected, Torin 1 (positive control) induced a marked mobility shift in TFEB under nutrient-rich conditions and also under either amino acid or glucose deprivation **(Figure 44a-c).** Additionally, DMSO (negative control), had no effect on the molecular weight of TFEB. Interestingly, the EGFR inhibitor caused a slight decrease in molecular weight of TFEB under nutrient-rich conditions whereas the ALK5 and PI3K inhibitors did not **(Figure 44a)**. All three inhibitors used were unable to prevent the mobility shift caused by amino acid or glucose starvation **(Figure 44b, c).**

Afterwards, we examined drug-induced changes on mTORC1 and mTORC2 signaling in the context of glucose deprivation by western blot analysis **(Figure 45a)**. In parallel, we performed immunofluorescence imaging using an antibody recognising endogenous TFEB to assess if the drugs were able to prevent TFEB nuclear translocation in response to glucose or amino acid deprivation **(Figure 45b)**. As before, mTORC1 signalling was again measured through the analysis of phosphorylation status of the downstream target S6 ribosomal protein. mTORC2 signalling was measured through the analysis of phosphorylation status of the downstream target AKT.

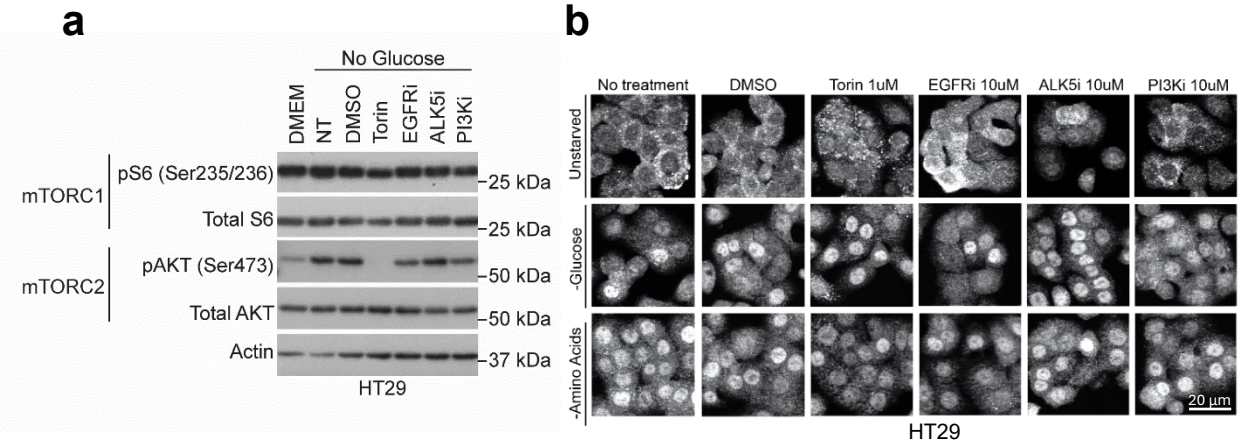

Figure 45. Commercially available kinase inhibitors are unable to re-capitulate changes in mTORC1 and mTORC2 and do not prevent TFEB nuclear translocation in response to glucose starvation, as observed with PKIS hits from drug screen 2
(a) Western blot analysis performed using HT29 unstarved (DMEM) compared to glucose deprived samples treated with DMSO (0.1%), Torin (250 nM), EGFR inhibitor 10 µM), ALK5 inhibitor (10 µM), or PI3K inhibitor (10 µM). (b) Immunofluorescence imaging demonstrating changes in TFEB subcellular localisation in response to glucose deprivation or amino acid deprivation compared to unstarved cells (DMEM). Cells were treated with either DMSO (0.1%), Torin (250 nM), EGFR inhibitor 10 µM), ALK5 inhibitor (10 µM), or PI3K inhibitor (10 µM). NT are non-treated samples where nothing additional was added (N=1)

Unexpectedly, we observed Torin 1 (positive control) only slightly reduced pS6 levels, indicating inefficient inhibition of mTORC1. However, Torin 1 did serve as a good positive control for mTORC2 inhibition, causing complete ablation of pAKT (Ser473) levels **(Figure 45a, Lane 4)**. Furthermore, glucose deprivation caused a marked increase in mTORC2 signaling as indicated by an increase in pAKT (Ser473) levels **(Figure 45a, Lane 2)**. Ultimately, there were no significant changes observed when using the three commercial inhibitors on either mTORC1 or mTORC2 **(Figure 45a, Lanes 5, 7)**. Additionally, the immunofluorescence experiment revealed no visually observable changes in TFEB subcellular localisation in response to drug treatment **(Figure 45b)**. The only notable result would be that under nutrient-rich conditions, the ALK5 inhibitor partially promoted TFEB nuclear translocation **(Figure 45b, Lane 5)**. Although Torin 1 promoted nuclear translocation of TFEB, we also observed punctate staining in the cytoplasm thought to be TFEB associated with lysosomes **(Figure 45b, Lane 3)**, which has also been observed by others (Jose A. Martina and Puertollano 2013)

Due to the inability to procure more of the hits from the screen as they are not commercially available, and not being able to reproduce the results using commercially available kinase inhibitors we chose to focus on one drug and try to elucidate its mode of action. We chose GW89516X due to its ability to prevent translocation in response to both amino acid and glucose deprivation.

To uncover the most likely target(s) responsible for the attenuation of nuclear translocation of TFEB in response to glucose and amino acid deprivation, we ranked the kinases that have been shown to be inhibited by GW89516X (**Table 13**). Most notably, GW89516X was able to inhibit AMPK *in vitro;* a kinase already known to be able to directly phosphorylate TFEB (a phosphorylation mark required for nuclear entry) but also act upstream of both the mTORC1 and mTORC2 pathways. Although the *in vitro* kinase assay data shows GW89516X has the ability to inhibit numerous kinases, it is worth noting that this is based on one *in vitro* kinase assay. Whether or not GW89516X can directly interact with all of these targets in living cells and to what capacity is not known. Furthermore, whether or not an interaction(s) is responsible for changes in TFEB localisation is yet to be determined.

Table 13. *In vitro* kinase data showing percentage (%) inhibition of kinases exhibited by Drug 6 (Regno: GW89516X, Compound ID: UNC10225084A, Chemotype: imidazotriazine, Smile: COc1cc(Nc2ncc3c(C)nc(-c4cc5ccccc5[nH]4)n3n2)cc(OC)c1OC) data obtained from PKSII library from GSK.

Rank	Kinase Name	% Inhibition
1	CIT	100%
2	CSNK2A2	99.7%
3	NEK7	99.7%
4	NEK6	99.6%
5	NEK5	99%
6	JAK1(JH2domain-pseudokinase)	98.5%
7	CSNK2A1	96.4%
8	FLT3	96.3%
9	MLK1	93.8%
10	RSK1(Kin.Dom.1-N-terminal)	91.7%
11	PIP5K2C	90.3%
12	SRC	90.1%
13	NEK9	90%
14	AMPK-alpha1	89%
15	MLK2	89%
16	NEK3	89%
17	PIP5K1C	89%
18	CLK1	88%
19	GCN2(Kin.Dom.2,S808G)	88%

We then repeated the immunofluorescence experiment to confirm the ability of GW89516X to prevent TFEB nuclear translocation in response to starvation was reproducible **(Figure 46)**.

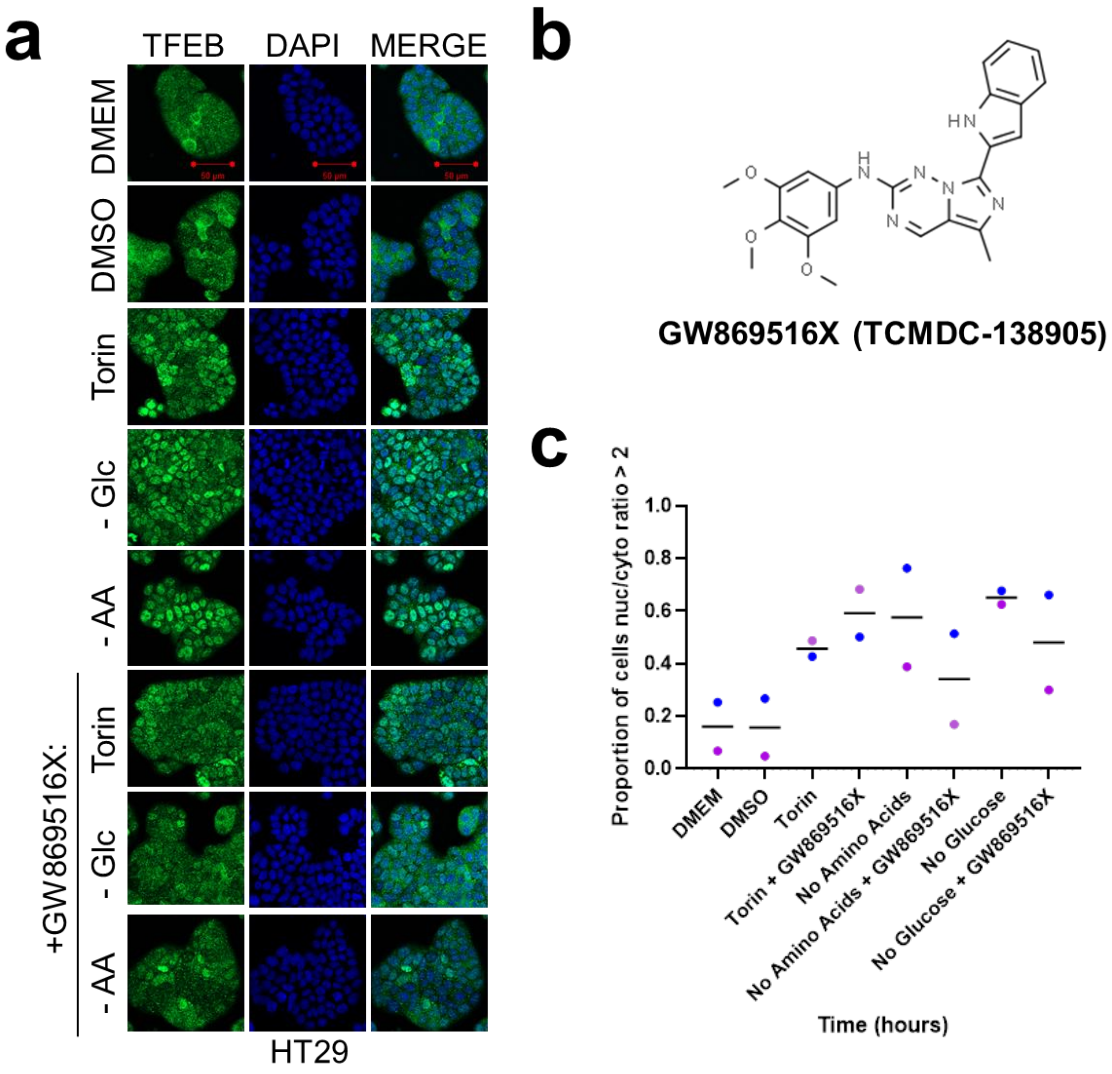

Figure 46. GW89516X reduces TFEB nuclear translocation in response to Glucose or Amino Acid Starvation but not in response to Torin 1 treatment
(a) Representative immunofluorescence images taken of HT29 starved of Amino Acids, Glucose or treated with Torin 1 (250 nM) for 2 hr with or without GW89516X (10 μM). To look at endogenous TFEB subcellular localisation, a TFEB (green) antibody were used and DAPI as a nuclear dye (blue). Pictures of the single channels along with merged images of both TFEB and DAPI are displayed to show co-localisation. Scale bars are shown in red (50 μm). (b) Chemical structure of GW89516X. (c) Scatter plot showing proportion of cells with a nuc/cyto ratio of 2 or greater from the immunofluorescence images (black bars = mean). Biological replicates are colour coded.

As anticipated, Torin 1, glucose starvation and amino acid starvation increased the proportion of cells with nuclear TFEB staining Promisingly, GW89516X reduced the proportion of cells

exhibiting nuclear TFEB staining in response to glucose starvation or amino acid starvation **(Figure 46a, c)**. Interestingly, not only was GW89516X unable to prevent translocation induced by Torin 1 treatment, it significantly increased the proportion of cells with nuclear TFEB staining **(Figure 46c)**.

5.2.3 GW89516X directly binds to and inhibits AMPK activity

After confirming the effect of GW89516X upon TFEB localisation was reproducible, we further explored the signaling pathways affected. To do this we immunoblotted against known mTORC1, mTORC2 and AMPK targets. In addition, we examined if GW89516X could prevent de-phosphorylation of TFEB, evident by western blot analysis as a 'mobility shift' **(Figure 47)**.

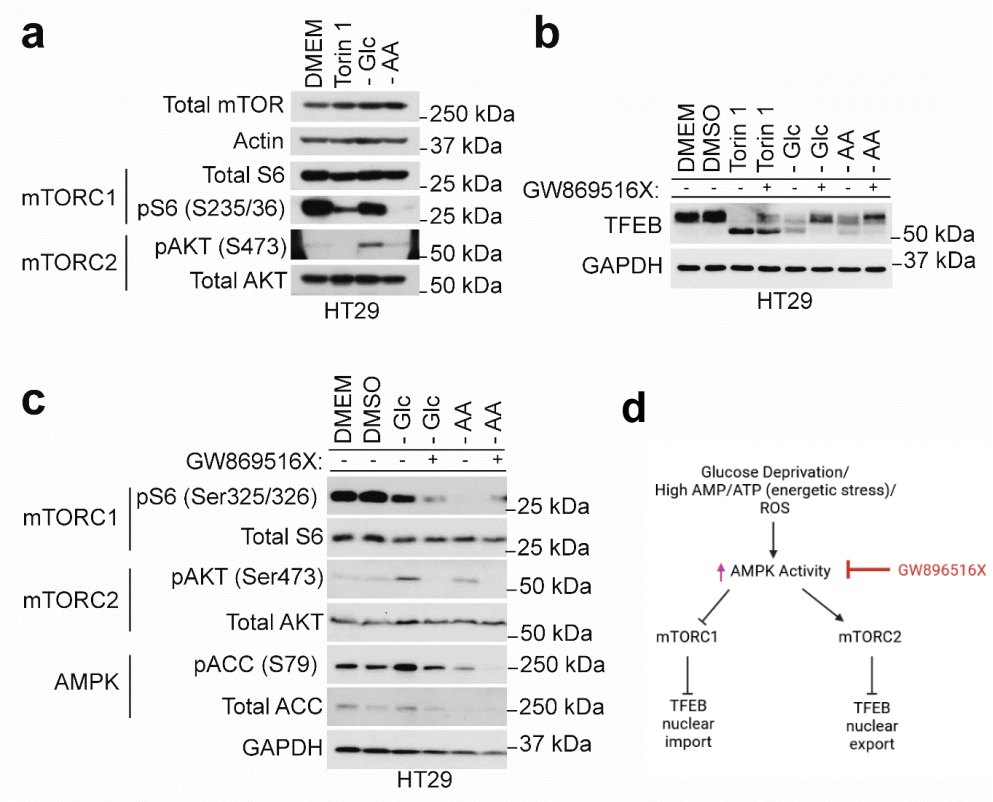

Figure 47. GW89516X impacts mTORC1, mTORC2 and AMPK signalling in response to glucose and amino acid starvation. (a) Western blot analysis performed using HT29 treated with control conditions (DMEM, Torin 1 (250 nM), no glucose or no amino acid medium for 2 hr. Torin 1 inhibits both mTORC1 and mTORC2 signalling as observed by a decrease in downstream targets; phosphorylation of protein S6 (Ser235/36) and AKT (Ser473) respectively. (b) Western blot analysis performed using samples from HT29 treated with control conditions: DMEM, DMSO (0.1%) Torin 1 (250 nM), no glucose or no amino acid medium for 2 hr with or without GW89516X (10 μM). GW89516X is able to prevent a decrease in molecular weight, indicative of de-phosphorylation required for nuclear translocation in response to starvation but only partially in response to Torin 1 treatment. (c) Western blot analysis performed using samples from HT29 treated with control conditions: DMEM, DMSO (0.1%), no glucose or no amino acid medium for 2 hr with or without GW89516X (10 μM). GW89516X is able to partially increase mTORC1 signaling and effectively abolish mTORC2 signalling induced by amino acid starvation and glucose starvation respectively. Treatment with GW89516X also decreases AMPK activity observed through a decrease in the phosphorylation of a direct downstream target; ACC (phosphorylation of Ser79. (d) Simplified schematic showing hypothetical model to explain observations when using GW89516X.

Firstly, we checked the control conditions (Torin 1, glucose starvation and amino acid starvation) induced the expected changes in mTORC1 and mTORC2 signaling **(Figure 47a)**. Indeed, as expected, Torin 1 decreased mTORC1 and mTORC2 activity. Furthermore, glucose starvation promoted mTORC2 activity whereas amino acid starvation reduced mTORC1 signaling. After, we assessed the ability of GW89516X to prevent the observed mobility shift in TFEB caused by Torin 1, glucose or amino acid starvation **(Figure 47b)**. We found that GW89516X could effectively block the mobility shift caused by glucose and amino acid deprivation, further corroborating the immunofluorescence data **(Figure 46)**. Interestingly, even though the immunofluorescence data demonstrated GW89516X was unable to prevent TFEB nuclear localisation in response to Torin 1 treatment, GW89516X seemingly reduced the proportion of TFEB that shifted to a lower molecular weight; observed by a higher molecular weight band remaining; representing the highly phosphorylated and cytoplasmic form of TFEB.

Using the same samples, we immunoblotted against downstream targets of mTORC1 and mTORC2 to assess the ability of GW89516X to impair changes promoted by either amino acid or glucose deprivation **(Figure 47c)**. Additionally, we immunoblotted against a known AMPK target; Acetyl-CoA Carboxylase (ACC). AMPK is known to inhibit ACC directly by phosphorylating Serine 79 (Ser79).

As anticipated, in response to glucose deprivation, we observed an increase in mTORC2 and AMPK signaling, visualised by an increase in pAKT and pACC respectively **(Figure 47c)**. We observed, treatment with GW89516X abolished pAKT and reduced pACC indicating inhibition of mTORC2 and AMPK activity respectively. One intriguing and unexpected finding is that when cells were starved of glucose and treated with GW89516X, a decrease in mTORC1 signaling was observed **(Figure 47c, Lanes 3, 4)**.

Conversely, amino acid deprivation resulted in a decrease in mTORC1 signaling as visualised by a decrease in pS6 (S325/6) relative to total S6 levels **(Figure 47c, Lanes 5, 6)** which was partially rescued by GW89516X treatment. It is worth noting that GW89516X also reduced pAKT and pACC levels under amino acid deprivation. These results support the hypothesis that the ability of GW89516X to prevent TFEB nuclear translocation could be via inhibition of AMPK. A simplistic schematic demonstrating a hypothetical model to explain how AMPK inhibition could lead to changes in mTORC1 and mTORC2 is shown in **(Figure 47d)**.

To assess if GW89516X can directly bind to the active site of AMPK in live cells, we used the NanoBRET TE Intracellular Kinase Assay. This assay employs the use of an energy transfer technique designed to measure the proximity of molecules in living cells. Firstly, the kinase of interest fused with luciferase (NanoLuc), is over-expressed in cells. After, the test compound

along with the NanoBRET tracer is added and luminescence is measured. The assay measures the affinity of test compounds by competitive displacement of the NanoBRET Tracer molecule. In essence, the more binding of the NanoBRET Tracer molecule to the target protein, the more BRET luminescence is measured. In the presence of a competitive inhibitor that can directly bind to the active site of the fusion-kinase, less BRET luminescence is measured **(Figure 48)**.

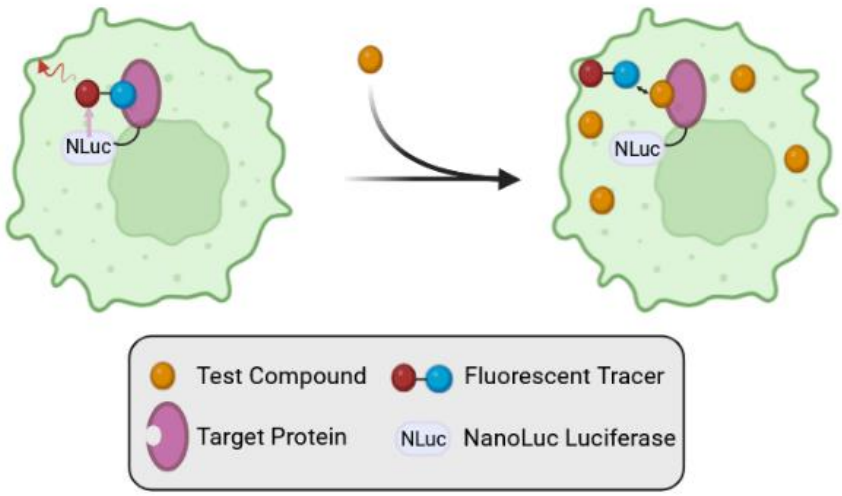

Figure 48. NanoBRET Target Engagement (TE) Intracellular Kinase Assay
The NanoBRET TE intracellular Kinase assay is based on the NanoBRET system, an energy transfer technique used to measure proximity of molecules in living cells. The NanoBRET TE Assays measure the affinity of test compounds by competitive displacement of the NanoBRET tracer, which is able to reversibly bind to the kinase of interest, over-expressed as a NanoLuc luciferase-kinase fusion. If a test compound is able to bind to the active site of the target protein, a decrease in the BRET signal will be observed.

Firstly, the NanoLuc-PRKAA1 (AMPK-α1) fusion protein was transiently over-expressed in HT29 cells. The next day, a serial dilution of GW89516X was performed and added to the cells, along with the NanoBRET Tracer Molecule (2.6 μM) and incubated for 2 hr. Afterwards, the Nano-Glo Substrate and NanoLuc Inhibitor were added and BRET luminescence was measured **(Figure 49)**.

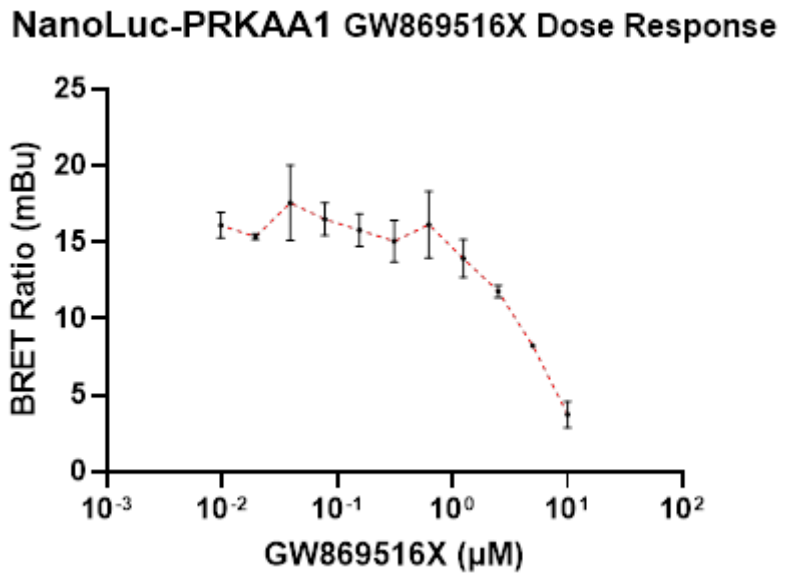

Figure 49. GW89516X can directly bind to the active site of AMPK in a dose dependent manner
GW89516X is able to directly bind to the active site of AMPK-α1, displacing the NanoBRET Tracer, in a dose-dependent manner as observed by a decrease in the BRET (ratio) signal. The BRET ratio shown as milliBRETs, is a calculation that determines the binding occupancy of the Tracer to the Fusion Kinase. It takes into account of the transfection efficiency of cells in different wells and is normalised to control wells without the NanoBRET Tracer. Each biological replicate was performed in technical duplicate (N=2, n=2). Error bars = SEM.

Using the NanoBRET TE Intracellular Kinase Assay, we observed that with increasing concentrations of GW89516X lower BRET ratios were measured **(Figure 49)**. Indicating the ability of GW89516X to bind directly to the active site of AMPK in a dose-dependent manner. This result supports our previous data demonstrating the ability of GW89516X reduce the phosphorylation of ACC at Serine 79; a phosphorylation site specific to AMPK. Additionally, this correlates with the ability of GW89516X to prevent TFEB nuclear translocation in response to glucose and amino acid deprivation in a dose-dependent manner as observed by immunofluorescence **(Figure 39)**.

5.3 Discussion and future perspectives

The MIT/TFE family of transcription factors have been implicated in a plethora of disease contexts. The importance of TFEB/3 in regulating lysosomal biogenesis and autophagy has been demonstrated by numerous studies and as such, they are often referred to as the ‘master regulators of autophagy and lysosomal biogenesis’.

During cancer development, cellular metabolism is rewired. Normal, healthy differentiated cells primarily rely upon mitochondrial oxidative phosphorylation to generate the energy needed for cellular processes. However, cancer cells instead often rely upon aerobic glycolysis which is referred to as the 'Warburg effect' (Kang et al. 2023), this can also be linked to different stages of disease progression, such as metastasis. Furthermore, the role of autophagy during cancer development is complex. Autophagy can inhibit cancer onset but promotes advanced tumour growth (Amaravadi et al. 2016). Pancreatic ductal adenocarcinoma (PDAC) for instance exhibits high levels of autophagy which is thought to contribute to therapy-resistance through the sequestration and degradation of anti-cancer drugs (S. Yang et al. 2011). Furthermore, others have shown PDAC cell lines exhibit constitutively nuclear MiT/TFE due to dysregulation of their nuclear import. As a result, the PDAC cell lines had high levels of MiT-TFE-dependent autophagy (Perera et al. 2015).

Given the MiT/TFE family have been implicated in mediating autophagy to promote pathogenesis in cancers such as PDAC, there is a clinical need to find drugs capable of preventing their activity. The aim of this chapter was to identify drugs that could attenuate nuclear translocation of TFEB in response to glucose and/or amino acid deprivation to prevent the adaptive response to starvation. To do this, we performed an image-based, high-throughput screen using the PKISI/II libraries of 758 compounds (GSK) to identify kinase inhibitors that could attenuate nuclear accumulation of TFEB in response to glucose or amino acid deprivation. This was a novel approach as most, if not all research laboratories that have performed TFEB drug screens have focused on promoting TFEB nuclear translocation.

We found, of 758 drugs, 10 were able to prevent accumulation of TFEB in response to amino acid and/or glucose deprivation. Four drugs blocked nuclear accumulation of TFEB in response to glucose deprivation (GW810372X, GSK2344444A, GSK1693850A, GSK2373723A), four drugs blocked nuclear accumulation of TFEB in response to amino acid deprivation (GSK2593067A, GW837331X, GW681251X, GW569716A) and two were able to block nuclear accumulation of TFEB in response to both amino acid and glucose starvation (GW869516X and GSK2373690A). These findings are interesting as glucose deprivation and amino acid deprivation promote nuclear accumulation of TFEB via two distinct mechanisms. As stated previously, glucose deprivation promotes nuclear accumulation of TFEB via inhibition of nuclear export, whereas amino acid deprivation promotes nuclear import of TFEB. Understanding how these compounds attenuate nuclear accumulation of TFEB can provide novel insights into how we can target either nuclear import and/or export to alter TFEB localisation for therapeutic benefit.

We found 4 out of 6 compounds that could prevent nuclear accumulation of TFEB in response to glucose deprivation (GSK2373690A, GSK2344444A, GSK1693850A and GSK2373723A) were annotated to be PI3K inhibitors. This is unsurprising given that PI3K is upstream of the AKT – mTORC2 pathway and five PI3K inhibitors have already been approved by the FDA for the treatment of breast cancer with PIK3CA mutations and blood disorders (Hongyao Li et al. 2024). Two compounds (GW810372X and GW869516X) were cited to have numerous targets making it difficult decipher their exact mode of action. For instance, GW810372X was annotated to target: PKY2, AurC, DK2/CycE, CDK2/CYCA, GSK3α, GSK3β, CLK2, HIPK1, HIPK4, DYRK1B and DYRK1A. Our lab previously showed GSK3β activity is required for TFEB nuclear export (Li et al. 2018), thus inhibiting GSK3β promotes TFEB nuclear accumulation. It is most likely that this drug prevents nuclear accumulation of TFEB through its ability to inhibit PKY2 (Proline-rich tyrosine kinase 2); a calcium-sensitive non-receptor tyrosine kinase which acts upstream of the PI3K/AKT/GSK3β pathway. Overall, it appeared most of these hits converged on the PI3K-AKT-GSK3β pathway.

Interestingly, the drugs that could prevent nuclear accumulation of TFEB in response to amino acid deprivation were annotated to have numerous targets. For instance, GSK2593067A was annotated to inhibit protein kinase R (PKR)-like endoplasmic reticulum kinase (PERK); a kinase involved in orchestrating the unfolded protein response. PERK is known to act upstream of the p-eIF2α/ATF4/CHOP axis and energetic stress can cause ER stress which can in turn, activate the PERK-AKT pathway and increase mTORC1 activity (Rozpędek et al. 2016). Unfortunately, we could not identify the full name of GSK2593067A as we could not find it in the library. We assume this was a case of the compound being misannotated by the TDI.

Another compound, GW569716A was annotated to be an inhibitor of the epidermal growth factor receptor (EGFR). Interestingly, EGFR acts upstream of numerous pathways involved in promoting cell survival, including the RAS/RAF/MAPK pathway, JAK/STAT pathway and the PI3K/AKT pathway (Wee and Wang 2017). The final kinase inhibitor, GW681251X was annotated to inhibit Activin receptor-like kinase-5 (ALK5); a member of the transforming growth factor-β (TGF-β) family. ALK5 also acts upstream of the RAS/RAF/MAPK pathway and the PI3K/AKT pathway (Papageorgis 2015). It appears that the likely mechanism through which inhibition of RAS would lead to attenuation of nuclear translocation of TFEB is via downstream effects upon PI3K/AKT. Overall, it appeared most of the ‘hits’ from the screen had impacts on the PI3K/AKT pathway either directly or indirectly. Furthermore, it is likely that GW89516X and GSK2373690A act upstream of both mTORC1 and mTORC2 pathways as they are able to prevent nuclear translocation of TFEB in response to both glucose and amino acid starvation.

GW89516X stood out as an interesting candidate to further validate as it has numerous targets including AMPK, a kinase already known to directly phosphorylate TFEB in response to energetic stress (Paquette et al. 2021). AMPK also acts upstream of both mTORC1 and mTORC2 and is activated in response to external 'stressors' including energetic stress.

Although the exact mode of action of the drugs were unclear, we demonstrated that GW869516X, GSK2373690A, GSK2593067A, GSK837331X, GW681251X, GW569716A could reproducibly prevent translocation of TFEB in our follow-up immunofluorescence imaging and that this effect was concentration-dependent. However, results differed from the screen for GSK2344444A; whereby in the drug screen it could only attenuate TFEB nuclear translocation in response to glucose deprivation but in our follow-up immunofluorescence experiment, it could prevent attenuation under both glucose and amino acid deprivation. Additionally, GSK1693850A; a hit that could prevent TFEB nuclear translocation in response to glucose starvation, no longer could and when using a concentration of 10 μM, actually promoted TFEB nuclear translocation in unstarved cells. A potential explanation could be the high concentration used; the compound may be causing ER stress which has been shown to induce TFEB nuclear translocation (Martina et al. 2016b). Overall, these discrepancies warrant further investigation.

Nonetheless, we investigated the pathways these compounds affected and whether this could explain the results we obtained. To do this, we first visualised changes in mTORC1 and mTORC2 signaling; arguably the main regulators of TFEB nuclear import and export respectively. Interestingly, we found GSK2373690 and GSK2344444 inhibited mTORC1 and activated mTORC2 signalling under nutrient-rich conditions. Although these changes are normally indicative of an increase in TFEB nuclear translocation due to mTORC1 inhibition, GSK2373690 and GSK2344444 did not promote nuclear accumulation of TFEB in our follow-up immunofluorescence experiment. Furthermore, GSK2373690 and GSK2344444 are annotated to be PI3K inhibitors in the library. Thus, one would expect to observe a decrease in phosphorylation of AKT in response to treatment with a PI3K inhibitor. However, it is worth noting that under amino acid starvation, both GSK2373690 and GSK2344444 decreased mTORC2 signaling. This demonstrates the effects of these drugs may be dependent on nutrient-availability.

Another interesting observation is that GSK16983850, another hit annotated to target PI3K, induced a large mobility shift in TFEB under all conditions, indicative of mass de-phosphorylation required for nuclear translocation of TFEB, corroborating the immunofluorescence images demonstrating that TFEB is nuclear under all conditions.

Ultimately, we are unclear as to why we observed these discrepancies when using GSK16983850.

The only drug that was that able to partially rescue mTORC1 signaling in response to amino acid deprivation, and inhibit mTORC2 signaling was GW869516X. These results also corroborated the immunofluorescence data, demonstrating that this drug could prevent nuclear attenuation of TFEB in response to amino acid and glucose deprivation respectively. However, we also observed that when unstarved or glucose-starved cells were treated with GW89516X, a decrease in mTORC1 signaling was observed; a finding that would not be explained if the drugs sole mode of action was via its suspected interaction with AMPK. However, the ability of GW89516X to mediate its effect upon mTORC1 and mTORC2 is likely dependent on nutrient availability; perhaps, under conditions whereby mTORC1 is active (where amino acids are plentiful), inhibition of mTORC2 could leads to inhibition of mTORC1 signaling, due to the ability of AKT to activate mTORC1 as part of a feedback loop (Szwed, Kim, and Jacinto 2021).

Due to the hits not being commercially available, we were unable to interrogate all hits further. To investigate their potential mode of action, we purchased commercially available inhibitors that targeted some of the kinases thought to be implicated. Western blot analysis revealed the commercial EGFR, ALK5 and PI3K inhibitors were unable to prevent de-phosphorylation of TFEB (visualised by no change in molecular weight) and nuclear accumulation of TFEB in response to glucose or amino acid starvation. Future studies would benefit from using phospho-specific antibodies to assess changes in the phosphorylation status of TFEB.

We found inhibition of EGFR, and PI3K caused a very minimal decrease in pAKT levels and ALK5 inhibition led to no observable changes in mTORC1 or mTORC2 signaling corroborating their inability to prevent nuclear accumulation of TFEB. These results provided evidence that perhaps the mode of action of some of these drugs were independent of EGFR, ALK5 and PI3K inhibition, despite being annotated to inhibit these kinases. However, there are many factors to consider when comparing the mode of action of different drugs targeting the same kinase. These include: differences in cell permeability or drug uptake, off-target effects and affinity/selectivity of the compounds for their respective targets. Additionally, we did not have a good control to check if the downstream targets of EGFR, ALK5 and PI3K were inhibited. Without knowing the effectiveness of these commercial inhibitors to inhibit EGFR, ALK5 and PI3K it is inconclusive as to whether the inhibitors were even inhibiting their known targets or to what capacity. Therefore, from these experiments alone, we cannot conclude if inhibition of EGFR, ALK5 and PI3K inhibition can alter TFEB subcellular localisation. Future experiments should be performed such as time-course experiments and dose-responses whilst checking

downstream targets to ensure sufficient inhibition of EGFR, ALK5 and PI3K so that conclusions can be drawn.

After being unable to recapitulate the results from the screen using commercially available inhibitors, we chose to focus on an interesting candidate known to inhibit numerous kinases; GW869516X. An interesting observation from the *in vitro* kinase assay data provided by GSK**,** was its ability inhibit AMPK; a kinase already implicated in regulating TFEB subcellular localisation. AMPK can regulate TFEB both directly through phosphorylation of Ser467 and via its downstream effectors; mTORC1, mTORC2 and AKT (Paquette et al. 2021). AMPK is a kinase implicated in many types of cancer; known to act as a tumour suppressor and tumour promotor depending on the type of cancer (Jiyong Liang and Mills 2013). Additionally, there are very few selective AMPK inhibitors on the market, the most commonly used is Compound C, known to have many off-target effects (Liu et al. 2014).

We found GW869516X was able to visually prevent nuclear accumulation of TFEB translocation in response to glucose and amino acid deprivation in our follow-up immunofluorescence experiments. Furthermore, we observed GW869516X could prevent de-phosphorylation of TFEB in response to glucose and amino acid deprivation (visualised by molecular weight) required for nuclear entry. Additionally, we observed GW869516X was able to inhibit mTORC2 and AMPK activity induced by glucose deprivation and partially rescue mTORC1 inhibition induced by amino acid starvation. As these results are consistent with AMPK inhibition, we investigated if GW869516X could directly bind to the active site of AMPK in live cells. By performing an intracellular kinase assay, we demonstrated GW869516X could directly bind to the active site of AMPK in a concentration-dependent manner.

Overall, although these results are consistent with GW869516X mediating its effects on TFEB subcellular localisation through inhibition of AMPK, we have not demonstrated that these effects are solely dependent on AMPK activity. In fact, the ability of GW869516X to prevent nuclear entry of TFEB in response to glucose and amino acid deprivation may be the result of inhibition of numerous kinases. Assuming that a drug would only inhibit one kinase would perhaps be naïve. Deciphering the exact mode of action is challenging as off-target effects are often seen even in commercially available kinase inhibitors.

To address these concerns, there are a plethora of experiments that should be performed. For instance, the use of AMPK knockout and over-expression cell lines would allow us to assess the AMPK-dependence of GW869516X. Additionally, comparing the activities of pharmacological inhibitors (Compound C) and activators (AICAR) and their effects on TFEB subcellular localisation would provide insights into the mechanism through which GW869516X acts.

Another consideration is the cell line we have used. In this study, we used HT29 which is known to harbour the $BRAF^{V600E}$ mutation which causes constitutive BRAF activation. The $BRAF^{V600E}$ mutation has been shown to uncouple liver kinase B1 (LKB1) from AMPK, leading to dampened AMPK activation in response to energetic stress (Esteve-Puig et al. 2009). Furthermore, inhibition of BRAF in $BRAF^{V600E}$ mutant cell lines lead to AMPK activation and autophagy, thought to contribute to therapy-resistance (Sueda et al. 2016). This is because LKB1 is one of the main kinases to phosphorylate AMPK on Thr172, a phosphorylation event required for activation of AMPK. Although LKB1 is the main kinase responsible for AMPK activation, Ca^{2+}/calmodulin-dependent protein kinase β (CaMKKβ), can also phosphorylate AMPK on Thr172 (Woods et al. 2005). Perhaps comparing the effectiveness of GW869516X to prevent nuclear translocation of TFEB in various cell lines with different mutations in this pathway, such as HeLa which is deficient in LKB1, or cancer cell lines that do not have the $BRAF^{V600E}$ mutation could provide us with more insight into the involvement of AMPK in mediating its effects. Additionally, other exciting experiments that could be performed include treating $BRAF^{V600E}$ mutant cell lines with a pharmacological inhibitor of BRAF, such as PLX4032 and co-treating with GW869516X to see how drug treatment would affect cell survival. In addition, it would be interesting to assess how GW869516X affects anchorage independent growth and metastasis in mouse models on various amino acid/glucose restricted diets.

Furthermore, we did not demonstrate that GW869516X is able to prevent TFEB transcriptional activity. However, based on the fact TFEB is a transcription factor and thus, has to be in the nucleus to bind to DNA, we theorise that treatment with GW869516X would reduce TFEB transcriptional activity induced by either glucose or amino acid starvation. Performing qRT-PCR to assess drug-induced changes in TFEB target genes would allow us to confirm this theory.

In summary, we performed a high-throughput, image-based screen using the PKISI/II library (GSK) to identify kinase inhibitors that can prevent the nuclear accumulation of TFEB in response to amino acid or glucose deprivation. Of the 758 drugs tested, we found 10 could prevent nuclear accumulation of TFEB in response to glucose and/or amino acid deprivation. Many of these drugs are annotated to inhibit the PI3K-AKT pathway either directly or indirectly. Furthermore, GW869516X was able to attenuate nuclear accumulation of TFEB in response to both amino acid and glucose deprivation in a dose-dependent manner. We observed GW869516X treatment inhibited mTORC1, mTORC2 and AMPK signalling and can directly bind to the active site of AMPK. Although GW869516X has been shown to inhibit numerous kinases *in vitro,* given what we currently know in regards to regulation of TFEB subcellular localisation, and the evidence presented in this chapter, we believe its mode of action is most

likely through inhibition of AMPK. Inhibition of AMPK is interesting target that has been implicated in cancer research. The commercially available AMPK inhibitor, Compound C commonly has been shown to lack specificity (Emerling et al. 2007). Finding novel inhibitors of AMPK would be beneficial from both an academic and therapeutic standpoint due to the lack of commercially available AMPK inhibitors. In addition, discovering more selective AMPK inhibitors would reduce the likelihood of unpleasant side effects exhibited by drug off-target effects.

Chapter 6: Discussion

6.1 Subcellular localisation of TFEB is controlled by numerous phosphorylation events and is regulated by mTORC1 and mTORC2.

Cells must be able to sense and adapt to changes in their environment in order to maintain cell homeostasis. The ability of cells to balance their nutrient supply with their demand is achieved in part through regulation of mTORC1 and mTORC2 signalling. Cancer cells acquire mutations that promote growth and proliferation independently of growth factors, whilst retaining the ability to sense nutrient levels, such as glucose and amino acids. Additionally, they acquire mutations in genes that promote uptake of glucose and amino acids, as well as rewiring their metabolism. The most commonly mutated oncogenes include: PI3K, AKT, RAS, RAF, ERK, MEK c-Myc, AMPK and mTOR.

As mentioned previously, cancer cells must adapt their behaviour in response to environmental stressors maintain survival and sustain tumorigenesis. For instance, in pancreatic ductal adenocarcinoma, tumours exhibit poor vascularisation, leading to high levels of TFEB-dependent autophagy which is required for pathogenesis (Perera et al. 2015). Moreover, tumours are comprised of subpopulations of cells displaying distinct phenotypes contributing to therapy resistance (Hoek and Goding 2010). The ability of cells to undergo phenotype-switching in response to changes in nutrient availability is essential for maintaining tumorigenesis. For instance, it has been demonstrated that melanoma cells can sense and adapt to glutamine withdrawal to induce translational reprogramming that impacts their metabolism (Falletta et al. 2017). Another study deprived non-small cell lung cancer (NSCLC) cells of each one of 20 amino acids and demonstrated that glutamine, arginine, methionine, and lysine all activated AKT to promote cell survival (Jin et al. 2021), highlighting the importance of other amino acids. Furthermore, the phenotype of melanoma cells also determines their responsiveness to stress, as demonstrated by observations that different melanoma cell lines representing different phenotypes respond differently to oxygen deprivation (Louphrasitthiphol et al. 2019).

One of the main ways cells promote catabolism in response to nutrient deprivation is via inhibition of mTORC1 and/or activation of mTORC2. One of the main effectors that promotes catabolism in response to mTORC1 inhibition are the MiT/TFE family of transcription factors. TFEB activity is regulated primarily through post-translational modifications, particularly phosphorylation, which alters its subcellular localisation. As a transcription factor, TFEB can only promote transcription when in the nucleus. How TFEB subcellular localisation is regulated by amino acids is well understood. Briefly, under nutrient-rich conditions, MAP4K3

phosphorylates TFEB on Ser3 (Hsu et al. 2018), allowing interaction with the Rags and recruitment to the surface of the lysosome. mTORC1 is then able to phosphorylate TFEB on numerous serine residues including Ser211, which promotes its cytoplasmic sequestration by the chaperone protein 14-3-3 and thus, prevents TFEB activity (Vega-Rubin-de-Celis et al. 2017). Conversely, in response to amino acid limitation mTORC1 is inhibited, allowing nuclear entry and transcriptional activity of TFEB.

Regulation of TFEB subcellular localisation is highly complex and involves integration of many signalling pathways. Numerous kinases and their respective phosphorylation events have been implicated in the regulation of TFEB localisation, transcriptional activity and stability such as: mTORC1 on Ser142, Ser122 and Ser211 (Martina et al. 2012; Vega-Rubin-de-Celis et al. 2017), MAP4K3 on Ser3 (Hsu et al. 2018), ERK2 on Ser142 (Settembre et al. 2011), GSK3β on Ser138 (Li et al. 2016), AKT on Ser467 (Palmieri et al. 2017), AMPK on Ser467 and Ser469 (Paquette et al. 2021) and PKC on Ser461, Ser466 and Ser468 (Ferron et al. 2013). In addition, TFEB can be actively dephosphorylated in response to an increase in intracellular calcium levels by calcineurin (Medina et al. 2015) and in response to oxidative stress by PP2A (José A. Martina and Puertollano 2018). Overall, the regulation of subcellular localisation and/or transcriptional activity of TFEB by phosphorylation is highly complex.

Although the nuclear import of TFEB in response to amino acid withdrawal is well understood, the ability of TFEB to respond to other nutrients such as glucose is not. The first part of this project explored the signalling pathways that are implicated in the response to glucose withdrawal and how TFEB subcellular localisation was affected. Through this work, we demonstrated that in response to glucose starvation, TFEB rapidly accumulates in the nucleus in an mTORC1-independent manner. Instead, glucose deprivation activates mTORC2. By immunofluorescence, we showed that localisation of TFEB was reversible and upon re-feeding, TFEB could return to being cytoplasmic. This work demonstrated that TFEB subcellular localisation is dynamic, and reversible and is controlled by both nuclear import and nuclear export. Moreover, our lab identified a novel, highly conserved nuclear export signal in the MiT/TFE family members with adjacent phospho-sites that when mutated, prevented nuclear export.

Downstream of mTORC2-AKT signalling is GSK3β, a kinase that has already been demonstrated to phosphorylate TFEB on Ser138 (Li et al. 2016). However, the group did not consider that GSK3β requires a priming phosphorylation event. This project demonstrated that GSK3β indeed phosphorylates TFEB on Ser138 but only after TFEB is phosphorylated on Ser142 by ERK2/mTORC1 (Li et al. 2018). This dual phosphorylation event provides cells with an ability to integrate amino acid and glucose levels to finely tune TFEB activity.

In a similar fashion, we showed GSK3β can phosphorylate Ser69 on MITF but only when first phosphorylated on Ser73 by ERK2 (Ngeow et al. 2018). Overall, the first part of this project contributed to the identification of a novel nuclear export signal in both TFEB and MITF which is controlled by a dual phosphorylation event (Li et al. 2018;Ngeow et al. 2018) and highlights the importance of nuclear export in the regulation of the MiT/TFE family.

6.2 Promoting TFEB activity as a therapy for neurodegenerative diseases

In neurodegenerative diseases, lysosomal biogenesis and autophagy are often impaired and contribute to disease pathogenesis. As TFEB is referred to as the 'master regulator of lysosomal biogenesis and autophagy' (Palmieri et al., 2011), it is no surprise that overexpression or activation of TFEB can ameliorate disease pathogenesis through promoting intracellular clearance in a variety of neurodegenerative diseases, including: Alzheimer's (Zhang & Zhao, 2015; Meng et al., 2016), Parkinson's (Zhuang et al., 2020;Chen et al., 2021), Huntington's (Ojalvo-Pacheco et al., 2024; (Tsunemi et al. 2012), and spinal and bulbar muscular atrophy (Cortes et al. 2014).

Due to the mounting evidence highlighting that promotion of TFEB activity is therapeutically beneficial in neurodegenerative diseases, the second part of this project aimed to identify drugs that could promote TFEB activity. To do this, we performed a high-throughput, image-based screen using an FDA-approved library of 1,600 small compounds and quantified drug-induced changes in subcellular localisation as a proxy for TFEB activity. A disadvantage of using this approach is that we effectively excluded drugs that could promote autophagy or lysosomal biogenesis via TFEB-independent mechanisms. However, a clear advantage is that, based on the evidence from numerous studies, it is clear that promoting TFEB activity should provide therapeutic benefit. Additionally, identifying drugs that can promote TFEB subcellular localisation may provide novel insights into the regulatory mechanisms involved.

In this study, we demonstrated that out of 1,600 drugs tested, 94 could promote nuclear accumulation of TFEB and/or TFE3. Rather than looking at TFEB-dependent drug-induced transcription by RT-qPCR, we performed a secondary, functional validation step, by assessing drug-induced changes in lysosomal staining. Our reasoning for this was that many anti-cancer drugs in the library have been reported to impair lysosomal function which could promote nuclear translocation of TFEB and thus transcriptional activity but overall, would not be therapeutically beneficial for the treatment of neurodegenerative diseases. For instance, we observed quinacrine hydrochloride was able to induce nuclear accumulation of TFEB and has been previously reported to permeabilise the lysosomal membrane (Bredahl Hansen et al. 2021).

Of the 94 drugs that could induce nuclear accumulation of TFEB, we found 50 that were able to increase lysosomal staining, indicative of an increase in lysosomal number. Notably, an increase in lysosomal number does not always equate to an increase in lysosomal biogenesis or activity but could be a consequence of impaired lysosomal degradation. In addition, many anti-cancer drugs that are weakly basic have been shown to accumulate in lysosomes, and thus, impair lysosomal function (Zhitomirsky and Assaraf 2017). However, the fact that numerous hits from our screen have been identified by independent studies to induce autophagy gave us confidence in our method. For instance, trifluoperazine, pimozide, loperamide were identified to induce autophagy in an independent screen (Zhang et al., 2007) and another screen identified ouabain as an inducer of TFEB nuclear translocation via inhibition of mTORC1 and exhibited neuroprotection in a cell-based model of Alzheimer's disease (Song et al. 2019).

Interestingly, pimozide and loperamide are calcium channel inhibitors and can reduce intracellular Ca^{2+} levels (Zielke et al. 2018). In addition, trifluoperazine can inhibit calmodulin (Kenigsberg, Côté, and Trifaró 1982). At first glance, it would appear unlikely that calcium channel inhibitors would be able to promote autophagy, as increased levels of cytosolic Ca^{2+} levels promote TFEB activity through activation of the phosphatase calcineurin (Medina et al. 2015) as well as through inhibition of mTORC1 by CAMKK2/CaMKKβ and AMPK (Høyer-Hansen et al. 2007). However, the role calcium plays in autophagy is complex, with some studies reporting that Ca^{2+} can act as an inhibitor of autophagy. For example, excess amino acids can induce intracellular levels of Ca^{2+} which can directly promote binding of Ca2+-CALM/calmodulin to PIK3C3/VPS34 and result in activation of mTORC1 and inhibition of autophagy (Gulati et al. 2008). Others have also demonstrated that inositol 1,4,5-trisphosphate receptor (ITPR)-dependent Ca^{2+} signalling acts to maintain mTORC1 activity and prevent autophagy (Khan and Joseph 2010). A decrease in intracellular cytosolic Ca^{2+} can also promote Ca^{2+} release from intracellular stores and activate Calcineurin (Park et al. 2020). Nevertheless, calcium signalling is important for neuronal function and has been implicated in neurodegenerative diseases (Pchitskaya, Popugaeva, and Bezprozvanny 2018). Future studies should measure changes in intracellular Ca^{2+} using calcium dyes such as Fura-2 AM (Barreto-Chang and Dolmetsch 2009) to confirm how these drugs affect intracellular calcium levels.

An alternative strategy to assess drug-induced changes on autophagic flux would be to use the dual fluorescent mCherry-EGFP-LC3B tandem vector (Kimura, Noda, and Yoshimori 2007) as previously mentioned (Chapter 4 discussion). Although we did generate a stable cell line expressing mCherry-EGFP-LC3B in HT29, we were unable to optimise the control conditions due to lack of time. Future experiments could use this cell line to look at drug-

induced changes in autophagic flux. In addition, performing dose and time-course experiments would allow us to assess drug pharmacokinetics, such as IC_{50} or the optimal time-point to use in order to visualise changes in autophagic flux.

Furthermore, we identified two neurotransmitter-related drugs that showed potential for drug re-purposing; nortriptyline hydrochloride and pimozide. We demonstrated by western blot analysis that both drugs could induce an increase in LC3B II and a further increase when used in combination with the autophagy inhibitor, bafilomycin A (BafA), indicative of increased autophagic flux (Mizushima and Yoshimori 2007). In addition, we demonstrated that they acted at least partially through TFEB and TFE3. Arguably, drug-induced changes in autophagic flux were only slightly reduced when TFEB or TFE3 was silenced, demonstrating that TFEB or TFE3 were not solely responsible for mediating their effects. However, we hypothesise that upon genetic ablation of both TFEB and TFE3, we would see an even greater reduction due to TFEB and TFE3 displaying functional redundancy (José A. Martina et al. 2014). Although recently, we have demonstrated that in the context of melanoma, TFEB, TFE3 and MITF exhibit differences in their transcriptional targets, driving radically distinct gene expression programs (Dias et al. 2024).

Nevertheless, knockout of TFEB or TFE3 significantly reduced the ability of pimozide to increase lysosomal staining, indicating that both TFEB and TFE3 mediate pimozide induced changes in lysosomal number. Additionally, we demonstrated that pimozide displayed neuroprotection in cell-based models of neurodegenerative diseases whereby SH-SY5Y cells were treated with either lipopolysaccharides or Amyloid β(1-42) oligomers. Although we did not demonstrate that the neuroprotective effect of pimozide is dependent upon TFEB and/or TFE3, given our understanding of the pathogenesis of neurodegenerative diseases, and having demonstrated an increase in lysosomal number and autophagic flux, it is plausible that TFEB is mediating these effects. Future studies should repeat these neuroprotective assays using a double knockout TFEB/3 cell line, as well as performing genetic rescue experiments to confirm this.

Overall, this work demonstrated that targeting TFEB/3 activity is feasible and can promote neuroprotection in cell models of neurodegenerative diseases. Future work should look toward defining drug mode of action as well as assessing the effect of these drugs in rodent models of neurodegenerative diseases. For example, one study demonstrated that a rat model of Alzheimer's disease, harbouring three familiar App mutations and humanized Aβ sequence knocked into the rat App gene exhibits pathologies and disease progression resembling those in human patients (Pang et al. 2022). This model would be a useful tool in understanding if these drugs would be suitable for drug re-purposing.

Furthermore, our screen has provided a reservoir of small molecules that can promote TFEB/3 nuclear accumulation and induce increases in lysosomal number. Given that these drugs are already clinically approved, the process of re-purposing them once their mode of actions are determined would be easier than developing new drugs to modulate TFEB activity. Taken together, this work has contributed to our understanding of how promoting TFEB/3 nuclear translocation may be beneficial in the context of neurodegenerative diseases.

6.3 Inhibiting TFEB activity as a therapy for cancer

The MiT/TFE family have been implicated in many types of cancer disease contexts. TFEB has been implicated in numerous types of tumours, particularly those exhibiting poor vascularisation. For example, TFEB promotes growth and proliferation of pancreatic ductal adenocarcinoma (PDAC) through promotion of autophagy (Perera et al. 2015) but also through its ability to increase glutamine catabolism (Kim et al., 2021). Preventing TFEB activity either by preventing nuclear import or conversely, promoting its nuclear export would provide clear therapeutic benefits in the context of cancers that exhibit high levels of autophagy, such as PDAC.

To assess the feasibility of inhibiting TFEB activity in response to amino acid or glucose deprivation, we performed a high-throughput image-based screen and assessed which drugs could reduce nuclear accumulation of TFEB. We found out of 758 drugs tested, only 10 could attenuate nuclear accumulation of TFEB in response to amino acid or glucose deprivation. Notably, many of these inhibitors converged on the PI3K-AKT pathway, either through directly inhibiting PI3K or via upstream signaling. Although we could not reproduce the results with commercially-available inhibitors (possibly due to drugs exhibiting various off-target effects and/or exhibiting different EC50s), our current understanding of TFEB subcellular localisation and the importance of PI3K-AKT signalling in cell homeostasis, it unsurprising that many of our hits were annotated to inhibit PI3K activity.

Furthermore, we identified GW869516X as a drug able to prevent nuclear accumulation of TFEB in response to both glucose and amino acid deprivation and impair mTORC1 and mTORC2 mediated responses. By western blot analysis we visualised in response to amino acid deprivation, GW869516X was able to partially rescue mTORC1 activity and in response to glucose withdrawal, GW869516X was able to inhibit mTORC2 signalling. These results implied that GW869516X acted upstream of both mTORC1 and mTORC2.

Although GW869516X is able to inhibit numerous kinases, AMPK stood out as it has already been shown to activate TFEB (Paquette et al. 2021), inhibit mTORC1 activity (Gwinn et al., 2008) and promote mTORC2 activity (Kazyken et al. 2019). In this study, we demonstrated

GW869516X was able to promote mTORC1 activity in response to amino acid deprivation and inhibit mTORC2 and AMPK activity. We also demonstrated that GW869516X could directly bind to AMPK in live cells in a concentration-dependent manner. However, we did not determine how the drug binds to AMPK to prevent tracer binding; either through directly binding to the active site of AMPK or through binding elsewhere and promoting a conformational change. Thus, understanding how GW869516X binds to AMPK warrants further investigation.

Targeting AMPK activity is an interesting area of research as it can act as both a tumour suppressor and tumour promoter depending on the context (Jiyong Liang and Mills 2013). For instance, cancers harbouring hyperactivating mutations in BRAF, such as the $BRAF^{V600E}$ mutation, display constitutively active ERK which uncouples LKB1 from AMPK, dampening AMPK activity and leading to increased mTORC1 activity (Esteve-Puig et al. 2009). In the context of cancers with mutations and/or hyperactivation of Ras, EGFR or PI3K/AKT signalling, activating AMPK would help restore regulation of mTORC1. Another interesting aspect of AMPK in BRAF mutant cancers is the idea of combination therapy. For instance, in thyroid cancer, inhibition of BRAF leads to AMPK-dependent cytoprotective autophagy and is thought to contribute to therapy resistance (Jiménez-Mora et al. 2021). Therefore, a clinical trial investigating the benefit of combined therapy versus using BRAF inhibitors alone would provide us with valuable insight into guiding future therapeutic strategies.

Others have demonstrated that AMPK can act as a tumour suppressor. For instance, activation of AMPK stabilises p53 and promotes apoptosis (Nieminen et al. 2013) and also inhibits the metastatic potential of melanoma cells by modulating ERK signalling and reducing the levels of the cyclooxygenase 2 (COX-2) protein (Kim et al., 2012), an enzyme required for Prostaglandin E2 (PGE2) synthesis which is involved in inflammation and lipid production. Additionally, genetic ablation of *Pten* and *Prkaa1* (encoding AMPK-α1) in mice promoted lymphoma development at an earlier age than *Pten* knockout mice which expressed wildtype AMPK and were also more aggressive (Vara-Ciruelos et al. 2019).

Overall, these studies highlight the complexities of AMPK activity in mediating tumorigenesis and warrant further investigation. Although there are many ways to activate AMPK, such as biguanides (metformin, phenformin), thiazolidinediones, polyphenols (resveratrol, berberine and quercetin), ginsenosides, and α-Lipoic acid, most indirectly activate AMPK through altering the levels of ATP. The first direct AMPK activator was 5-aminoimidazole-4-carboxamide riboside (AICAR), an adenosine analog that when taken up into cells, generates the AMP-mimetic, AICAR monophosphate (ZMP). In 2006, a direct activator of AMPK, A-769662 was identified by Abbott Laboratories (Cool et al. 2006). In addition to providing

researchers with a direct activator of AMPK with fewer off-target effects, it proved targeting AMPK with non-nucleotide ligands was possible. Since then, many more direct activators have been developed such as Salicylate (Hawley et al. 2012), Compound-13 (Gómez-Galeno et al. 2010), PT-1 (Pang et al. 2008) and MT 63–78 (Zadra et al. 2014) that can allosterically activate AMPK.

Although there has been success in the development of AMPK activators, the development of selective AMPK inhibitors has been less successful. The only cell-permeable AMPK inhibitor that is commercially available is Compound C. Compound C has been shown to inhibit other kinases and as a result, has many off-target effects (Jin et al., 2009; Emerling et al., 2007; Liu et al., 2014). Therefore, there is a clinical need to discover new, more potent inhibitors of AMPK in order to study how AMPK is implicated in cancers.

Our work has contributed to the identification of a new AMPK inhibitor that once fully-validated, could be useful to study AMPK activity. In addition, knowing GW869516X directly binds to AMPK may provide novel insights into how we can develop more selective AMPK inhibitors in the future.

6.4 Conclusion

This work has contributed to our understanding of how subcellular localisation of TFEB is regulated by not only amino acids, but also by glucose. We demonstrated that in response to glucose withdrawal, mTORC1 activity is largely unaffected, whereas mTORC2 activity increases. Furthermore, we demonstrated that GSK3β, downstream of mTORC2 can phosphorylate serines adjacent to a conserved nuclear export signal in both TFEB (Ser138) and MITF (Ser69) but only when a priming phosphorylation event by ERK2/mTORC1 (Ser142/Ser73 in TFEB/MITF) occurs first. This work contributed to our understanding of how a dual phosphorylation event on TFEB (Li et al., 2018) and MITF (Ngeow et al. 2018) controls nuclear export and enables the integration of amino acid and glucose availability. Prior to this work, the TFEB field has focused primarily on regulation of nuclear import in response to amino acid starvation. Here we demonstrate that regulation of nuclear export is also important as TFEB subcellular localisation is highly dynamic and readily reversible. Furthermore, the ability of TFEB to respond to low glucose levels highlights its other roles in metabolism. Investigation into the regulation of TFEB nuclear export gives rise to another avenue for targeting TFEB activity therapeutically.

Through the use of a high-throughput, image-based screen, we identified 50 FDA-approved drugs that promote nuclear accumulation of TFEB and increase lysosomal staining. We identified pimozide, a neuro-transmitter related drug, which was able to induce changes in

autophagic flux and lysosomal staining in a partially TFEB or TFE3 dependent manner. In addition, pimozide displayed neuroprotection in cell-based models of neurodegenerative diseases, highlighting it as a potential therapeutic agent that could be re-purposed in the future.

Conversely, we performed a second screen, through which we identified 10 kinase inhibitors that were able to attenuate nuclear accumulation of TFEB in response to amino acid or glucose deprivation. Of these 10 kinases, we identified GW869516X as a novel AMPK inhibitor, that can directly bind to the active site of AMPK. This finding is critical for furthering our understanding of how TFEB subcellular localisation is regulated, but also provides insight into how we can also target AMPK activity.

Overall, our screens have provided a reservoir of compounds that can either activate, or inhibit TFEB activity through regulation of its subcellular localisation. The implications of these findings are useful to a variety of diseases that TFEB is implicated in. In addition, the identification of a novel AMPK inhibitor may provide researchers with an alternative to compound c to study the role of AMPK activity in disease.

Reference list

Aksan, I, and C R Goding. 1998. 'Targeting the Microphthalmia Basic Helix-Loop-Helix-Leucine Zipper Transcription Factor to a Subset of E-Box Elements In Vitro and In Vivo'. *MOLECULAR AND CELLULAR BIOLOGY*. Vol. 18.

Ali, Adnan, Klaus P. Hoeflich, and James R. Woodgett. 2001. 'Glycogen Synthase Kinase-3: Properties, Functions, and Regulation'. *Chemical Reviews* 101 (8): 2527–40. https://doi.org/10.1021/cr000110o.

Almuhaideb, Ahmad, Nikolaos Papathanasiou, and Jamshed Bomanji. 2011. '18F-FDG PET/CT Imaging in Oncology'. *Annals of Saudi Medicine*. https://doi.org/10.4103/0256-4947.75771.

Amaravadi, Ravi, Alec C Kimmelman, and Eileen White. 2016. 'Recent Insights into the Function of Autophagy in Cancer'. https://doi.org/10.1101/gad.287524.

Argani, Pedram, Marick Laé, Brian Hutchinson, Victor E Reuter, Margaret H Collins, John Perentesis, John E Tomaszewski, et al. 2005. 'Renal Carcinomas With the t(6;11)(P21;Q12) Clinicopathologic Features and Demonstration of the Specific Alpha-TFEB Gene Fusion by Immunohistochemistry, RT-PCR, and DNA PCR'. *Am J Surg Pathol*. Vol. 29. http://journals.lww.com/ajsp.

Ascierto, Paolo A, John M Kirkwood, Jean-Jacques Grob, Ester Simeone, Antonio M Grimaldi, Michele Maio, Giuseppe Palmieri, Alessandro Testori, Francesco M Marincola, and Nicola Mozzillo. 2012. 'The Role of BRAF V600 Mutation in Melanoma'. http://www.translational-medicine.com/content/10/1/85.

Aubel-Sadron, Geneviève, and Danielle Londos-Gagliardi. 1984. 'Daunorubicin and Doxorubicin, Anthracycline Antibiotics, a Physicochemical and Biological Review'. *Biochimie* 66 (5): 333–52. https://doi.org/10.1016/0300-9084(84)90018-X.

Baffi, Timothy R., Gema Lorden, Jacob M. Wozniak, Andreas Feichtner, Wayland Yeung, Alexandr P. Kornev, Charles C. King, et al. 2021a. 'TORC2 Controls the Activity of PKC and Akt by Phosphorylating a Conserved TOR Interaction Motif'. *Science Signaling* 14 (678). https://doi.org/10.1126/scisignal.abe4509.

———. 2021b. 'TORC2 Controls the Activity of PKC and Akt by Phosphorylating a Conserved TOR Interaction Motif'. *Science Signaling* 14 (678). https://doi.org/10.1126/scisignal.abe4509.

Bar-Peled, Liron, Lynne Chantranupong, Andrew D. Cherniack, Walter W. Chen, Kathleen A. Ottina, Brian C. Grabiner, Eric D. Spear, Scott L. Carter, Matthew Meyerson, and David M. Sabatini. 2013. 'A Tumor Suppressor Complex with GAP Activity for the Rag GTPases That Signal Amino Acid Sufficiency to MTORC1'. *Science* 340 (6136): 1100–1106. https://doi.org/10.1126/science.1232044.

Bar-Peled, Liron, Lawrence D. Schweitzer, Roberto Zoncu, and David M. Sabatini. 2012. 'Ragulator Is a GEF for the Rag GTPases That Signal Amino Acid Levels

to MTORC1'. *Cell* 150 (6): 1196–1208. https://doi.org/10.1016/j.cell.2012.07.032.

Barreto-Chang, Odmara L., and Ricardo E. Dolmetsch. 2009. 'Calcium Imaging of Cortical Neurons Using Fura-2 AM'. *Journal of Visualized Experiments*, no. 23. https://doi.org/10.3791/1067.

Barthel, Andreas, Steven T. Okino, Jinfang Liao, Kaname Nakatani, Jinping Li, James P. Whitlock, and Richard A. Roth. 1999. 'Regulation of GLUT1 Gene Transcription by the Serine/Threonine Kinase Akt1'. *Journal of Biological Chemistry* 274 (29): 20281–86. https://doi.org/10.1074/JBC.274.29.20281.

Beckmann, Holger, Li-Kuo Su, and Tom Kadesch. 1990. 'TFE3: A Helix-Loop-Helix Protein That Activates Transcription through the Immunoglobulin Enhancer IxE3 Motif'.

Ben-Sahra, Issam, Jessica J. Howell, John M. Asara, and Brendan D. Manning. 2013. 'Stimulation of de Novo Pyrimidine Synthesis by Growth Signaling through MTOR and S6K1'. *Science* 339 (6125): 1323–28. https://doi.org/10.1126/science.1228792.

Ben-Sahra, Issam, Gerta Hoxhaj, Stéphane J.H. Ricoult, John M. Asara, and Brendan D. Manning. 2016. 'MTORC1 Induces Purine Synthesis through Control of the Mitochondrial Tetrahydrofolate Cycle'. *Science* 351 (6274): 728–33. https://doi.org/10.1126/science.aad0489.

Berchtold, Doris, Manuele Piccolis, Nicolas Chiaruttini, Isabelle Riezman, Howard Riezman, Aurélien Roux, Tobias C. Walther, and Robbie Loewith. 2012. 'Plasma Membrane Stress Induces Relocalization of Slm Proteins and Activation of TORC2 to Promote Sphingolipid Synthesis'. *Nature Cell Biology* 14 (5): 542–47. https://doi.org/10.1038/ncb2480.

Bouché, Valentina, Alma Perez Espinosa, Luigi Leone, Marco Sardiello, Andrea Ballabio, and Juan Botas. 2016. 'Drosophila Mitf Regulates the V-ATPase and the Lysosomal-Autophagic Pathway'. *Autophagy* 12 (3): 484–98. https://doi.org/10.1080/15548627.2015.1134081.

Brand, Karl. 1985. 'Glutamine and Glucose Metabolism during Thymocyte Proliferation* Pathways of Glutamine and Glutamate Metabolism'. *Morell & Froesch*. Vol. 228. Lang & Weber. http://portlandpress.com/biochemj/article-pdf/228/2/353/583571/bj2280353.pdf.

Bredahl Hansen, Malene, Maria Postol, Siri Tvingsholm, Inger Ødum Nielsen, Tiina Naumanen Dietrich, Pietri Puustinen, Kenji Maeda, et al. 2021. 'Identification of Lysosome-Targeting Drugs with Anti-Inflammatory Activity as Potential Invasion Inhibitors of Treatment Resistant HER2 Positive Cancers'. https://doi.org/10.1007/s13402-021-00603-2/Published.

Brown, Joel S., Sarah R. Amend, Robert H. Austin, Robert A. Gatenby, Emma U. Hammarlund, and Kenneth J. Pienta. 2023. 'Updating the Definition of Cancer'. *Molecular Cancer Research* 21 (11): 1142–47. https://doi.org/10.1158/1541-7786.MCR-23-0411.

Burgdorf, Sven, and Christian Kurts. 2008. 'Endocytosis Mechanisms and the Cell Biology of Antigen Presentation'. *Current Opinion in Immunology* 20 (1): 89–95. https://doi.org/10.1016/J.COI.2007.12.002.

Burnett, Patrick E, Roxanne K Barrow, Noam A Cohen, Solomon H Snyder* † ‡ §, and David M Sabatini. 1998. 'RAFT1 Phosphorylation of the Translational Regulators P70 S6 Kinase and 4E-BP1'. *Biochemistry*. Vol. 95. www.pnas.org.

Byun, Jun Kyu, Yeon Kyung Choi, Ji Hyun Kim, Ji Yun Jeong, Hui Jeon Jeon, Mi Kyung Kim, Ilseon Hwang, et al. 2017. 'A Positive Feedback Loop between Sestrin2 and MTORC2 Is Required for the Survival of Glutamine-Depleted Lung Cancer Cells'. *Cell Reports* 20 (3): 586–99. https://doi.org/10.1016/J.CELREP.2017.06.066.

Cafferkey, R., P.R. Young, M.M. McLaughlin, D.J. Bergsma, Y. Koltin, G.M. Sathe, L. Faucette, W.-K. Eng, R.K. Johnson, and G.P. Livi. 1993. 'Dominant Missense Mutations in a Novel Yeast Protein Related to Mammalian Phosphatidylinositol 3-Kinase and VPS34 Abrogate Rapamycin Cytotoxicity'. *Molecular and Cellular Biology* 13 (10): 6012–23.

Caliò, Anna, Shuko Harada, Matteo Brunelli, Serena Pedron, Diego Segala, Sofia Canete Portillo, Cristina Magi-Galluzzi, George J. Netto, Alexander C. Mackinnon, and Guido Martignoni. 2021. 'TFEB Rearranged Renal Cell Carcinoma. A Clinicopathologic and Molecular Study of 13 Cases. Tumors Harboring MALAT1-TFEB, ACTB-TFEB, and the Novel NEAT1-TFEB Translocations Constantly Express PDL1'. *Modern Pathology* 34 (4): 842–50. https://doi.org/10.1038/S41379-020-00713-6.

Carling, Phillippa J, Brent J Ryan, William McGuinness, Shikha Kataria, Stewart W Humble, Stefan Milde, James A Duce, et al. 2023. 'Multiparameter Phenotypic Screening for Endogenous TFEB and TFE3 Translocation Identifies Novel Chemical Series Modulating Lysosome Function Multiparameter Phenotypic Screening for Endogenous TFEB and TFE3 Translocation Identifies Novel Chemical Series Modulating Lysosome Function Multiparameter Phenotypic Screening for Endogenous TFEB and TFE3 Translocation Identifies Novel Chemical Series Modulating Lysosome Function'. *Autophagy* 19 (2): 692–705. https://doi.org/10.1080/15548627.2022.2095834.

Carr, Cynthia S, and Phillip A Sharp. 1990. 'A Helix-Loop-Helix Protein Related to the Immunoglobulin E Box-Binding Proteins'. *MOLECULAR AND CELLULAR BIOLOGY*.

Carrière, Audrey, Marie Cargnello, Louis André Julien, Huanhuan Gao, Éric Bonneil, Pierre Thibault, and Philippe P. Roux. 2008. 'Oncogenic MAPK Signaling Stimulates MTORC1 Activity by Promoting RSK-Mediated Raptor Phosphorylation'. *Current Biology* 18 (17): 1269–77. https://doi.org/10.1016/J.CUB.2008.07.078.

Castellano, Brian M., Ashley M. Thelen, Ofer Moldavski, McKenna Feltes, Reini E.N. Van Der Welle, Laurel Mydock-McGrane, Xuntian Jiang, et al. 2017.

'Lysosomal Cholesterol Activates MTORC1 via an SLC38A9-Niemann-Pick C1 Signaling Complex'. *Science* 355 (6331): 1306–11. https://doi.org/10.1126/science.aag1417.

Chantranupong, Lynne, Sonia M. Scaria, Robert A. Saxton, Melanie P. Gygi, Kuang Shen, Gregory A. Wyant, Tim Wang, J. Wade Harper, Steven P. Gygi, and David M. Sabatini. 2016. 'The CASTOR Proteins Are Arginine Sensors for the MTORC1 Pathway'. *Cell* 165 (1): 153–64. https://doi.org/10.1016/j.cell.2016.02.035.

Chantranupong, Lynne, Rachel L. Wolfson, Jose M. Orozco, Robert A. Saxton, Sonia M. Scaria, Liron Bar-Peled, Eric Spooner, Marta Isasa, Steven P. Gygi, and David M. Sabatini. 2014. 'The Sestrins Interact with Gator2 to Negatively Regulate the Amino-Acid-Sensing Pathway Upstream of MTORC1'. *Cell Reports* 9 (1): 1–8. https://doi.org/10.1016/j.celrep.2014.09.014.

Chen, Jialong, Kanmin Mao, Honglin Yu, Yue Wen, Hua She, He Zhang, Linhua Liu, Mingque Li, Wenjun Li, and Fei Zou. 2021. 'P38-TFEB Pathways Promote Microglia Activation through Inhibiting CMA-Mediated NLRP3 Degradation in Parkinson's Disease'. *Journal of Neuroinflammation* 18 (1). https://doi.org/10.1186/s12974-021-02349-y.

Chu, Qiaoyun, Jing An, Ping Liu, Yihan Song, Xuewei Zhai, Ronghui Yang, Jing Niu, Chuanzhen Yang, and Binghui Li. 2023. 'Repurposing a Tricyclic Antidepressant in Tumor and Metabolism Disease Treatment through Fatty Acid Uptake Inhibition'. *Journal of Experimental Medicine* 220 (3). https://doi.org/10.1084/jem.20221316.

Chung, Jongkyeong, Calvin J. Kuo, Gerald R. Crabtree, and John Blenis. 1992. 'Rapamycin-FKBP Specifically Blocks Growth-Dependent Activation of and Signaling by the 70 Kd S6 Protein Kinases'. *Cell* 69 (7): 1227–36. https://doi.org/10.1016/0092-8674(92)90643-Q.

Collins, Shannon E., Mollie E. Wiegand, Alyssa N. Werner, Isabella N. Brown, Mary I. Mundo, Douglas J. Swango, Ghassan Mouneimne, and Pascale G. Charest. 2023. 'Ras-Mediated Activation of MTORC2 Promotes Breast Epithelial Cell Migration and Invasion'. *Molecular Biology of the Cell* 34 (2). https://doi.org/10.1091/mbc.E22-06-0236.

Conrad, Marcus, and Hideyo Sato. 2012. 'The Oxidative Stress-Inducible Cystine/Glutamate Antiporter, System x c-: Cystine Supplier and Beyond'. In *Amino Acids*, 42:231–46. https://doi.org/10.1007/s00726-011-0867-5.

Cool, Barbara, Bradley Zinker, William Chiou, Lemma Kifle, Ning Cao, Matthew Perham, Robert Dickinson, et al. 2006. 'Identification and Characterization of a Small Molecule AMPK Activator That Treats Key Components of Type 2 Diabetes and the Metabolic Syndrome'. *Cell Metabolism* 3 (6): 403–16. https://doi.org/10.1016/J.CMET.2006.05.005.

Cortes, Constanza J., Helen C. Miranda, Harald Frankowski, Yakup Batlevi, Jessica E. Young, Amy Le, Nishi Ivanov, et al. 2014. 'Polyglutamine-Expanded

Androgen Receptor Interferes with TFEB to Elicit Autophagy Defects in SBMA'. *Nature Neuroscience* 17 (9): 1180–89. https://doi.org/10.1038/nn.3787.

Cross, DA, DR Alessi, P Cohen, M Andjelkovich, and BA Hemmings. 1995. 'Inhibition of Glycogen Synthase Kinase-3 by Insulin Mediated by Protein Kinase B'. *Nature*, December. https://doi.org/10.1038/378785a0.

Cui, Libin, Hyunkyung Jeong, Fran Borovecki, Christopher N. Parkhurst, Naoko Tanese, and Dimitri Krainc. 2006. 'Transcriptional Repression of PGC-1α by Mutant Huntingtin Leads to Mitochondrial Dysfunction and Neurodegeneration'. *Cell* 127 (1): 59–69. https://doi.org/10.1016/J.CELL.2006.09.015.

Davies, Helen, Graham R Bignell, Charles Cox, Philip Stephens, Sarah Edkins, Sheila Clegg, Jon Teague, et al. 2002. 'Mutations of the BRAF Gene in Human Cancer'. www.nature.com/nature.

Davis, Ian J, Bae-Li Hsi, Jason D Arroyo, Sara O Vargas, Y Albert Yeh, Gabriela Motyckova, Patricia Valencia, et al. 2003. 'Cloning of an Alpha-TFEB Fusion in Renal Tumors Harboring the t(6;11)(P21;Q13) Chromosome Translocation'. *PNAS May*. Vol. 13. www.pnas.orgcgidoi10.1073pnas.0931430100.

Decressac, Mickael, Bengt Mattsson, Pia Weikop, Martin Lundblad, Johan Jakobsson, and Anders Björklund. 2013. 'TFEB-Mediated Autophagy Rescues Midbrain Dopamine Neurons from α-Synuclein Toxicity'. *Proceedings of the National Academy of Sciences of the United States of America* 110 (19). https://doi.org/10.1073/pnas.1305623110.

deGraffenried, L. A., L. Fulcher, W. E. Friedrichs, V. Grünwald, R. B. Ray, and Manuel Hidalgo. 2004. 'Reduced PTEN Expression in Breast Cancer Cells Confers Susceptibility to Inhibitors of the PI3 Kinase/Akt Pathway'. *Annals of Oncology* 15 (10): 1510–16. https://doi.org/10.1093/ANNONC/MDH388.

Dehay, Benjamin, Marta Martinez-Vicente, Guy A. Caldwell, Kim A. Caldwell, Zhenyue Yue, Mark R. Cookson, Christine Klein, Miquel Vila, and Erwan Bezard. 2013. 'Lysosomal Impairment in Parkinson's Disease'. *Movement Disorders*. https://doi.org/10.1002/mds.25462.

Dias, Diogo, Erica Oliveira, Román Martí-Díaz, Sarah Andrews, Ana Chocarro-Calvo, Alice Bellini, Laura Mosteo, et al. 2024. 'Functional Specialization of MITF, TFEB and TFE3 Drives Radically Distinct Adaptive Gene Expression Programs in Melanoma'. https://doi.org/10.1101/2024.12.23.629393.

Dibble, Christian C., Winfried Elis, Suchithra Menon, Wei Qin, Justin Klekota, John M. Asara, Peter M. Finan, David J. Kwiatkowski, Leon O. Murphy, and Brendan D. Manning. 2012. 'TBC1D7 Is a Third Subunit of the TSC1-TSC2 Complex Upstream of MTORC1'. *Molecular Cell* 47 (4): 535–46. https://doi.org/10.1016/j.molcel.2012.06.009.

Dodd, K. M., J. Yang, M. H. Shen, J. R. Sampson, and A. R. Tee. 2015. 'MTORC1 Drives HIF-1α and VEGF-A Signalling via Multiple Mechanisms Involving 4E-

BP1, S6K1 and STAT3'. *Oncogene* 34 (17): 2239–50. https://doi.org/10.1038/onc.2014.164.

Du, Jinyan, Arlo J Miller, Hans R Widlund, Martin A Horstmann, Sridhar Ramaswamy, and David E Fisher. 2003. 'MLANA/MART1 and SILV/PMEL17/GP100 Are Transcriptionally Regulated by MITF in Melanocytes and Melanoma'. *American Journal of Pathology*.

Du, Wei, Jennifer S Searle, Mammalian Rb, and Family Proteins. 2009. 'The Rb Pathway and Cancer Therapeutics Rb AND E2F FAMILY PROTEINS NIH Public Access'. *Curr Drug Targets*. Vol. 10.

Dumont, Francis J., and Qingxiang Su. 1995. 'Mechanism of Action of the Immunosuppressant Rapamycin'. *Life Sciences* 58 (5): 373–95. https://doi.org/10.1016/0024-3205(95)02233-3.

Eagle, Harry. 1955.
'The Minimum Vitamin Requirements of the L and HeLa Cells in Tissue Culture, the Production of Specific Vitamin Deficiencies, and Their Cure.' *Journal of Experimental Medicine*. http://rupress.org/jem/article-pdf/102/5/595/1643749/595.pdf.

Eberhardy, Scott R., and Peggy J. Farnham. 2001. 'C-Myc Mediates Activation of the Cad Promoter via a Post-RNA Polymerase II Recruitment Mechanism'. *Journal of Biological Chemistry* 276 (51): 48562–71. https://doi.org/10.1074/JBC.M109014200.

Eema, S, S Inghal, J Ayesh, M Ehta, R Aman, D Esikan, An A Yers, et al. 1927. 'ANTITUMOR ACTIVITY OF THALIDOMIDE IN REFRACTORY MULTIPLE MYELOMA A BSTRACT Background Patients with Myeloma Who Relapse'. Vol. 341.

El-Houjeiri, Leeanna, Elite Possik, Tarika Vijayaraghavan, Mathieu Paquette, José A. Martina, Jalal M. Kazan, Eric H. Ma, et al. 2019a. 'The Transcription Factors TFEB and TFE3 Link the FLCN-AMPK Signaling Axis to Innate Immune Response and Pathogen Resistance'. *Cell Reports* 26 (13): 3613-3628.e6. https://doi.org/10.1016/j.celrep.2019.02.102.

———. 2019b. 'The Transcription Factors TFEB and TFE3 Link the FLCN-AMPK Signaling Axis to Innate Immune Response and Pathogen Resistance'. *Cell Reports* 26 (13): 3613-3628.e6. https://doi.org/10.1016/J.CELREP.2019.02.102.

Emerling, Brooke M, Benoit Viollet, Kathryn V Tormos, and Navdeep S Chandel. 2007. 'Compound C Inhibits Hypoxic Activation of HIF-1 Independent of AMPK'.

Eng, C P, S N Sehgalt, and Claude Vezina. 1984. 'Activity of Rapamycin (AY-22,989) against Transplanted Tumors'. *THE JOURNAL OF ANTIBIOTICS*.

Esteve-Puig, Rosaura, Francesc Canals, Núria Colomé, Glenn Merlino, and Juan Ángel Recio. 2009. 'Uncoupling of the LKB1-AMPKα Energy Sensor Pathway

by Growth Factors and Oncogenic BRAFV600E'. *PLoS ONE* 4 (3). https://doi.org/10.1371/journal.pone.0004771.

Fadaka, Adewale, Basiru Ajiboye, Oluwafemi Ojo, Olusola Adewale, Israel Olayide, and Rosemary Emuowhochere. 2017. 'Biology of Glucose Metabolization in Cancer Cells'. *Journal of Oncological Sciences* 3 (2): 45–51. https://doi.org/10.1016/J.JONS.2017.06.002.

Falletta, Paola, Colin R. Goding, and Yurena Vivas-García. 2022. 'Connecting Metabolic Rewiring With Phenotype Switching in Melanoma'. *Frontiers in Cell and Developmental Biology*. Frontiers Media S.A. https://doi.org/10.3389/fcell.2022.930250.

Falletta, Paola, Luis Sanchez-del-Campo, Jagat Chauhan, Maike Effern, Amy Kenyon, Christopher J. Kershaw, Robert Siddaway, et al. 2017. 'Translation Reprogramming Is an Evolutionarily Conserved Driver of Phenotypic Plasticity and Therapeutic Resistance in Melanoma'. *Genes and Development* 31 (1): 18–33. https://doi.org/10.1101/gad.290940.116.

Ferron, Mathieu, Carmine Settembre, Junko Shimazu, Julie Lacombe, Shigeaki Kato, David J. Rawlings, Andrea Ballabio, and Gerard Karsenty. 2013. 'A RANKL-PKCβ-TFEB Signaling Cascade Is Necessary for Lysosomal Biogenesis in Osteoclasts'. *Genes and Development* 27 (8): 955–69. https://doi.org/10.1101/gad.213827.113.

Forbes, Simon A., Nidhi Bindal, Sally Bamford, Charlotte Cole, Chai Yin Kok, David Beare, Mingming Jia, et al. 2011. 'COSMIC: Mining Complete Cancer Genomes in the Catalogue of Somatic Mutations in Cancer'. *Nucleic Acids Research* 39 (SUPPL. 1). https://doi.org/10.1093/nar/gkq929.

Frias, Maria A., Carson C. Thoreen, Jacob D. Jaffe, Wayne Schroder, Tom Sculley, Steven A. Carr, and David M. Sabatini. 2006a. 'MSin1 Is Necessary for Akt/PKB Phosphorylation, and Its Isoforms Define Three Distinct MTORC2s'. *Current Biology* 16 (18): 1865–70. https://doi.org/10.1016/J.CUB.2006.08.001.

———. 2006b. 'MSin1 Is Necessary for Akt/PKB Phosphorylation, and Its Isoforms Define Three Distinct MTORC2s'. *Current Biology* 16 (18): 1865–70. https://doi.org/10.1016/J.CUB.2006.08.001.

Fukuda, Hiroshi, Taiju Matsuzawa, Yoshinao Abe, Satoshi Endo, Kenji Yamada, Kazuo Kubota, Jun Hatazawa, et al. 1982. 'Experimental Study for Cancer Diagnosis with Positron-Labeled Fluorinated Glucose Analogs: [18F]-2-Fluoro-2-Deoxy-D-Mannose: A New Tracer for Cancer Detection'. *Eur J Nucl Med*. Vol. 7.

Funes, Juan M, Marisol Quintero, Stephen Henderson, Dolores Martinez, Uzma Qureshi, Claire Westwood, Mark O Clements, et al. 2007. 'Transformation of Human Mesenchymal Stem Cells Increases Their Dependency on Oxidative Phosphorylation for Energy Production'. www.pnas.orgcgidoi10.1073pnas.0700690104.

Gan, Xiaoqing, Jiyong Wang, Bing Su, and Dianqing Wu. 2011. 'Evidence for Direct Activation of MTORC2 Kinase Activity by Phosphatidylinositol 3,4,5-Trisphosphate'. *Journal of Biological Chemistry* 286 (13): 10998–2. https://doi.org/10.1074/JBC.M110.195016.

Gao, Ping, Irina Tchernyshyov, Tsung Cheng Chang, Yun Sil Lee, Kayoko Kita, Takafumi Ochi, Karen I. Zeller, et al. 2009. 'C-Myc Suppression of MiR-23a/b Enhances Mitochondrial Glutaminase Expression and Glutamine Metabolism'. *Nature* 458 (7239): 762–65. https://doi.org/10.1038/nature07823.

Gao, Sumei, Xiaoyan Li, Xia Ding, and Wenwen Qi. 2017. 'The Effect of Cepharanthine on Breast Cancer Cells Cellular Physiology and Biochemistry Cellular Physiology and Biochemistry Apoptosis and Cell Cycle Arrest in Breast Cancer Cells'. *Cell Physiol Biochem* 41:1633–48. https://doi.org/10.1159/000471234.

Gayatri, Meher Bolisetti, Navya Naidu Gajula, Suresh Chava, and Aramati B.M. Reddy. 2022. 'High Glutamine Suppresses Osteogenesis through MTORC1-Mediated Inhibition of the MTORC2/AKT-473/RUNX2 Axis'. *Cell Death Discovery* 8 (1). https://doi.org/10.1038/s41420-022-01077-3.

Gehlert, Sebastian, Wilhelm Bloch, and Frank Suhr. 2015. 'Ca 2+-Dependent Regulations and Signaling in Skeletal Muscle: From Electro-Mechanical Coupling to Adaptation'. *OPEN ACCESS Int. J. Mol. Sci* 16:16. https://doi.org/10.3390/ijms16011066.

Ghosh, Arindam P, Christopher B Marshall, Tatjana Coric, Eun-Hee Shim, Richard Kirkman, Mary E Ballestas, Mitsuhiko Ikura, Mary-Ann Bjornsti, and Sunil Sudarshan. 2015. 'Point Mutations of the MTOR-RHEB Pathway in Renal Cell Carcinoma'. *Oncotarget*. Vol. 6. www.impactjournals.com/oncotarget/.

Giatromanolaki, Alexandra, Dimitra Kalamida, Efthimios Sivridis, Ilias V. Karagounis, Kevin C. Gatter, Adrian L. Harris, and Michael I. Koukourakis. 2015. 'Increased Expression of Transcription Factor EB (TFEB) Is Associated with Autophagy, Migratory Phenotype and Poor Prognosis in Non-Small Cell Lung Cancer'. *Lung Cancer* 90 (1): 98–105. https://doi.org/10.1016/J.LUNGCAN.2015.07.008.

Glick, Danielle, Sandra Barth, and Kay F. Macleod. 2010. 'Autophagy: Cellular and Molecular Mechanisms'. *Journal of Pathology*. https://doi.org/10.1002/path.2697.

GNS, Hema Sree, Saraswathy GR, Manikanta Murahari, and Mamatha Krishnamurthy. 2019. 'An Update on Drug Repurposing: Re-Written Saga of the Drug's Fate'. *Biomedicine and Pharmacotherapy*. Elsevier Masson SAS. https://doi.org/10.1016/j.biopha.2018.11.127.

Goding, Colin R., and Heinz Arnheiter. 2019. 'Mitf—the First 25 Years'. *Genes and Development*. Cold Spring Harbor Laboratory Press. https://doi.org/10.1101/gad.324657.119.

Goldstein, Joseph L., and Michael S. Brown. 2015. 'A Century of Cholesterol and Coronaries: From Plaques to Genes to Statins'. *Cell*. Cell Press. https://doi.org/10.1016/j.cell.2015.01.036.

Gómez-Galeno, Jorge E., Qun Dang, Thanh H. Nguyen, Serge H. Boyer, Matthew P. Grote, Zhili Sun, Mingwei Chen, et al. 2010. 'A Potent and Selective AMPK Activator That Inhibits de Novo Lipogenesis'. *ACS Medicinal Chemistry Letters* 1 (9): 478–82. https://doi.org/10.1021/ml100143q.

Goodall, Megan L., Tong Wang, Katie R. Martin, Matthew G. Kortus, Audra L. Kauffman, Jeffrey M. Trent, Stephen Gately, and Jeffrey P. MacKeigan. 2014. 'Development of Potent Autophagy Inhibitors That Sensitize Oncogenic BRAF V600E Mutant Melanoma Tumor Cells to Vemurafenib'. *Autophagy* 10 (6): 1120–36. https://doi.org/10.4161/auto.28594.

Grabiner, Brian C., Valentina Nardi, Kivanç Birsoy, Richard Possemato, Kuang Shen, Sumi Sinha, Alexander Jordan, Andrew H. Beck, and David M. Sabatini. 2014. 'A Diverse Array of Cancer-Associated MTOR Mutations Are Hyperactivating and Can Predict Rapamycin Sensitivity'. *Cancer Discovery* 4 (5): 554–63. https://doi.org/10.1158/2159-8290.CD-13-0929.

Gray, Matthew A., Christopher H. Choy, Roya M. Dayam, Erika Ospina-Escobar, Alexander Somerville, Xuan Xiao, Shawn M. Ferguson, and Roberto J. Botelho. 2016. 'Phagocytosis Enhances Lysosomal and Bactericidal Properties by Activating the Transcription Factor TFEB'. *Current Biology* 26 (15): 1955–64. https://doi.org/10.1016/j.cub.2016.05.070.

Grimes, D. A., and D. E. Bulman. 2002. 'Parkinson's Genetics—Creating Exciting New Insights'. *Parkinsonism & Related Disorders* 8 (6): 459–64. https://doi.org/10.1016/S1353-8020(02)00030-5.

Gulati, Pawan, Lawrence D. Gaspers, Stephen G. Dann, Manel Joaquin, Takahiro Nobukuni, Francois Natt, Sara C. Kozma, Andrew P. Thomas, and George Thomas. 2008. 'Amino Acids Activate MTOR Complex 1 via Ca2+/CaM Signaling to HVps34'. *Cell Metabolism* 7 (5): 456–65. https://doi.org/10.1016/j.cmet.2008.03.002.

Gulhati, Pat, Qingsong Cai, Jing Li, Jianyu Liu, Piotr G. Rychahou, Suimin Qiu, Eun Y. Lee, et al. 2009. 'Targeted Inhibition of Mammalian Target of Rapamycin Signaling Inhibits Tumorigenesis of Colorectal Cancer'. *Clinical Cancer Research* 15 (23): 7207–16. https://doi.org/10.1158/1078-0432.CCR-09-1249.

Gutiérrez-Martínez, Enric, Remi Planès, Giorgio Anselmi, Matthew Reynolds, Shinelle Menezes, Aimé Cézaire Adiko, Loredana Saveanu, and Pierre Guermonprez. 2015. 'Cross-Presentation of Cell-Associated Antigens by MHC Class I in Dendritic Cell Subsets'. *Frontiers in Immunology*. Frontiers Research Foundation. https://doi.org/10.3389/fimmu.2015.00363.

Gwinn, Dana M., David B. Shackelford, Daniel F. Egan, Maria M. Mihaylova, Annabelle Mery, Debbie S. Vasquez, Benjamin E. Turk, and Reuben J. Shaw. 2008a. 'AMPK Phosphorylation of Raptor Mediates a Metabolic Checkpoint'. *Molecular Cell* 30 (2): 214–26. https://doi.org/10.1016/j.molcel.2008.03.003.

———. 2008b. ‘AMPK Phosphorylation of Raptor Mediates a Metabolic Checkpoint’. *Molecular Cell* 30 (2): 214–26. https://doi.org/10.1016/j.molcel.2008.03.003.

Haginaka, Jun, Tomoko Kitabatake, Iyo Hirose, Hisami Matsunaga, and Koshien Kyuban-cho. 2015. ‘HHS Public Access’ 434 (1): 202–6. https://doi.org/10.1016/j.ab.2012.11.010.Interaction.

Han, Xie, Yanling Tang, Yuanli Zhang, Jingjing Zhang, Zeyu Hu, Wanjing Xu, Shangzhi Xu, and Qiang Niu. 2022. ‘Impaired V-ATPase Leads to Increased Lysosomal PH, Results in Disrupted Lysosomal Degradation and Autophagic Flux Blockage, Contributes to Fluoride-Induced Developmental Neurotoxicity’. *Ecotoxicology and Environmental Safety* 236 (May):113500. https://doi.org/10.1016/J.ECOENV.2022.113500.

Hanahan, Douglas, and Robert A. Weinberg. 2000. ‘The Hallmarks of Cancer’. *Cell* 100 (1): 57–70. https://doi.org/10.1016/S0092-8674(00)81683-9.

Hannun, Yusuf A., and Lina M. Obeid. 2018. ‘Sphingolipids and Their Metabolism in Physiology and Disease’. *Nature Reviews Molecular Cell Biology*. Nature Publishing Group. https://doi.org/10.1038/nrm.2017.107.

Hara, Kenta, Yoshiko Maruki, Xiaomeng Long, Ken ichi Yoshino, Noriko Oshiro, Sujuti Hidayat, Chiharu Tokunaga, Joseph Avruch, and Kazuyoshi Yonezawa. 2002. ‘Raptor, a Binding Partner of Target of Rapamycin (TOR), Mediates TOR Action’. *Cell* 110 (2): 177–89. https://doi.org/10.1016/S0092-8674(02)00833-4.

Harding, Heather P., Yuhong Zhang, Huiquing Zeng, Isabel Novoa, Phoebe D. Lu, Marcella Calfon, Navid Sadri, et al. 2003. ‘An Integrated Stress Response Regulates Amino Acid Metabolism and Resistance to Oxidative Stress’. *Molecular Cell* 11 (3): 619–33. https://doi.org/10.1016/S1097-2765(03)00105-9.

Haruta, Tetsuro, Tatsuhito Uno, Junko Kawahara, Atsuko Takano, Katsuya Egawa, Prem M Sharma, Jerrold M Olefsky, and Masashi Kobayashi. 2000. ‘A Rapamycin-Sensitive Pathway Down-Regulates Insulin Signaling via Phosphorylation and Proteasomal Degradation of Insulin Receptor Substrate-1’. https://academic.oup.com/mend/article/14/6/783/2747701.

Haughey, Norman J., Veera V.R. Bandaru, Mihyun Bae, and Mark P. Mattson. 2010. ‘Roles for Dysfunctional Sphingolipid Metabolism in Alzheimer’s Disease Neuropathogenesis’. *Biochimica et Biophysica Acta - Molecular and Cell Biology of Lipids*. https://doi.org/10.1016/j.bbalip.2010.05.003.

Hawley, Simon A., Morgan D. Fullerton, Fiona A. Ross, Jonathan D. Schertzer, Cyrille Chevtzoff, Katherine J. Walker, Mark W. Peggie, et al. 2012. ‘The Ancient Drug Salicylate Directly Activates AMP-Activated Protein Kinase’. *Science* 336 (6083): 918–22. https://doi.org/10.1126/science.1215327.

Hay, Nissim, and Nahum Sonenberg. 2004. ‘Upstream and Downstream of MTOR’. *Genes and Development*. https://doi.org/10.1101/gad.1212704.

Hemesath, Timothy J, Eirikur Steingrimsson, Gael Mcgill, Michael J Hansen, James Vaught, Colin A Hodgkinson, Heinz Amheiter, Neal G Copeland, Nancy A Jenkins, and David E Fisher^'. 1994. 'Microphthalmia, a Critical Factor in Melanocyte Development, Defines a Discrete Transcription Factor Family'.

Herbert, Katharine, Romuald Binet, Jean Philippe Lambert, Pakavarin Louphrasitthiphol, Halime Kalkavan, Laura Sesma-Sanz, Carla Daniela Robles-Espinoza, et al. 2019. 'BRN2 Suppresses Apoptosis, Reprograms DNA Damage Repair, and Is Associated with a High Somatic Mutation Burden in Melanoma'. *Genes and Development* 33 (5–6): 310–32. https://doi.org/10.1101/gad.314633.118.

Hershey, Christine L., and David E. Fisher. 2005. 'Genomic Analysis of the Microphthalmia Locus and Identification of the MITF-J/Mitf-J Isoform'. *Gene* 347 (1): 73–82. https://doi.org/10.1016/j.gene.2004.12.002.

Hertwig, Paula. n.d. 'NEUE MUTATIONEN UND KOPPELUNGSGRUPPEN BEI DER HAUSMAUS'.

Hodgkinson, Colin A, Karen J Moore, Atsuo Nakayama, Eirfkur Steingrfmsson, Neal G Copeland, Nancy A Jenkins, and Heinz Arnheiter'. 1993. 'Mutations at the Mouse Microphthalmia Locus Are Associated with Defects in a Gene Encoding a Novel Basic-Helix-Loop-Helix-Zipper Protein'. *Cell*. Vol. 74.

Hoek, Keith S., and Colin R. Goding. 2010a. 'Cancer Stem Cells versus Phenotype-Switching in Melanoma'. *Pigment Cell and Melanoma Research*. https://doi.org/10.1111/j.1755-148X.2010.00757.x.

———. 2010b. 'Cancer Stem Cells versus Phenotype-Switching in Melanoma'. *Pigment Cell and Melanoma Research*. https://doi.org/10.1111/j.1755-148X.2010.00757.x.

Hoek, Keith S., Natalie C. Schlegel, Ossia M. Eichhoff, Daniel S. Widmer, Christian Praetorius, Steingrimur O. Einarsson, Sigridur Valgeirsdottir, et al. 2008. 'Novel MITF Targets Identified Using a Two-Step DNA Microarray Strategy'. *Pigment Cell and Melanoma Research* 21 (6): 665–76. https://doi.org/10.1111/j.1755-148X.2008.00505.x.

Horton, Jay D., Joseph L. Goldstein, and Michael S. Brown. 2002. 'SREBPs: Activators of the Complete Program of Cholesterol and Fatty Acid Synthesis in the Liver'. *Journal of Clinical Investigation* 109 (9): 1125–31. https://doi.org/10.1172/jci200215593.

Hoxhaj, Gerta, and Brendan D. Manning. 2020. 'The PI3K–AKT Network at the Interface of Oncogenic Signalling and Cancer Metabolism'. *Nature Reviews Cancer*. Nature Research. https://doi.org/10.1038/s41568-019-0216-7.

Høyer-Hansen, Maria, Lone Bastholm, Piotr Szyniarowski, Michelangelo Campanella, György Szabadkai, Thomas Farkas, Katiuscia Bianchi, et al. 2007. 'Control of Macroautophagy by Calcium, Calmodulin-Dependent Kinase Kinase-β, and Bcl-2'. *Molecular Cell* 25 (2): 193–205. https://doi.org/10.1016/j.molcel.2006.12.009.

Hsu, Cynthia L., Elian X. Lee, Kara L. Gordon, Edwin A. Paz, Wen Chuan Shen, Kohta Ohnishi, Jill Meisenhelder, Tony Hunter, and Albert R. La Spada. 2018. 'MAP4K3 Mediates Amino Acid-Dependent Regulation of Autophagy via Phosphorylation of TFEB'. *Nature Communications* 9 (1). https://doi.org/10.1038/s41467-018-03340-7.

Hsu, Peggy P., and David M. Sabatini. 2008. 'Cancer Cell Metabolism: Warburg and Beyond'. *Cell*. Elsevier B.V. https://doi.org/10.1016/j.cell.2008.08.021.

Huan, Chongmin, Matthew L Kelly, Ryan Steele, Iuliana Shapira, Susan R S Gottesman, and Christopher A J Roman. 2006. 'Transcription Factors TFE3 and TFEB Are Critical for CD40 Ligand Expression and Thymus-Dependent Humoral Immunity'. *Nat Immunol*. Vol. 7.

Huan, Chongmin, Deepa Sashital, Tiruneh Hailemariam, Matthew L. Kelly, and Christopher A.J. Roman. 2005. 'Renal Carcinoma-Associated Transcription Factors TFE3 and TFEB Are Leukemia Inhibitory Factor-Responsive Transcription Activators of E-Cadherin'. *Journal of Biological Chemistry* 280 (34): 30225–35. https://doi.org/10.1074/jbc.M502380200.

Hughes, Anne E, Valerie E Newton, Xue Z Liu, and Andrew P Read. 1994. 'A Gene for Waardenburg Syndrome Type 2 Maps Close to the Human Homologue of the Microphthalmia Gene at Chromosome 3p12-P14.1'. http://www.nature.com/naturegenetics.

Hunn, Benjamin H.M., Siv Vingill, Sarah Threlfell, Javier Alegre-Abarrategui, Morgane Magdelyns, Thierry Deltheil, Nora Bengoa-Vergniory, et al. 2019. 'Impairment of Macroautophagy in Dopamine Neurons Has Opposing Effects on Parkinsonian Pathology and Behavior'. *Cell Reports* 29 (4): 920-931.e7. https://doi.org/10.1016/J.CELREP.2019.09.029.

Hyun, Teresa, Alan Yam, Salvatore Pece, Xiaozhen Xie, Jie Zhang, Toru Miki, J. Silvio Gutkind, and Weiqun Li. 2000. 'Loss of PTEN Expression Leading to High Akt Activation in Human Multiple Myelomas'. *Blood* 96 (10): 3560–68. https://doi.org/10.1182/BLOOD.V96.10.3560.

Inoki, Ken, Yong Li, Tian Xu, and Kun Liang Guan. 2003. 'Rheb GTpase Is a Direct Target of TSC2 GAP Activity and Regulates MTOR Signaling'. *Genes and Development* 17 (15): 1829–34. https://doi.org/10.1101/gad.1110003.

Inoki, Ken, Yong Li, Tianquan Zhu, Jun Wu, and Kun Liang Guan. 2002a. 'TSC2 Is Phosphorylated and Inhibited by Akt and Suppresses MTOR Signalling'. *Nature Cell Biology* 4 (9): 648–57. https://doi.org/10.1038/ncb839.

Inoki, Ken, Yong Li, Tianquan Zhu, Jun Wu, and Kun-Liang Guan. 2002b. 'TSC2 Is Phosphorylated and Inhibited by Akt and Suppresses MTOR Signalling'. *NATURE CELL BIOLOGY* 4. https://doi.org/10.1038/ncb839.

Inoki, Ken, Hongjiao Ouyang, Tianqing Zhu, Charlotta Lindvall, Yian Wang, Xiaojie Zhang, Qian Yang, et al. 2006. 'TSC2 Integrates Wnt and Energy Signals via a Coordinated Phosphorylation by AMPK and GSK3 to Regulate Cell Growth'. *Cell* 126 (5): 955–68. https://doi.org/10.1016/J.CELL.2006.06.055.

Inoki, Ken, Tianqing Zhu, and Kun Liang Guan. 2003a. 'TSC2 Mediates Cellular Energy Response to Control Cell Growth and Survival'. *Cell* 115 (5): 577–90. https://doi.org/10.1016/S0092-8674(03)00929-2.

Inoki, Ken, Tianqing Zhu, and Kun-Liang Guan. 2003b. 'TSC2 Mediates Cellular Energy Response to Control Cell Growth and Survival Phosphorylation Decreases the Ability of TSC2 to Inhibit the Phosphorylation of Ribosomal S6 Kinase (S6K) and Eukaryotic Initiation Factor 4E Binding Protein-1 (4EBP1)'. *Cell*. Vol. 115. www.cell.com/cgi/content/full/115/5/577/DC1.

Ishida, Seiichi, Erich Huang, Harry Zuzan, Rainer Spang, Gustavo Leone, Mike West, and Joseph R. Nevins. 2001. 'Role for E2F in Control of Both DNA Replication and Mitotic Functions as Revealed from DNA Microarray Analysis'. *Molecular and Cellular Biology* 21 (14): 4684–99. https://doi.org/10.1128/mcb.21.14.4684-4699.2001.

Jamaspishvili, Tamara, David M. Berman, Ashley E. Ross, Howard I. Scher, Angelo M. De Marzo, Jeremy A. Squire, and Tamara L. Lotan. 2018. 'Clinical Implications of PTEN Loss in Prostate Cancer'. *Nature Reviews Urology*. Nature Publishing Group. https://doi.org/10.1038/nrurol.2018.9.

Jewell, Jenna L.;, Young Chul; Kim, Ryan C.; Russel, Fa-Xing; Yu, Hyun Woo; Park, Steven W.; Plouffe, Vincent S.; Tagliabracci, and Kun-Liang Guan. 2015. 'Differential Regulation of MTORC1 by Leucine and Glutamine'. *Science* 347 (6218): 194–98. https://doi.org/10.1126/science.1259472.

Jia, Rui, and Juan S. Bonifacino. 2019. 'Lysosome Positioning Influences MTORC2 and AKT Signaling'. *Molecular Cell* 75 (1): 26-38.e3. https://doi.org/10.1016/j.molcel.2019.05.009.

Jiménez-Mora, Eva, Beatriz Gallego, Sergio Díaz-Gago, Marina Lasa, Pablo Baquero, and Antonio Chiloeches. 2021. 'V600e Braf Inhibition Induces Cytoprotective Autophagy through Ampk in Thyroid Cancer Cells'. *International Journal of Molecular Sciences* 22 (11). https://doi.org/10.3390/ijms22116033.

Jin, Hyeon Ok, Sung Eun Hong, Ji Young Kim, Se Kyeong Jang, and In Chul Park. 2021. 'Amino Acid Deprivation Induces AKT Activation by Inducing GCN2/ATF4/REDD1 Axis'. *Cell Death and Disease* 12 (12): 1–10. https://doi.org/10.1038/s41419-021-04417-w.

Jin, Junfei, Thomas D. Mullen, Qi Hou, Jacek Bielawski, Alicja Bielawska, Xiaoming Zhang, Lina M. Obeid, Yusuf A. Hannun, and Yi Te Hsu. 2009. 'AMPK Inhibitor Compound C Stimulates Ceramide Production and Promotes Bax Redistribution and Apoptosis in MCF7 Breast Carcinoma Cells'. *Journal of Lipid Research* 50 (12): 2389–97. https://doi.org/10.1194/JLR.M900119-JLR200.

Jong, Bauke de, Ineke M. Molenaar, J. Albertus Leeuw, Vera J.S. Idenberg, and J. Wolter Oosterhuis. 1986. 'Cytogenetics of a Renal Adenocarcinoma in a 2-Year-Old Child'. *Cancer Genetics and Cytogenetics* 21 (2): 165–69. https://doi.org/10.1016/0165-4608(86)90042-7.

Juárez-López, Daniel, and Alejandro Schcolnik-Cabrera. 2021. 'Drug Repurposing: Considerations to Surpass While Re-Directing Old Compounds for New Treatments'. *Archives of Medical Research*. Elsevier Inc. https://doi.org/10.1016/j.arcmed.2020.10.021.

Kang, Hyunkoo, Byeongsoo Kim, Junhyeong Park, Hye Sook Youn, and Bu Hyun Youn. 2023. 'The Warburg Effect on Radioresistance: Survival beyond Growth'. *Biochimica et Biophysica Acta - Reviews on Cancer*. Elsevier B.V. https://doi.org/10.1016/j.bbcan.2023.188988.

Karuman, Philip, Or Gozani, Robert D. Odze, Xun Clare Zhou, Hong Zhu, Reuben Shaw, Tom P. Brien, et al. 2001. 'The Peutz-Jegher Gene Product LKB1 Is a Mediator of P53-Dependent Cell Death'. *Molecular Cell* 7 (6): 1307–19. https://doi.org/10.1016/S1097-2765(01)00258-1.

Kasanami, Yoshihito, Chihiro Ishikawa, Takahiro Kino, Momoka Chonan, Naoki Toyooka, Yasuhiro Takashima, Yuriko Iba, et al. 2022. 'Discovery of Pimozide Derivatives as Novel T-Type Calcium Channel Inhibitors with Little Binding Affinity to Dopamine D2 Receptors for Treatment of Somatic and Visceral Pain'. *European Journal of Medicinal Chemistry* 243 (August): 114716. https://doi.org/10.1016/j.ejmech.2022.114716.

Kauffman, Eric C., Christopher J. Ricketts, Soroush Rais-Bahrami, Youfeng Yang, Maria J. Merino, Donald P. Bottaro, Ramaprasad Srinivasan, and W. Marston Linehan. 2014. 'Molecular Genetics and Cellular Features of TFE3 and TFEB Fusion Kidney Cancers'. *Nature Reviews Urology*. Nature Publishing Group. https://doi.org/10.1038/nrurol.2014.162.

Kazyken, Dubek, Brian Magnuson, Cagri Bodur, Hugo A Acosta-Jaquez, Deqiang Zhang, Xin Tong, Tammy M Barnes, et al. 2019. 'AMPK Directly Activates MTORC2 to Promote Cell Survival during Acute Energetic Stress'. *Sci. Signal*. Vol. 12. https://www.science.org.

Ke, Rong, Qicao Xu, Cong Li, Lingyu Luo, and Deqiang Huang. 2018. 'Mechanisms of AMPK in the Maintenance of ATP Balance during Energy Metabolism'. *Cell Biology International*. Wiley-Blackwell Publishing Ltd. https://doi.org/10.1002/cbin.10915.

Kenigsberg, R. L., A. Côté, and J. M. Trifaró. 1982. 'Trifluoperazine, a Calmodulin Inhibitor, Blocks Secretion in Cultured Chromaffin Cells at a Step Distal from Calcium Entry'. *Neuroscience* 7 (9): 2277–86. https://doi.org/10.1016/0306-4522(82)90138-5.

Khan, M. Tariq, and Suresh K. Joseph. 2010. 'Role of Inositol Trisphosphate Receptors in Autophagy in DT40 Cells'. *Journal of Biological Chemistry* 285 (22): 16912–20. https://doi.org/10.1074/jbc.M110.114207.

Kim, Do Hyung, Dos D. Sarbassov, Siraj M. Ali, Robert R. Latek, Kalyani V.P. Guntur, Hediye Erdjument-Bromage, Paul Tempst, and David M. Sabatini. 2003. 'GβL, a Positive Regulator of the Rapamycin-Sensitive Pathway Required for the Nutrient-Sensitive Interaction between Raptor and MTOR'. *Molecular Cell* 11 (4): 895–904. https://doi.org/10.1016/S1097-2765(03)00114-X.

Kim, Hak Su, Myung Jin Kim, Eun Ju Kim, Young Yang, Myeong Sok Lee, and Jong Seok Lim. 2012. 'Berberine-Induced AMPK Activation Inhibits the Metastatic Potential of Melanoma Cells via Reduction of ERK Activity and COX-2 Protein Expression'. *Biochemical Pharmacology* 83 (3): 385–94. https://doi.org/10.1016/J.BCP.2011.11.008.

Kim, James H, and Anthony R Scialli. 2011. 'Thalidomide: The Tragedy of Birth Defects and the Effective Treatment of Disease'. *TOXICOLOGICAL SCIENCES* 122 (1): 1–6. https://doi.org/10.1093/toxsci/kfr088.

Kim, Ji Hye, Jinyoung Lee, Young Ra Cho, So Yeon Lee, Gi Jun Sung, Dong Myung Shin, Kyung Chul Choi, and Jaekyoung Son. 2021. 'Tfeb Supports Pancreatic Cancer Growth through the Transcriptional Regulation of Glutaminase'. *Cancers* 13 (3): 1–14. https://doi.org/10.3390/cancers13030483.

Kimura, Shunsuke, Takeshi Noda, and Tamotsu Yoshimori. 2007. 'Dissection of the Autophagosome Maturation Process by a Novel Reporter Protein, Tandem Fluorescent-Tagged LC3'. *Autophagy* 3 (5): 452–60. https://doi.org/10.4161/auto.4451.

Klionsky, Daniel J, and Scott D Emr. 2000. 'Autophagy as a Regulated Pathway of Cellular Degradation'. *Science*. Vol. 290.

Knopman, David S., Helene Amieva, Ronald C. Petersen, Gäel Chételat, David M. Holtzman, Bradley T. Hyman, Ralph A. Nixon, and David T. Jones. 2021. 'Alzheimer Disease'. *Nature Reviews Disease Primers* 7 (1). https://doi.org/10.1038/s41572-021-00269-y.

Koo, Junghui, Xuerong Wang, Taofeek K Owonikoko, Suresh S Ramalingam, Fadlo R Khuri, and Shi-Yong Sun. 2015. 'GSK3 Is Required for Rapalogs to Induce Degradation of Some Oncogenic Proteins and to Suppress Cancer Cell Growth'. Vol. 6. www.impactjournals.com/oncotarget.

Kremer, Berry, Paul Goldberg, Susan E. Andrew, Jane Theilmann, Hakan Telenius, Jutta Zeisler, Ferdinando Squitieri, et al. 1994. 'A Worldwide Study of the Huntington's Disease Mutation: The Sensitivity and Specificity of Measuring CAG Repeats'. *New England Journal of Medicine* 330 (20): 1401–6. https://doi.org/10.1056/nejm199405193302001.

Kwon, Hyock Joo, Lina Abi-Mosleh, Michael L. Wang, Johann Deisenhofer, Joseph L. Goldstein, Michael S. Brown, and Rodney E. Infante. 2009. 'Structure of N-Terminal Domain of NPC1 Reveals Distinct Subdomains for Binding and Transfer of Cholesterol'. *Cell* 137 (7): 1213–24. https://doi.org/10.1016/j.cell.2009.03.049.

Lang, Florian, Nathalie Strutz-Seebohm, Guiscard Seebohm, and Undine E. Lang. 2010. 'Significance of SGK1 in the Regulation of Neuronal Function'. *Journal of Physiology*. https://doi.org/10.1113/jphysiol.2010.190926.

Laplante, Mathieu, and David M. Sabatini. 2012. 'MTOR Signaling in Growth Control and Disease'. *Cell*. Elsevier B.V. https://doi.org/10.1016/j.cell.2012.03.017.

Larsson, Christer. 2006. 'Protein Kinase C and the Regulation of the Actin Cytoskeleton'. *Cellular Signalling* 18 (3): 276–84. https://doi.org/10.1016/J.CELLSIG.2005.07.010.

Lee, Dung Fang, Hsu Ping Kuo, Chun Te Chen, Jung Mao Hsu, Chao Kai Chou, Yongkun Wei, Hui Lung Sun, et al. 2007. 'IKKβ Suppression of TSC1 Links Inflammation and Tumor Angiogenesis via the MTOR Pathway'. *Cell* 130 (3): 440–55. https://doi.org/10.1016/J.CELL.2007.05.058.

Lee, J.-M, E M Ramos, J.-H Lee, T Gillis, J S Mysore, Bsc M R Hayden, S C Warby, et al. 2012. 'CAG Repeat Expansion in Huntington Disease Determines Age at Onset in a Fully Dominant Fashion'. www.neurology.org.

Lee, Jong Ho, Rui Liu, Jing Li, Chuanbao Zhang, Yugang Wang, Qingsong Cai, Xu Qian, et al. 2017a. 'Stabilization of Phosphofructokinase 1 Platelet Isoform by AKT Promotes Tumorigenesis'. *Nature Communications* 8 (1). https://doi.org/10.1038/s41467-017-00906-9.

———. 2017b. 'Stabilization of Phosphofructokinase 1 Platelet Isoform by AKT Promotes Tumorigenesis'. *Nature Communications* 8 (1). https://doi.org/10.1038/s41467-017-00906-9.

Lee, Jong Kil, Hee Kyung Jin, Min Hee Park, Bo Ra Kim, Phil Hyu Lee, Hiromitsu Nakauchi, Janet E. Carter, Xingxuan He, Edward H. Schuchman, and Jae Sung Bae. 2014. 'Acid Sphingomyelinase Modulates the Autophagic Process by Controlling Lysosomal Biogenesis in Alzheimer's Disease'. *Journal of Experimental Medicine* 211 (8): 1551–70. https://doi.org/10.1084/jem.20132451.

Li, Haiyan, Jun Lin, Xiaokai Wang, Guangyu Yao, Liping Wang, Hang Zheng, Cuilan Yang, Chunhong Jia, Anling Liu, and Xiaochun Bai. 2012. 'Targeting of MTORC2 Prevents Cell Migration and Promotes Apoptosis in Breast Cancer'. *Breast Cancer Research and Treatment* 134 (3): 1057–66. https://doi.org/10.1007/s10549-012-2036-2.

Li, Hongyao, Xiang Wen, Yueting Ren, Zhichao Fan, Jin Zhang, Gu He, and Leilei Fu. 2024. 'Targeting PI3K Family with Small-Molecule Inhibitors in Cancer Therapy: Current Clinical Status and Future Directions'. *Molecular Cancer* 23 (1): 1–42. https://doi.org/10.1186/s12943-024-02072-1.

Li, Jiao, Peng Qu, Xing Zhi Zhou, Yun Xia Ji, Shuo Yuan, Shuang Ping Liu, and Qing Gao Zhang. 2022. 'Pimozide Inhibits the Growth of Breast Cancer Cells by Alleviating the Warburg Effect through the P53 Signaling Pathway'. *Biomedicine and Pharmacotherapy* 150 (May): 113063. https://doi.org/10.1016/j.biopha.2022.113063.

Li, Linxin, Hans J. Friedrichsen, Sarah Andrews, Sarah Picaud, Laurent Volpon, Kaochin Ngeow, Georgina Berridge, et al. 2018. 'A TFEB Nuclear Export Signal Integrates Amino Acid Supply and Glucose Availability'. *Nature Communications* 9 (1). https://doi.org/10.1038/s41467-018-04849-7.

Li, Mengqi, Xiaoyan Wei, Jinye Xiong, Jin Wei Feng, Chen Song Zhang, and Sheng Cai Lin. 2023. 'Hierarchical Inhibition of MTORC1 by Glucose Starvation-Triggered AXIN Lysosomal Translocation and by AMPK'. *Life Metabolism* 2 (3). https://doi.org/10.1093/lifemeta/load005.

Li, Shun, Ying Song, Christine Quach, Hongrui Guo, Gyu Beom Jang, Hadi Maazi, Shihui Zhao, et al. 2019. 'Transcriptional Regulation of Autophagy-Lysosomal Function in BRAF-Driven Melanoma Progression and Chemoresistance'. *Nature Communications* 10 (1). https://doi.org/10.1038/s41467-019-09634-8.

Li, Yang, Meng Xu, Xiao Ding, Chen Yan, Zhiqin Song, Lianwan Chen, Xiahe Huang, et al. 2016a. 'Protein Kinase C Controls Lysosome Biogenesis Independently of MTORC1'. *Nature Cell Biology* 18 (10): 1065–77. https://doi.org/10.1038/ncb3407.

———. 2016b. 'Protein Kinase C Controls Lysosome Biogenesis Independently of MTORC1'. *Nature Cell Biology* 18 (10): 1065–77. https://doi.org/10.1038/ncb3407.

Liang, Jing, Xinfeng Jia, Kun Wang, and Niankun Zhao. 2018. 'High Expression of TFEB Is Associated with Aggressive Clinical Features in Colorectal Cancer'. *OncoTargets and Therapy* 11:8089–98. https://doi.org/10.2147/OTT.S180112.

Liang, Jiyong, and Gordon B. Mills. 2013. 'AMPK: A Contextual Oncogene or Tumor Suppressor?' *Cancer Research*. https://doi.org/10.1158/0008-5472.CAN-12-3876.

Lieberman, Brian P., Karl Ploessl, Limin Wang, Wenchao Qu, Zhihao Zha, David R. Wise, Lewis A. Chodosh, George Belka, Craig B. Thompson, and Hank F. Kung. 2011. 'PET Imaging of Glutaminolysis in Tumors by 18F-(2S,4R)4-Fluoroglutamine'. *Journal of Nuclear Medicine* 52 (12): 1947–55. https://doi.org/10.2967/jnumed.111.093815.

Liu, Pengda, Wenjian Gan, Y. Rebecca Chin, Kohei Ogura, Jianping Guo, Jinfang Zhang, Bin Wang, et al. 2015. 'Ptdins(3,4,5) P3 -Dependent Activation of the MTORC2 Kinase Complex'. *Cancer Discovery* 5 (11): 1194–11209. https://doi.org/10.1158/2159-8290.CD-15-0460.

Liu, Pengda, Wenjian Gan, Hiroyuki Inuzuka, Adam S. Lazorchak, Daming Gao, Omotooke Arojo, Dou Liu, et al. 2013. 'Sin1 Phosphorylation Impairs MTORC2 Complex Integrity and Inhibits Downstream Akt Signalling to Suppress Tumorigenesis'. *Nature Cell Biology* 15 (11): 1340–50. https://doi.org/10.1038/ncb2860.

Liu, Xiaona, Rishi Raj Chhipa, Ichiro Nakano, and Biplab Dasgupta. 2014. 'The AMPK Inhibitor Compound C Is a Potent AMPK-Independent Antiglioma Agent'. *Molecular Cancer Therapeutics* 13 (3): 596–605. https://doi.org/10.1158/1535-7163.MCT-13-0579.

Long, Xiaomeng, Yenshou Lin, Sara Ortiz-Vega, Kazuyoshi Yonezawa, and Joseph Avruch. 2005. 'Rheb Binds and Regulates the MTOR Kinase'. *Current Biology* 15 (8): 702–13. https://doi.org/10.1016/J.CUB.2005.02.053.

Louphrasitthiphol, Pakavarin, Ioanna Ledaki, Jagat Chauhan, Paola Falletta, Robert Siddaway, Francesca M. Buffa, David R. Mole, Tomoyoshi Soga, and Colin R. Goding. 2019. 'MITF Controls the TCA Cycle to Modulate the Melanoma Hypoxia Response'. *Pigment Cell and Melanoma Research* 32 (6): 792–808. https://doi.org/10.1111/pcmr.12802.

Lowings, P, U Yavuzer, and C R Goding. 1992. 'Positive and Negative Elements Regulate a Melanocyte-Specific Promoter'. *MOLECULAR AND CELLULAR BIOLOGY*.

Lu, Ssu Yi, Hsiao Ching Wan, Mengtao Li, and Yi Ling Lin. 2010. 'Subcellular Localization of Mitf in Monocytic Cells'. *Histochemistry and Cell Biology* 133 (6): 651–58. https://doi.org/10.1007/s00418-010-0703-0.

MacDonald, Marcy E., Christine M. Ambrose, Mabel P. Duyao, Richard H. Myers, Carol Lin, Lakshmi Srinidhi, Glenn Barnes, et al. 1993. 'A Novel Gene Containing a Trinucleotide Repeat That Is Expanded and Unstable on Huntington's Disease Chromosomes'. *Cell* 72 (6): 971–83. https://doi.org/10.1016/0092-8674(93)90585-E.

Mansueto, Gelsomina, Andrea Armani, Carlo Viscomi, Luca D'Orsi, Rossella De Cegli, Elena V. Polishchuk, Costanza Lamperti, et al. 2017a. 'Transcription Factor EB Controls Metabolic Flexibility during Exercise'. *Cell Metabolism* 25 (1): 182–96. https://doi.org/10.1016/J.CMET.2016.11.003.

———. 2017b. 'Transcription Factor EB Controls Metabolic Flexibility during Exercise'. *Cell Metabolism* 25 (1): 182–96. https://doi.org/10.1016/j.cmet.2016.11.003.

Manteuffel, Sabine R Von, Patrick B Dennis, Nicholas Pullen, Anne-Claude Gingras, Nahum Sonenberg, and George Thomas. 1997. 'The Insulin-Induced Signalling Pathway Leading to S6 and Initiation Factor 4E Binding Protein 1 Phosphorylation Bifurcates at a Rapamycin-Sensitive Point Immediately Upstream of P70 S6k'. *MOLECULAR AND CELLULAR BIOLOGY*. Vol. 17.

Martina, Jose A., Yong Chen, Marjan Gucek, and Rosa Puertollano. 2012. 'MTORC1 Functions as a Transcriptional Regulator of Autophagy by Preventing Nuclear Transport of TFEB'. *Autophagy* 8 (6): 903–14. https://doi.org/10.4161/auto.19653.

Martina, José A, Heba I Diab, Owen A Brady, and Rosa Puertollano. 2016. ' TFEB and TFE 3 Are Novel Components of the Integrated Stress Response '. *The EMBO Journal* 35 (5): 479–95. https://doi.org/10.15252/embj.201593428.

Martina, José A., Heba I. Diab, Li Lishu, Lim Jeong-A, Simona Patange, Nina Raben, and Rosa Puertollano. 2014. 'The Nutrient-Responsive Transcription Factor TFE3 Promotes Autophagy, Lysosomal Biogenesis, and Clearance of Cellular Debris'. *Science Signaling* 7 (309). https://doi.org/10.1126/scisignal.2004754.

Martina, Jose A., and Rosa Puertollano. 2013. 'Rag GTPases Mediate Amino Acid-Dependent Recruitment of TFEB and MITF to Lysosomes'. *Journal of Cell Biology* 200 (4): 475–91. https://doi.org/10.1083/jcb.201209135.

Martina, José A., and Rosa Puertollano. 2018. 'Protein Phosphatase 2A Stimulates Activation of TFEB and TFE3 Transcription Factors in Response to Oxidative Stress'. *Journal of Biological Chemistry* 293 (32): 12525–34. https://doi.org/10.1074/jbc.RA118.003471.

Maruotti, Julien, Thuzar Thein, Donald J. Zack, and Noriko Esumi. 2012. 'MITF-M, a "melanocyte-Specific" Isoform, Is Expressed in the Adult Retinal Pigment Epithelium'. *Pigment Cell and Melanoma Research*. https://doi.org/10.1111/j.1755-148X.2012.01033.x.

Masri, Janine, Andrew Bernath, Jheralyn Martin, Oak D. Jo, Raffi Vartanian, Alexander Funk, and Joseph Gera. 2007. 'MTORC2 Activity Is Elevated in Gliomas and Promotes Growth and Cell Motility via Overexpression of Rictor'. *Cancer Research* 67 (24): 11712–20. https://doi.org/10.1158/0008-5472.CAN-07-2223.

Mazur, Magdalena A., Marcus Winkler, Elvira Ganić, Jesper K. Colberg, Jenny K. Johansson, Hedvig Bennet, Malin Fex, Ulrike A. Nuber, and Isabella Artner. 2013. 'Microphthalmia Transcription Factor Regulates Pancreatic β-Cell Function'. *Diabetes* 62 (8): 2834–42. https://doi.org/10.2337/db12-1464.

Meacham, Corbin E, and Sean J Morrison. 2013. 'Tumor Heterogeneity and Cancer Cell Plasticity'. *Nature*.

Medina, Diego L., Alessandro Fraldi, Valentina Bouche, Fabio Annunziata, Gelsomina Mansueto, Carmine Spampanato, Claudia Puri, et al. 2011. 'Transcriptional Activation of Lysosomal Exocytosis Promotes Cellular Clearance'. *Developmental Cell* 21 (3): 421–30. https://doi.org/10.1016/J.DEVCEL.2011.07.016.

Medina, Diego L, Simone Di Paola, Ivana Peluso, Andrea Armani, Diego De Stefani, Rossella Venditti, Sandro Montefusco, et al. 2015. 'Lysosomal Calcium Signalling Regulates Autophagy through Calcineurin and TFEB'. *NATURE CELL BIOLOGY* 17 (3). https://doi.org/10.1038/ncb3114.

Meng, Delong, Qianmei Yang, Huanyu Wang, Chase H. Melick, Rishika Navlani, Anderson R. Frank, and Jenna L. Jewell. 2020. 'Glutamine and Asparagine Activate MTORC1 Independently of Rag GTPases'. *Journal of Biological Chemistry*. American Society for Biochemistry and Molecular Biology Inc. https://doi.org/10.1074/jbc.AC119.011578.

Meng, Xiangbao, Yun Luo, Tian Liang, Mengxia Wang, Jingyu Zhao, Guibo Sun, and Xiaobo Sun. 2016. 'Gypenoside XVII Enhances Lysosome Biogenesis and Autophagy Flux and Accelerates Autophagic Clearance of Amyloid-β through TFEB Activation'. *Journal of Alzheimer's Disease* 52 (3): 1135–50. https://doi.org/10.3233/JAD-160096.

Milam, Michael R., Joseph Celestino, Weiguo Wu, Russell R. Broaddus, Kathleen M. Schmeler, Brian M. Slomovitz, Pamela T. Soliman, et al. 2007. 'Reduced Progression of Endometrial Hyperplasia with Oral MTOR Inhibition in the Pten Heterozygote Murine Model'. *American Journal of Obstetrics and Gynecology* 196 (3): 247.e1-247.e5. https://doi.org/10.1016/J.AJOG.2006.10.872.

Miller, Donald M., Shelia D. Thomas, Ashraful Islam, David Muench, and Kara Sedoris. 2012. 'C-Myc and Cancer Metabolism'. *Clinical Cancer Research*. https://doi.org/10.1158/1078-0432.CCR-12-0977.

Mizushima, Noboru, and Tamotsu Yoshimori. 2007. 'How to Interpret LC3 Immunoblotting'. *Autophagy*. Taylor and Francis Inc. https://doi.org/10.4161/auto.4600.

Moloughney, Joseph G., Peter K. Kim, Nicole M. Vega-Cotto, Chang Chih Wu, Sisi Zhang, Matthew Adlam, Thomas Lynch, et al. 2016a. 'MTORC2 Responds to Glutamine Catabolite Levels to Modulate the Hexosamine Biosynthesis Enzyme GFAT1'. *Molecular Cell* 63 (5): 811–26. https://doi.org/10.1016/J.MOLCEL.2016.07.015.

———. 2016b. 'MTORC2 Responds to Glutamine Catabolite Levels to Modulate the Hexosamine Biosynthesis Enzyme GFAT1'. *Molecular Cell* 63 (5): 811–26. https://doi.org/10.1016/j.molcel.2016.07.015.

Mothi, Meghana, and Stephanie Sampson. 2013. 'Pimozide for Schizophrenia or Related Psychoses'. *Cochrane Database of Systematic Reviews* 2013 (11). https://doi.org/10.1002/14651858.CD001949.pub3.

Muller, Maéline, Jasmine Bélanger, Imane Hadj-Aissa, Conghao Zhang, Chantelle F. Sephton, and Paul A. Dutchak. 2024. 'GATOR1 Mutations Impair PI3 Kinase-Dependent Growth Factor Signaling Regulation of MTORC1'. *International Journal of Molecular Sciences* 25 (4). https://doi.org/10.3390/ijms25042068.

Murakami, Takashi, Toshihiko Nishiyama, Tetsuya Shirotani, Yasuo Shinohara, Masaharu Kan, Kazuo Ishii, Fumihiko Kanai, Shoichi Nakazuru, and Yousuke Ebina. 1992. 'Identification of Two Enhancer Elements in the Gene Encoding the Type 1 Glucose Transporter from the Mouse Which Are Responsive to Serum, Growth Factor, and Oncogenes.' *Journal of Biological Chemistry* 267 (13): 9300–9306. https://doi.org/10.1016/S0021-9258(19)50423-9.

Napolitano, Gennaro, and Andrea Ballabio. 2016. 'TFEB at a Glance'. https://doi.org/10.1242/jcs.146365.

Napolitano, Gennaro, Alessandra Esposito, Heejun Choi, Maria Matarese, Valerio Benedetti, Chiara Di Malta, Jlenia Monfregola, Diego Luis Medina, Jennifer Lippincott-Schwartz, and Andrea Ballabio. 2018. 'MTOR-Dependent Phosphorylation Controls TFEB Nuclear Export'. *Nature Communications* 9 (1). https://doi.org/10.1038/s41467-018-05862-6.

Ngeow, Kao Chin, Hans J. Friedrichsen, Linxin Li, Zhiqiang Zeng, Sarah Andrews, Laurent Volpon, Hannah Brunsdon, et al. 2018. 'BRAF/MAPK and GSK3

Signaling Converges to Control MITF Nuclear Export'. *Proceedings of the National Academy of Sciences of the United States of America* 115 (37): E8668–77. https://doi.org/10.1073/pnas.1810498115.

Nicklin, Paul, Philip Bergman, Bailin Zhang, Ellen Triantafellow, Henry Wang, Beat Nyfeler, Haidi Yang, et al. 2009. 'Bidirectional Transport of Amino Acids Regulates MTOR and Autophagy'. *Cell* 136 (3): 521–34. https://doi.org/10.1016/j.cell.2008.11.044.

Nieminen, Anni I., Vilja M. Eskelinen, Heidi M. Haikala, Topi A. Tervonen, Yan Yan, Johanna I. Partanen, and Juha Klefström. 2013. 'Myc-Induced AMPK-Phospho P53 Pathway Activates Bak to Sensitize Mitochondrial Apoptosis'. *Proceedings of the National Academy of Sciences of the United States of America* 110 (20). https://doi.org/10.1073/pnas.1208530110.

Northrup, H, M K Koenig, and D A Pearson. 1999. 'Tuberous Sclerosis Complex'.

Oh, Won Jun, Chang Chih Wu, Sung Jin Kim, Valeria Facchinetti, Louis André Julien, Monica Finlan, Philippe P. Roux, Bing Su, and Estela Jacinto. 2010. 'MTORC2 Can Associate with Ribosomes to Promote Cotranslational Phosphorylation and Stability of Nascent Akt Polypeptide'. *EMBO Journal* 29 (23): 3939–51. https://doi.org/10.1038/emboj.2010.271.

Ojalvo-Pacheco, Javier, Sokhna M.S. Yakhine-Diop, José M. Fuentes, Marta Paredes-Barquero, and Mireia Niso-Santano. 2024. 'Role of TFEB in Huntington's Disease'. *Biology*. Multidisciplinary Digital Publishing Institute (MDPI). https://doi.org/10.3390/biology13040238.

Okosun, Jessica, Rachel L. Wolfson, Jun Wang, Shamzah Araf, Lucy Wilkins, Brian M. Castellano, Leire Escudero-Ibarz, et al. 2016. 'Recurrent MTORC1-Activating RRAGC Mutations in Follicular Lymphoma'. *Nature Genetics* 48 (2): 183–88. https://doi.org/10.1038/ng.3473.

O'reilly, Kathryn E, Fredi Rojo, Qing-Bai She, David Solit, Gordon B Mills, Debra Smith, Heidi Lane, et al. 2006. 'MTOR Inhibition Induces Upstream Receptor Tyrosine Kinase Signaling and Activates Akt'. *Cancer Res* 66 (3): 1500–1508. https://doi.org/10.1158/0008-5472.CAN-05-2925.

Ostrerova, Natalie, Leonard Petrucelli, Matthew Farrer, Nitinkumar Mehta, Peter Choi, John Hardy, and Benjamin Wolozin. 1999. 'Synuclein Shares Physical and Functional Homology with 14-3-3 Proteins'.

Otto Warburg, BY, Franz Wind, and N Negelein. 1927. 'THE METABOLISM OF TUMORS IN THE BODY'.

Pallett, Laura J., Sarah Dimeloe, Linda V. Sinclair, Adam J. Byrne, and Anna Schurich. 2021. 'A Glutamine "Tug-of-War": Targets to Manipulate Glutamine Metabolism for Cancer Immunotherapy'. *Immunotherapy Advances*. Oxford University Press. https://doi.org/10.1093/immadv/ltab010.

Palm, Wilhelm, Youngkyu Park, Kevin Wright, Natalya N. Pavlova, David A. Tuveson, and Craig B. Thompson. 2015. 'The Utilization of Extracellular

Proteins as Nutrients Is Suppressed by MTORC1'. *Cell* 162 (2): 259–70. https://doi.org/10.1016/j.cell.2015.06.017.

Palmieri, Michela, Soren Impey, Hyojin Kang, Alberto di Ronza, Carl Pelz, Marco Sardiello, and Andrea Ballabio. 2011a. 'Characterization of the CLEAR Network Reveals an Integrated Control of Cellular Clearance Pathways'. *Human Molecular Genetics* 20 (19): 3852–66. https://doi.org/10.1093/hmg/ddr306.

———. 2011b. 'Characterization of the CLEAR Network Reveals an Integrated Control of Cellular Clearance Pathways'. *Human Molecular Genetics* 20 (19): 3852–66. https://doi.org/10.1093/hmg/ddr306.

Palmieri, Michela, Rituraj Pal, Hemanth R. Nelvagal, Parisa Lotfi, Gary R. Stinnett, Michelle L. Seymour, Arindam Chaudhury, et al. 2017. 'MTORC1-Independent TFEB Activation via Akt Inhibition Promotes Cellular Clearance in Neurodegenerative Storage Diseases'. *Nature Communications* 8 (February). https://doi.org/10.1038/ncomms14338.

Pang, Keliang, Richeng Jiang, Wei Zhang, Zhengyi Yang, Lin Lin Li, Makoto Shimozawa, Simone Tambaro, et al. 2022. 'An App Knock-in Rat Model for Alzheimer's Disease Exhibiting Aβ and Tau Pathologies, Neuronal Death and Cognitive Impairments'. *Cell Research* 32 (2): 157–75. https://doi.org/10.1038/s41422-021-00582-x.

Pang, Tao, Zhen Shan Zhang, Min Gu, Bei Ying Qiu, Li Fang Yu, Peng Rong Cao, Wei Shao, et al. 2008. 'Small Molecule Antagonizes Autoinhibition and Activates AMP-Activated Protein Kinase in Cells'. *Journal of Biological Chemistry* 283 (23): 16051–60. https://doi.org/10.1074/jbc.M710114200.

Papageorgis, Panagiotis. 2015. 'TGF β Signaling in Tumor Initiation, Epithelial-to-Mesenchymal Transition, and Metastasis'. *Journal of Oncology* 2015. https://doi.org/10.1155/2015/587193.

Paquette, Mathieu, Leeanna El-Houjeiri, Linda C. Zirden, Pietri Puustinen, Paola Blanchette, Hyeonju Jeong, Kurt Dejgaard, Peter M. Siegel, and Arnim Pause. 2021. 'AMPK-Dependent Phosphorylation Is Required for Transcriptional Activation of TFEB and TFE3'. *Autophagy* 17 (12): 3957–75. https://doi.org/10.1080/15548627.2021.1898748.

Park, Yune Jung, Seung Ah Yoo, Mingyo Kim, and Wan Uk Kim. 2020. 'The Role of Calcium–Calcineurin–NFAT Signaling Pathway in Health and Autoimmune Diseases'. *Frontiers in Immunology* 11 (March): 1–14. https://doi.org/10.3389/fimmu.2020.00195.

Parmar, Nitika, and Fuyuhiko Tamanoi. 2010. 'Rheb G-Proteins and the Activation of MTORC1'. In *Enzymes*, 27:39–56. Academic Press. https://doi.org/10.1016/S1874-6047(10)27003-8.

Pastore, Nunzia, Owen A. Brady, Heba I. Diab, José A. Martina, Lu Sun, Tuong Huynh, Jeong A. Lim, et al. 2016. 'TFEB and TFE3 Cooperate in the Regulation

of the Innate Immune Response in Activated Macrophages'. *Autophagy* 12 (8): 1240–58. https://doi.org/10.1080/15548627.2016.1179405.

Pastore, Nunzia, Tuong Huynh, Niculin J. Herz, Alessia Calcagni', Tiemo J. Klisch, Lorenzo Brunetti, Kangho Ho Kim, et al. 2020. 'TFEB Regulates Murine Liver Cell Fate during Development and Regeneration'. *Nature Communications* 11 (1). https://doi.org/10.1038/s41467-020-16300-x.

Pavlova, Natalya N., and Craig B. Thompson. 2016. 'The Emerging Hallmarks of Cancer Metabolism'. *Cell Metabolism*. Cell Press. https://doi.org/10.1016/j.cmet.2015.12.006.

Pchitskaya, Ekaterina, Elena Popugaeva, and Ilya Bezprozvanny. 2018. 'Calcium Signaling and Molecular Mechanisms Underlying Neurodegenerative Diseases'. *Cell Calcium*. Elsevier Ltd. https://doi.org/10.1016/j.ceca.2017.06.008.

Pearce, Laura R., Xu Huang, Jérôme Boudeau, Rafał Pawłowski, Stephan Wullschleger, Maria Deak, Adel F.M. Ibrahim, Robert Gourlay, Mark A. Magnuson, and Dario R. Alessi. 2007. 'Identification of Protor as a Novel Rictor-Binding Component of MTOR Complex-2'. *Biochemical Journal* 405 (3): 513–22. https://doi.org/10.1042/BJ20070540.

Perera, Rushika M., Svetlana Stoykova, Brandon N. Nicolay, Kenneth N. Ross, Julien Fitamant, Myriam Boukhali, Justine Lengrand, et al. 2015. 'Transcriptional Control of Autophagy-Lysosome Function Drives Pancreatic Cancer Metabolism'. *Nature* 524 (7565): 361–65. https://doi.org/10.1038/nature14587.

Peskin, C S, D Tranchina, D Y Vargas, S Tyagi, A Van Oudenaarden, E K O Shea, J W Hong, et al. 2009. 'A Gene Network Regulating Biogenesis and Function', no. July, 473–77.

Peterson, Timothy R., Mathieu Laplante, Carson C. Thoreen, Yasemin Sancak, Seong A. Kang, W. Michael Kuehl, Nathanael S. Gray, and David M. Sabatini. 2009. 'DEPTOR Is an MTOR Inhibitor Frequently Overexpressed in Multiple Myeloma Cells and Required for Their Survival'. *Cell* 137 (5): 873–86. https://doi.org/10.1016/j.cell.2009.03.046.

Peterson, Timothy R., Shomit S. Sengupta, Thurl E. Harris, Anne E. Carmack, Seong A. Kang, Eric Balderas, David A. Guertin, et al. 2011. 'MTOR Complex 1 Regulates Lipin 1 Localization to Control the Srebp Pathway'. *Cell* 146 (3): 408–20. https://doi.org/10.1016/j.cell.2011.06.034.

Piffoux, Max, Erwan Eriau, and Philippe A. Cassier. 2021. 'Autophagy as a Therapeutic Target in Pancreatic Cancer'. *British Journal of Cancer*. Springer Nature. https://doi.org/10.1038/s41416-020-01039-5.

Ploper, Diego, Vincent F. Taelman, Lidia Robert, Brian S. Perez, Björn Titz, Hsiao Wang Chen, Thomas G. Graeber, Erika Von Euw, Antoni Ribas, and Edward M. De Robertis. 2015. 'MITF Drives Endolysosomal Biogenesis and Potentiates Wnt Signaling in Melanoma Cells'. *Proceedings of the National Academy of*

Sciences of the United States of America 112 (5): E420–29. https://doi.org/10.1073/pnas.1424576112.

Polito, Vinicia A, Hongmei Li, Heidi Martini-Stoica, Baiping Wang, Li Yang, Yin Xu, Daniel B Swartzlander, et al. 2014. 'Selective Clearance of Aberrant Tau Proteins and Rescue of Neurotoxicity by Transcription Factor EB'. *EMBO Molecular Medicine* 6 (9): 1142–60. https://doi.org/10.15252/emmm.201303671.

Porstmann, Thomas, Claudio R. Santos, Beatrice Griffiths, Megan Cully, Mary Wu, Sally Leevers, John R. Griffiths, Yuen Li Chung, and Almut Schulze. 2008. 'SREBP Activity Is Regulated by MTORC1 and Contributes to Akt-Dependent Cell Growth'. *Cell Metabolism* 8 (3): 224–36. https://doi.org/10.1016/J.CMET.2008.07.007.

Pringsheim, Tamara, and Connie Marras. 2009. 'Pimozide for Tics in Tourette's Syndrome'. *Cochrane Database of Systematic Reviews*, no. 2. https://doi.org/10.1002/14651858.CD006996.pub2.

Puertollano, Rosa, Shawn M Ferguson, James Brugarolas, and Andrea Ballabio. 2018. ' The Complex Relationship between TFEB Transcription Factor Phosphorylation and Subcellular Localization '. *The EMBO Journal* 37 (11). https://doi.org/10.15252/embj.201798804.

Puigserver, Pere, and Bruce M. Spiegelman. 2003. 'Peroxisome Proliferator-Activated Receptor-γ Coactivator 1α (PGC-1α): Transcriptional Coactivator and Metabolic Regulator'. *Endocrine Reviews*. https://doi.org/10.1210/er.2002-0012.

Raices, Marcela, and Maximiliano A. D'Angelo. 2012. 'Nuclear Pore Complex Composition: A New Regulator of Tissue-Specific and Developmental Functions'. *Nature Reviews Molecular Cell Biology*. https://doi.org/10.1038/nrm3461.

Ramanathan, Arvind, Connie Wang, and Stuart L Schreiber. 2005. 'Perturbational Profiling of a Cell-Line Model of Tumorigenesis by Using Metabolic Measurements'. www.pnas.orgcgidoi10.1073pnas.0502267102.

Ranjan, Alok, Itishree Kaushik, and Sanjay K. Srivastava. 2020. 'Pimozide Suppresses the Growth of Brain Tumors by Targeting Stat3-Mediated Autophagy'. *Cells* 9 (9): 1–19. https://doi.org/10.3390/cells9092141.

Rathmell, Jeffrey C., Casey J. Fox, David R. Plas, Peter S. Hammerman, Ryan M. Cinalli, and Craig B. Thompson. 2003. 'Akt-Directed Glucose Metabolism Can Prevent Bax Conformation Change and Promote Growth Factor-Independent Survival'. *Molecular and Cellular Biology* 23 (20): 7315–28. https://doi.org/10.1128/mcb.23.20.7315-7328.2003.

Rathmell, Jeffrey C., Mathew G.Vander Heiden, Marian H. Harris, Kenneth A. Frauwirth, and Craig B. Thompson. 2000. 'In the Absence of Extrinsic Signals, Nutrient Utilization by Lymphocytes Is Insufficient to Maintain Either Cell Size

or Viability'. *Molecular Cell* 6 (3): 683–92. https://doi.org/10.1016/S1097-2765(00)00066-6.

Rebsamen, Manuele, Lorena Pochini, Taras Stasyk, Mariana E.G. De Araújo, Michele Galluccio, Richard K. Kandasamy, Berend Snijder, et al. 2015. 'SLC38A9 Is a Component of the Lysosomal Amino Acid Sensing Machinery That Controls MTORC1'. *Nature* 519 (7544): 477–81. https://doi.org/10.1038/nature14107.

Ricciarelli, Roberta, and Ernesto Fedele. 2017. 'The Amyloid Cascade Hypothesis in Alzheimer's Disease: It's Time to Change Our Mind'. *Current Neuropharmacology* 15 (6). https://doi.org/10.2174/1570159x15666170116143743.

Roberts, D. J., and S. Miyamoto. 2015. 'Hexokinase II Integrates Energy Metabolism and Cellular Protection: Akting on Mitochondria and TORCing to Autophagy'. *Cell Death and Differentiation*. Nature Publishing Group. https://doi.org/10.1038/cdd.2014.173.

Roberts, David J., Valerie P. Tan-Sah, Jeffery M. Smith, and Shigeki Miyamoto. 2013. 'Akt Phosphorylates HK-II at Thr-473 and Increases Mitochondrial HK-II Association to Protect Cardiomyocytes'. *Journal of Biological Chemistry* 288 (33): 23798–806. https://doi.org/10.1074/jbc.M113.482026.

Rock, Kenneth L., and Lianjun Shen. 2005. 'Cross-Presentation: Underlying Mechanisms and Role in Immune Surveillance'. *Immunological Reviews*. https://doi.org/10.1111/j.0105-2896.2005.00301.x.

Roock, Wendy De, Veerle De Vriendt, Nicola Normanno, Fortunato Ciardiello, and Sabine Tejpar. 2011. 'KRAS, BRAF, PIK3CA, and PTEN Mutations: Implications for Targeted Therapies in Metastatic Colorectal Cancer'. *The Lancet Oncology* 12 (6): 594–603. https://doi.org/10.1016/S1470-2045(10)70209-6.

Ross, Christopher A, and Sarah J Tabrizi. 2011. 'Huntington's Disease: From Molecular Pathogenesis to Clinical Treatment'. *Lancet Neurol*. Vol. 10. www.thelancet.com/.

Rosset, Clévia, Cristina Brinckmann Oliveira Netto, and Patricia Ashton-Prolla. 2017. 'TSC1 and TSC2 Gene Mutations and Their Implications for Treatment in Tuberous Sclerosis Complex: A Review'. *Genetics and Molecular Biology*. Brazilian Journal of Genetics. https://doi.org/10.1590/1678-4685-GMB-2015-0321.

Rousseau, Adrien, and Anne Bertolotti. 2016. 'An Evolutionarily Conserved Pathway Controls Proteasome Homeostasis'. *Nature* 536 (7615): 184–89. https://doi.org/10.1038/nature18943.

Rozpędek, W, D Pytel, B Mucha, H Leszczyńska, J Alan Diehl, I Majsterek, and (I Majsterek. 2016. 'The Role of the PERK/EIF2α/ATF4/CHOP Signaling Pathway in Tumor Progression During Endoplasmic Reticulum Stress HHS Public Access'. *Curr Mol Med*. Vol. 16.

Sabatini, David M, Hediye Erdjument-Bromage, Mary Lui, Paul Tempst, and Solomon H Snyder. 1994. 'RAFTI: A Mammalian Protein That Binds to FKBP12 in a Rapamycin-Dependent Fashion and Is Homologous to Yeast TORs'. *Cell*. Vol. 78.

Sahu, Umakant, and Issam Ben-Sahra. 2023. 'GATOR2 Rings GATOR1 to Speak to MTORC1'. *Molecular Cell*. Cell Press. https://doi.org/10.1016/j.molcel.2022.12.011.

Samie, Mohammad, and Peter Cresswell. 2015. 'The Transcription Factor TFEB Acts as a Molecular Switch That Regulates Exogenous Antigen-Presentation Pathways'. *Nature Immunology* 16 (7): 729–36. https://doi.org/10.1038/ni.3196.

Samuels, Yardena, Zhenghe Wang, Alberto Bardelli, Natalie Silliman, Janine Ptak, Steve Szabo, Hai Yan, et al. 2004. 'High Frequency of Mutations of the PIK3CA Gene in Human Cancers'. *Science* 304 (5670): 554. https://doi.org/10.1126/science.1096502.

Sancak, Yasemin, Liron Bar-Peled, Roberto Zoncu, Andrew L. Markhard, Shigeyuki Nada, and David M. Sabatini. 2010. 'Ragulator-Rag Complex Targets MTORC1 to the Lysosomal Surface and Is Necessary for Its Activation by Amino Acids'. *Cell* 141 (2): 290–303. https://doi.org/10.1016/j.cell.2010.02.024.

Sancak, Yasemin, Timothy R. Peterson, Yoav D. Shaul, Robert A. Lindquist, Carson C. Thoreen, Liron Bar-Peled, and David M. Sabatini. 2008. 'The Rag GTPases Bind Raptor and Mediate Amino Acid Signaling to MTORC1'. *Science* 320 (5882): 1496–1501. https://doi.org/10.1126/science.1157535.

Sancak, Yasemin, Carson C. Thoreen, Timothy R. Peterson, Robert A. Lindquist, Seong A. Kang, Eric Spooner, Steven A. Carr, and David M. Sabatini. 2007. 'PRAS40 Is an Insulin-Regulated Inhibitor of the MTORC1 Protein Kinase'. *Molecular Cell* 25 (6): 903–15. https://doi.org/10.1016/J.MOLCEL.2007.03.003.

Santarpia, Libero, Scott M. Lippman, and Adel K. El-Naggar. 2012. 'Targeting the MAPKRASRAF Signaling Pathway in Cancer Therapy'. *Expert Opinion on Therapeutic Targets*. https://doi.org/10.1517/14728222.2011.645805.

Sarantis, Panagiotis, Evangelos Koustas, Adriana Papadimitropoulou, Athanasios G. Papavassiliou, and Michalis V. Karamouzis. 2020. 'Pancreatic Ductal Adenocarcinoma: Treatment Hurdles, Tumor Microenvironment and Immunotherapy'. *World Journal of Gastrointestinal Oncology*. Baishideng Publishing Group Co. https://doi.org/10.4251/wjgo.v12.i2.173.

Sarbassov DD, DA Guertin, SM Ali, and DM Sabatini. 2005. 'Phosphorylation and Regulation of Akt/PKB by the Rictor-MTOR Complex'. *Science* 95 (February):57. https://doi.org/10.1126/science.1106148.

Sarbassov, Dos D, Siraj M Ali, Do-Hyung Kim, David A Guertin, Robert R Latek, Hediye Erdjument-Bromage, Paul Tempst, and David M Sabatini. 2004. 'Rictor, a Novel Binding Partner of MTOR, Defines a Rapamycin-Insensitive

and Raptor-Independent Pathway That Regulates the Cytoskeleton'. *Current Biology* 14:1296–1302. https://doi.org/10.1016/j.

Sardiello, Marco, Michela Palmieri, Alberto di Ronza, Diego Luis Medina, Marta Valenza, Vincenzo Alessandro Gennarino, Chiara Di Malta, et al. 2009. 'A Gene Network Regulating Lysosomal Biogenesis and Function'. *Science*, June. https://doi.org/10.1126/science.1174447.

Sato, S, K Roberts, G Gambino, A Cook, T Kouzarides, and C R Goding. 1997. 'CBP/P300 as a Co-Factor for the Microphthalmia Transcription Factor'. *Oncogene*.

Schafer, Zachary T., Alexandra R. Grassian, Loling Song, Zhenyang Jiang, Zachary Gerhart-Hines, Hanna Y. Irie, Sizhen Gao, Pere Puigserver, and Joan S. Brugge. 2009. 'Antioxidant and Oncogene Rescue of Metabolic Defects Caused by Loss of Matrix Attachment'. *Nature* 461 (7260): 109–13. https://doi.org/10.1038/nature08268.

Schuchman, Edward H. 2010. 'Acid Sphingomyelinase, Cell Membranes and Human Disease: Lessons from Niemann-Pick Disease'. *FEBS Letters*. https://doi.org/10.1016/j.febslet.2009.11.083.

Sehgal, S. N., H. Baker, and Claude Vézina. 1975. 'Rapamycin (Ay-22,989), a New Antifungal Antibiotic. II. Fermentation, Isolation and Characterization'. *The Journal of Antibiotics* 28 (10): 727–32. https://doi.org/10.7164/antibiotics.28.727.

Sen, Buer, Zhihui Xie, Natasha Case, William R. Thompson, Gunes Uzer, Maya Styner, and Janet Rubin. 2014. 'MTORC2 Regulates Mechanically Induced Cytoskeletal Reorganization and Lineage Selection in Marrow-Derived Mesenchymal Stem Cells'. *Journal of Bone and Mineral Research* 29 (1): 78–89. https://doi.org/10.1002/jbmr.2031.

Settembre, Carmine, Rossella De Cegli, Gelsomina Mansueto, Pradip K. Saha, Francesco Vetrini, Orane Visvikis, Tuong Huynh, et al. 2013. 'TFEB Controls Cellular Lipid Metabolism through a Starvation-Induced Autoregulatory Loop'. *Nature Cell Biology* 15 (6): 647–58. https://doi.org/10.1038/ncb2718.

Settembre, Carmine, Chiara Di Malta, Vinicia Assunta Polito, Moises Garcia, Francesco Vetrini, Serpil Uckac Serkan Erdin, Serpil Uckac Serkan Erdin, et al. 2011. 'TFEB Links Autophagy to Lysosomal Biogenesis'. *Science* 332 (6036): 1429–33. https://doi.org/10.1126/science.1204592.TFEB.

Settembre, Carmine, Roberto Zoncu, Diego L. Medina, Francesco Vetrini, Serkan Erdin, Serpiluckac Erdin, Tuong Huynh, et al. 2012. 'A Lysosome-to-Nucleus Signalling Mechanism Senses and Regulates the Lysosome via MTOR and TFEB'. *EMBO Journal* 31 (5): 1095–1108. https://doi.org/10.1038/emboj.2012.32.

Shain, A. Hunter, and Boris C. Bastian. 2016. 'From Melanocytes to Melanomas'. *Nature Reviews Cancer*. Nature Publishing Group. https://doi.org/10.1038/nrc.2016.37.

Shi, Yijiang, Huajun Yan, Patrick Frost, Joseph Gera, and Alan Lichtenstein. 2005. 'Mammalian Target of Rapamycin Inhibitors Activate the AKT Kinase in Multiple Myeloma Cells by Up-Regulating the Insulin-like Growth Factor Receptor/Insulin Receptor Substrate-1/Phosphatidylinositol 3-Kinase Cascade'. https://doi.org/10.1158/1535-7163.MCT-05-0068.

Shibahara, Shigeki, Kazuhisa Takeda, Ken-Ichi Yasumoto, Tetsuo Udono, Ken-Ichi Watanabe, Hideo Saito, and Kazuhiro Takahashi. 2001. 'Microphthalmia-Associated Transcription Factor (MITF): Multiplicity in Structure, Function, and Regulation'. *Journal of Investigative Dermatology Symposium Proceedings*. Vol. 6.

Shields, Janiel M., Kevin Pruitt, Aidan McFall, Amy Shaub, and Channing J. Der. 2000. 'Understanding Ras: "It Ain't over "til It's over"'. *Trends in Cell Biology* 10 (4): 147–54. https://doi.org/10.1016/S0962-8924(00)01740-2.

Shipley, J M, S Birdsall, J Clark, J Crew, S Gill, M Linehan, J Gnarra, S Fisher, 1 W Craig, and C S Cooper2. 1995. 'Mapping the X Chromosome Breakpoint in Two Papillary Renal Cell Carcinoma Cell Lines with a t(X; 1)(P11.2;Q21.2) and the First Report of a Female Case'. *Cytogenet Cell Genet*. Vol. 7. http://karger.com/cgr/article-pdf/71/3/280/2323940/000134127.pdf.

Sjödahl, Gottfrid, Martin Lauss, Sigurdur Gudjonsson, Fredrik Liedberg, Christer Halldén, Gunilla Chebil, Wiking Månsson, Mattias Höglund, and David Lindgren. 2011. 'A Systematic Study of Gene Mutations in Urothelial Carcinoma; Inactivating Mutations in Tsc2 and Pik3r1'. *PLoS ONE* 6 (4). https://doi.org/10.1371/journal.pone.0018583.

Śmiech, Magdalena, Paweł Leszczyński, Hidetoshi Kono, Christopher Wardell, and Hiroaki Taniguchi. 2020. 'Emerging Braf Mutations in Cancer Progression and Their Possible Effects on Transcriptional Networks'. *Genes* 11 (11): 1–14. https://doi.org/10.3390/genes11111342.

Song, Ha Lim, Atanas Vladimirov Demirev, Na Young Kim, Dong Hou Kim, and Seung Yong Yoon. 2019. 'Ouabain Activates Transcription Factor EB and Exerts Neuroprotection in Models of Alzheimer's Disease'. *Molecular and Cellular Neuroscience* 95 (March):13–24. https://doi.org/10.1016/J.MCN.2018.12.007.

Sooyeon, Lee, Sato Yutaka, and Ralph A. Nixon. 2011. 'Primary Lysosomal Dysfunction Causes Cargo-Specific Deficits of Axonal Transport Leading to Alzheimer-like Neuritic Dystrophy.' 7 (November): 1308–15.

Spada, A, E Wilson, D Lubahn, A Harding, and K Fischbeck. 1991. 'Androgen Receptor Gene in X-Linked spinal and Bulbar Muscular Atrophy'. *Nature*, no. 352, 77–79. https://doi.org/https://doi.org/10.1038/352077a0.

Stark, Michal, Tomás F.D. Silva, Guy Levin, Miguel Machuqueiro, and Yehuda G. Assaraf. 2020. 'The Lysosomotropic Activity of Hydrophobic Weak Base Drugs Is Mediated via Their Intercalation into the Lysosomal Membrane'. *Cells* 9 (5). https://doi.org/10.3390/cells9051082.

Steingrimsson, Eirikur, Karen J Moore, M Lynn Lamoreux, Adrian R Ferre-D'amare, Stephen K Burlef, Debra C Sanders Zimring\, Loren C Skow\, et al. 1994. 'Molecular Basis of Mouse Microphthalmia (Mi) Mutations Helps Explain Their Developmental and Phenotypic Consequences'. *Nature Genetics*. http://www.nature.com/naturegenetics.

Sueda, Toshinori, Daisuke Sakai, Koichi Kawamoto, Masamitsu Konno, Naohiro Nishida, Jun Koseki, Hugh Colvin, et al. 2016. 'BRAFV600E Inhibition Stimulates AMP-Activated Protein Kinase-Mediated Autophagy in Colorectal Cancer Cells'. *Scientific Reports* 6 (January): 1–7. https://doi.org/10.1038/srep18949.

Sun, Yanan, Huihui Wang, Taiqi Qu, Junjie Luo, Peng An, Fazheng Ren, Yongting Luo, and Yixuan Li. 2023. 'MTORC2: A Multifaceted Regulator of Autophagy'. *Cell Communication and Signaling*. BioMed Central Ltd. https://doi.org/10.1186/s12964-022-00859-7.

Szwed, Angelia, Eugene Kim, and Estela Jacinto. 2021. 'REGULATION AND METABOLIC FUNCTIONS OF MTORC1 AND MTORC2'. *Physiological Reviews* 101 (3): 1371–1426. https://doi.org/10.1152/physrev.00026.2020.

Takebayashi, Kimiko, Kazuhiro Chida, Ikuyo Tsukamoto, Eiichi Morii, Hiroshi Munakata, Heinz Arnheiter, Toshio Kuroki, Yukihiko Kitamura, and Shintaro Nomura. 1996. 'The Recessive Phenotype Displayed by a Dominant Negative Microphthalmia-Associated Transcription Factor Mutant Is a Result of Impaired Nuclear Localization Potential'. *MOLECULAR AND CELLULAR BIOLOGY*. Vol. 16.

Tan, An S., James W. Baty, Lan Feng Dong, Ayenachew Bezawork-Geleta, Berwini Endaya, Jacob Goodwin, Martina Bajzikova, et al. 2015. 'Mitochondrial Genome Acquisition Restores Respiratory Function and Tumorigenic Potential of Cancer Cells without Mitochondrial DNA'. *Cell Metabolism* 21 (1): 81–94. https://doi.org/10.1016/J.CMET.2014.12.003.

Tanji, Kunikazu, Fumiaki Mori, Akiyoshi Kakita, Hitoshi Takahashi, and Koichi Wakabayashi. 2011. 'Alteration of Autophagosomal Proteins (LC3, GABARAP and GATE-16) in Lewy Body Disease'. *Neurobiology of Disease* 43 (3): 690–97. https://doi.org/10.1016/j.nbd.2011.05.022.

Tassabehjil, Mayada, Valerie E Newton, and Andrew P Read. 1994. 'Waarclenburg Syndrome Type 2 Caused by Mutations in the Human Microphthalmia (MlTf) Gene' 8 (november): 251–55.

Tcw, Julia, and Alison M. Goate. 2017. 'Genetics of β-Amyloid Precursor Protein in Alzheimer's Disease'. *Cold Spring Harbor Perspectives in Medicine*. https://doi.org/10.1101/cshperspect.a024539.

Thompson, C B. 2011. 'Rethinking the Regulation of Cellular Metabolism'. *Cold Spring Harbor Laboratory Press*. https://doi.org/10.1101/sqb.2012.76.010496.

Tian, Yangzi, and Weinan Guo. 2020. 'A Review of the Molecular Pathways Involved in Resistance to BRAF Inhibitors in Patients with Advanced-Stage Melanoma'. *Medical Science Monitor* 26 (April). https://doi.org/10.12659/MSM.920957.

Tran, Sharon, W. Douglas Fairlie, and Erinna F. Lee. 2021. 'Beclin1: Protein Structure, Function and Regulation'. *Cells*. MDPI. https://doi.org/10.3390/cells10061522.

Tshori, Sagi, Dan Gilon, Ronen Beeri, Hovav Nechushtan, Dmitry Kaluzhny, Eli Pikarsky, and Ehud Razin. 2006. 'Transcription Factor MITF Regulates Cardiac Growth and Hypertrophy'. *Journal of Clinical Investigation* 116 (10): 2673–81. https://doi.org/10.1172/JCI27643.

Tsun, Zhi Yang, Liron Bar-Peled, Lynne Chantranupong, Roberto Zoncu, Tim Wang, Choah Kim, Eric Spooner, and David M. Sabatini. 2013. 'The Folliculin Tumor Suppressor Is a GAP for the RagC/D GTPases That Signal Amino Acid Levels to MTORC1'. *Molecular Cell* 52 (4): 495–505. https://doi.org/10.1016/j.molcel.2013.09.016.

Tsunemi, Taiji, Travis D. Ashe, Bradley E. Morrison, Kathryn R. Soriano, Jonathan Au, Ruben A.Vázquez Roque, Eduardo R. Lazarowski, Vincent A. Damian, Eliezer Masliah, and Albert R. La Spada. 2012. 'PGC-1a Rescues Huntington's Disease Proteotoxicity by Preventing Oxidative Stress and Promoting TFEB Function'. *Science Translational Medicine* 4 (142). https://doi.org/10.1126/scitranslmed.3003799.

Turco, Eleonora, Dorotea Fracchiolla, and Sascha Martens. 2020. 'Recruitment and Activation of the ULK1/Atg1 Kinase Complex in Selective Autophagy'. *Journal of Molecular Biology* 432 (1): 123–34. https://doi.org/10.1016/J.JMB.2019.07.027.

Vara-Ciruelos, Diana, Madhumita Dandapani, Fiona M. Russell, Katarzyna M. Grzes, Abdelmadjid Atrih, Marc Foretz, Benoit Viollet, Douglas J. Lamont, Doreen A. Cantrell, and D. Grahame Hardie. 2019. 'Phenformin, But Not Metformin, Delays Development of T Cell Acute Lymphoblastic Leukemia/Lymphoma via Cell-Autonomous AMPK Activation'. *Cell Reports* 27 (3): 690-698.e4. https://doi.org/10.1016/j.celrep.2019.03.067.

Vega-Rubin-de-Celis, Silvia, Samuel Peña-Llopis, Meghan Konda, and James Brugarolas. 2017. 'Multistep Regulation of TFEB by MTORC1'. *Autophagy* 13 (3): 464–72. https://doi.org/10.1080/15548627.2016.1271514.

Visvikis, Orane, Nnamdi Ihuegbu, Sid A. Labed, Lyly G. Luhachack, Anna Maria F. Alves, Amanda C. Wollenberg, Lynda M. Stuart, Gary D. Stormo, and Javier E. Irazoqui. 2014. 'Innate Host Defense Requires TFEB-Mediated Transcription of Cytoprotective and Antimicrobial Genes'. *Immunity* 40 (6): 896–909. https://doi.org/10.1016/j.immuni.2014.05.002.

Vogelstein, Bert, and Kenneth W. Kinzler. 2004. 'Cancer Genes and the Pathways They Control'. *Nature Medicine*. https://doi.org/10.1038/nm1087.

Wang, Bo, Xiaoqin Yin, Weidong Gan, Fan Pan, Shiyuan Li, Zou Xiang, Xiaodong Han, and Dongmei Li. 2021. 'PRCC-TFE3 Fusion-Mediated PRKN/Parkin-Dependent Mitophagy Promotes Cell Survival and Proliferation in PRCC-TFE3 Translocation Renal Cell Carcinoma'. *Autophagy* 17 (9): 2475–93. https://doi.org/10.1080/15548627.2020.1831815.

Wang, Liyuan, Chuchu Zhao, Tao Zheng, Yi Zhang, Hanruo Liu, Xi Wang, Xianling Tang, Baowen Zhao, and Ping Liu. 2022. 'Torin 1 Alleviates Impairment of TFEB-Mediated Lysosomal Biogenesis and Autophagy in TGFBI (p.G623_H626del)-Linked Thiel-Behnke Corneal Dystrophy'. *Autophagy* 18 (4): 765–82. https://doi.org/10.1080/15548627.2021.1955469.

Wang, Yudong, Johan Palmfeldt, Niels Gregersen, Alexander M. Makhov, James F. Conway, Meicheng Wang, Stephen P. McCalley, et al. 2019. 'Mitochondrial Fatty Acid Oxidation and the Electron Transport Chain Comprise a Multifunctional Mitochondrial Protein Complex'. *Journal of Biological Chemistry* 294 (33): 12380–91. https://doi.org/10.1074/jbc.RA119.008680.

Warburg, Otto. 1956. 'Injuring of Respiration On the Origin of Cancer Cells'. *Science* 123:3191. https://www.science.org.

Wee, Ping, and Zhixiang Wang. 2017. 'Epidermal Growth Factor Receptor Cell Proliferation Signaling Pathways'. *Cancers*. MDPI AG. https://doi.org/10.3390/cancers9050052.

Wise, David R, Ralph J Deberardinis, Anthony Mancuso, Nabil Sayed, Xiao-Yong Zhang, Harla K Pfeiffer, Ilana Nissim, et al. 2008. 'Myc Regulates a Transcriptional Program That Stimulates Mitochondrial Glutaminolysis and Leads to Glutamine Addiction'. www.pnas.org/cgi/content/full/.

Wisner, Katherine L., and Christof Schaefer. 2015. *Psychotropic Drugs*. *Drugs During Pregnancy and Lactation: Treatment Options and Risk Assessment: Third Edition*. Elsevier. https://doi.org/10.1016/B978-0-12-408078-2.00012-3.

Wolfson, Rachel L., Lynne Chantranupong, Robert A. Saxton, Kuang Shen, Sonia M. Scaria, Jason R. Cantor, and David M. Sabatini. 2016. 'Sestrin2 Is a Leucine Sensor for the MTORC1 Pathway'. *Science* 351 (6268): 43–48. https://doi.org/10.1126/science.aab2674.

Woods, Angela, Kristina Dickerson, Richard Heath, Seung Pyo Hong, Milica Momcilovic, Stephen R. Johnstone, Marian Carlson, and David Carling. 2005. 'Ca2+/Calmodulin-Dependent Protein Kinase Kinase-β Acts Upstream of AMP-Activated Protein Kinase in Mammalian Cells'. *Cell Metabolism* 2 (1): 21–33. https://doi.org/10.1016/J.CMET.2005.06.005.

Wu, Di, and Jie Liang. 2024. 'Activating Transcription Factor 4: A Regulator of Stress Response in Human Cancers'. *Frontiers in Cell and Developmental Biology*. Frontiers Media SA. https://doi.org/10.3389/fcell.2024.1370012.

Wu, Dianqing, and Weijun Pan. 2010. 'GSK3: A Multifaceted Kinase in Wnt Signaling'. *Trends in Biochemical Sciences*. https://doi.org/10.1016/j.tibs.2009.10.002.

Xia, Jing, Rong Wang, Tianlong Zhang, and Jianping Ding. 2016. 'Structural Insight into the Arginine-Binding Specificity of CASTOR1 in Amino Acid-Dependent MTORC1 Signaling'. *Cell Discovery* 2 (September). https://doi.org/10.1038/celldisc.2016.35.

Xiao, Qingli, Ping Yan, Xiucui Ma, Haiyan Liu, Ronaldo Perez, Alec Zhu, Ernesto Gonzales, et al. 2014. 'Enhancing Astrocytic Lysosome Biogenesis Facilitates Aβ Clearance and Attenuates Amyloid Plaque Pathogenesis'. *Journal of Neuroscience* 34 (29): 9607–20. https://doi.org/10.1523/JNEUROSCI.3788-13.2014.

Xiao, Xin, Wei Wang, Yuqian Li, Di Yang, Xiaokang Li, Chao Shen, Yan Liu, Xianzhu Ke, Shuo Guo, and Zheng Guo. 2018. 'HSP90AA1-Mediated Autophagy Promotes Drug Resistance in Osteosarcoma'. *Journal of Experimental and Clinical Cancer Research* 37 (1): 1–13. https://doi.org/10.1186/s13046-018-0880-6.

Yamamoto, Hiromasa, Hisayuki Shigematsu, Masaharu Nomura, William W. Lockwood, Mitsuo Sato, Naoki Okumura, Junichi Soh, et al. 2008. 'PIK3CA Mutations and Copy Number Gains in Human Lung Cancers'. *Cancer Research* 68 (17): 6913–21. https://doi.org/10.1158/0008-5472.CAN-07-5084.

Yanagida, Osamu, Yoshikatsu Kanai, Arthit Chairoungdua, Do Kyung Kim, Hiroko Segawa, Tomoko Nii, Seok Ho Cha, et al. 2001. 'Human L-Type Amino Acid Transporter 1 (LAT1): Characterization of Function and Expression in Tumor Cell Lines'. *Biochimica et Biophysica Acta (BBA) - Biomembranes* 1514 (2): 291–302. https://doi.org/10.1016/S0005-2736(01)00384-4.

Yang, Guang, Danielle S. Murashige, Sean J. Humphrey, and David E. James. 2015. 'A Positive Feedback Loop between Akt and MTORC2 via SIN1 Phosphorylation'. *Cell Reports* 12 (6): 937–43. https://doi.org/10.1016/J.CELREP.2015.07.016.

Yang, Shenghong, Xiaoxu Wang, Gianmarco Contino, Marc Liesa, Ergun Sahin, Haoqiang Ying, Alexandra Bause, et al. 2011. 'Pancreatic Cancers Require Autophagy for Tumor Growth'. *Genes and Development* 25 (7): 717–29. https://doi.org/10.1101/gad.2016111.

Yao, Xiaohao, Xiaochu Chen, Charisa Cottonham, and Lan Xu. 2008. 'Preferential Utilization of Imp7/8 in Nuclear Import of Smads'. *Journal of Biological Chemistry* 283 (33): 22867–74. https://doi.org/10.1074/JBC.M801320200.

Yasumoto, Ken Ichi, Shintaro Amae, Tetsuo Udono, Nobuo Fuse, Kazuhisa Takeda, and Shigeki Shibahara. 1998. 'A Big Gene Linked to Small Eyes Encodes Multiple Mitf Isoforms: Many Promoters Make Light Work'. *Pigment Cell Research*. Blackwell Publishing Ltd. https://doi.org/10.1111/j.1600-0749.1998.tb00491.x.

Yasumoto,' Kouji Yokoyama,', Ken-Ichi, Koushi Shibata,', Yasushi Tomita, and Shigeki Shibaharai. 1994. 'Microphthalmia-Associated Transcription Factor

as a Regulator for Melanocyte-Specific Transcription of the Human Tyrosinase Gene'. *MOLECULAR AND CELLULAR BIOLOGY*.

Ye, Jiangbin, Wilhelm Palm, Min Peng, Bryan King, Tullia Lindsten, Ming O. Li, Constantinos Koumenis, and Craig B. Thompson. 2015. 'GCN2 Sustains MTORC1 Suppression upon Amino Acid Deprivation by Inducing Sestrin2'. *Genes and Development* 29 (22): 2331–36. https://doi.org/10.1101/gad.269324.115.

Yoneshima, Erika, Kuniaki Okamoto, Eiko Sakai, Kazuhisa Nishishita, Noriaki Yoshida, and Takayuki Tsukuba. 2016. 'The Transcription Factor EB (TFEB) Regulates Osteoblast Differentiation Through ATF4/CHOP-Dependent Pathway'. *Journal of Cellular Physiology* 231 (6): 1321–33. https://doi.org/10.1002/jcp.25235.

Yoneyama, Yosuke, Tomomi Inamitsu, Kazuhiro Chida, Shun Ichiro Iemura, Tohru Natsume, Tatsuya Maeda, Fumihiko Hakuno, and Shin Ichiro Takahashi. 2018. 'Serine Phosphorylation by MTORC1 Promotes IRS-1 Degradation through SCFβ-TRCP E3 Ubiquitin Ligase'. *IScience* 5 (July):1–18. https://doi.org/10.1016/j.isci.2018.06.006.

Yun, Jihye, Carlo Rago, Ian Cheong, Ray Pagliarini, Philipp Angenendt, Harith Rajagopalan, Kerstin Schmidt, et al. 2009. 'Glucose Deprivation Contributes to the Development of KRAS Pathway Mutations in Tumor Cells'. *Science* 325 (5947): 1555–59. https://doi.org/10.1126/science.1174229.

Yun, Seongseok, Nicole D. Vincelette, Xiaoqing Yu, Gregory W. Watson, Mario R. Fernandez, Chunying Yang, Taro Hitosugi, et al. 2021. 'TFEB Links MYC Signaling to Epigenetic Control of Myeloid Differentiation and Acute Myeloid Leukemia'. *Blood Cancer Discovery* 2 (2): 162–85. https://doi.org/10.1158/2643-3230.BCD-20-0029.

Zadra, Giorgia, Cornelia Photopoulos, Svitlana Tyekucheva, Pedram Heidari, Qing Ping Weng, Giuseppe Fedele, Hong Liu, et al. 2014. ' A Novel Direct Activator of AMPK Inhibits Prostate Cancer Growth by Blocking Lipogenesis '. *EMBO Molecular Medicine* 6 (10): 1357–1357. https://doi.org/10.15252/emmm.201470070.

Zhang, Jing, Thomas M. Roberts, and Ramesh A. Shivdasani. 2011. 'Targeting PI3K Signaling as a Therapeutic Approach for Colorectal Cancer'. *Gastroenterology* 141 (1): 50–61. https://doi.org/10.1053/J.GASTRO.2011.05.010.

Zhang, Lihong, Jia Yu, Heling Pan, Ping Hu, Yan Hao, Wenqing Cai, Hong Zhu, et al. 2007. 'Small Molecule Regulators of Autophagy Identified by an Image-Based High-Throughput Screen'. *Proceedings of the National Academy of Sciences of the United States of America* 104 (48): 19023–28. https://doi.org/10.1073/pnas.0709695104.

Zhang, Tianyi, Qingxiang Zhou, Margret Helga Ogmundsdottir, Katrin Möller, Robert Siddaway, Lionel Larue, Michael Hsing, et al. 2015. 'Mitf Is a Master Regulator of the V-ATPase, Forming a Control Module for Cellular Homeostasis with v-

ATPase and TORC1'. *Journal of Cell Science* 128 (15): 2938–50. https://doi.org/10.1242/jcs.173807.

Zhang, Wei, Hui Tu Liu, and Hui Tu. 2002. 'MAPK Signal Pathways in the Regulation of Cell Proliferation in Mammalian Cells'. *Cell Research*. http://www.cell-research.com.

Zhang, Wen Hua, Hongyan Wang, Xin Wang, Malini V. Narayanan, Irina G. Stavrovskaya, Bruce S. Kristal, and Robert M. Friedlander. 2008. 'Nortriptyline Protects Mitochondria and Reduces Cerebral Ischemia/Hypoxia Injury'. *Stroke* 39 (2): 455–62. https://doi.org/10.1161/STROKEAHA.107.496810.

Zhang, Xinbo, Naimei Tang, Timothy J. Hadden, and Arun K. Rishi. 2011. 'Akt, FoxO and Regulation of Apoptosis'. *Biochimica et Biophysica Acta (BBA) - Molecular Cell Research* 1813 (11): 1978–86. https://doi.org/10.1016/J.BBAMCR.2011.03.010.

Zhang, Yi Dan, and Jian Jun Zhao. 2015. 'TFEB Participates in the Aβ-Induced Pathogenesis of Alzheimer's Disease by Regulating the Autophagy-Lysosome Pathway'. *DNA and Cell Biology* 34 (11): 661–68. https://doi.org/10.1089/dna.2014.2738.

Zhang, Zengli, Hongfeng Wang, Qifeng Ding, Yufei Xing, Delai Xu, Zhonghua Xu, Tong Zhou, et al. 2017. 'The Tumor Suppressor P53 Regulates Autophagosomal and Lysosomal Biogenesis in Lung Cancer Cells by Targeting Transcription Factor EB'. *Biomedicine & Pharmacotherapy* 89 (May):1055–60. https://doi.org/10.1016/J.BIOPHA.2017.02.103.

Zhao, Guang-Quan, Q I Zhao, Xin Zhou, Marie-Genevieve Matfrei, and Benoit De Crombrugghel. 1993. 'TFEC, a Basic Helix-Loop-Helix Protein, Forms Heterodimers with TFE3 and Inhibits TFE3-Dependent Transcription Activation'. *MOLECULAR AND CELLULAR BIOLOGY*. Vol. 13.

Zhao, Mantong, and Daniel J. Klionsky. 2011. 'AMPK-Dependent Phosphorylation of ULK1 Induces Autophagy'. *Cell Metabolism*. Cell Press. https://doi.org/10.1016/j.cmet.2011.01.009.

Zhitomirsky, Benny, and Yehuda G Assaraf. 2017. 'Lysosomal Accumulation of Anticancer Drugs Triggers Lysosomal Exocytosis'. *Oncotarget*. Vol. 8. www.impactjournals.com/oncotarget/.

Zhou, Ying, Elizabeth Hopper-Borge, Tong Shen, Xiao Cong Huang, Zhi Shi, Ye Hong Kuang, Tatsuhiko Furukawa, et al. 2009. 'Cepharanthine Is a Potent Reversal Agent for MRP7(ABCC10)-Mediated Multidrug Resistance'. *Biochemical Pharmacology* 77 (6): 993–1001. https://doi.org/10.1016/j.bcp.2008.12.005.

Zhu, Chunyang, Yangyang Lu, Shasha Wang, Jialin Song, Yixin Ding, Yan Wang, Chen Dong, Jiani Liu, Wensheng Qiu, and Weiwei Qi. 2024. 'Nortriptyline Hydrochloride, a Potential Candidate for Drug Repurposing, Inhibits Gastric Cancer by Inducing Oxidative Stress by Triggering the Keap1-Nrf2 Pathway'. *Scientific Reports* 14 (1): 1–16. https://doi.org/10.1038/s41598-024-56431-5.

Zhuang, Xu Xu, Sheng Fang Wang, Yuan Tan, Ju Xian Song, Zhou Zhu, Zi Ying Wang, Ming Yue Wu, et al. 2020. 'Pharmacological Enhancement of TFEB-Mediated Autophagy Alleviated Neuronal Death in Oxidative Stress-Induced Parkinson's Disease Models'. *Cell Death and Disease* 11 (2). https://doi.org/10.1038/s41419-020-2322-6.

Zielke, Svenja, Nina Meyer, Muriel Mari, Khalil Abou-El-Ardat, Fulvio Reggiori, Sjoerd J L Van Wijk, Donat Kögel, and Simone Fulda. 2018. 'Loperamide, Pimozide, and STF-62247 Trigger Autophagy-Dependent Cell Death in Glioblastoma Cells'. *Cell Death and Disease*. https://doi.org/10.1038/s41419-018-1003-1.

Zinzalla, Vittoria, Daniele Stracka, Wolfgang Oppliger, and Michael N. Hall. 2011. 'Activation of MTORC2 by Association with the Ribosome'. *Cell* 144 (5): 757–68. https://doi.org/10.1016/J.CELL.2011.02.014.

Supplementary materials

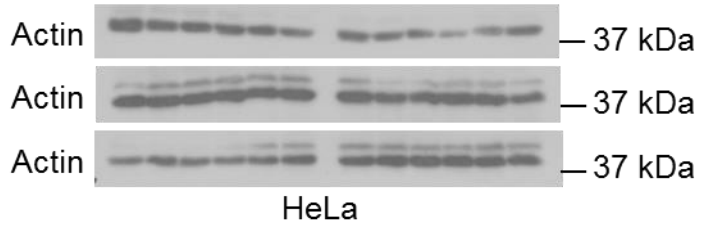

Supplemental Figure 1. Additional loading controls from western blot analysis shown in figure 10

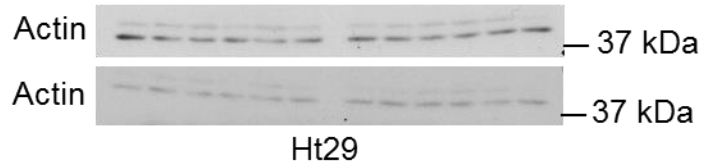

Supplemental Figure 2. Additional loading controls from western blot analysis shown in for Figure 11

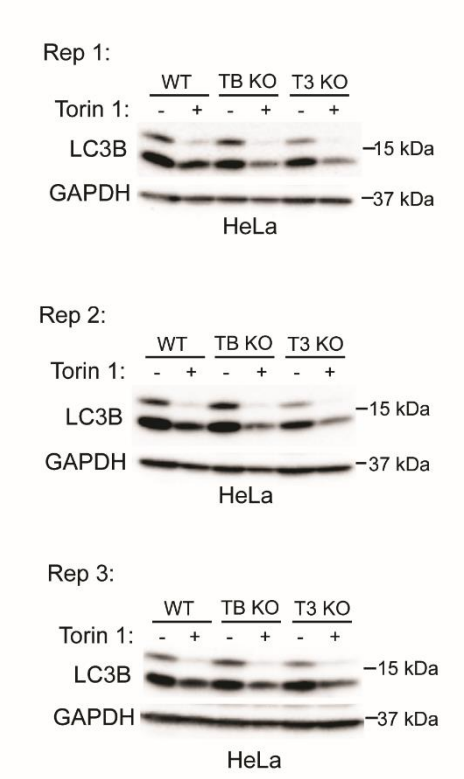

Supplemental Figure 3. Quantification of LC3BI/II-fold changes were calculated by densitometry from three independent experiments (N=3).

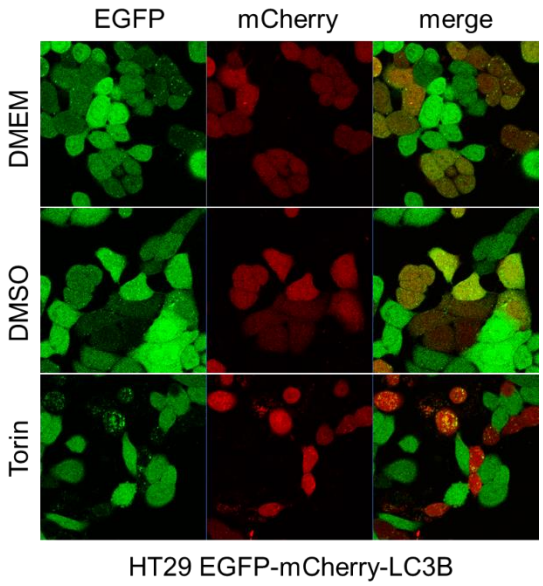

Supplemental Figure 4. Live microscopy images taken of HT29 EGFP-mCherry-LC3B cell line
HT29 were either untreated (DMEM), treated with DMSO (0.1%) or Torin (250 nM) for 4 hours prior to images taken. *Cell line generated by the candidate but not used for experiments in this study due to lack of time.*

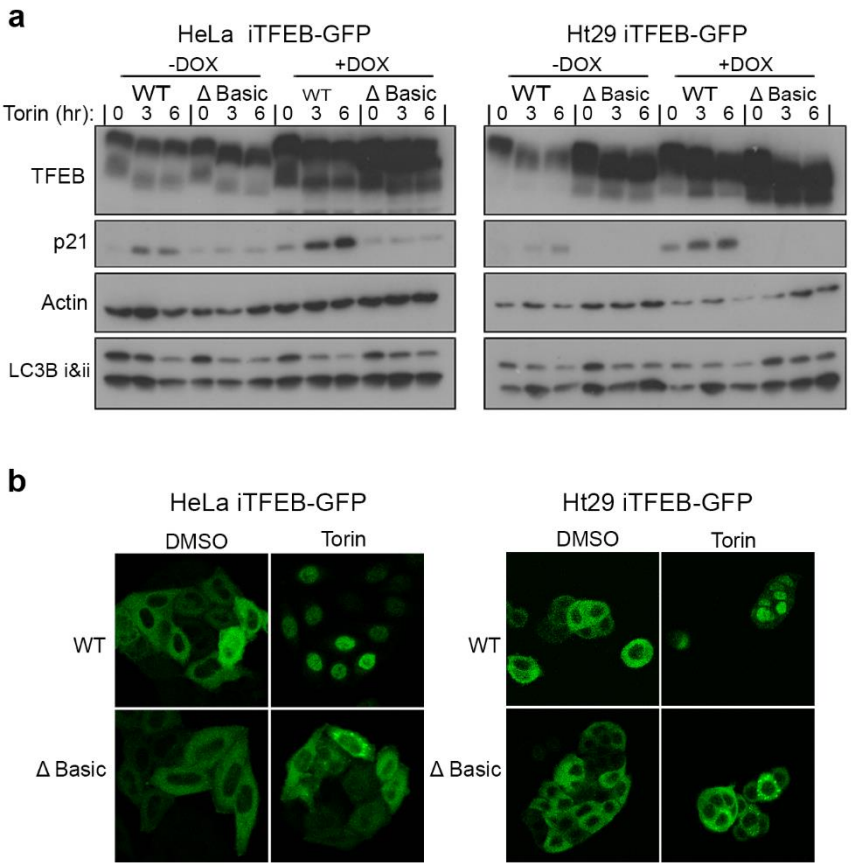

Supplemental Figure 5. Western blot analysis and live microscopy images demonstrating functional consequences of over-expressing wildtype vs ΔBasic TFEB-GFP mutant when treated with or without Torin.
(a) Western blot analysis of HeLa and HT29 cell lines stably expressing DOX-inducible WT TFEB-GFP or △ Basic TFEB-GFP, treated with and without DOX (10 ng/mL, overnight). The next day, cells were treated with or without Torin (250 nM) for up to 6 hr. Western blot shows induction of p21 when over-expressing wildtype TFEB-GFP but not when overexpressing △ Basic TFEB-GFP. (b) Live microscopy images demonstrating that in response to Torin (250 nM, 2 hr) wildtype TFEB-GFP translocates to the nucleus whereas △Basic TFEB-GFP does not. D*isclaimer: cell lines not generated by the candidate. Experiments designed and performed by the candidate. These cell lines were not used in this study due to lack of time.*

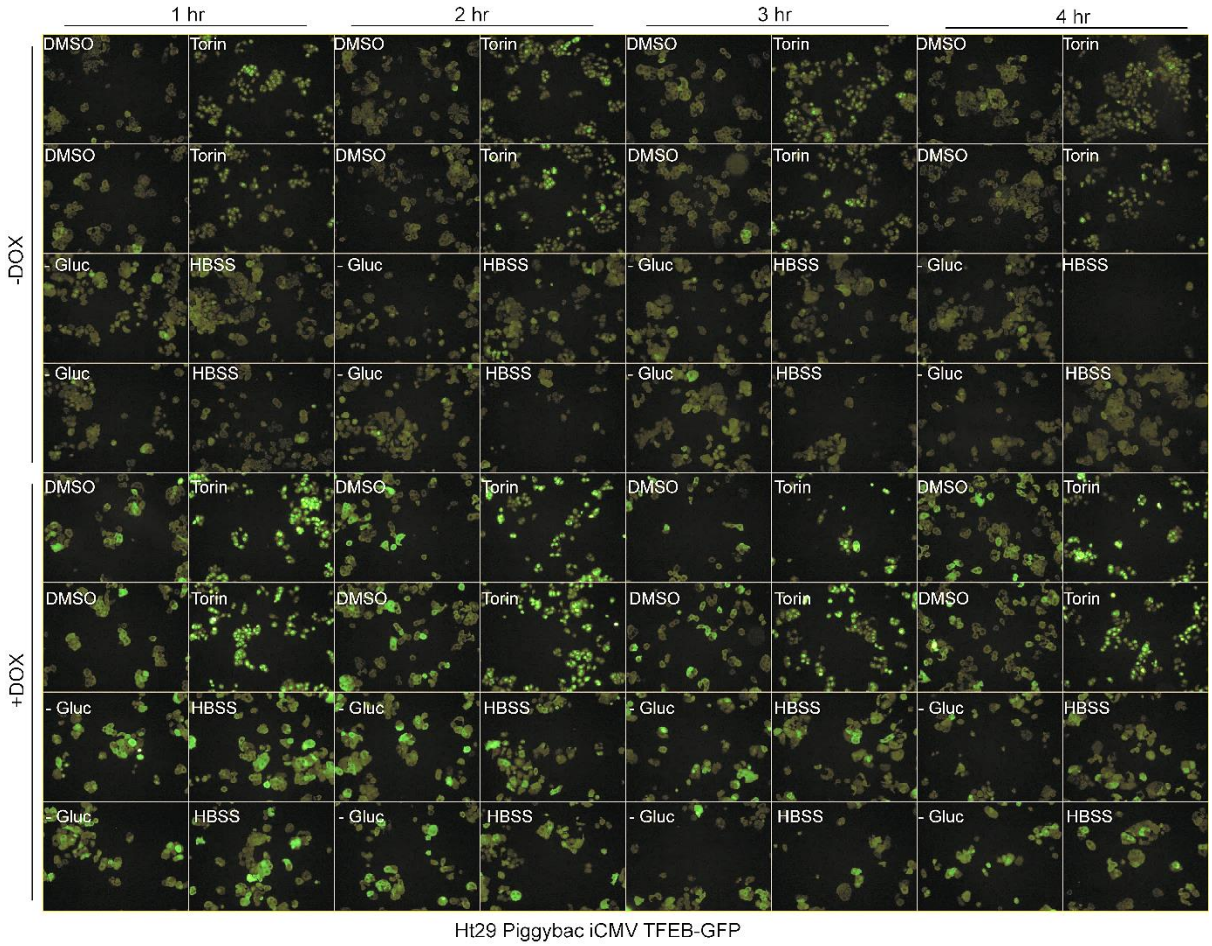

Supplemental Figure 6. Immunofluorescence microscopy images demonstrating wild-type TFEB-GFP does not respond to glucose or amino acid deprivation but does respond to Torin treatment

Surprisingly, the wildtype TFEB-GFP protein does not translocate to the nucleus upon glucose or amino acid deprivation. We could not find out an explanation for this despite our best efforts. Due to lack of time, we were unable to use this cell like for the second drug screen (Chapter 5).

Supplementary 7. Macro used for measuring nuclear/cytoplasmic TFEB staining and generation of ROIs

```
// Set the measurements to be acquired by this macro

run("Set Measurements...", "area mean shape integrated display redirect=None decimal=2");

// These lines select the source and destination directories/folders for the macro

dir1 = getDirectory("Choose a folder");

dir2 = getDirectory("Pick a folder");

//These lines define the list of files to be used and ensure that only .CZI files from the source folder are selected for processing

list = getFileList(dir1);

setBatchMode(false);

for (loop=0; loop<lengthOf(list);loop++){

        if(endsWith(list[loop],".czi")){

run("Bio-Formats", "open=["+dir1+list[loop]+"] color_mode=Default rois_import=[ROI manager] view=Hyperstack stack_order=XYCZT series_1");

Title = getTitle();

// This function allows the scale of the parent image to be imported to duplications and label images.

run("Set Scale...","global");

// This command splits the image stack into two channels

run("Split Channels");

selectWindow("C2-"+Title);

//close();

//select the nuclei (DAPI) channel

//selectWindow("C1-"+Title);

//Duplicate channel to allow a rename for Stardist

run("Duplicate...", "title=nuclei");

//Segment nuclei by running Stardist on its default settings on the window labelled nuclei;

run("Command From Macro", "command=[de.csbdresden.stardist.StarDist2D], args=['input':'nuclei', 'modelChoice':'Versatile (fluorescent nuclei)', 'normalizeInput':'true', 'percentileBottom':'28.90000000002', 'percentileTop':'99.8', 'probThresh':'0.479071', 'nmsThresh':'0.3', 'outputType':'Both', 'nTiles':'1', 'excludeBoundary':'20', 'roiPosition':'Automatic', 'verbose':'false', 'showCsbdeepProgress':'false', 'showProbAndDist':'false'], process=[false]");

selectImage("Label Image");

close();

close();

//This section superimposed the Stardist generated ROIs onto the original nuclear signal and saves an overlaid image to allow for manual QC
```

```
selectWindow("C2-"+Title);
roiManager("Show All");
run("Flatten");
saveAs("TIFF", dir2+Title+"QC_Overlay");
close();
//selects the window to be examined for nuclear signal
selectWindow("C1-"+Title);
roiManager("Show All");
for (i = 0; i < roiManager("count"); i++) {
        roiManager("Select", i);
        run("Enlarge...", "enlarge=-0.5");
        roiManager("Update");}
        roiManager("Measure");
saveAs("Results",dir2+Title+"green_nucleus"+".csv");
run("Clear Results");
// Convert the circular ROIs into rings within which signal will be measured
for (i = 0; i < roiManager("count"); i++) {
        roiManager ("Select", i);
        run("Make Band...", "band=4");
        roiManager("Update");
}
// constrict the rings to ensure that none are touching borders which will crash the macro
for (i = 0; i < roiManager("count"); i++) {
        roiManager("Select", i);
        run("Enlarge...", "enlarge=-2");
        roiManager("Update");
}
// perform the measurement of the regions of interest
for (i = 0; i < roiManager("count"); i++) {
        roiManager("Select", i);
        roiManager("Measure");
}
run("Flatten");
saveAs("Tiff", dir2+Title+"Green_Cytoplasm_QC_Overlay");
```

```
saveAs("Results",dir2+Title+"Results_cytoplasm"+".csv");
run("Clear Results");
//Close the images to allow the cycle to continue
//selectWindow("C3-"+Title);
//close();
//selectWindow("C1-"+Title);
close();
run("Close All");
//save the results as a .csv before clearing for the next image
// Clear the existing ROIs to allow for the next image to be segmented
roiManager("Select All");
roiManager("Reset");
        }
}
// A signal that the macro has been performed successfully without any failures stopping it.
print("Analysis complete please see dir2 for results");
/*To use this macro users will need to install the following plugins to FIJI
CBSDEEP
STARDIST.*/
```

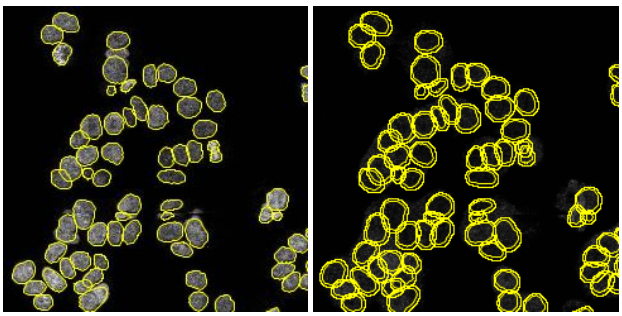

Supplemental Figure 8. Macro-generated Regions Of Interest (ROI)
Left panel: the nuclear area ROI was determined using DAPI as a nuclear dye and after, eroded by decreasing the size of the ring by a set number of pixels to remove cytoplasmic contamination. Right panel: the cytoplasmic ROI was determined by expanding the ring encompassing the nuclear ROI. After a second outer ring several pixels away was made to generate a cytoplasmic collar.

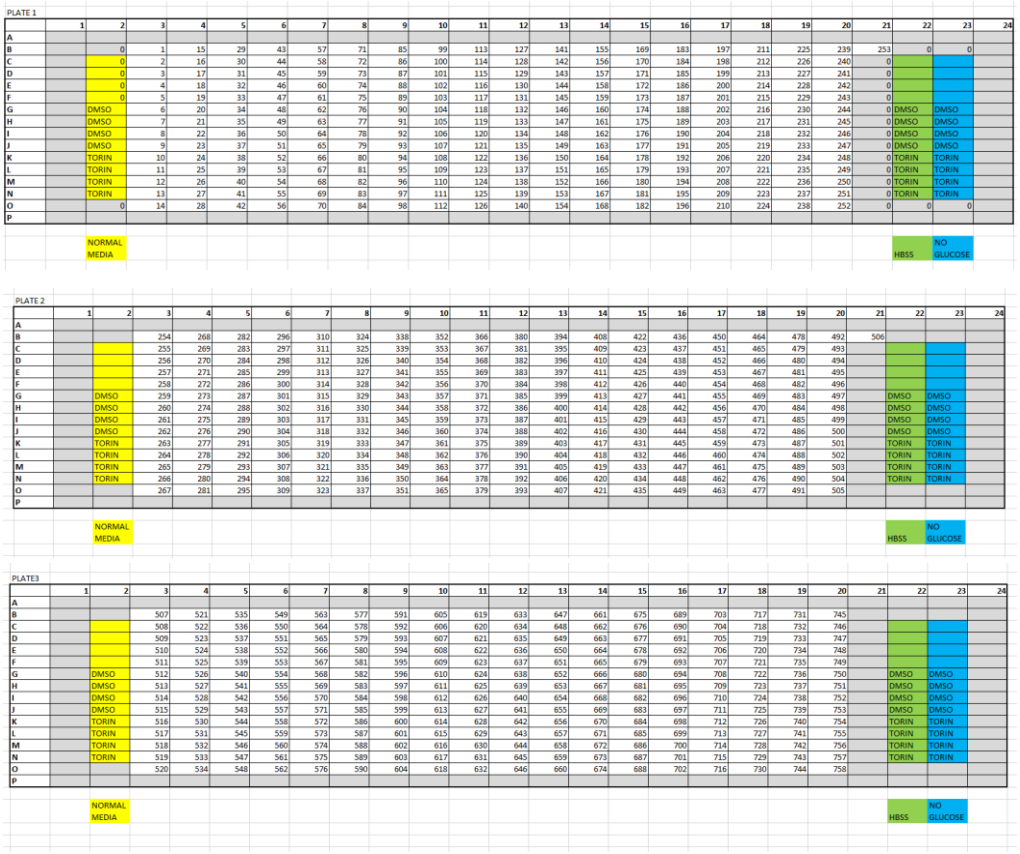

PLATE 1

	1	2	3	4	5	6	7	8	9	10	11	12	13	14	15	16	17	18	19	20	21	22	23	24
A																								
B		0	1	15	29	43	57	71	85	99	113	127	141	155	169	183	197	211	225	239	253	0	0	
C		0	2	16	30	44	58	72	86	100	114	128	142	156	170	184	198	212	226	240	0			
D		0	3	17	31	45	59	73	87	101	115	129	143	157	171	185	199	213	227	241	0			
E		0	4	18	32	46	60	74	88	102	116	130	144	158	172	186	200	214	228	242	0			
F		0	5	19	33	47	61	75	89	103	117	131	145	159	173	187	201	215	229	243	0			
G		DMSO	6	20	34	48	62	76	90	104	118	132	146	160	174	188	202	216	230	244	0	DMSO	DMSO	
H		DMSO	7	21	35	49	63	77	91	105	119	133	147	161	175	189	203	217	231	245	0	DMSO	DMSO	
I		DMSO	8	22	36	50	64	78	92	106	120	134	148	162	176	190	204	218	232	246	0	DMSO	DMSO	
J		DMSO	9	23	37	51	65	79	93	107	121	135	149	163	177	191	205	219	233	247	0	DMSO	DMSO	
K		TORIN	10	24	38	52	66	80	94	108	122	136	150	164	178	192	206	220	234	248	0	TORIN	TORIN	
L		TORIN	11	25	39	53	67	81	95	109	123	137	151	165	179	193	207	221	235	249	0	TORIN	TORIN	
M		TORIN	12	26	40	54	68	82	96	110	124	138	152	166	180	194	208	222	236	250	0	TORIN	TORIN	
N		TORIN	13	27	41	55	69	83	97	111	125	139	153	167	181	195	209	223	237	251	0	TORIN	TORIN	
O		0	14	28	42	56	70	84	98	112	126	140	154	168	182	196	210	224	238	252	0	0	0	
P																								

NORMAL MEDIA — HBSS — NO GLUCOSE

PLATE 2

	1	2	3	4	5	6	7	8	9	10	11	12	13	14	15	16	17	18	19	20	21	22	23	24
A																								
B			254	268	282	296	310	324	338	352	366	380	394	408	422	436	450	464	478	492	506			
C			255	269	283	297	311	325	339	353	367	381	395	409	423	437	451	465	479	493				
D			256	270	284	298	312	326	340	354	368	382	396	410	424	438	452	466	480	494				
E			257	271	285	299	313	327	341	355	369	383	397	411	425	439	453	467	481	495				
F			258	272	286	300	314	328	342	356	370	384	398	412	426	440	454	468	482	496				
G		DMSO	259	273	287	301	315	329	343	357	371	385	399	413	427	441	455	469	483	497		DMSO	DMSO	
H		DMSO	260	274	288	302	316	330	344	358	372	386	400	414	428	442	456	470	484	498		DMSO	DMSO	
I		DMSO	261	275	289	303	317	331	345	359	373	387	401	415	429	443	457	471	485	499		DMSO	DMSO	
J		DMSO	262	276	290	304	318	332	346	360	374	388	402	416	430	444	458	472	486	500		DMSO	DMSO	
K		TORIN	263	277	291	305	319	333	347	361	375	389	403	417	431	445	459	473	487	501		TORIN	TORIN	
L		TORIN	264	278	292	306	320	334	348	362	376	390	404	418	432	446	460	474	488	502		TORIN	TORIN	
M		TORIN	265	279	293	307	321	335	349	363	377	391	405	419	433	447	461	475	489	503		TORIN	TORIN	
N		TORIN	266	280	294	308	322	336	350	364	378	392	406	420	434	448	462	476	490	504		TORIN	TORIN	
O			267	281	295	309	323	337	351	365	379	393	407	421	435	449	463	477	491	505				
P																								

NORMAL MEDIA — HBSS — NO GLUCOSE

PLATE3

	1	2	3	4	5	6	7	8	9	10	11	12	13	14	15	16	17	18	19	20	21	22	23	24
A																								
B			507	521	535	549	563	577	591	605	619	633	647	661	675	689	703	717	731	745				
C			508	522	536	550	564	578	592	606	620	634	648	662	676	690	704	718	732	746				
D			509	523	537	551	565	579	593	607	621	635	649	663	677	691	705	719	733	747				
E			510	524	538	552	566	580	594	608	622	636	650	664	678	692	706	720	734	748				
F			511	525	539	553	567	581	595	609	623	637	651	665	679	693	707	721	735	749				
G		DMSO	512	526	540	554	568	582	596	610	624	638	652	666	680	694	708	722	736	750		DMSO	DMSO	
H		DMSO	513	527	541	555	569	583	597	611	625	639	653	667	681	695	709	723	737	751		DMSO	DMSO	
I		DMSO	514	528	542	556	570	584	598	612	626	640	654	668	682	696	710	724	738	752		DMSO	DMSO	
J		DMSO	515	529	543	557	571	585	599	613	627	641	655	669	683	697	711	725	739	753		DMSO	DMSO	
K		TORIN	516	530	544	558	572	586	600	614	628	642	656	670	684	698	712	726	740	754		TORIN	TORIN	
L		TORIN	517	531	545	559	573	587	601	615	629	643	657	671	685	699	713	727	741	755		TORIN	TORIN	
M		TORIN	518	532	546	560	574	588	602	616	630	644	658	672	686	700	714	728	742	756		TORIN	TORIN	
N		TORIN	519	533	547	561	575	589	603	617	631	645	659	673	687	701	715	729	743	757		TORIN	TORIN	
O			520	534	548	562	576	590	604	618	632	646	660	674	688	702	716	730	744	758				
P																								

NORMAL MEDIA — HBSS — NO GLUCOSE

Supplemental Figure 9. Example of plate layouts used for high-throughput image-based screen.
Plate layout demonstrating compound and control conditions. There were 6x plates treated by compounds diluted in media containing no glucose (DMEM no glucose) and 6x plates treated by compounds diluted in in media containing no amino acids (HBSS). Each plate was performed in duplicate, giving a total of 12 plates. Each plate had control conditions: DMEM only, DMSO 0.1%, Torin 1 (250 nM), HBSS, DMEM no glucose.

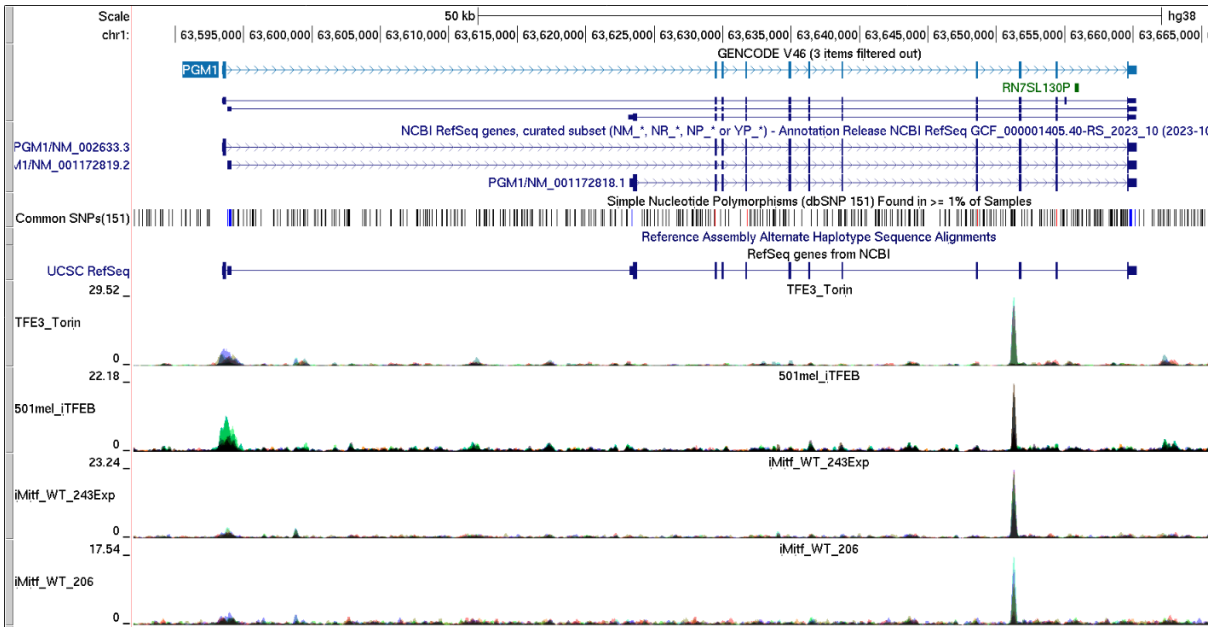

Supplemental Figure 10 Snapshot of USC browser demonstrating TFEB and MITF can directly bind to the PGM1 promoter provided by Pakavarin Louphrasitthiphol

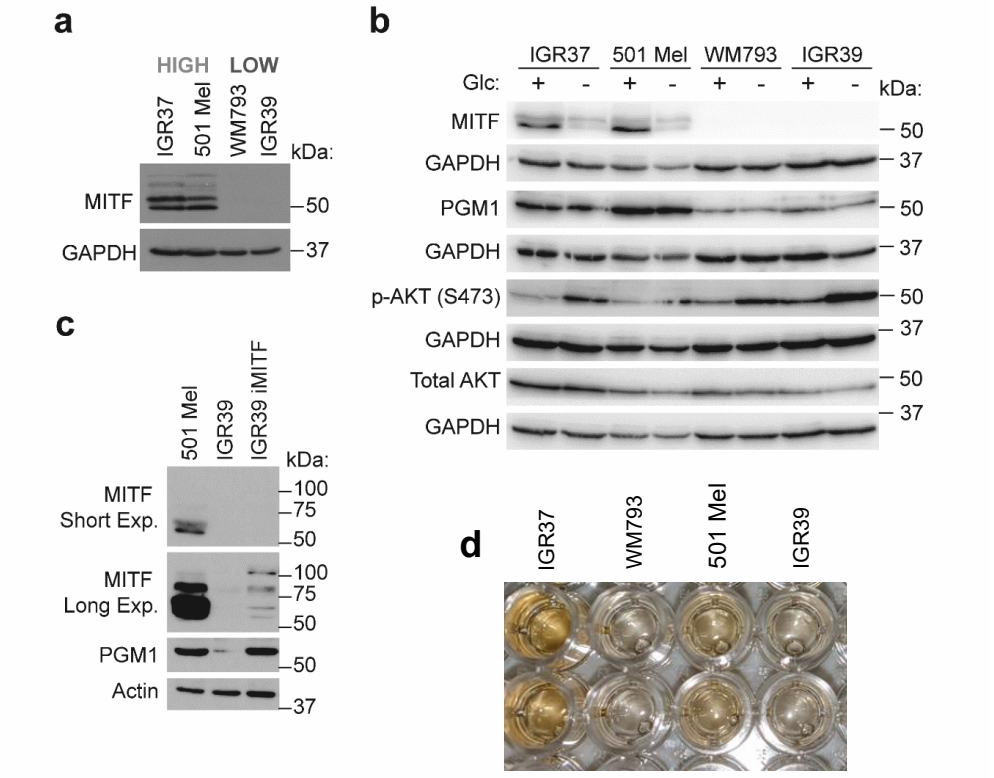

Supplemental Figure 11. MITF high melanoma cell lines have higher levels of PGM1, lower levels of mTORC2 signalling and more glycogen than compared to low MITF melanoma cell lines

(a) Western blot analysis demonstrating 1GR37 and 501 Mel express high levels of MITF, compared to WM793 and IGR39. (b) Western blot analysis demonstrating that in response to glucose deprivation (4 hr), MITF low cell lines exhibit a greater induction of mTORC2 activity compared to MITF high cell lines. Furthermore, MITF high cell lines express more PGM1 than MITF low cell lines. Notably, there is also a visible decrease in total MITF levels in response to glucose withdrawal. (c) Over-expression of MITF increases PGM1 expression in IGR39. (d) MITF high cell lines have visibly more glycogen than MITF low cell lines. Quantification could not be performed due to lack of time.

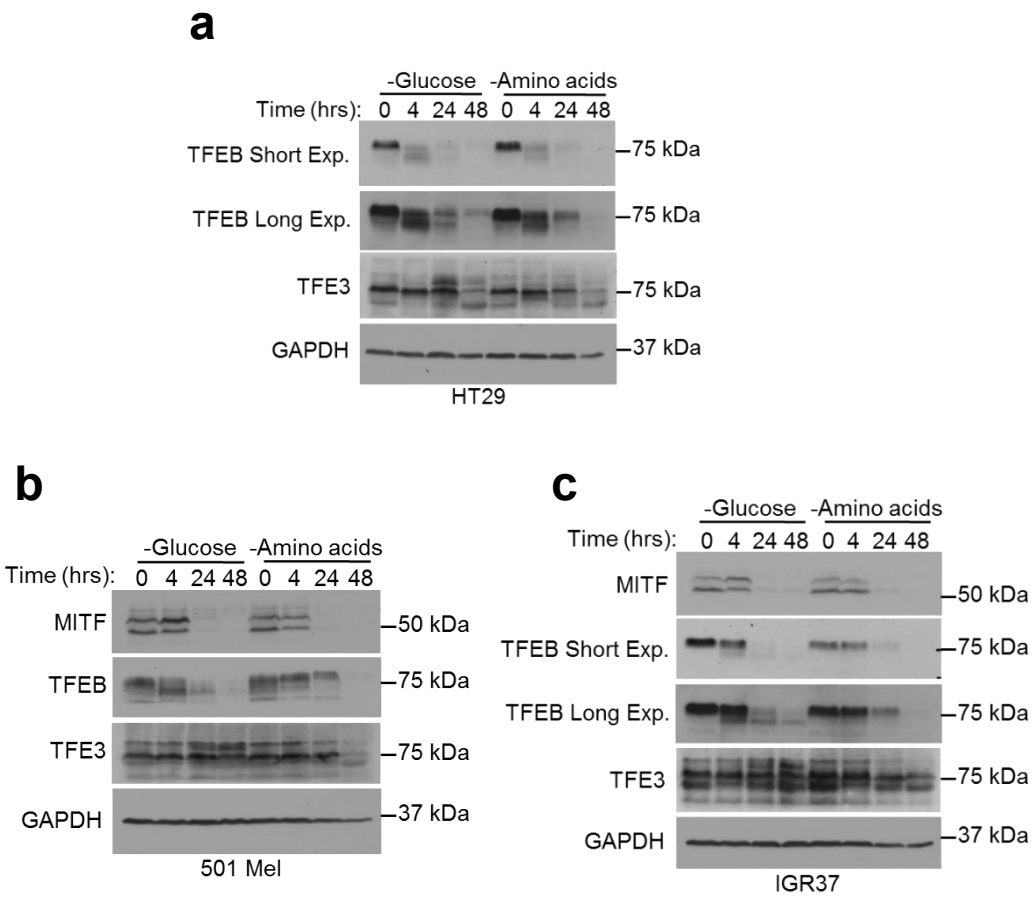

Supplemental Figure 12 Glucose starvation leads to a decrease in levels of MITF and TFEB but not TFE3.
(a) Western blot analysis of HT29 starved of glucose or amino acids for up to 48 hrs. (b) Western blot analysis of 501 Mel starved of glucose or amino acids for up to 48 hrs. (c) Western blot analysis of IGR37 starved of glucose or amino acids for up to 48 hrs. *Data produced by the candidate and published in (Dias et al., 2024)*

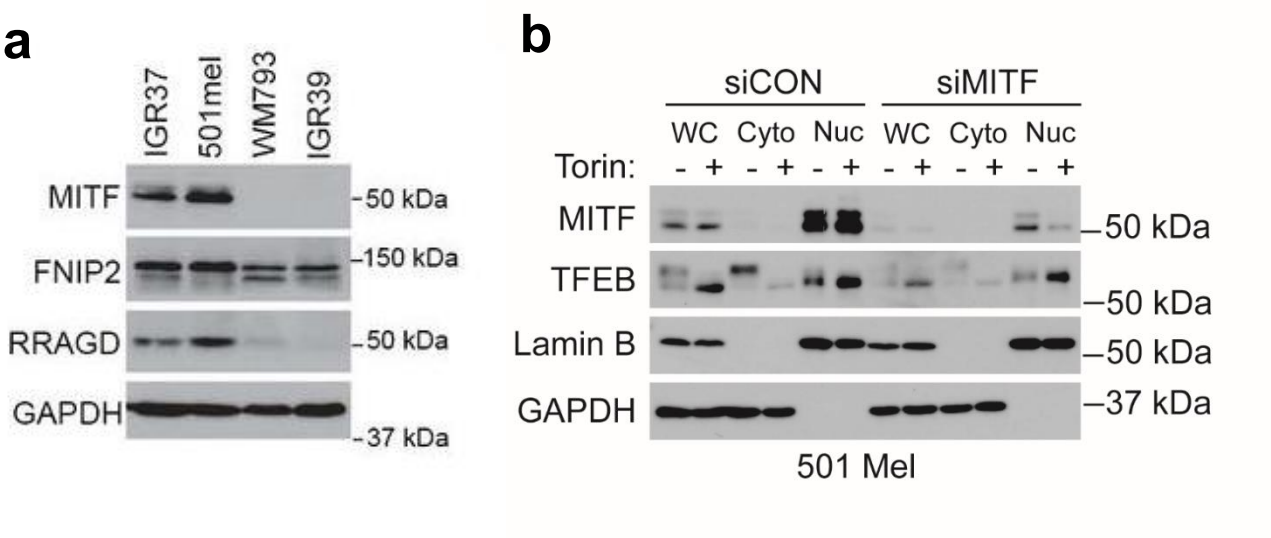

Supplemental Figure 13 MITF levels correlate with mTORC1 signaling *(a) Western blot analysis demonstrating that MITF high cell lines have higher levels of mTORC1 signalling as visualised by FNIP2 and RRAGD than MITF low cell lines. (b) Western blot analysis showing when MITF is silenced by siRNA, TFEB levels decrease and the proportion of TFEB in the nucleus increases. Data produced by the candidate and published in* (Dias et al. 2024)

Publication list

Dias, D., Oliveira, E., Martí-Díaz, R., Andrews, S., Chocarro-Calvo, A., Bellini, A., Mosteo, L., Vivas García, Y., Chauhan, J., Li, L., García-Martinez, J. M., Rodriguez-López, J. N., Maria-Engler, S. S., García-Jiménez, C., Sanchez-del-Campo, L., Louphrasitthiphol, P., & Goding, C. R. (2024). Functional specialization of MITF, TFEB and TFE3 drives radically distinct adaptive gene expression programs in melanoma. BioRxive.

Herbert, K., Binet, R., Lambert, J. P., Louphrasitthiphol, P., Kalkavan, H., Sesma-Sanz, L., Robles-Espinoza, C. D., Sarkar, S., Suer, E., Andrews, S., Chauhan, J., Roberts, N. D., Middleton, M. R., Gingras, A. C., Masson, J. Y., Larue, L., Falletta, P., & Goding, C. R. (2019). BRN2 suppresses apoptosis, reprograms DNA damage repair, and is associated with a high somatic mutation burden in melanoma. Genes and Development, 33(5–6), 310–332.

Li, L., Friedrichsen, H. J., Andrews, S., Picaud, S., Volpon, L., Ngeow, K., Berridge, G., Fischer, R., Borden, K. L. B., Filippakopoulos, P., & Goding, C. R. (2018). A TFEB nuclear export signal integrates amino acid supply and glucose availability. *Nature Communications*, *9*(1).

Ngeow, K. C., Friedrichsen, H. J., Li, L., Zeng, Z., Andrews, S., Volpon, L., Brunsdon, H., Berridge, G., Picaud, S., Fischer, R., Lisle, R., Knapp, S., Filippakopoulos, P., Knowles, H., Steingrímsson, E., Borden, K. L. B., Patton, E. E., & Goding, C. R. (2018). BRAF/MAPK and GSK3 signaling converges to control MITF nuclear export. *Proceedings of the National Academy of Sciences of the United States of America*, *115*(37), E8668–E8677.